1-1-1999

Polyelectrolyte multilayer assemblies.

Meng Che Hsieh
University of Massachusetts Amherst

POLYELECTROLYTE MULTILAYER ASSEMBLIES

A Dissertation Presented

by

MENG CHE HSIEH

Submitted to the Graduate School of the
University of Massachusetts Amherst in partial fulfillment
of the degree requirements for the degree of

DOCTOR OF PHILOSOPHY

September 1999

Polymer Science and Engineering

POLYELECTROLYTE MULTILAYER ASSEMBLIES

A Dissertation Presented

by

MENG CHE HSIEH

Approved as to style and content by:

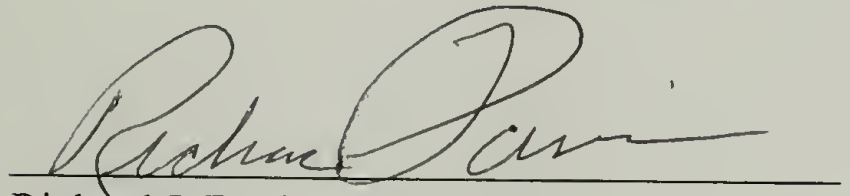

Richard J. Farris, Co-Chairman

Thomas J. McCarthy, Co-Chairman

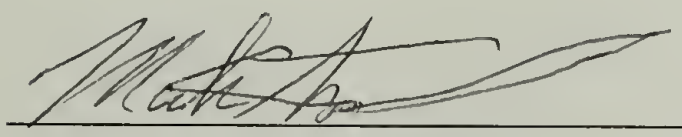

Mark T. Tuominen, Member

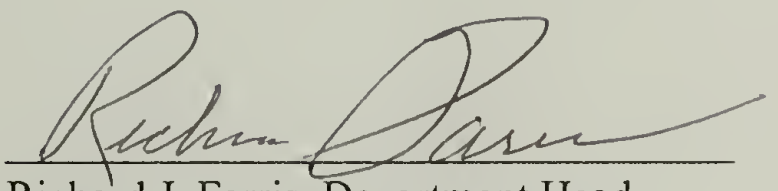

Richard J. Farris, Department Head
Polymer Science and Engineering

To my parents

ACKNOWLEDGMENTS

I would like to start by acknowledging my co-advisors, Tom McCarthy and Dr. Richard Farris. I am grateful for all their kindness, advice, and help. In addition, I want to thank them for allowing me to pursue research that was to my interest, independent of my dissertation. Dr. Mark Tuominen deserves my gratitude, as well, for his suggestions and time that he has given for the past 2 years.

Next, I want to thank the past and current members of the McCarthy and Farris research groups for making graduate school enjoyable and memorable. Jack deserves recognition as he maintained "my old" XPS, organized the in-coming lab supplies, and helped me on vacuum issues (among many other things). I am grateful for the input of those people (Wei, Vip, Gene, and Juha) whom have worked on the layer-by-layer system. I want to thank Rick for the skiing and hockey outings (and for not running me over in those hockey games). I want to thank Wei, Vip, Jeff, and Chris for keeping me company in the labs on the weekends and for the good times we had outside the lab. I appreciate the friendship we have.

Finally, I want to thank my family for their love and support throughout the years. I appreciate the sacrifices my parents made when they decided to move to the "States", for the sole reason that my brother and I could obtain a better education. I thank my brother for all the good times we have had: from the skiing trips to the hiking outings.

ABSTRACT

POLYELECTROLYTE MULTILAYER ASSEMBLIES

SEPTEMBER 1999

MENG CHE HSIEH, B.S., CORNELL UNIVERSITY

M.S., UNIVERSITY OF MASSACHUSETTS AMHERST

Ph.D., UNIVERSITY OF MASSACHUSETTS AMHERST

Directed by: Professor Richard J. Farris and Professor Thomas J. McCarthy

The overall objective of the projects that constitute this Ph.D. thesis is an in-depth understanding of layer-by-layer assemblies. The approaches taken in this quest include: a general method of surface modification for adsorbing polyelectrolytes (Chapter 2), the mechanical integrity of layer-by-layer assemblies (Chapter 3), and the adhesion of these assemblies to a substrate (Chapter 4).

The approach taken toward the development of a general method to incorporate charges on any surface to promote layer-by-layer assembly of polyelectrolytes is plasma polymerization of allylamine onto poly(tetrafluoroethylene). Plasma polymerization (10 W, 50 W) produces substrates that yield higher surface densities of amine groups at lower power. Well-defined multilayer structures , composed of poly(allylamine hydrochloride) (PAH) and poly(sodium styrenesulfonate) (PSS), are apparent in samples with greater than ~10 layers. XPS and contact angle data indicate stratified layers. XPS analysis also indicates that the stoichiometry of the assembly process is 2 ammonium ions per sulfonate group. The average individual layer thickness for the 10 W samples and for the 50 W samples are ~6.1 Å and 4.7 Å, respectively.

The mechanical properties of layer-by-layer assemblies are determined by forming polyelectrolyte multilayer assemblies of PAH and PSS on nitrogen/hydrogen-plasma modified spandex films and yarns. XPS analysis indicates that the stoichiometry of the assembly process is 1.7 ammonium ions per sulfonate group. The tensile modulus of the yarns decreased to 1.24 MPa from 2.61 MPa after plasma-modification. Upon adsorption of 50 layers of polyelectrolytes, the tensile modulus increased to 7.42 MPa resulting in a calculated modulus of the 50 layers of 8.8 GPa. These layer-by-layer assemblies fail at 2.5% strain.

The adhesion strength of the layer-by-layer assemblies is measured by studying the mean crack spacing of these assemblies on LPDE with varying surface charge. LDPE films, oxidized using chromic acid followed by adsorption of 50 layers, show cracks after 150% strain due to the failure of the multilayer assembly. Gold-coated LDPE films, adsorbed with an acid thiol followed by adsorption of 50 layers, show cracks after 50% strain due to the failure of the gold coating. The work of adhesion for the layers on oxidized LDPE is 370 mJ/m^2, which is greater than that on plasma-modified spandex (200 mJ/m^2) due to the higher surface charge density on the oxidized LDPE.

TABLE OF CONTENTS

LIST OF TABLES

LIST OF FIGURES

LIST OF ABBREVIATIONS

AFM	atomic force microscopy
ATR-IR	attenuated total reflectance infrared spectroscopy
EHFB	ethyl heptafluorobutyrate
FESEM	field emission SEM
FTIR	Fourier transform infrared spectroscopy
HFBA	2,2,3,3,4,4,4-heptafluorobutyl acrylate
HFIA	1,1,1,3,3,3-hexafluoroisopropyl acrylate
L-by-L	layer-by-layer
LDPE	low density polyethylene
LDPE-COOH	chromic acid oxidized LDPE
LDPE-Au-S-x-COOH	gold-coated LDPE adsorbed with mercaptohexadecanoic acid
Lycra-COOH	chromic acid oxidized Lycra
Lycra-NH_3^+	nitrogen/hydrogen plasma-modified Lycra
Lycra-PPAAM	allylamine plasma polymerized at 50W onto Lycra
NFH	3,3,4,4,5,5,6,6,6-nonafluoro-1-hexene
PAH	poly(allylamine hydrochloride)
PCTFE	poly(chlorotrifluoroethylene)
PEI	polyethylenimine
PET	poly(ethylene terephthalate)
PFH	perfluorohexane
PFMP	perfluoro-2-methyl-2-pentene

PFPA	2,2,3,3,3-pentafluoropropyl acrylate
PMP	poly(4-methyl-1-pentene)
PSS	poly(sodium styrenesulfonate)
PTFE	poly(tetrafluoroethylene)
^{10}PTFE-NH_3^+	allylamine plasma polymerized at 10W onto PTFE
^{50}PTFE-NH_3^+	allylamine plasma polymerized at 50W onto PTFE
rf	radiofrequency
SEM	scanning electron microscopy
XPS	x-ray photoelectron spectroscopy

CHAPTER 1

INTRODUCTION

Overview

This thesis describes three research projects that I have worked on for my dissertation. The overall objective of these projects is an in-depth understanding of layer-by-layer assemblies. The approaches taken in this quest include: a general method of surface modification for adsorbing polyelectrolytes, the mechanical integrity of layer-by-layer assemblies, and the adhesion of these assemblies to a substrate with different surface charge densities.

This first chapter covers background material that is common throughout this thesis: the layer-by-layer assembly technique and the methods used in this thesis to characterize these assemblies. In the first section, the substrates and the polyelectrolyte solutions that have been used, the variables for controlling the deposition process, and previous methods used to characterize these assemblies are discussed. In the second section, XPS and dynamic contact angle measurements are reviewed.

Chapter 2 examines the plasma polymerization of allylamine onto the surface of poly(tetrafluoroethylene) (PTFE) to generate a surface that is activated to promote layer-by-layer deposition. Currently, different methods are needed to initiate layer-by-layer

(L-by-L) deposition on different substrates. Successful demonstration of this technique on PTFE implies that this technique can be used as a general method of surface modification for the adsorption of polyelectrolytes on other substrates.

Chapter 3 describes the modification of Lycra® and the study of the mechanical properties of these multilayer assemblies on the modified Lycra®. As many potential applications of layer-by-layer assemblies have been discussed in recent publications, it is important that the mechanical properties of these assemblies be known. The tensile strength, the strain to failure, and the tensile modulus of these nano-assemblies are measured from uniaxial tension tests.

Chapter 4 investigates the adhesion strength of these layer-by-layer assemblies on low density polyethylene films of varying charge density. In the reported research on envisioned applications, the layer-by-layer assemblies are, in all cases, supported on a substrate (there have been no reports of free-standing multilayer films). If these assemblies are to be used in any application, it is vital to learn the adhesion strength of these assemblies on a substrate and the importance of the surface charge density on the adhesion strength. The adhesion strength of these assemblies is determined by measuring mean crack spacing of these assemblies.

Layer-by-Layer Deposition

Layer-by-layer (L-by-L) deposition of polyelectrolytes to build multilayer assemblies was recently reported by Decher *et.al.*[1-6] as a new and versatile spontaneous assembly tool to prepare modified surfaces and supramolecular ordered structures.[7-9] Other widely used methods for preparing structures of this type, Langmuir-Blodgett (LB) and self-assembled monolayer (SAM) techniques, are restricted by the limited range of substances that are useful self-assembly components and by the inability to prepare multilayer structures using the SAM technique. The L-by-L process has several important advantages: 1) it is simple as the adsorptions are driven by electrostatic attraction of opposite charges, 2) a wide variety of water-soluble polyions can be used as assembly components, 3) any substrate that can be modified to contain a charge can be used - independent of its shape, topography or topology, and 4) the overall thickness can be controlled precisely and accurately. The utility of the method is demonstrated by the applications that have been reported including conducting thin films,[10-13] films for nonlinear optics,[14] light-emitting and electrochromic thin films,[15-18] lithographic development,[19] sequential enzyme reactors,[20] biosensors,[21] humidity sensors,[22] and asymmetric gas separation membranes.[23]

The procedure for assembling these films is generalized as follows. A charged substrate (e.g. positive) is dipped into a solution containing a polyelectrolyte of opposite charge (e.g. negative). The concentration of the polyelectrolyte is in excess so that upon the completion of polyelectrolyte adsorption, a number of charged groups on the

polyelectrolyte chains remains exposed and the charge on the substrate is reversed (e.g. from positive to negative). The (negatively) charged substrate is rinsed and immersed into a (cationie) polyelectrolyte solution, which adsorbs and reverses the surface charge, restoring the original charge of the substrate (positive). Alternating adsorptions of anionie and eationie polyeleetrolytes lead to multilayer films. A simplified pieture of this proeess is shown in figure 1.1. This pieture is simplified as the layers are indieated as stratified with no interpenetration and the eharges have a one to one eorrelation.

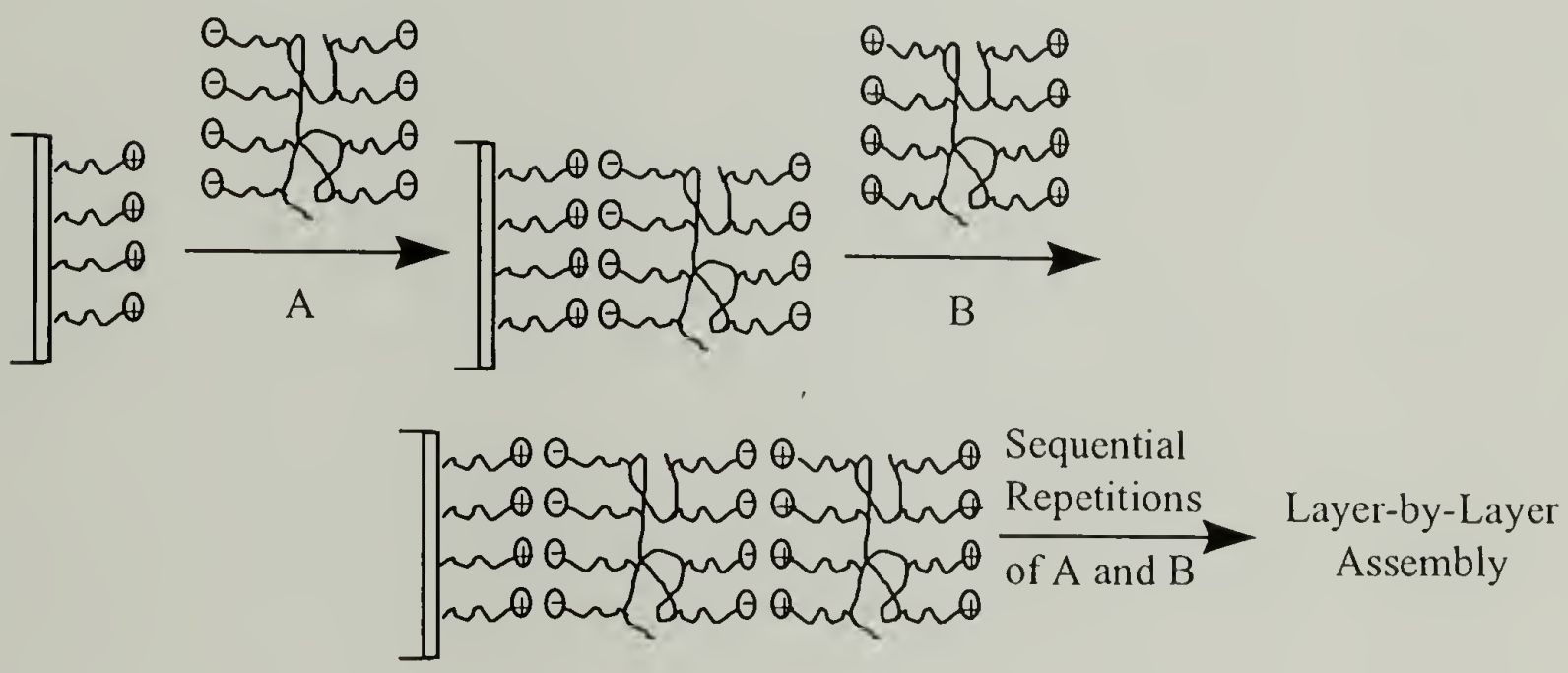

Figure 1.1. A simplified pieture of the L-by-L deposition proeess.

Substrates

Any substrate, independent of size, topology, and topography ean be used for the L-by-L teehnique. Numerous types of substrates, charged and neutral, have been used. Among inorganic substrates, glass (ineluding siliea, fused quartz, and the oxide layer on a

silicon wafer) and gold are the most common. L-by-L adsorptions have been accomplished on many types of surface-modified glass including hydrophilic (cleaning),[30] hydrophobic (plasma treatment with hexamethyldisilazane),[30] positively charged (reacting with a silane coupling agent containing amine groups[1,13,30-32] or adsorbing poly(ethylene imine) (PEI)[13,33]), and negatively charged (plasma treatment with methane and oxygen).[28] Gold has been modified by reacting with mercaptohexadecanoic acid[19] or mercaptopropionic acid.[34]

L-by-L deposition on organic substrates has also been examined. Using an initial adsorption of PEI, multilayer assemblies have been formed on PET, poly(methyl methacrylate), and poly(styrene).[35] Insufficient amounts of PEI adsorbs onto poly(propylene), but initial adsorption of poly(choline methacrylate) did initiate L-by-L adsorption.[35] In our laboratory, the common approach to initiate L-by-L deposition was surface modification of the polymeric substrate. In addition to the work that is reported here, multilayer assemblies have been studied on PMP,[23] PET and its derivatives,[24] and PCTFE.[25]

Adsorption Solutions

The adsorption solutions can contain any charged species since adsorption is driven by electrostatic attraction between opposite charges. The usual solvent is water but cosolvents have been added to enhance the solubility of the solute.[12,13] Addition of

acid or base adjusts the pH of the solutions while addition of salt adjusts the ionic strength of the solutions.

Organic polyelectrolytes are the most common materials used for the L-by-L deposition technique. The most widely used are PAH,[1-6,10,19,28,31,34] PEI,[5,6] and poly(dimethyldiallylammonium chloride) (PDDA)[19,36,37] for the cationic species and poly(sodium styrenesulfonate) (PSS)[1-6,10,19,28,31,34,35] and poly(vinyl sulfate)[1,3,5,6,38] for the anionic species. Among biological materials, proteins,[21,33] a virus,[39] and DNA[40] have been used as polyelectrolytes. Conjugated polymers such as poly(*p*-phenylene vinylene),[10,15,16] sulfonated polyaniline,[10,16,32] and p-doped poly(aniline)[11,12,13] have been incorporated into the multilayer assembly to make conductive or light-emitting thin films. Electrochromic thin films have been made by using poly(viologens)[17,18] as a polyelectrolyte layer. Components for L-by-L deposition are not limited to linear polyelectrolytes; dendrimers have also been used.[32,41]

Inorganic components for self-assembly have also been reported. Clays, such as synthetic hectorite[22,36] and montmorillonite,[42] have been incorporated into the multilayer assembly. L-By-L assembly has also been reported for nanoparticles of silica and TiO_2 (both negatively charged at pH=10) and CeO_2 (positively charged at pH=3.5)[37] and for "coupled" colloids of TiO_2/PbS.[43]

Variables for Controlling Polyelectrolyte Deposition

The amount of polyelectrolytes adsorbed is controlled by the surface charge density of the substrate, the pH and ionic strength of the solution, the polymer concentration and molecular weight, and on the adsorption time. Theoretical predictions on how these variables affect polyelectrolyte adsorption are based on the lattice theory for polymer adsorption of Scheutjens and Fleer.[44-47] Results from experiments support these predictions, except for the affect of surface charge density.

For polyelectrolyte adsorption, the amount of charge on the substrate surface determines how the chains adsorb. On a neutral substrate, the amount of adsorption increases with molecular weight due to the growth of the average size of loops and tails.[48,49] On a charged substrate (charge opposite to the polyelectrolyte), increasing the charge density has an uncertain effect. Cosgrove demonstrates that increasing the surface charge decreases the adsorbed amount as the chains adsorb in a flatter configuration.[50] Conversely, Evers and Blaakmeer show that increasing surface charge increases the amount adsorbed due to the electrostatic contribution to the adsorption energy of the segments.[46,51] Perhaps, the type of polyelectrolyte used attributed to the differences as Cosgrove used a strong polyelectrolyte while Evers and Blaakmeer used a weak polyelectrolyte in a regime where it behaves like a strong polyelectrolyte.

The adsorption of weak polyelectrolytes is dependent on the degree of dissociation which varies with the concentration and the solution pH. At low

concentrations, there is a high degree of ionization and low amounts of polymer are adsorbed. Similarly at high pH (above pK_o), the polyelectrolyte ionizes and behaves like a strong polyelectrolyte; the amount adsorbed is independent of the molecular weight and the pH and increases with salt content. As the concentration increases, the degree of dissociation decreases and greater amounts of polymer adsorb. At low pH, the polyelectrolyte adsorbs like a neutral polymer, the adsorbed amount increases with molecular weight and with decreasing solvent quality.[46,51] In the presence of a highly charged surface, the amount adsorbed is decreased as the salt ions in the solution preferentially adsorb onto the surface, displacing the uncharged polyelectrolyte. At intermediate pH (about 1-1.5 pH units below pK_0), there is a maximum in adsorption because the electrostatic attraction between segments and surface is stronger than the repulsion between segments. The pH dependence on the polyelectrolyte adsorption is shown in figure 1.2.

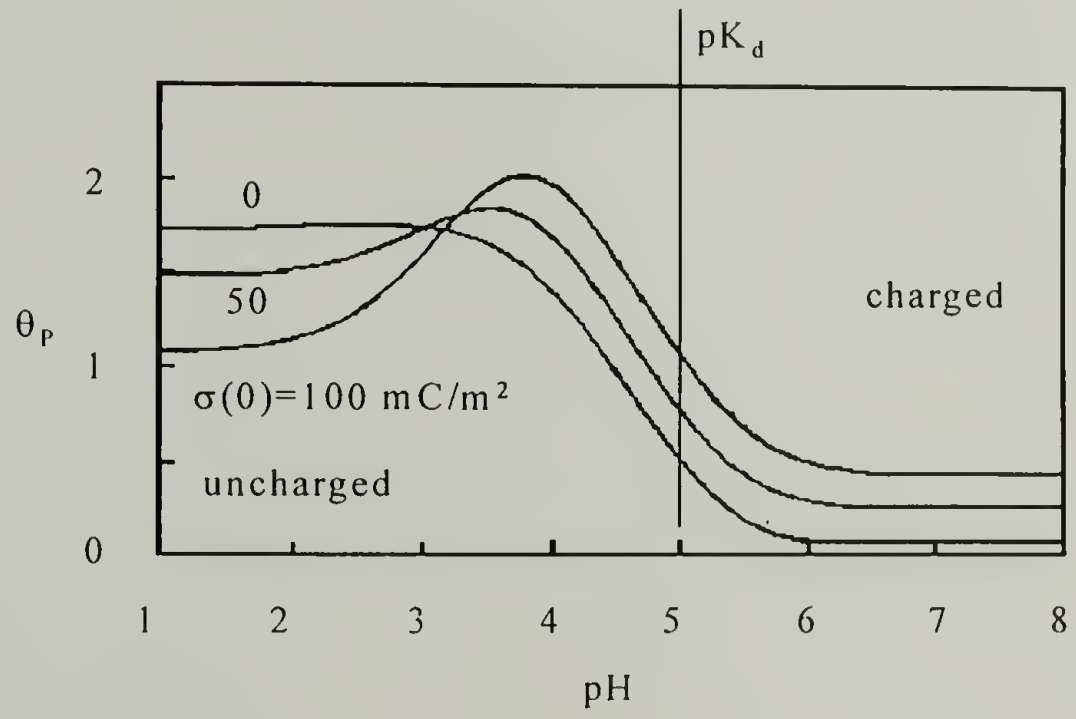

Figure 1.2 Adsorbed amounts of a weak polyacid (pK_d=5) as a function of pH for three fixed surface charges: 0, 50, and 100 mC/m^2.[47]

Electrostatic forces can be minimized by incorporating salt in the polyelectrolyte solution. In the absence of salt, the polyelectrolyte chains adsorb in a flat conformation, with 90% of the chains in contact with the charged surface. As the ionic strength is increased, the electrostatic repulsions between the segments are screened leading to a more flexible chain. The chains adsorbed from polyelectrolyte solutions containing salt adopt configurations with more loops and result in thicker layers (figure 1.3).[44,47,50] The variation in the relative amounts of loops, tails, and trains as a function of salt concentration is shown in figure 1.4. The amount of adsorption on any substrate increases with ionic strength. At high salt concentrations, the polyelectrolyte behaves similarly to neutral polymers as the charges on the chains are screened and the adsorption becomes molecular weight dependent.[45]

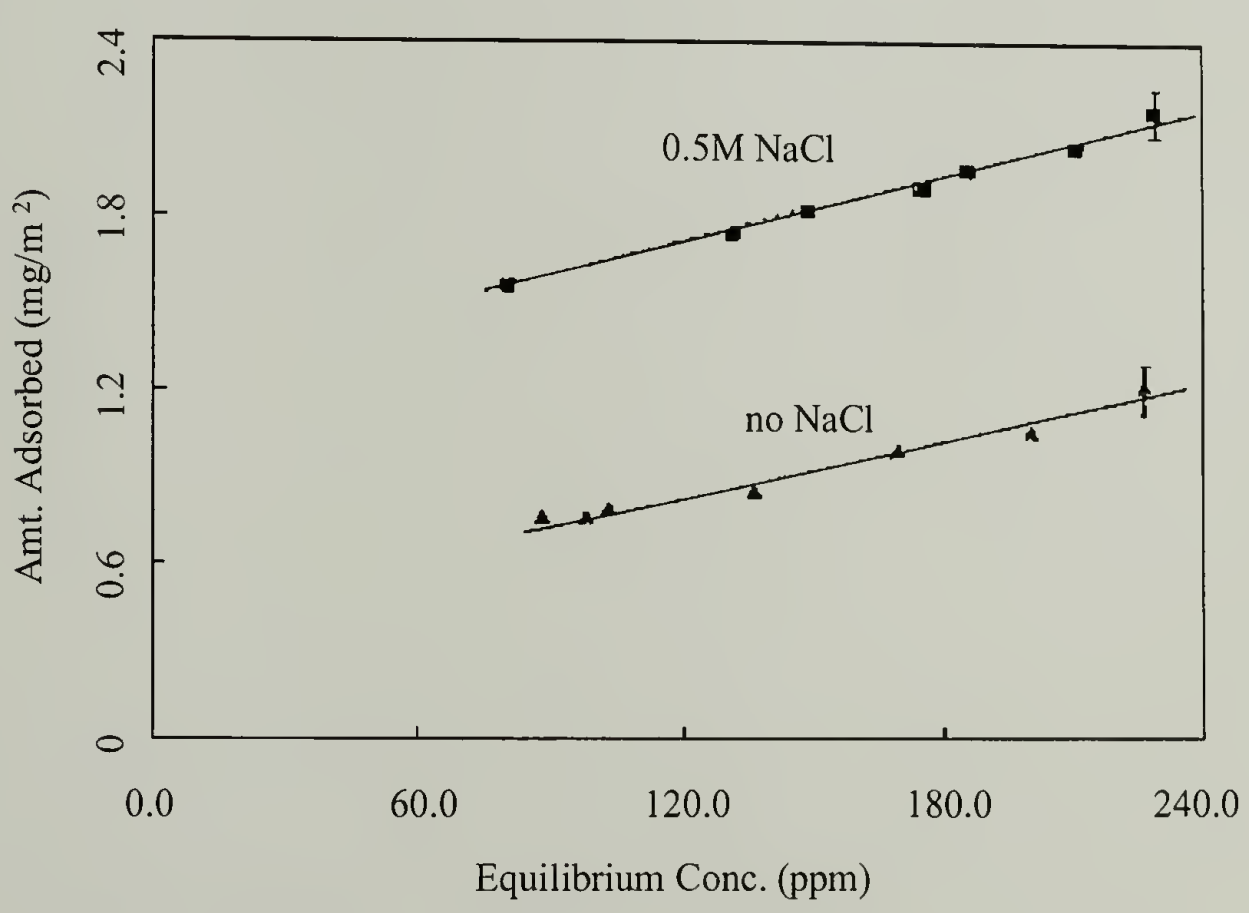

Figure 1.3. Adsorption isotherm for PSS (MW=780k) at two different salt concentrations.[50]

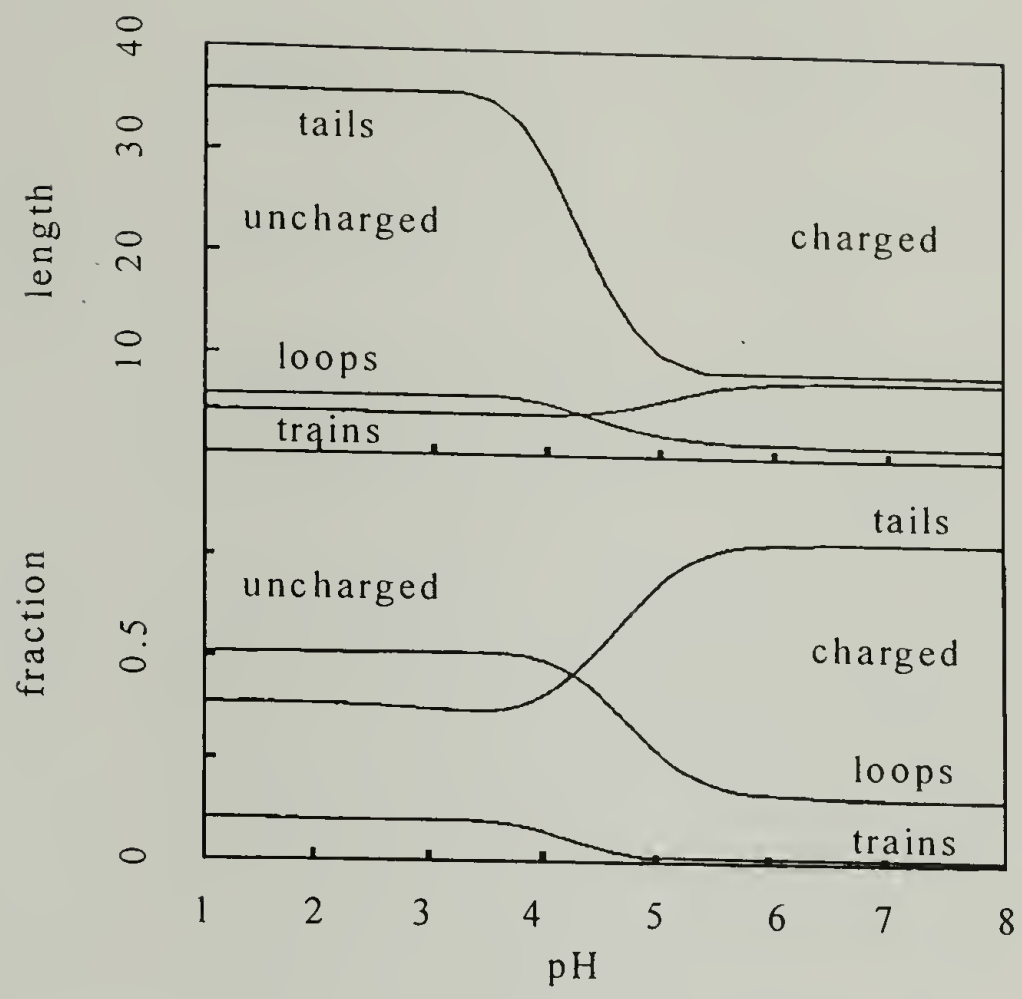

Figure 1.4. Average length and fraction of segments in trains, loops, and tails as a function of pH for a weak polyacid adsorbing onto a charged surface of 50 mC/m^2.[47]

Two other variables are polyelectrolyte concentration and adsorption time. For strong polyelectrolytes, the amount of adsorption increases as the polymer concentration is increased. A certain amount of time is required for complete polymer adsorption, usually less then 20 minutes.

Characterization of Layer-by-Layer Assemblies

Early analyses of these multilayer assemblies have focused on proving the viability of the L-by-L deposition technique as a method to form thin film assemblies. This has been done by measuring the thickness of the assemblies by small angle X-ray

and neutron reflectivity[1-5,31,38-41] as layers are deposited. Another method was to follow the intensity of adsorption of a characteristic band of one of the polyelectrolytes as layers are deposited using UV-Vis spectroscopy.[1,10-13] Recently, the quartz crystal microbalance[21,22,36,37,42] and surface plasmon resonance spectroscopy[21,34] have been used to indirectly measure the mass as layers are deposited. Other methods to follow the thickness of the layers are profilometry[10-13,30] and ellipsometry.[13,18,19,30,32] The atomic composition of multilayer assemblies have been analyzed by X-ray photoelectron spectroscopy (XPS),[18,32,34,35,38] time-of-flight secondary ion mass spectroscopy,[35,38] and energy dispersive X-ray spectroscopy.[43] Cross-sections of multilayer assemblies were observed using optical microscopy.[1] Other techniques have been used to examine the surfaces of these structures including atomic force microscopy (AFM),[13,19,32,37,43] scanning electron microscopy (SEM),[37,42] and transmission electron microscopy.[43]

Surface Analysis Techniques

Two techniques used throughout this dissertation in the analysis of surfaces are XPS and contact angle measurements. XPS, also know as Electron Spectroscopy for Chemical Analysis (ESCA), is used to determine the atomic composition and to obtain qualitative information on the functional groups present in the outermost 10-100 Å of a surface. Contact angle measurements are made to follow the wettability of the surface as the surface is modified.

XPS

XPS provides atomic composition data and qualitative information on functional groups due to the photoelectric effect. By exposing a sample to a beam of monoenergetic soft x-rays (most commonly Al K_α or Mg K_α), core shell electrons are ejected from the sample as shown in figure 1.5. A detector collects and analyzes the kinetic energy, E_k, of the ejected electron. From this measurement and knowing the energy of the x-rays ($h\nu$) and the work function of the spectrometer, ϕ, the binding energy E_b of the electron in an atomic orbital of the source element can be calculated by:

$$E_b = h\nu - E_\kappa - \phi. \qquad (1.1)$$

As each element has a unique set of core electrons, the elements present in samples can be identified from the obtained spectrum. The atomic composition is calculated by measuring the peak areas and using atomic sensitivity factors obtained from samples with known composition. Qualitative information concerning the functional groups at the surface is provided due to the affects of valence states on the energy of the core electrons.

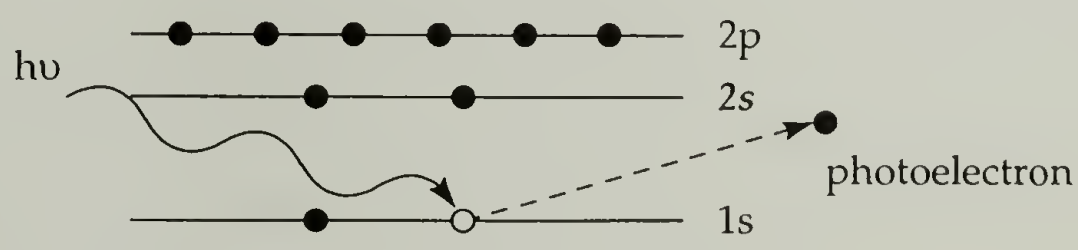

Figure 1.5. An x-ray hits a 1s core electron transferring energy to the electron resulting in its ejection from the sample with a characteristic kinetic energy.

For atoms that are bound to electroncgative speeies, such as carbon bound to oxygen, the electrons from the carbon are attracted to oxygen. As there are less negative charges to interact with the carbon nucleus, there is less electrostatic shielding of 1s core electrons and these electrons are more strongly attracted to the nucleus. These core electrons have higher binding energies and thus have lower kinetic energies.

XPS is a surface technique and not a bulk technique due to the finite escape depth of the ejected core electrons. The number of electrons detected, N, at sampling depth t is related to the number of electrons ejected, N_0, by

$$N = N_0 e^{-(t/\lambda \sin\theta)} \tag{1.2}$$

where λ is the electron mean free path and θ is the angle between the plane of the sample surface and the detector. The electron mean free path is defined as the mean distance an electron travels before colliding with a particle and losing energy. The most common experimental method for measuring the mean free path is the overlayer technique in which a homogeneous film of know thickness is deposited on a substrate. As the intensity of the film and substrate peaks are dependent on the thickness of the overlayer, it is expected that the signal intensity from the substrate will exponentially decay with increasing thickness and that the overlayer signal intensity will increase until the substrate is not detected. Electron mean free path is a function of kinetic energy and the values in organic polymers should be similar to metals and semiconductors.[52] A wide range of values has been reported, from 7 Å to 65 Å. The higher values are usually those measured from samples involving Langmuir-Blodgett films.[53,54] It has been recognized that these values are higher due to a channeling phenomena whereby electrons can travel

nearly parallel to the long chains. For carbon film and films of poly(*p*-xylylene), such phenomena is not possible and lower values were measured.[52,55] Theoretical predictions made by Ashley based on the electron energy, the material density, the molecular weight of the monomer unit, and the number of valence electrons per monomer unit result in mean free paths that agree with experimental results.[56-58]

Since the number of electrons detected is dependent on the depth, it is possible to obtain the depth profile of a sample by using variable take-off angles (the angle between the sample surface and the detector). Figure 1.6 shows the sample/detector geometry. XPS data obtained at smaller take-off angles are more surface sensitive as only photoelectrons ejected from the outermost surface can reach the detector. The sampling depth, the depth from which 95% of the photoelectrons originates, based on eq. 1.2. is $3\lambda\sin\theta$. The mean free path for C_{1s} electrons used in this dissertation is 14 Å (from Clark)[52] which translates to sampling depths of ~10 Å and ~40 Å for the 15° and 75° take-off angles, respectively.

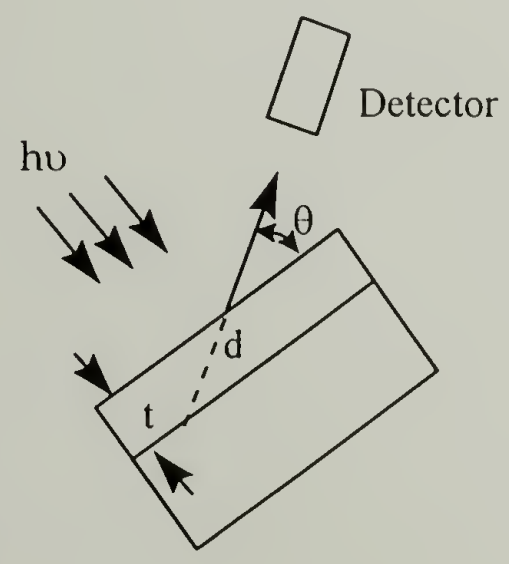

Figure 1.6. Sample/detector geometry in variable angle XPS.

Dynamic Contact Angle Measurements

Contact angle measurement is used to determine the critical surface tension of a material and consequently the wettability of the materials. A high energy surface will tend to be wetted by a probe fluid as the wetting of the fluid decreases the energy of the system. Conversely, a probe fluid will dewet a low energy surface so as to maintain the low energy state of the system. The angle θ formed by a probe fluid on a material is determined by the balance of three surface tensions (shown in figure 1.7): that existing at the solid-vapor interface γ^{SV}, the solid-liquid interface γ^{SL}, and the liquid-vapor interface γ^{LV}. This is mathematically represented by Young's equation:[59]

$$\gamma^{SV}-\gamma^{SL}=\gamma^{LV}\cos\theta. \qquad (1.3)$$

In this dissertation, dynamic contact angle measurements are made as the probe fluid is advanced onto the surface (to measure the advancing angle θ_A) and withdrawn from the surface (to measure the receding angle θ_R). The results from dynamic measurements are more informative than static measurements. The hysteresis, the difference between the

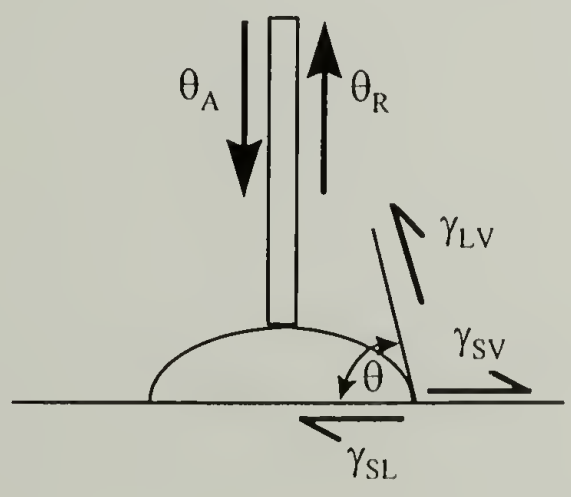

Figure 1.7. Dynamic contact angle measurement.

advancing and receding angle, may give information concerning the heterogeneity of the surface[60,61] or the roughness of the surface.[62-66] Hysteresis is also present if there is surface reorientation, surface deformation due to the moving droplet, or sample swelling.

Heterogeneous Surfaces. For a surface consisting of high contact angle regions (low energy), the advancing angle is associated with the high contact angle regions. An extreme example is the pinning effect where the advancing droplet is stopped by the low energy region and the contact angle increases until the angle approaches that of the low energy region at which point the droplet will advance across the region. The contact angle of heterogeneous surfaces was first approximated by Cassie to be an average of the phases present:

$$\cos\theta = \sum Q_n \cos\theta_n \qquad (1.4)$$

where Q_n is the fraction of the surface having contact angle θ_n and n is the number of phases present on the surface.[60] Johnson and Dettre developed a more complex model for a binary surface (figure 1.8).[61] These curves show that advancing angles are closer to the that of low energy surfaces (receding angles to high energy surfaces), advancing angles increase greatly when a small amount of a low-energy phase is present on a high-energy surface (receding angles decrease on low surface energy surface with high energy phase), and the behavior approaches Cassie's approximation as the size of the heterogeneity decreases (vibrational state of the liquid becomes greater). For patches below 0.1 μ, there is negligible contribution to hysteresis.

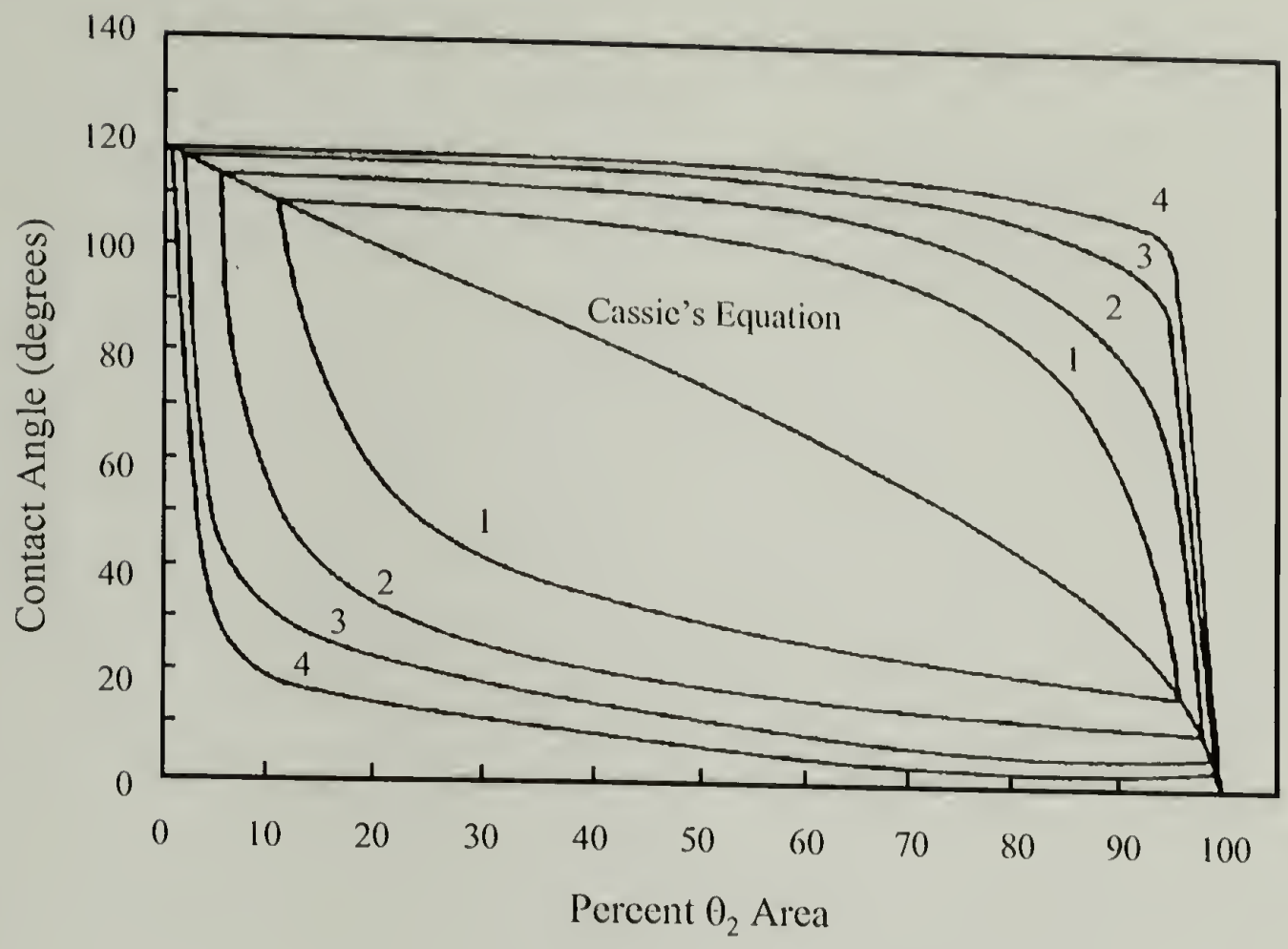

Figure 1.8. Contact angle hysteresis on a model heterogeneous surface with different energy barrier heights represented by E_d. Curve 1, E_d=0.2 cm; curve 2, E_d=0.1 cm; curve 3, E_d=0.05 cm; curve 4, E_d=0.025 cm.

Surface Roughness. The effect of surface roughness on wettability was first reported in 1936 by Wenzel.[62] In this report, he suggests that a rough surface has a greater intensity of surface energy compared to a smooth surface. For a nonwetting surface ($\theta>90°$), a rough solid should be more strongly repellent than a smooth solid. This behavior is described by Wenzel's equation:

$$\cos\theta' = r\cos\theta \tag{1.5}$$

where θ' is the contact angle on a rough surface and r is a roughness factor described by:

$$r = \frac{\text{actual surface}}{\text{geometric surface}}. \tag{1.6}$$

The actual surface is the surface area of the rough solid and the geometric surface is the area when the surface is projected onto a plane (smooth). This theory was extended by Cassie and Baxter for porous surfaces which adds an additional term to account for the liquid-air interface:[63]

$$\cos \theta' = Q_1 \cos \theta + Q_2 \qquad (1.7)$$

where Q_1 is the fractional area of the solid-liquid interface and Q_2 is the fractional area of the liquid-air interface beneath the drop. In order to explain contact angle hysteresis, Johnson and Dettre studied the wettability of an idealized sinusoidal surface with varying degrees of roughness.[64,65] They suggest that the contact angle hysteresis is explained by a balance between the macroscopic vibrational energy of the liquid drop and the heights of energy barriers separating metastable states such that the hysteresis decreases as the energy barrier decreases or as the vibrational energy increases. For hydrophobic surfaces at low roughness ratios, the hysteresis increases with roughness ratio up to a critical roughness ratio. At this critical roughness ratio, there is a transition from a noncomposite to a composite surface, the existence of liquid-air and liquid-solid interfaces under the drop are created, and the hysteresis decreases as the roughness ratio is increased further as shown in figure 1.9. This is due to the very low free energy barriers for composite surfaces.

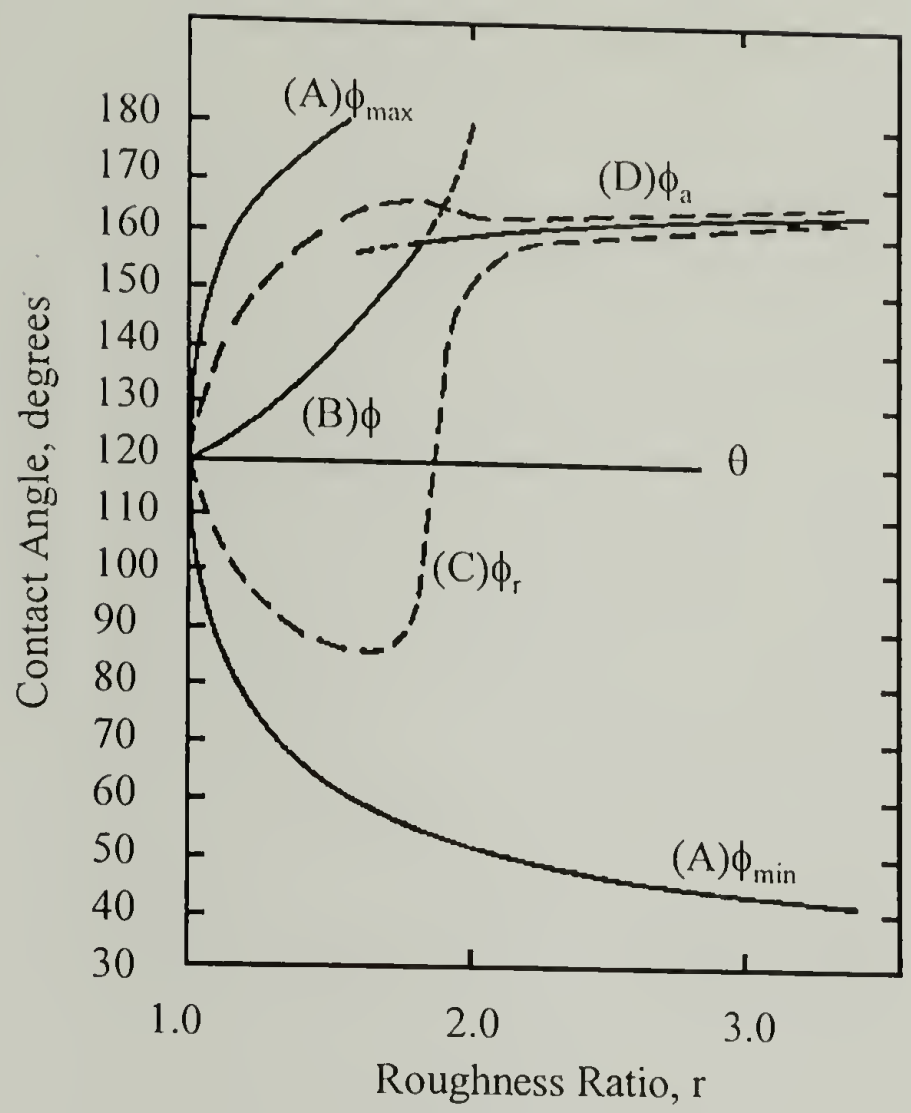

Figure 1.9. Effect of roughness on contact angle for a hydrophobic surface, θ=120°. Curve (A) shows the maximum and minimum possible angles. Curve (B) shows the most probable contact angle as calculated from Wenzel's equation (low roughness) and from Cassie and Baxter's equation (high roughness). Possible curves of receding and advancing angles are shown as Curves (C) and (D), respectively.[64]

Notes and References

(1) Decher, G.; Hong, J.-D.; Schmitt, J. *Thin Solid Films* **1992**, *210/211*, 831.

(2) Decher, G.; Schmitt, J. *Progr. Colloid. Polym. Sci.* **1992**, *89*, 160.

(3) Lvov, Y.; Decher, G.; Möhwald, H. *Langmuir* **1993**, *9*, 481.

(4) Decher, G.; Lvov, Y.; Schmitt, J. *Thin Solid Films* **1994**, *244*, 772.

(5) Sukhorukov, G.B.; Schmitt, J.; and Decher, G. *Ber. Bunsenges. Phys. Chem.* **1996**, *100*, 948.

(6) Decher, G. *Multilayer Films (Polyelectrolytes)*, in *The Polymeric Materials Encyclopedia: Synthesis, Properties and Applications*; Salamone, J.C., Ed., Vol. 6, CRC Press: Boca Raton, 1996, p 4540.

(7) Ulman, A. *An Introduction to Ultrathin Organic Films from Langmuir-Blodgett to Self-Assembly*; Academic Press: New York, 1991.

(8) Ulman, A., Ed. *Thin Films, vol. 20, Organic Thin Films and Surfaces: Directions for the Nineties*; Academic Press: New York, 1995.

(9) Vögtle, F. *Supramolecular Chemistry*; Wiley: Chichester, 1993.

(10) Ferreira, M.; Rubner, M.F. *Macromolecules* **1995**, *28*, 7107.

(11) Fou, A.C.; Rubner, M.F. *Macromolecules* **1995**, *28*, 7115.

(12) Cheung, J.H.; Stockton, W.B.; Rubner, M.F. *Macromolecules* **1997**, *30*, 2712.

(13) Stockton, W.B.; Rubner, M.F. *Macromolecules* **1997**, *30*, 2717.

(14) Laschewsky, A.; Bayer, B.; Wischerhoff, E.; Arys, X.; Bertrand, P.; Delacorte, A.; Jonas, A. *Thin Solid Films* **1996**, *284*, 334.

(15) Fou, A.C.; Onitsuka, O.; Ferreira, M.; Rubner, M.F.; Hsieh, B.R. *J. Appl. Phys.* **1996**, *79*, 7501.

(16) Onoda, M.; Yoshino, K. *Jpn. J. Appl. Phys.* **1995**, *34*, L260.

(17) Stepp, J.; Schlenoff, J.B. *J. Electrochem. Soc.* **1997**, *144*, L155.

(18) Laurent, D.; Schlenoff, J.B. *Langmuir* **1997**, *13*, 1552.

(19) Hammond, P.T.; Whitesides, G.M. *Macromolecules* **1995**, *28*, 7569.

(20) Onda, M.; Lvov, Y.; Ariga, K.; Kunitake, T. *J. Ferment. Bioeng.* **1996**, *82*, 502.

(21) Caruso, F.; Niikura, K.; Furlong, D.N.; Okahata, Y. *Langmuir*, **1997**, *13*, 3427.

(22) Kleinfeld, E.R.; Ferguson, G.S. *Chem. Mater.* **1995**, *7*, 2327.

(23) Leväsalmi, J.-M.; McCarthy, T.J. *Macromolecules* **1997**, *30*, 1752.

(24) Chen, W.; McCarthy, T.J. *Macromolecules* **1997**, *30*, 78.

(25) Phuvanartnuruks, V.; McCarthy, T.J. *Macromolecules* **1998**, *31*, 1906.

(26) Dias, A.J.; McCarthy, T.J. *Macromolecules* **1987**, *20*, 2068.

(27) Gombotz, W.R.; Hoffman, A.S. *J. Appl. Polym. Sci.: Polym. Symp.* **1988**, *42*, 285.

(28) Lvov, Y.; Haas, H. Decher, G.; Möhwald, H.; Kalachev, A. *J. Phys. Chem.* **1993**, *97*, 12835.

(29) Vargo, T.G.; Gardella, Jr., J.A.; Meyer, A.E.; Baier, R.E. *J. Polym. Sci.: Part A: Polym. Chem.* **1991**, *29*, 555.

(30) Ferreira, M.; Cheung, J.H.; Rubner, M.F. *Thin Solid Films*, **1994**, *244*, 806.

(31) Schmitt, J.; Grunewald, G,; Decher, G.; Pershan, P.S.; Kjaer, K.; Losche, M. *Macromolecules* **1993**, *26*, 7058.

(32) Watanabe, S.; Regan, S.L. *J. Am. Chem. Soc.* **1994**, *116*, 8855.

(33) Lvov, Y.; Ariga, K.; Kunitake, T. *Chem. Lett.* **1994**, 2323.

(34) Caruso, F.; Niikura, K.; Furlong, D.N.; Okahata, Y. *Langmuir* **1997**, *13*, 3422.

(35) Delcorte, A.; Bertrand, P.; Wischerhoff, E.; Laschewsky, A. *Langmuir* **1997**, *13*, 5125.

(36) Kleinfeld, E.R.; Ferguson, G.S. *Science* **1994**, *265*, 370.

(37) Lvov, Y.; Ariga, K.; Onda, M.; Ichinose, I.; Kunitakc, T. *Langmuir* **1997**, *13*, 6195.

(38) Delcorte, A.; Bertrand, P.; Arys, X.; Jonas, A.; Wischerhoff, E.; Mayer, B.; Laschewsky, A. *Surface Science* **1996**, *366*, 149.

(39) Lvov, Y.; Haas, H.; Decher, G.; Möhwald, H. *Langmuir* **1994**, *10*, 4232.

(40) Lvov, Y.; Decher, G.; Sukhorukov, G. *Macromolecules* **1993**, *26*, 5397.

(41) Tsukruk, V.V.; Rinderspacher, F.; Bliznyuk, V. *Langmuir* **1997**, *13*, 2171.

(42) Lvov, Y.; Ariga, K.; Ichinose, I.; Kunitake, T. *Langmuir* **1996**, *12*, 3038.

(43) Sun, Y.; Hao, E.; Zhang, X.; Yang, B.; Shen, J.; Chi, L.; Fuchs, H. *Langmuir* **1997**, *13*, 5168.

(44) Van der Schee, H.A.; Lyklema, J. *J. Phys. Chem.* **1984**, 88, 6661.

(45) Papenhuijzen, J.; van der Schee, H.A.; Fleer, G.J. *J. Colloid Interface Sci.* **1985**, *104*, 540.

(46) Evers, O.A.; Fleer, G.J.; Scheutjens, J.M.H.M.; Lyklema, J. *J. Colloid Interface Sci.* **1986**, *111 (2)*, 446.

(47) Böhmer, M.R.; Evers, O.A.; Scheutjens, J.M.H.M. *Macromolecules* **1990**, 23, 2288.

(48) Marra, J.; van der Schee, H.A.; Fleer, G.J.; Lyklema, J. In *Adsorption from Solution*; Ottewill, R.H., Rochester, C.H., Eds.; Academic Press: New York, 1983, p 245.

(49) Papenhuijzen, J.; Fleer, G.J; Bijsterbosch, B.H. *J. Colloid Interface Sci.* **1985**, *104*, 530.

(50) Cosgrove, T.; Obey, T.M.; Vincent, B. *J. Colloid Interface Sci.* **1986**, *111 (2)*, 409.

(51) Blaakmeer, J.; Böhmer, M.R.; Cohen Stuart, M.A.; Fleer, G.J. *Macromolecules* **1990**, 23, 2301.

(52) Clark, D.T.; Thomas, H.R. *J. Polym. Sci., Polym. Chem. Ed.* **1977**, *15*, 2843.

(53) Powell, C.J. *Surface Science* **1974**, *44*, 29.

(54) Hall, S.M.; Andrade, J.D.; Ma, S.M.; King, R.N. *J. Electron Spectroscopy* **1979**, *17*, 181.

(55) Steinhardt, R.G.; Hudis, J.; Perlman, M.L. *Phys. Rev.* **1972**, *B5*, 1016.

(56) Ashley, J.C. *IEEE Trans. Nucl. Sci.* **1980**, *NS-27*, 1454.

(57) Ashley, J.C.; Williams, M.W. *Rad. Res.* **1980**, *81*, 364.

(58) Ashley, J.C. *J. Electron Spectroscopy* **1982**, *29*, 177.

(59) Young, T. *Phil. Trans.* **1805**, *95*, 65.

(60) Cassie, A.B.D. *Discuss. Faraday Soc.* **1948**, *3*, 11.

(61) Johnson, R.E., Jr.; Dettre, R.H. *J. Phys. Chem.* **1964**, *68*, 1744.

(62) Wenzel, R.N. *Ind. Eng. Chem.* **1936**, *28*, 988.

(63) Cassie, A.B.D; Baxter, S. *Trans. Faraday Soc.* **1944**, *40*, 546.

(64) Johnson, R.E., Jr.; Dettre, R.H. *Adv. Chem. Ser.* **1964**, *43*, 112.

(65) Dettre, R.H.; Johnson, R.E., Jr. *Adv. Chem. Ser.* **1964**, *43*, 136.

CHAPTER 2

A GENERAL METHOD FOR MODIFYING SUBSTRATE SURFACES TO FORM LAYER-BY-LAYER ASSEMBLIES

Introduction

Recently[1-3] the L-by-L deposition technique has been extended to organic polymer substrates by preparing supported polyelectrolyte multilayers on surface-modified (and in one case, unmodified) polymer film samples. Poly(4-methyl-1-pentene) (PMP) was oxidized[1] to prepare a carboxylic acid - functionalized PMP surface (PMP-CO_2^-) that is negatively charged at sufficiently high pH and that adsorbs cationic polyelectrolytes. Poly(ethylene terephthalate)[2] (PET) was hydrolyzed (PET-CO_2^-) and amidated (PET-NH_3^+) to form surfaces that, respectively, cationic and anionic polyelectrolytes adsorb to and initiate L-by-L deposition. Poly(chlorotrifluoroethylene) (PCTFE) was modified to introduce alcohol functionality[4] and poly(allylamine hydrochloride) (PAH) was adsorbed to PCTFE-OH to promote L-by-L assembly.[3] Virgin PET (a neutral surface) also supports L-by-L deposition initiated with PAH and it is suspected that hydrogen bonding is the primary interaction driving adsorption of the first layer with PET and PCTFE-OH substrates.

In these studies PAH and PSS were used as polyelectrolytes and direct comparisons can be made between the multilayer assemblies on the different substrates. No limit to the number of layers that can be deposited on any substrate was found, but the

multilayer assemblies differ significantly on different substrates. Individual layer thicknesses vary from less than an angstrom to ~10 Å and the stoichiometry of the assembly process (ammonium ion : sulfonate ion ratio) varies from ~1:1 to ~1.6:1. The assembly process is remarkably forgiving, adapting to different substrates and exerting layer thickness and stoichiometry control. XPS indicates that the layers are stratified on all substrates, but the extremely small average thicknesses measured indicate that the individual layers are not close-packed and must be interdigitated at functional group dimensions. Stratification and interdigitation are observed in assemblies with thicker layers on silicon substrates.[5] Contact angle data indicate that wettability is controlled by the outermost layer when the layers are sufficiently thick, but by at least 2 layers when the layers are thinner. The mechanical integrity of the multilayer films on PET, PET-CO_2^- and PET-NH_3^+ was assessed using a peel test with pressure-sensitive adhesive tape. The results indicate that PAH/PSS multilayer assemblies have significant mechanical strength: failures occur in the adhesive for PET-CO_2^- - and PET-NH_3^+ - supported films and in the PET substrate for virgin PET-supported films.

These previous studies indicate that L-by-L deposition can be used to modify polymer surfaces, however they also point out that the method is not generally applicable. Different surface modifications are required to initiate L-by-L deposition on different polymer substrates. In this chapter, a general method for priming polymer surfaces for L-by-L deposition is proposed: we report that allylamine can be plasma-polymerized onto poly(tetrafluoroethylene) (PTFE) and that this polymer layer initiates layer-by-layer

deposition of PSS and PAH. PTFE was chosen as a substrate because it is difficult to surface-modify and is resistant to plasma modification,[6] thus it is a severe test of this method. Allylamine has been plasma polymerized on other polymer substrates[7] and the resulting plasma polymers have been shown to contain amine functionality. L-by-L deposition has been reported on an oxygen plasma - treated plasma-polymerized methane film supported on glass.[8]

Poly(tetrafluoroethylene)

The polymerization process of poly(tetrafluoroethylene) (PTFE) was developed by Plunkett in 1938.[9] The polymerization is a free-radical reaction in an aqueous dispersion at temperatures between 55 and 240 °C under 7 MPa of pressure. The resulting polymer has molecular weights ranging between 500,000 to 5,000,000, a density of about 2.2 g/cm^3, and is highly crystalline (90-95%). PTFE is a thermoplastic with a melting point at 327 °C and a glass transition temperature of 126 °C, however it is not a liquid until above 500 °C. It is chemically resistant, solvent resistant (soluble only in a few fluorinated solvents), and resistant to plasma modification.[6]

Processing and bonding of PTFE is rather difficult due its inherent properties. To form samples of desired shape, granular PTFE is first pressed into the desired shape under pressures ranging from 13 to 70 MPa and then sintered (fused) at 360-380 °C. Once the desired form is obtained, joining PTFE to another material requires a treatment to the surface. The most common treatment uses naphthalenide in tetrahydrofuran (THF) which

forms a black carbonaceous layer that is bondable. Other methods include: treatment in a solution of sodium in liquid ammonia (-33 °C), electrochemical reduction, and alkali-metal amalgams.

Plasma Chemistry

Plasma describes the state of ionized gas that consists of positively charged molecules or atoms and electrons. It can be generated by several methods but the most common is the glow discharge whereby the plasma is formed by the transfer of power from an electric field to electrons. A molecule or atom is ionized upon colliding with electrons of sufficient energy. All species generated are very reactive with surfaces exposed to the plasma and with other species. Three types of reaction occur at the exposed surfaces: ablation, surface reaction, and plasma polymerization. Using one or more of these reactions, polymer surfaces can be modified to possess functional groups.

Glow Discharge and Setup

Glow discharge can be generated using either direct-current (DC) or alternating current (AC). For a DC glow discharge, the cathode is bombarded by positive ions and generates secondary electrons which accelerate away from the cathode. At a certain distance away, the electrons will have gained enough energy to ionize molecules by inelastic collision. For AC at low frequencies (below 500 kHz), the glow discharge is formed in a similar manner to that of the DC discharge with the exception that the

polarity is alternating. At frequencies above 500 kHz, electrons oscillate with its velocity 90° out of phase with the electric field. Electrons, interacting with the electric field, gain energy by random collisions with gas atoms until enough energy is acquired to make inelastic collisions.

The reactor geometry for DC and low frequency AC glow discharge requires that the electrodes be inside the reactor whereas the electrodes can be placed outside the chamber for radio frequency (rf) plasma. Some common reactors are shown in figure 2.1.[10] In all cases, the chamber is connected to a vacuum pump and has monomer inlets. The type of reactor used and the placement of the monomer inlets affect the deposition rate of plasma polymers. This will be discussed briefly in a later section.

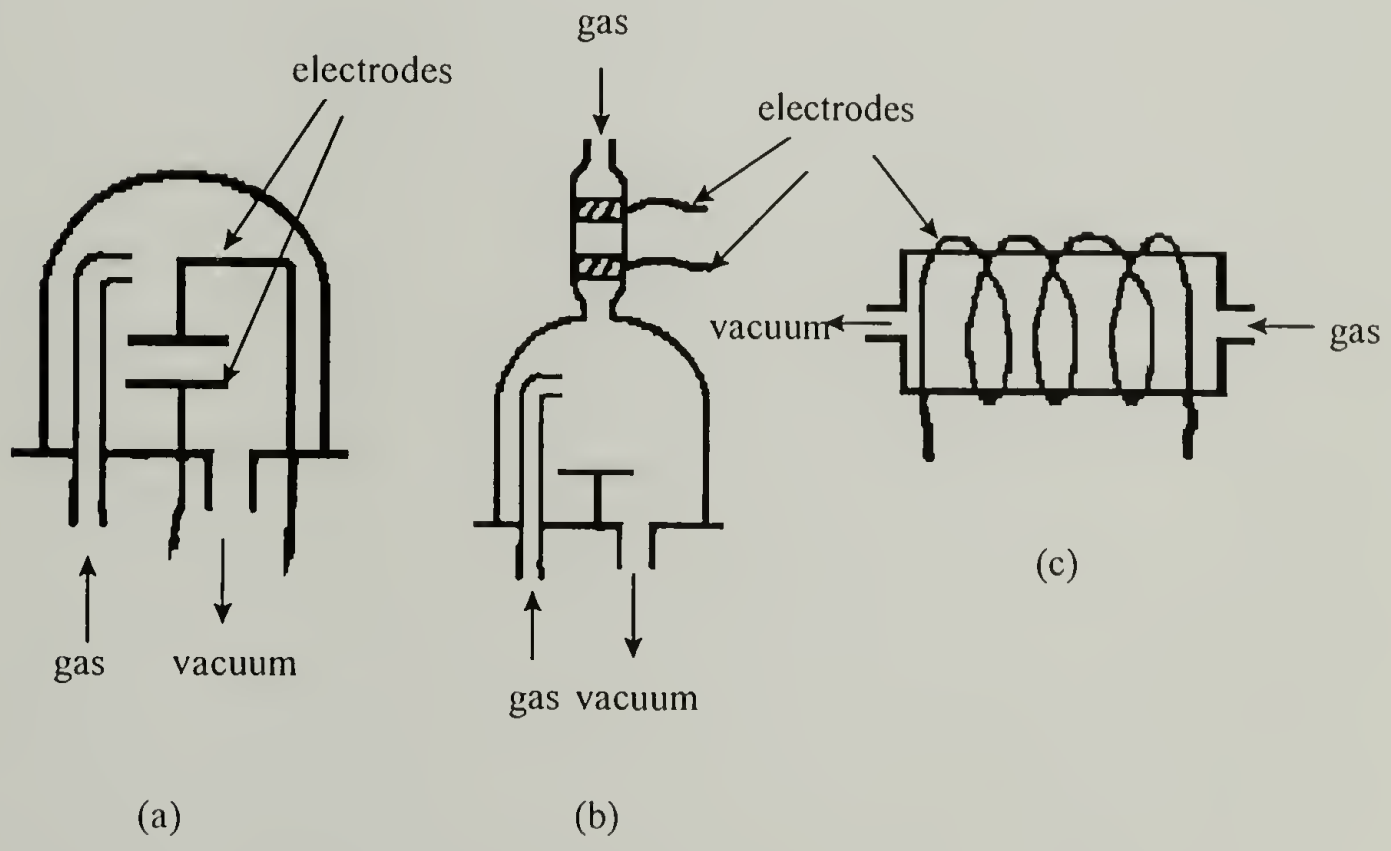

Figure 2.1. Three common plasma reactors: (a) and (b) are two typical DC or low frequency glow discharge reactors and (c) is an inductively coupled rf reactor.

Plasma Gas

Several types of gases can be used in a plasma reactor. These gases form two classes: nonpolymerizing gases (noble gases, oxygen-containing gases, nitrogen-containing gases, and fluorinated gases) and polymerizing gases (hydrocarbons, hydrocarbons with polar groups, halocarbons, organosilicon compounds, and organometallic compounds). As the names imply the gases used in the plasma reaction either react with the surface or polymerize onto the surface changing the surface properties.

Nonpolymerizing gas plasmas react with the surface to produce functional groups, form crosslinks, or etch the surface. Inert gases such as argon are commonly used for cleaning surfaces to improve adhesion. Adhesion is improved by removing low-molecular-weight materials or converting them to high-molecular-weight by crosslinking reactions.[11] Oxygen and oxygen-containing plasmas are used to incorporate oxygen functional groups to polymer surfaces. In these reactions, two competing processes occur simultaneously: etching of the polymer surface to give volatile reaction products and formation of oxygen-containing functional groups. Reaction of PTFE with an oxygen plasma demonstrates this competitive process.[12] In the initial stages of the reaction, surface modification is dominant but is overwhelmed by the etching process at later stages. Utilization of nitrogen-containing plasmas improves wettability and biocompatibility of polymer surfaces. Collagen was covalently attached to plasma-modified PTFE grafts with alkylamine surfaces using a glutaraldehyde crosslinker.[13]

Fluorine-containing plasmas, depending on the gas type, operating parameters, polymer substrate, and electrode, can react with the surface or polymerize onto the surface.[14] Etching of silicon is accomplished using hexafluoroacetone.[15] Surface wettability decreases when polyurethanes are treated with C_xF_y but increases when treated with O_2 and O_2/CF_4.[16]

Plasma-deposited films can also be formed on substrates using appropriate gases (monomers). Plasma polymer films are deposited as a result of two simultaneous reactions: plasma-induced polymerization and plasma-state polymerization. In a plasma-induced polymerization, free-radicals induce polymerization by reacting with unsaturated carbon-carbon bonds. In a plasma-state polymerization, any organic compound can be used as it is the decomposition products caused by energetic electrons (or other reactive species) breaking bonds that recombine to form a "polymer." Hydrocarbons used in plasma polymerizations are divided into three subclasses, each with a different deposition rate: (1) triple bond containing structures (including benzene), (2) double bond containing and cyclic structures, and (3) saturated monomers.[17] These plasma polymers have good microhardness and good barrier properties. Plasma polymers of ethane have been used as a protective coating for alkali halide crystals for IR detectors.[18] Monomers of hydrocarbons with polar groups such as allyl amine have been plasma polymerized to incorporate amino groups on polymeric films.[7,19,20] Halocarbons are used to produce hydrophobic coatings. Expanded PTFE grafts treated with a hexafluoroethane/hydrogen plasma exhibit 87% reduced platelet deposition.[21] Organosilicon monomers include

silanes, siloxanes, and silazanes. Plasma polymers from these monomers have excellent thermal and chemical resistance and outstanding electrical, optical, and biomedical properties.

Basic Plasma Parameters

The four basic plasma parameters that affect the plasma process are the electron density, n_e; the electron energy distribution, $f(E)$; the gas density, N; and the residence time for a gas molecule in a plasma, τ.[22] The first two parameters are difficult to measure but their relationship to the plasma process are understood. The electron density is proportional to the current through the plasma and the electron energy distribution has a Maxwellian energy distribution. Generally, the average electron energy in a plasma is insufficient to break chemical bonds and it is the electrons in the tail of the energy distribution, having sufficient energy, that contribute to the ionization and fragmentation in the plasma. The gas density can be determined from the pressure in the reactor p_0, and the residence time is related to p_0, volume of the plasma V, and flow rate F by the following equation: $\tau = p_0 V / F$. Using these four concepts, the effect of the process variables on the deposition rate can be explained.

Parameters for Controlling Deposition Rate

The plasma polymerization deposition rate can be controlled by varying the frequency of the potential, the excitation power, the monomer flow rate, the plasma

pressure, and to a certain extent the reactor geometry. A combined parameter, W/F, governing the deposition process has been formed by relating the deposition rate to the excitation power, W, and the monomer flow rate, F.

The deposition rate as a function of frequency, from 50 Hz to 13.56 MHz, has been studied. It was found that for frequencies below 500 Hz (including DC plasmas) the deposition rate is higher due to a higher density of ions and activated species.[23] However, there is a greater variation in deposition rate as a function of the sample placement. For the plasma polymerization of ethylene, the deposition rate was more homogenous across the substrate for a rf plasma (13.56 MHz) and became more heterogeneous as the frequency was decreased, from rf to audio frequencies (AF) to AC (figure 2.2).[24]

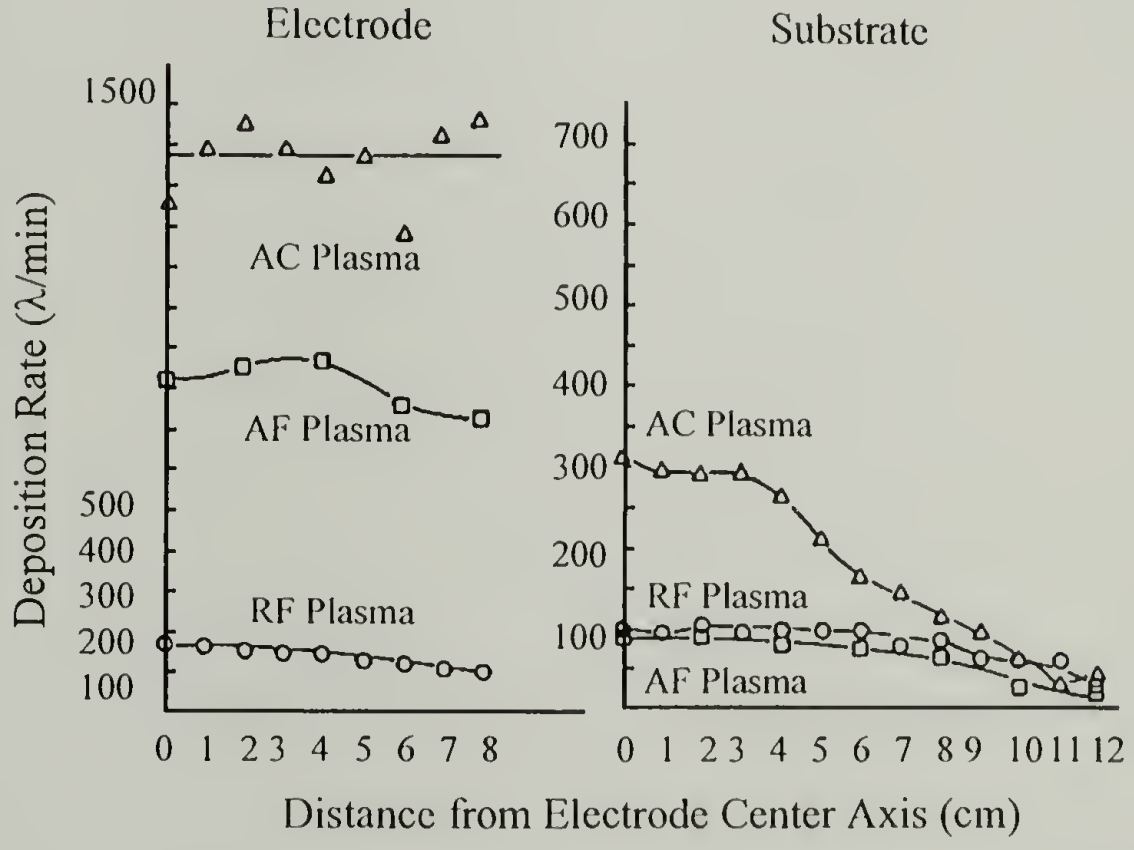

Figure 2.2. Plasma deposition rate of ethylene plasma polymer as a function of distance from the center of the electrode, location in the interelectrode gap, and frequency at 135 cm^3/min flow rate. (RF=13.56 MHz, AF=10 kHz, AC=60 Hz).

The excitation power limits the deposition rate by controlling the electron density. At high powers, the electron density is high as observed in a rf glow discharge by the expansion of the glow region outside the vicinity of the electrodes. Under these conditions, the deposition rate increases with the flow rate. As the excitation power is decreased, a critical point at a flow rate is reached where the deposition rate decreases with increasing flow rate (figure 2.3). A reactive specie in the glow region requires a certain amount of time for it to react. When the excitation power is decreased, the electron density in the glow decreases as does the number of reactive species. The amount of time the reactive specie is available to react is governed by the residence time which is related to the monomer flow rate. At low flow rates, there is enough time for the

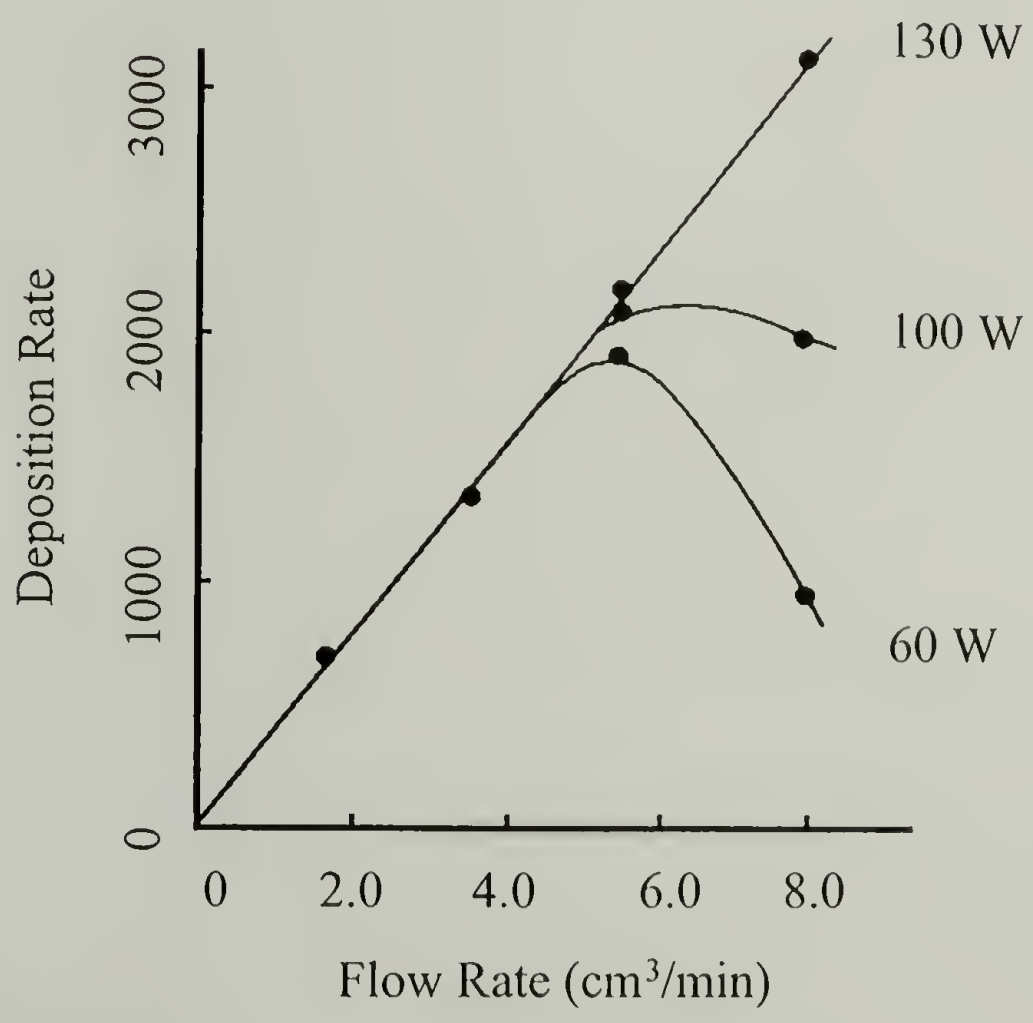

Figure 2.3. Deposition rate of acrylonitrile as a function of flow rate for three input powers.[25]

plasma reaction to occur. But as the flow rate is increased, the residence time decreases and less time is available for species to react. So for low excitation power and high flow rate, the few active species that are available to react, cannot due to time constraints. With such a direct correlation, it is apparent that these two variables can be used together to formulate a new composite parameter. One such parameter is *W/FM* where *W* is the power, *F* is the flow rate, and *M* is the molecular weight of the monomer. When plotted as a function of deposition rate (figure 2.4), two regimes are observed. At high values of (*W/FM*) above the critical point (region III), the deposition rate is independent of the composite parameter. In this region, it is called the monomer-deficient region because sufficient discharge power is available but not enough monomer is present. For values below the critical (*W/FM*) in region II, the deposition rate increases with (*W/FM*). This is the power-deficient transient region where the power input is insufficient to activate all

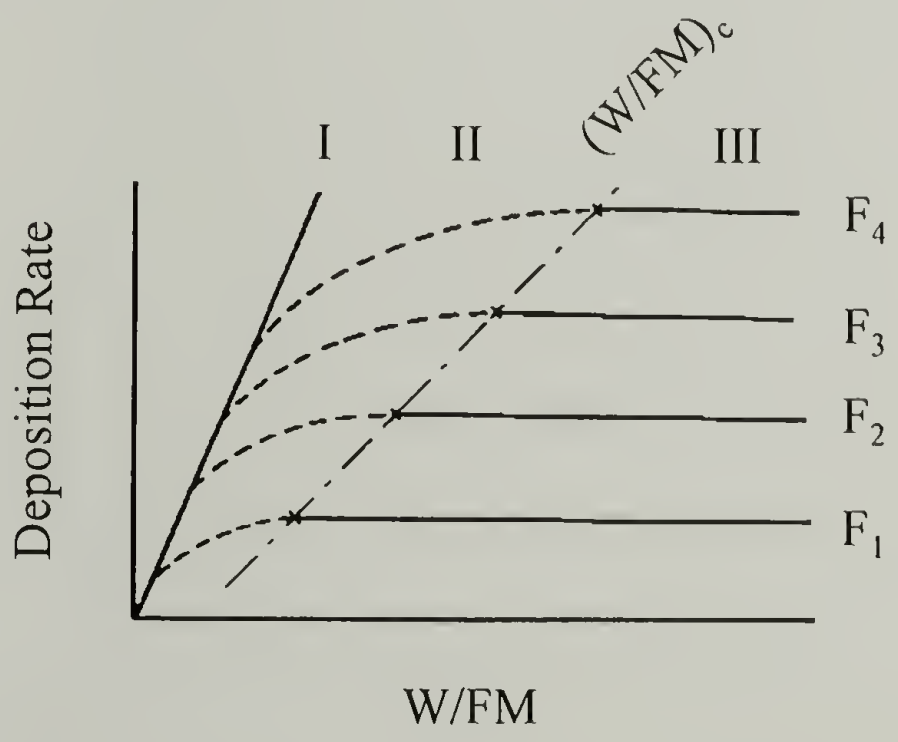

Figure 2.4. The plasma polymerization domains is observed by the variation in deposition rate with respect to (*W/FM*).[17]

the monomer. The deposition rate increase becomes linear in extreme cases as shown in region I. The critical (*W/FM*) value increases with flow rate for hydrocarbons of type (2) and (3) and is independent of flow rate for type (1) hydrocarbons, triple bond or benzene containing structures.[17]

The plasma pressure affects the deposition rate by the change in the residence time, the average electron energy, the gas density, the electron density, and the mean free path of a molecule. As the pressure is increased, the residence time of molecules and the gas density increases. In addition, the mean free path of molecules λ decreases as it is related to the number density of a gas, η, by:

$$\lambda = \frac{1}{4\pi r^2 \eta} \qquad (2.1)$$

where r is the radius of the molecule. These three variables would lead us to conclude that increasing pressure would increase deposition rate. However, the effect of pressure on the average electron energy and electron density plays a greater role in determining the deposition rate. The concentration of electrons decreases as more molecules are introduced and with the higher number of gas molecules, the average electron energy decreases as well as the deposition rate. Since the electron density is affected by pressure change, it implies that there might be some effect with change in flow rate. This has been observed and is shown in figure 2.5.[26] The figure shows that the plasma polymerization can be classified into two regions similar to excitation power and a similar argument concerning their existence can be made. Initially with increasing flow rate, the deposition rate is independent of the pressure and increases with flow rate (monomer-deficient

region). At a critical pressure and flow rate, the residence time is insufficient for the activated molecule to react with the surface and the polymer deposition rate decreases with increasing flow rate (energy-deficient region).

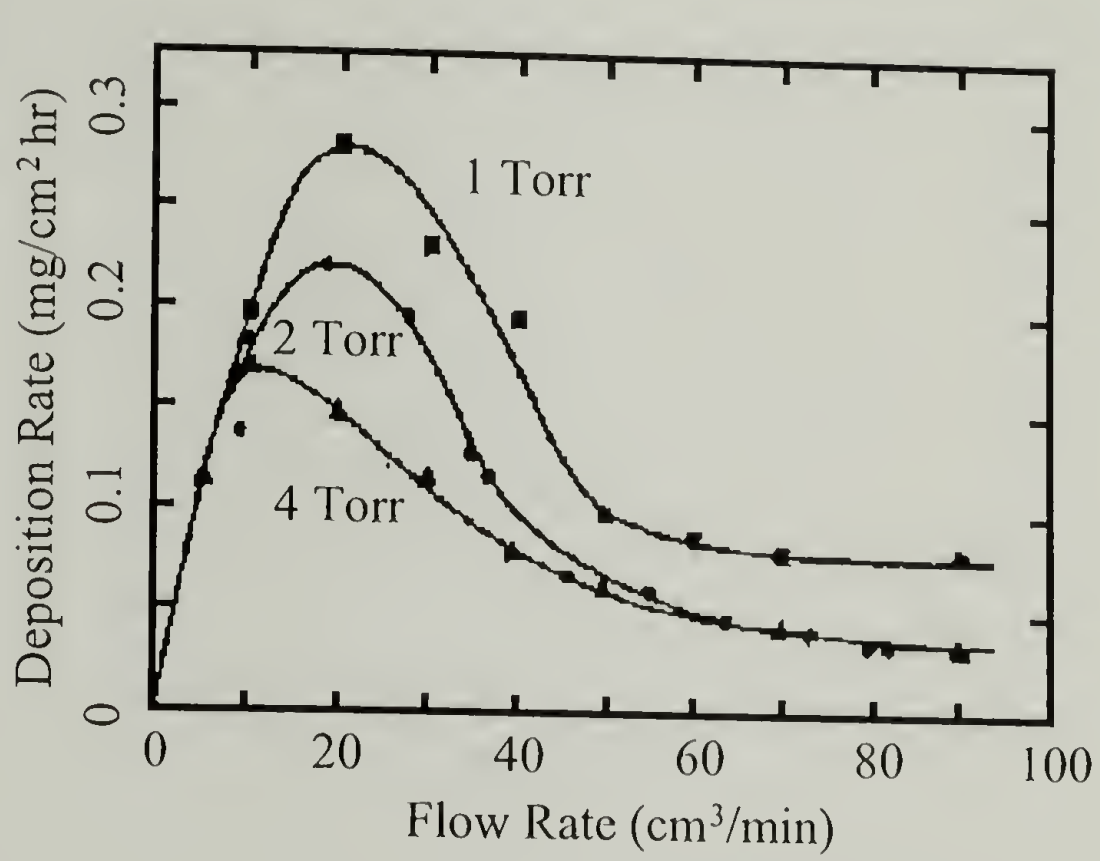

Figure 2.5. Effects of pressure and flow rate on the deposition rate of ethane plasma polymer at 100 W.

Controlling the Plasma Polymer Structure

The structure of the deposited polymer can be adjusted by changing the plasma processing parameters, the excitation power, the flow rate, and the pressure. Adjusting these processing parameters results in changing either the energetic state of the gas plasma or the residence time which affect the retention of monomer structure in the plasma polymer and/or the crosslink density.

The degradation of the monomer structure can be minimized by limiting the input power, working at high pressures, and limiting the residence time of molecules in the plasma. The first two factors control the energy of the electrons in the plasma. By working at low input powers or at high pressures, the amount of energy present is enough to break the weakest bonds thus preserving the monomer structure (dissociation energy for carbon-carbon π bond is 2.72 eV versus 3.61 eV for carbon-carbon sigma bond). Using high flow rates limits the amount of time the monomer is exposed to the plasma region and results in good structure retention. However, the monomer must adsorb at a high rate so that the modified monomer does not escape in the by-product gas stream. This is achieved by using either a cryogenically cooled substrate or monomers having low vapor pressures at room temperature.

The crosslink density is controlled by the number of active sites present in the plasma polymer. Films with a low crosslink density, desirable for reverse osmosis membranes, have been deposited by using either a comonomer or minimizing the contact of monomer with the plasma. A comonomer gas, such as nitrogen, acts as a scavenger of hydrocarbon radicals in the plasma polymerization process and reduces the number of radicals that can participate in the formation of crosslinks.[27] Instead of using radical scavengers to limit the number of active sites, another method to reduce the number of sites is by limiting the contact of monomer with the glow discharge. An inert gas can be used to transfer the energy from the glow region to the monomer to produce plasma polymers with less active sites for crosslinking.[19] Highly crosslinked films for permselective separation of gases are made by using conditions between the monomer-

deficient region and the power-deficient region. Higher input power, which increases crosslink density, is not desirable because the intrinsic stress will increase with the result of introducing gross defects.[28]

Characterization

Three approaches are taken to characterize plasma polymer films: surface analysis, microstructural analysis, and morphological analysis. Wettability of the plasma polymer surface is analyzed using contact angle measurements.[6,12,13,29] XPS provides information on the surface elemental composition[6,7,12,13,29,30] and attenuated total reflectance FTIR identifies the type of functional groups present in the near-surface.[6,7] The microstructures of plasma polymers are studied using pyrolysis/gas chromatography, pyrolysis/mass spectrometry, solid state ^{13}C nuclear magnetic resonance spectroscopy,[30] secondary-ion mass spectrometry,[29] FTIR,[13,19,20,30] and elemental analysis.[20,29] Electron spin resonance is an important technique to find the density of free radicals, to determine the nature and environment of the free radical, and to identify the chemical nature of the free radical.[27,31] The surfaces of plasma polymer films have been examined by SEM[6,12,13,20] and AFM.[29] Ellipsometry is used to measure the thickness of plasma polymer films.[7]

Experimental

Materials

PTFE was obtained from Norton Performance Plastics as 4 mil skived film (DuPont teflon®). Poly(allylamine hydrochloride) (PAH) (Aldrich, M_n = 50,000-65,000), and poly(sodium styrene sulfonate) (PSS) (Aldrich, M_n = 70,000) were used as received. Allylamine (99+%, Aldrich) was degassed using freeze-pump-thaw cycles. Water was purified using a Millipore Milli-Q® system that involves reverse osmosis followed by ion-exchange and filtration steps.

General Procedures

Plasma modification reactions were carried out in a home-built inductively coupled pyrex reactor in which flow rate, power (13.56 MHz - supplied by an Astron RS-35A power supply and a Yaesu FT-840 HF transceiver), and pressure can be controlled. X-ray photoelectron spectra (XPS) were recorded on a Perkin-Elmer - Physical Electronics 5100 spectrometer with Al K_α excitation (15 kV, 400 W) at a take-off angle of 75° (between the plane of the sample surface and the entrance lens of the detector optics). Atomic concentration data were determined using sensitivity factors obtained from samples of known composition: C_{1s}, 0.200; O_{1s}, 0.501; N_{1s}, 0.352; S_{2p}, 0.540; F_{1s}, 1.00. Attenuated total reflectance infrared (ATR IR) spectra were recorded using a Bio-Rad FTS 175C FTIR at 1 cm^{-1} resolution with a 10 x 5 x 1 mm 45° KRS-5 internal

reflection element. Contact angle measurements were made with a Ramé-Hart telescopic goniometer and a Gilmont syringe with a 24-gauge flat-tipped needle. Dynamic advancing (θ_A) and receding angles (θ_R) were recorded while the probe fluid (water, purified as described above) was added to and withdrawn from the drop, respectively. Interferometric microscopy was performed with a Zygo Maxim 3D® Model 5800. Peel tests were performed manually with an angle of 180° between the delaminated film surface and the tape (3M no. 810).

Plasma Chemistry

PTFE film samples were inserted into the reactor which was then evacuated to ~0.05 mm. Air was introduced using a needle valve and the pressure was equilibrated to 0.2 mm by adjusting the needle valve. After equilibrium pressure was reached, radiofrequency at 50 W was applied for 30 minutes. The air inlet was then closed and the reactor was evacuated to ~0.05 mm. The inlet to a vessel containing allylamine was then opened and the monomer pressure was adjusted to 0.3 mm. The flow rate was measured to be ~1.7 sccm. The allylamine plasma was operated at the desired power for the desired period of time. Most of the experiments were conducted at 10 W for 30 min or at 50 W for 5 min. After the radiofrequency was turned off, allylamine was allowed to flow through the system for two minutes before evacuating the chamber to ~0.05 mm for 15 minutes and isolating the PTFE film samples.

Polyelectrolyte Deposition

0.02 M PAH and 0.02 M PSS (concentrations based on repeat units) deposition solutions were prepared and adjusted to pH 2.2 and 2.9, respectively, by adding small amounts of dilute HCl and NaOH solutions and using a Fisher 825MP pH meter. Alternating monolayers of PAH and PSS were deposited onto the plasma-treated PTFE substrate by alternating submersions of the film samples in the polyelectrolyte solutions to build multilayer structures of up to 30 layers. Between the 20-minute-depositions, the films were rinsed with three aliquots of water.

Results and Discussions

Plasma Chemistry

Our home-built plasma reactor was modeled after the one described by Morosoff[10] and consists of an 85 mm diameter pyrex tube attached to a ballasted vacuum manifold with ports to introduce compressed gases and volatile liquids through needle valves. The stationary electrode is 10 turns of $^{3}/_{16}$" soft copper tubing around a 15 cm section of the tube and is powered by a radio transmitter that has been set to broadcast at 13.56 MHz. Samples are supported by a glass plate that rests in the center of the tube within the volume defined by the electrode.

Film samples of PTFE were cut to dimensions appropriate for our analytical techniques (generally 1 x 5 cm) and were exposed to an air plasma (50 W) for 30 min. X-ray photoelecton spectroscopy (XPS) of samples treated in this manner indicate the incorporation of small amounts of oxygen (~2 atom %) and no nitrogen. Gardella[6] has reviewed and discussed the chemical inertness of fluoropolymers toward air and other plasmas; our objective in using the air plasma was not to incorporate functionality, but to clean the samples and remove any weak boundary layer that would adversely affect adhesion. The water contact angles of PTFE change from θ_A/θ_R = 120°/92° to θ_A/θ_R = 131°/49° and we attribute the increase in the hysteresis to the incorporation of small amounts of hydrophilic oxygen-containing functionality that pin the drop during advancing or receding analysis and to the change in the surface roughness of the PTFE as the surface is etched by the oxygen plasma. From equation (1.5), the surface roughness of the etched PTFE is 1.3 using θ_A. The change in contact angle versus oxygen plasma treated time on PTFE has been reported previously.[12] Normally the samples were not isolated from the plasma reactor after this treatment, but the system was evacuated and allylamine vapor was introduced. After equilibration of pressure/flow rate, the radiofrequency power was applied at the desired power for the desired period of time. After the RF power was turned off, allylamine vapor was allowed to flow through the system for two minutes before evacuating the chamber and isolating the samples. The majority of samples were prepared using two optimized conditions that were determined to be reasonably reproducible: one set of samples was prepared at low power (10 W) for 30 min and the other at high power (50 W) for 5 min. The power (and also the flow rate and pressure) affects the plasma chemistry. Low power plasmas retain the structure of the

monomer more than do high power plasmas[22] and the products tend to be less highly crosslinked. Figure 2.6 shows ATR IR spectra of the two plasma-modified samples which we abbreviate ^{10}PTFE-NH_3^+ and ^{50}PTFE-NH_3^+, where the superscript indicates the radiofrequency power used in the synthesis. They are named as the ammonium ion because the amines present in the sample are protonated during the L-by-L depositions described below. Both spectra indicate the presence of primary amine groups (3400-3600 cm^{-1}) and clearly they are present in higher concentration on ^{10}PTFE-NH_3^+ than on ^{50}PTFE-NH_3^+. Also indicated are secondary amines and/or imines (3300-3400 cm^{-1}), nitriles (2240 cm^{-1}) and isonitriles (2180 cm^{-1}). Other functionality including C-C unsaturation as well as signals from the PTFE substrate are observed in portions of the spectra not shown. XPS spectra showed significant nitrogen concentration (discussed quantitatively below) and the disappearance of fluorine, indicating a continuous coating.

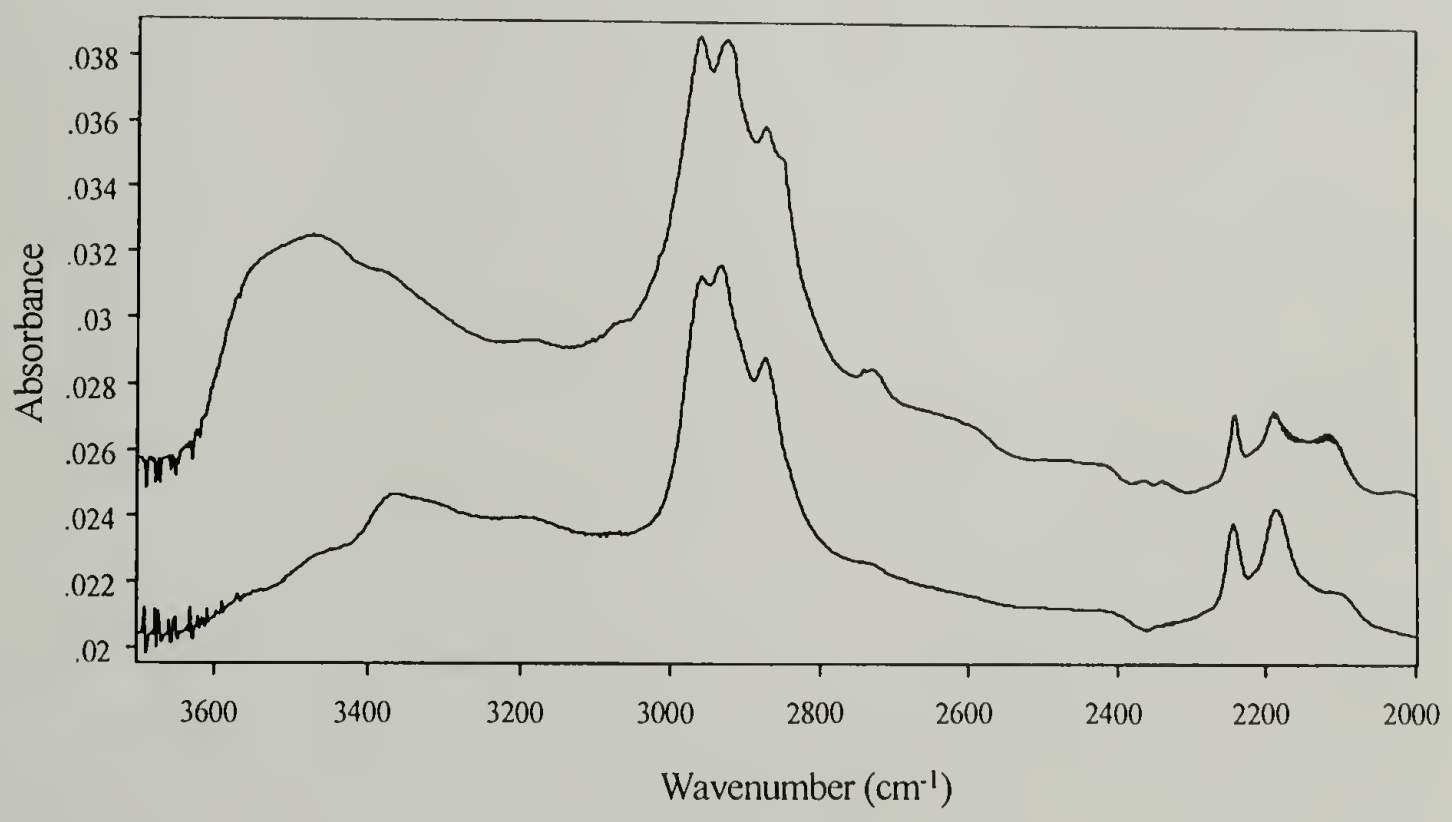

Figure 2.6. ATR IR spectra of allylamine plasma-modified PTFE samples: ^{50}PTFE-NH_3^+, lower spectrum; ^{10}PTFE-NH_3^+, upper spectrum.

of plasma polymer. Interferometric microscopy was used to measure the thickness of the plasma polymers. Allylamine was plasma polymerized onto microscope slides with half the slide masked using the conditions for preparation of ^{10}PTFE-NH_3^+ and ^{50}PTFE-NH_3^+. The step height was measured indicating thicknesses of ~720 Å and ~120 Å for the 10 W, 30 min and 50 W, 5 min polymerizations, respectively. Water contact angles are significantly lower than PTFE and air plasma - treated PTFE: θ_A/θ_R = 64°/6° and 52°/8° for ^{10}PTFE-NH_3^+ and ^{50}PTFE-NH_3^+, respectively. The mechanical integrity of the plasma-polymerized films and the adhesion of the plasma polymers to PTFE was assessed using a 180° peel test with a pressure-sensitive adhesive tape. For samples prepared using both plasma conditions, XPS analysis of the delaminated tape showed the absence of nitrogen. Analysis of the plasma-modified PTFE films after delamination showed increased carbon and oxygen content and decreased nitrogen content. These results indicate that failure occurs within the tape and that the plasma polymers have a higher cohesive strength than the adhesive and also that the adhesion between the plasma polymers and PTFE is quite good.

Polyelectrolyte Deposition

Both ^{10}PTFE-NH_3^+ and ^{50}PTFE-NH_3^+ were used as substrates for layer-by-layer deposition of PSS and PAH. Film samples were alternately placed in unstirred aqueous solutions of the two polyelectrolytes at room temperature, rinsing with pure water between deposition steps. The polyelectrolyte concentrations used were chosen, based on data for other substrates, to be well within the platcau region of concentration isotherms.

The kinetics of the first layer (PSS) adsorptions were determined by XPS over 2 h and sulfur concentration values indicate that the adsorption is complete within 20 minutes as shown in figure 2.7. The 1st PSS layer in all multilayer assemblies was deposited using a 30 min adsorption time and subsequent layers were deposited using 20 minute adsorption times. Adsorption solutions used for 1st-layer depositions were discarded and replaced by fresh solutions to ensure that the adsorption solutions were not contaminated by impurities that may desorb from the plasma polymer. A build-up of PSS and PAH layers by L-by-L deposition occurred on both ^{10}PTFE-NH_3^+ and ^{50}PTFE-NH_3^+ substrates. Untreated PTFE films and air-plasma treated films were also dipped into PSS solutions as controls. XPS indicates that PSS does not adsorb from aqueous solution to PTFE or air plasma-treated PTFE (no sulfur was detected).

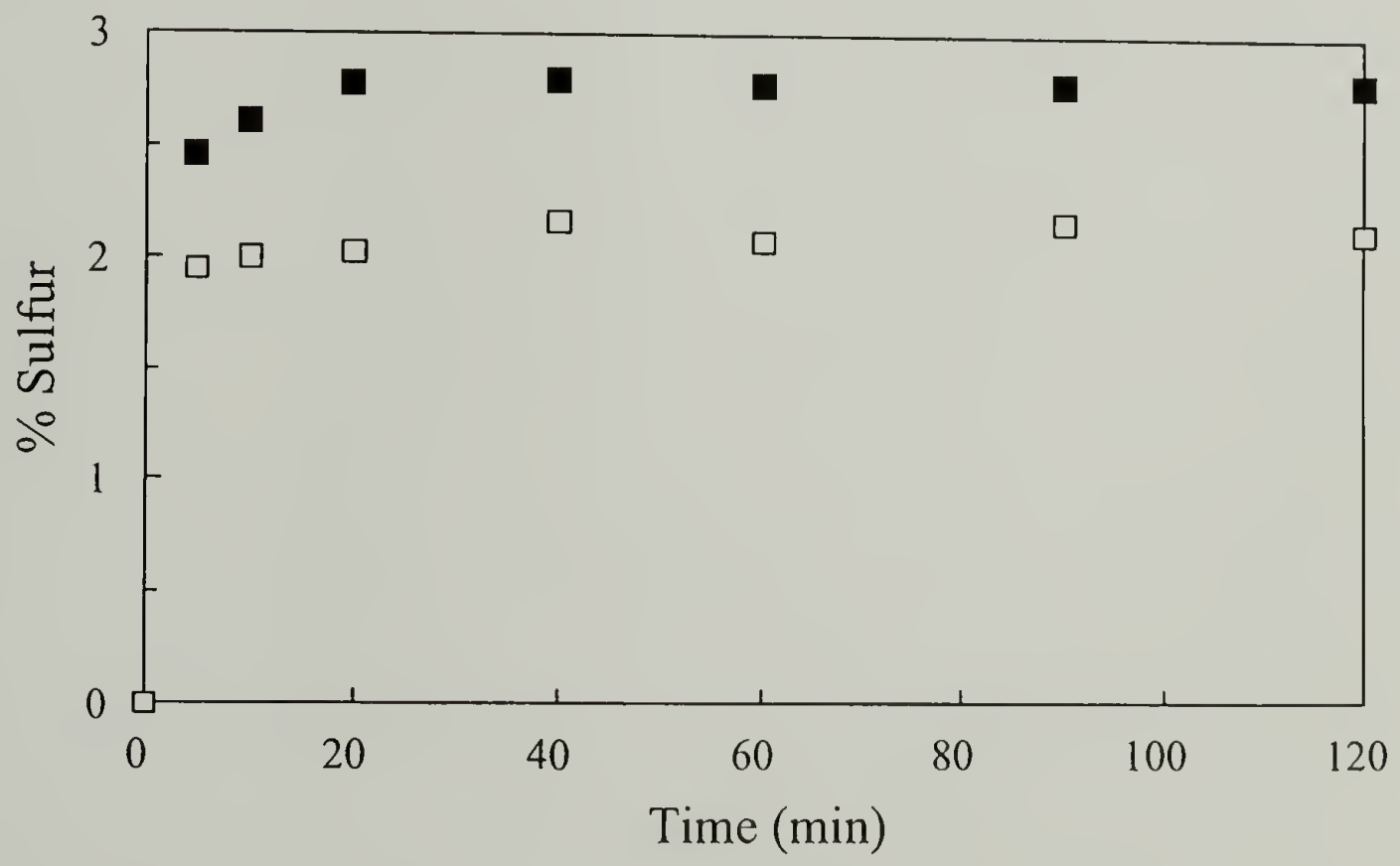

Figure 2.7. The atomic sulfur concentration present at 15° (□) and 75° (■) take-off angles as a function of the adsorption time.

^{10}PTFE-NH_3^+. XPS analysis of ^{10}PTFE-NH_3^+ indicates that the plasma polymer contains ~17 atom % nitrogen. Upon L-by-L deposition of PSS and PAH this value decreases and levels at ~6.5% after 6-10 layers (3-5 PSS/PAH bilayers) have been deposited. The polyelectrolyte layers build up on top of the plasma polymer and attenuate the strong nitrogen signal from ^{10}PTFE-NH_3^+. Figure 2.8 shows a representative XPS survey spectrum of a ^{10}PTFE-NH_3^+-supported multilayer assembly (11 layers) and figure 2.9 shows the nitrogen content, determined by XPS at 75° take-off angle, versus the number of layers deposited. A take-off angle of 75° was used because we have measured a photoelectron mean free path in a series of $(PSS/PAH)_n$ samples at this angle and can use these data and this value to estimate individual layer thickness.[1-3] Chen has discussed the angular dependence of electron mean free paths in these multilayer assemblies.[2] The sampling depth of XPS under these conditions is the thickness of the 6-10 polyelectrolyte

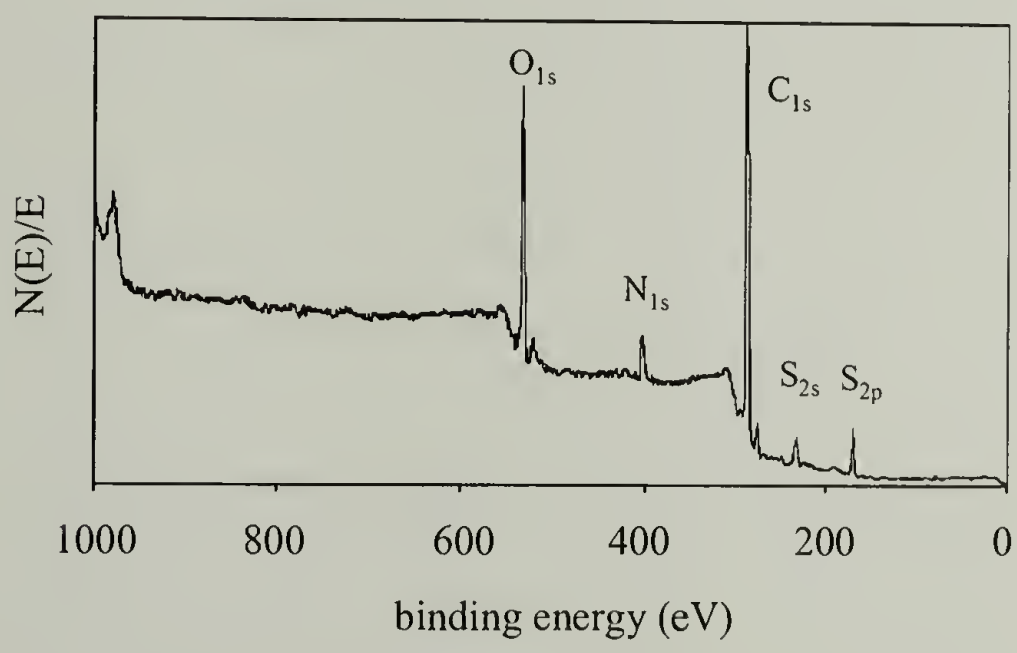

Figure 2.8. Survey XPS spectrum of an 11-layer polyelectrolyte film (^{10}PTFE-NH_3^+-$(PSS,PAH)_5$-PSS).

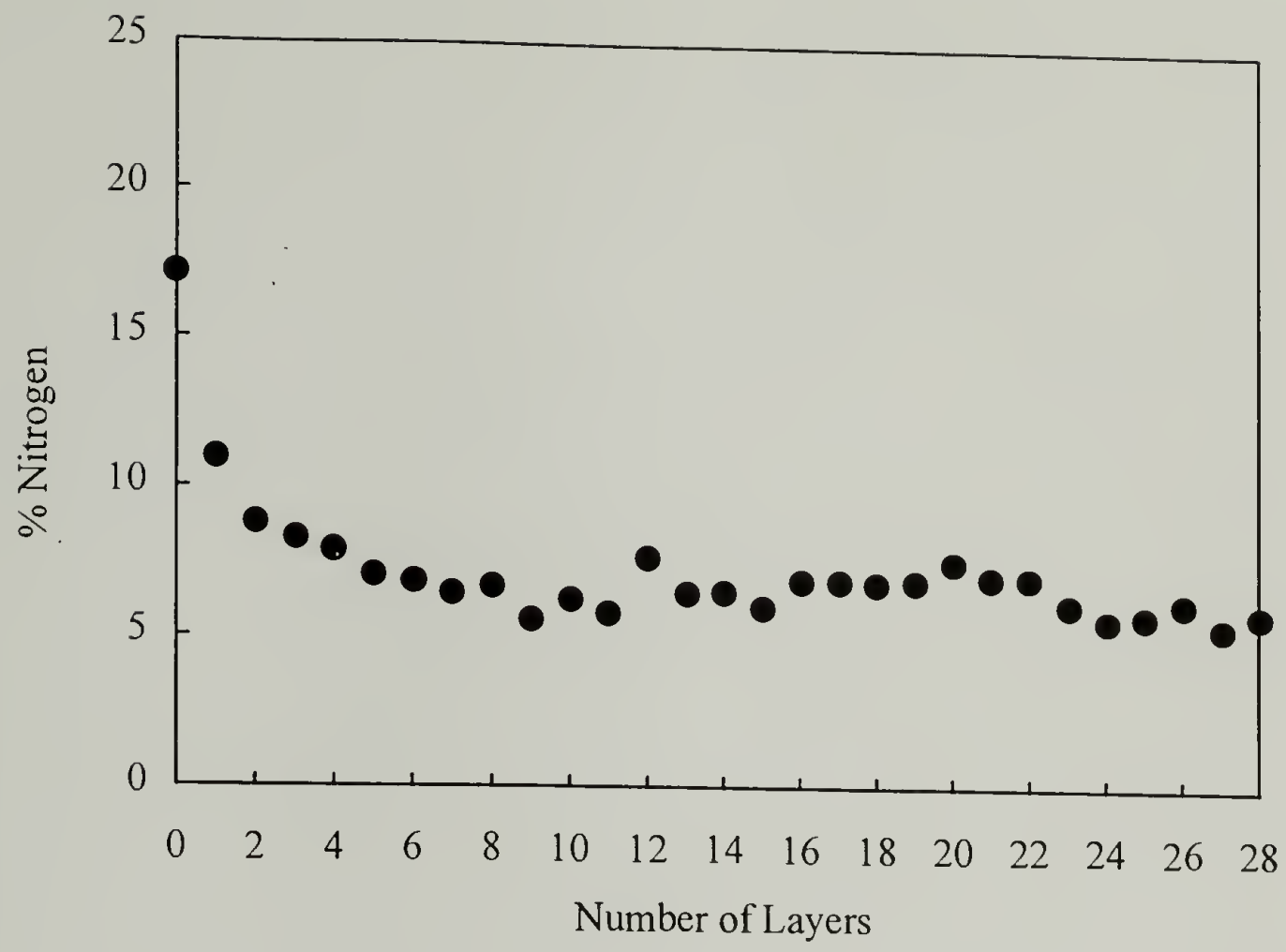

Figure 2.9. Nitrogen atomic concentrations determined by XPS as a function of the number of layers in the PSS/PAH multilayer film.

layers; the scatter in the data precludes a more precise determination than 6-10, but other data (below) indicates that ~10 layers is a better estimate. Some degree of scatter in the data is expected due to the fact that separate samples (each prepared by multistep procedures) are used for analysis of each multilayer assembly; samples were not reused as substrates for additional layer adsorption after analysis. We emphasize, however, that the scatter is not great and is significantly less than that in individual samples of the ^{10}PTFE-NH_3^+ substrate: all of the nitrogen concentration values between 6 and 28 layers vary between 5.52% (27 layers) and 7.75% (12 layers). The sulfur content increases with the first 10-12 layer depositions and levels at 3.3 ± 0.4% (the average and scatter of the data

for all multilayer assemblies with 10-28 layers). The S_{2p} photoelectron has only a slightly longer mean free path that the N_{1s} photoelectron (20.5 Å vs. 19.8 Å - see below) so sulfur and nitrogen compositions are expected to level with the same number of layers. From the sulfur and nitrogen data we estimate that the sampling depth of XPS under these conditions is the thickness of ~10 polyelectrolyte layers.

The average thickness of the individual layers is calculated using the nitrogen XPS data (figure 2.9) plotted according to equation 2.2.[2] This equation relates the

$$-\ln(N/N_o)\sin\theta = nz/\lambda \qquad (2.2)$$

attenuation of a substrate photoelectron signal to the thickness of a multilayer assembly where N is the number of substrate photoelectrons that reach the detector through the assembly, N_O is the number of substrate photoelectrons detected without a L-by-L deposited overlayer, θ is the take-off angle, n is the number of layers, z is the average thickness of the individual layers and λ is the photoelectron mean free path. The attenuation of the F_{1s} signal in PCTFE-OH and the carbonyl C_{1s} signal in PET derivatives was observed as layers were deposited and determine average layer thicknesses.[2,3] The $^{10}PTFE\text{-}NH_3^+$ substrate, however, does not contain an element that is not present in the polyelectrolytes (the F_{1s} signal from PTFE is completely attenuated by the plasma polymer layer), so the analysis is less straight-forward. In this system we have to measure the attenuation of the nitrogen signal from the substrate as polyelectrolytes, one of which contains nitrogen (of lower concentration), are deposited. Figure 2.10 shows a plot of $-\ln(N/N_O)\sin\theta$ versus n where N and N_O are the observed nitrogen concentrations minus the final (leveled) nitrogen concentration. The slope of the line (z/λ - equation 2.2) is

the average layer thickness divided by the N_{1s} photoelectron mean free path; this analysis indicates that the average layer thickness is ~0.3λ. This is the average thickness of layers 2-7; the first PSS layer was thicker than the others and was not included in the analysis because it would have biased the average high. Leväsalmi has measured a mean free path of 20Å for the Mg K_α-excited Si_{2p} electron in a $(PAH/PSS)_n$ assembly supported on a silicon wafer using XPS (75° take-off angle) and X-ray reflectivity data[1] and we can use this value to calculate[32] a mean free path of 19.8 Å for the Al K_α-excited N_{1s} photoelectron. Assuming that the electron mean free path in $^{10}PTFE\text{-}NH_3^+$-supported $(PAH/PSS)_n$ is the same as that determined for Si-supported $(PAH/PSS)_n$, the average layer thickness is 6.1 Å.

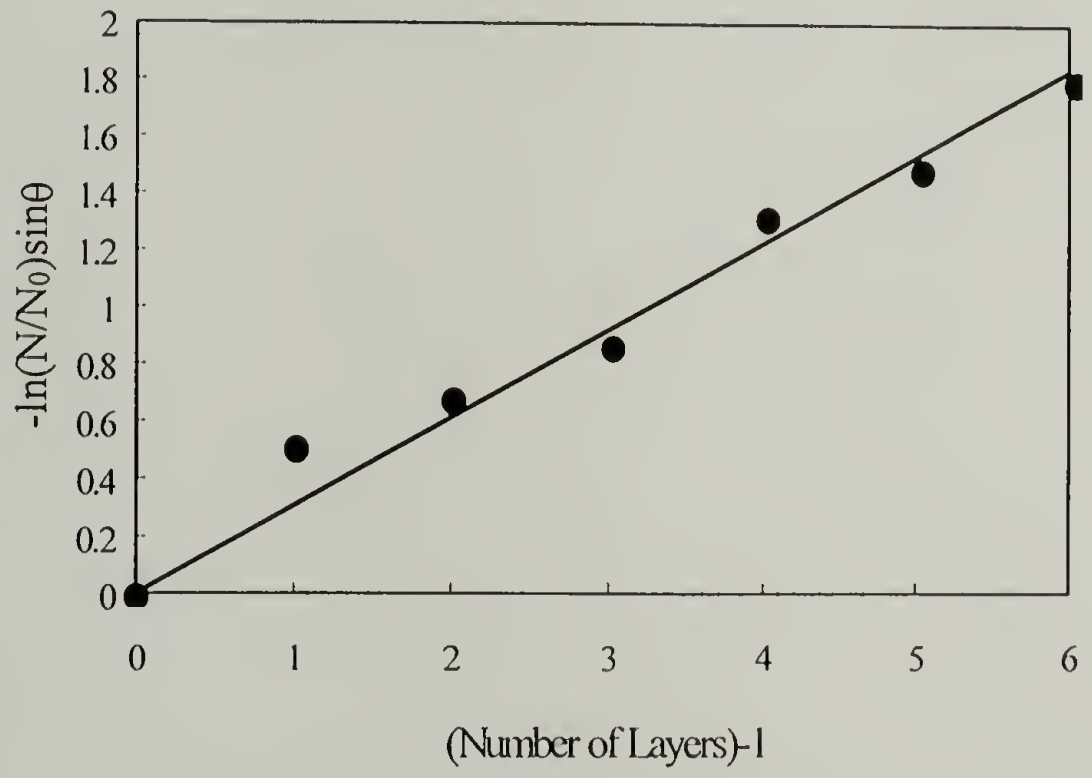

Figure 2.10. Plot of $-\ln(N/N_o)\sin\theta$ vs. number of layers in the PSS/PAH multilayer film.

In other polymer-supported $(PAH/PSS)_n$ films,[1-3] pronounced odd-even effects are observed in the surface composition and in the wettability. Nitrogen:sulfur ratios oscillate between relatively high values when PAH is the outermost layer and relatively low values when PSS is top-most. The oscillations indicate that the layers are stratified and the amplitude of the oscillation is proportional to the thickness of the layers and their degree of stratification (versus interpenetration). Figure 2.11 shows the nitrogen:sulfur ratio (calculated from 75° take-off angle XPS atomic composition data) as a function of the number of layers deposited on $^{10}PTFE\text{-}NH_3^+$. The ratio decreases with increasing number of layers and levels after ~10 layers have been deposited and the nitrogen signal

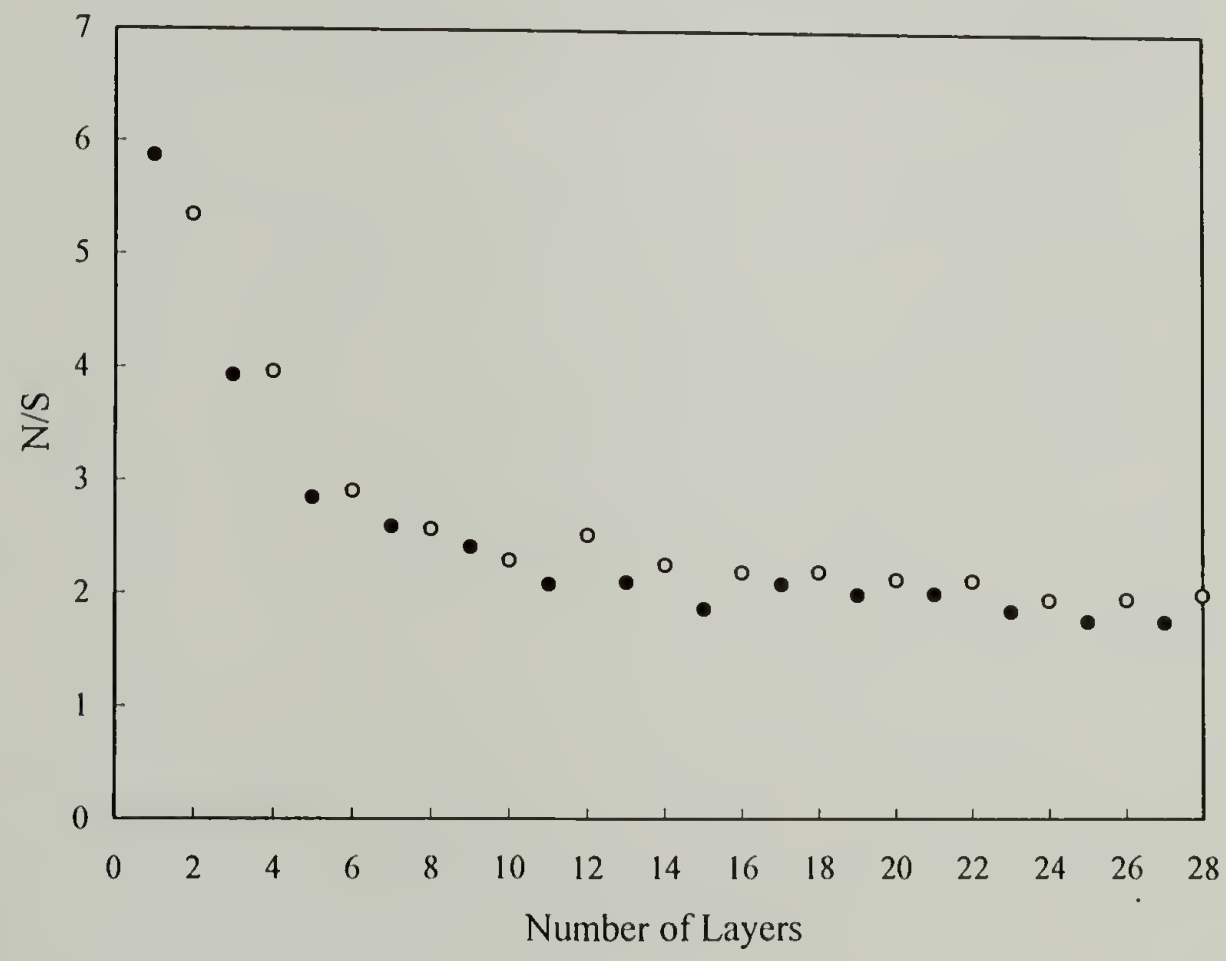

Figure 2.11. Nitrogen:sulfur atomic ratio data (XPS) versus the number of layers in the PSS/PAH multilayer film on $^{10}PTFE\text{-}NH_3^+$: closed (●) and open (○) symbols indicate an odd and even number of layers, respectively.

from $^{10}PTFE\text{-}NH_3^+$ is attenuated. For the samples with 10 or more layers, an odd-even effect consistent with the composition of the outermost layer is observed. There is not an obvious odd-even trend in the data for samples with fewer than 10 layers (we note that the decreases in N:S ratio between 2 and 3 layers and between 4 and 5 layers are consistent with the adsorption of a PSS layer) and this could be due to variability in the nitrogen content of the $^{10}PTFE\text{-}NH_3^+$ substrate and/or to less well-defined layers being formed in the initial depositions. Water contact angle data (figure 2.12) show a pronounced odd-even trend that is consistent across the series of samples (the 11-layer sample is anomalous) with samples containing PSS as the top layer exhibiting greater wettability than those with PAH as the outermost layer. The strong amplitude at low layer numbers suggests that the initial layers are stratified and well defined and that scatter in the N:S ratio data is due primarily to composition differences in $^{10}PTFE\text{-}NH_3^+$ samples.

The N:S ratio data converge on a value of ~2 indicating that the stoichiometry of the assembly process is 2 ammonium ions per sulfonate ion. This suggests that chlorine (as chloride) should have been observed in XPS spectra, but it rarely was and only in very small quantities; we rationalize its absence by assuming that HCl is lost from the excess ammonium ions to form the free base of PAH under the conditions of analysis (high vacuum). The stoichiometry also suggests that the multilayer assemblies have a net positive charge when in contact with acidic aqueous media and that this charge should

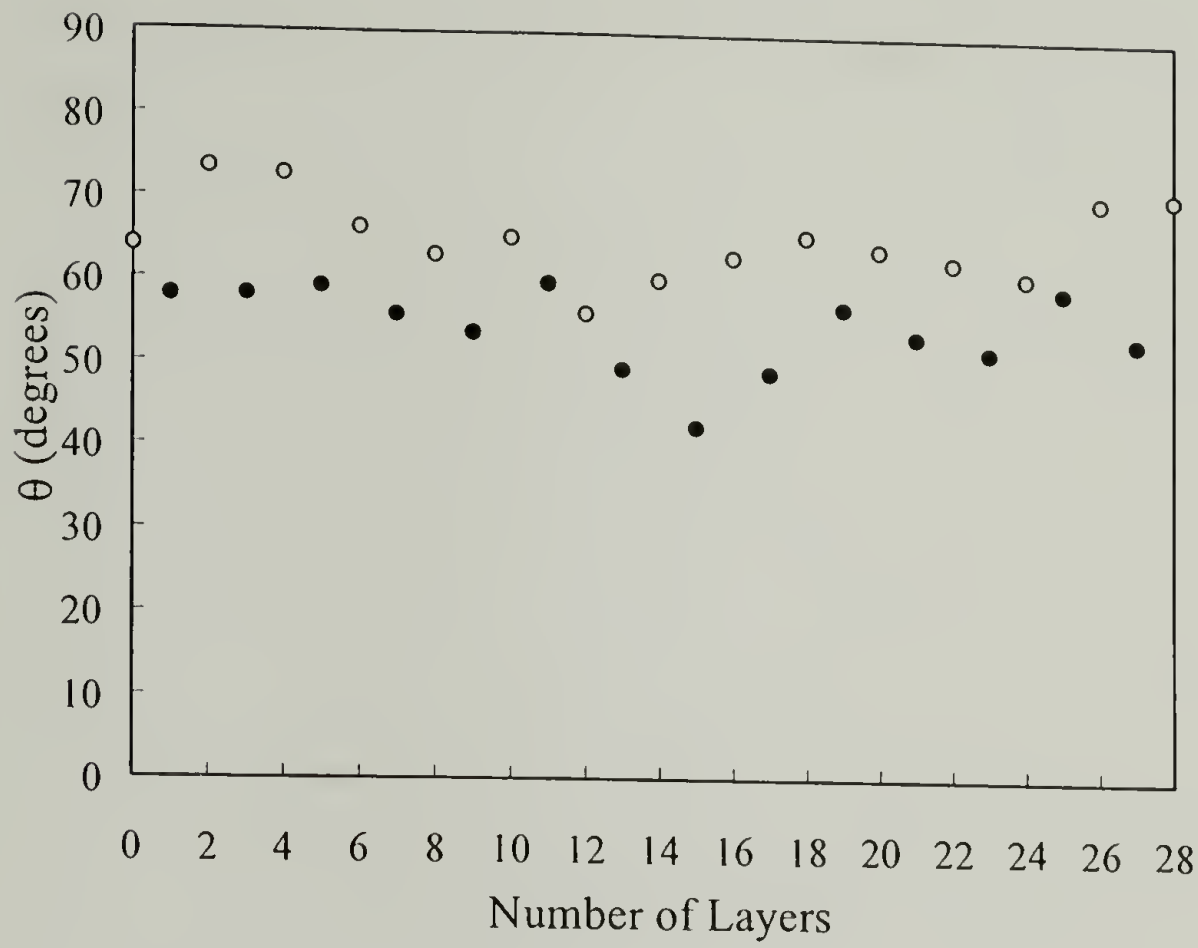

Figure 2.12. Advancing water contact angle data versus the number of layers in the PSS/PAH multilayer film on ^{10}PTFE-NH_3^+: closed (●) and open (○) symbols indicate an odd and even number of layers, respectively.

increase with increasing number of layers deposited. This may be the case, but apparently chloride ions effectively screen this positive charge so that assemblies with PSS as the outermost layer have available sulfonate groups, function as negatively charged surfaces and adsorb cationic polyelectrolytes. We must qualify these analyses by emphasizing that the XPS data were obtained on dry samples at high vacuum and the extent to which these data reflect the structure of the surfaces in contact with acidic polyelectrolyte solutions must be questioned.

^{50}PTFE-NH_3^+. Polyelectrolyte multilayer assemblies were also prepared using ^{50}PTFE-NH_3^+ samples as substrates and the results were qualitatively similar to those obtained using ^{10}PTFE-NH_3^+. XPS analysis of ^{50}PTFE-NH_3^+ indicates that the plasma polymer contains ~24 atom % nitrogen. Upon L-by-L deposition of PSS and PAH this value decreases and levels at ~7.0% after 7-10 layers (3-5 PSS/PAH bilayers) have been deposited. Similar to ^{10}PTFE-NH_3^+ substrates, the nitrogen concentration values between 7 and 20 layers vary between 6.37% (15 layers) and 7.80% (7 layers) and show insignificant scatter. The sulfur content increases with the first 10-12 layer depositions and levels at 3.3 ± 0.4% (the average and scatter of the data for all multilayer assemblies with 10-20 layers). The average thickness of the individual layers is calculated using the attenuation of the nitrogen signal from the substrate and equation 2.2. By plotting - $\ln(N/N_O)\sin\theta$ versus n, the average thickness of layers 2-7 is 4.7 Å.

Figure 2.13 shows the nitrogen:sulfur ratio (calculated from 75° take-off angle XPS atomic composition data) as a function of the number of layers deposited on ^{50}PTFE-NH_3^+. The ratio decreases with increasing number of layers and levels after ~10 layers have been deposited and the nitrogen signal from ^{10}PTFE-NH_3^+ is attenuated. An odd-even effect consistent with the composition of the outermost layer is observed for samples with 10 or more layers,. There is not an obvious odd-even trend in the data for samples with fewer than 10 layers (we note that the decreases in N:S ratio between 2 and 3 layers, 4 and 5 layers, 6 and 7 layers, and 8 and 9 layers are consistent with the adsorption of a PSS layer) and this could be due to variability in the nitrogen content of the ^{50}PTFE-NH_3^+ substrate and/or to less well-defined layers being formed in the initial

depositions. Water contact angle data (Figure 2.14) show a pronounced odd-even trend that is consistent for samples with greater than 13 layers; samples containing PSS as the top layer exhibit greater wettability than those with PAH as the outermost layer.

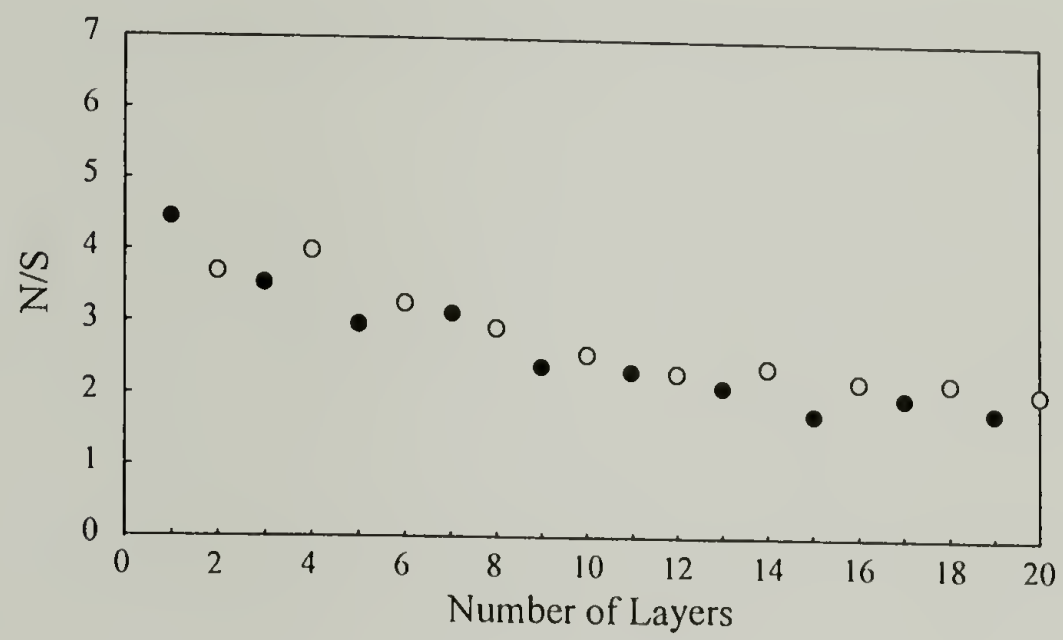

Figure 2.13. Nitrogen:sulfur atomic ratio data (XPS) versus the number of layers in the PSS/PAH multilayer film on ^{50}PTFE-NH_3^+: closed (●) and open (○) symbols indicate an odd and even number of layers, respectively.

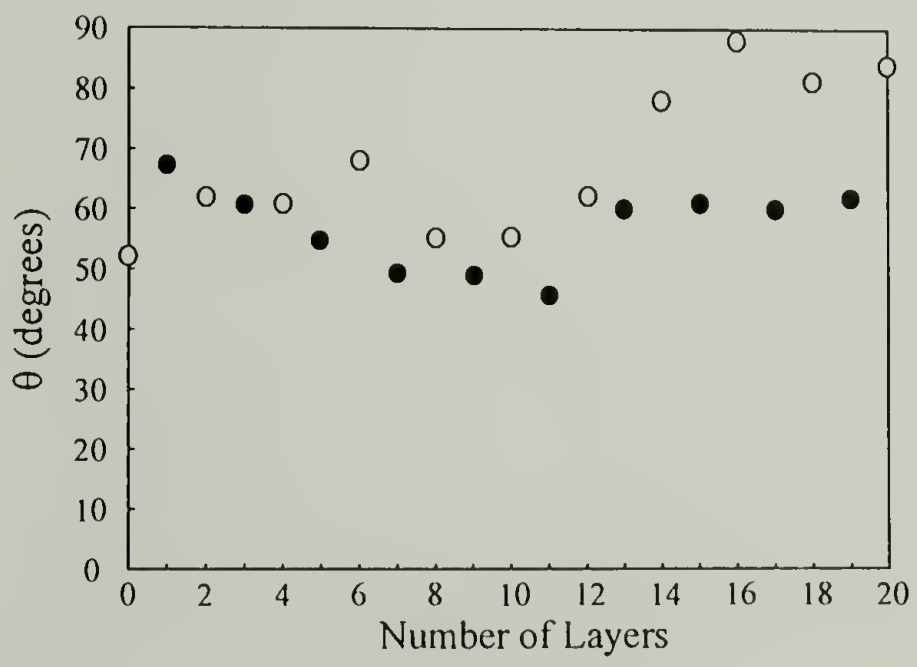

Figure 2.14. Advancing water contact angle data versus the number of layers in the PSS/PAH multilayer film on ^{50}PTFE-NH_3^+: closed (●) and open (○) symbols indicate an odd and even number of layers, respectively.

The weak amplitude at low layer numbers suggests that the initial layers are not well defined. However with successive depositions, defects are "healed" and the layers become more stratified.

The data for the first ~10 layers has significantly more scatter and we suspect that the initial layers on this substrate are not as well-defined. A lower initial surface charge (fewer $-NH_3^+$ groups) may be the cause of this. The adsorptions become more well behaved after 10 layers have been adsorbed and odd-even trends in XPS and contact angle data indicating layer stratification are apparent in samples with higher numbers of layers. The thickness of the individual layers is comparable to that of layers supported on $^{10}PTFE\text{-}NH_3^+$ and the stoichiometry of the assembly is also ~2:1 ammonium:sulfonate ions.

Conclusions

PTFE can be surface-modified using an allylamine plasma polymerization to contain amine groups; the modified surfaces support layer-by-layer deposition of polyelectrolytes. The conditions of the plasma polymerization affect the chemical structure of the resulting polymer layer. In particular, a higher surface concentration of primary amines is formed at lower radiofrequency power and this translates to higher surface charge density and more reproducible polyelectrolyte adsorptions. Multilayer assemblies of PSS and PAH form by sequential polyelectrolyte adsorption and XPS and contact angle data indicate stratified layers. XPS analysis also indicates that the stoichiometry of the assembly process is 2 ammonium ions per sulfonate group and that the average individual layer thickness is ~6.1 Å for ^{10}PTFE-NH_3^+ and ~4.7 Å for ^{50}PTFE-NH_3^+. The assembly stoichiometry is determined by the initial substrate chemistry and the adsorption behavior of the polyelectrolytes in the first few layer formation steps. The established stoichiometry is maintained throughout multiple polyelectrolyte adsorption steps and differs from that of different substrates. The successful surface modification of PTFE by this sequential protocol (plasma polymerization/layer-by-layer deposition) suggests that this is a general method for polymer surface modification.

Notes and References

(1) Leväsalmi, J.-M.; McCarthy, T.J. *Macromolecules* **1997**, *30*, 1752.

(2) Chen, W.; McCarthy, T.J. *Macromolecules* **1997**, *30*, 78.

(3) Phuvanartnuruks, V.; McCarthy, T.J. *Macromolecules* **1998**, *31*, 1906.

(4) Dias, A.J.; McCarthy, T.J. *Macromolecules* **1987**, *20*, 2068.

(5) Schmitt, J.; Grunewald, G,; Decher, G.; Pershan, P.S.; Kjaer, K.; Losche, M. *Macromolecules* **1993**, *26*, 7058.

(6) Vargo, T.G.; Gardella, Jr., J.A.; Meyer, A.E.; Baier, R.E. *J. Polym. Sci.: Part A: Polym. Chem.* **1991**, *29*, 555.

(7) Gombotz, W.R.; Hoffman, A.S. *J. Appl. Polym. Sci.: Polym. Symp.* **1988**, *42*, 285.

(8) Lvov, Y.; Haas, H. Decher, G.; Möhwald, H.; Kalachev, A. *J. Phys. Chem.* **1993**, *97*, 12835.

(9) Plunkett, R.J. U.S. Pat. 2,230,654, **1941**.

(10) Morosoff, N. *Surface Modification by Plasma Polymerization*, in *Innovations in Materials Processing*, Bruggeman, G., Weiss, V., Eds., Plenum: New York, 1985.

(11) Liston, E.M.; Martinu, L.; Wertheimer, M.R. *Plasma Surface Modification of Polymers for Improved Adhesion: A Critical Review*, in *Plasma Surface Modification of Polymers*, Strobel, M.; Lyons, C.; Mittal, K.L., Eds., Utrecht: The Netherlands, 1994.

(12) Morra, M.; Occhiello, E.; Garbassi, F. *Langmuir* **1989**, *5*, 872.

(13) Tran, C.N.B.; Walt, D.R. *J. Colloid Interface Sci.* **1989**, *132*, 373.

(14) d'Agostino, R. *J. Vac. Sci. Technol. A* **1985**, *3(6)*, 2627.

(15) Coburn, J.W.; Kay, E. *IBM J. Res. Develop.* **1979**, *23*, 33.

(16) Sterrett, T.L.; Sachdeva, R.; Jerabek, P. *J. Mater. Sci. Mater. Med.* **1992**, *3*, 402.

(17) Yasuda, H. *Plasma Polymerization*; Academic Press: New York, 1985.

(18) Yamagishi, F.G.; Granger, D.D.; Schmitz, A.E.; Miller, L.J. *Thin Solid Films* **1981**, *84*, 427.

(19) Hollahan, J.R.; Wydeven, T. *Science* **1973**, *179*, 500..

(20) Krishnamurthy, V.; Kamel, I.L.; Wei, Y. *J. Polym. Sci.: Part A: Polym. Chem.* **1989**, *27*, 1211.

(21) Yeh, Y.-S.; Iriyama, Y.; Matsuzawa, Y.; Hanson, S.R.; Yasuda, H. *J. Biomed. Mater. Res.* **1988**, *22*, 795.

(22) Morosoff, N. *An Introduction to Plasma Polymerization*, in *Plasma Deposition, Treatment, and Etching of Polymers*, d'Agostino, R., Ed., Academic Press: San Diego, 1990.

(23) Morita, S.; Bell, A.T.; Shen, M. *J. Polym. Sci.: Polym. Chem. Ed.* **1979**, *17*, 2775.

(24) Morosoff, N.; Newton, W.; Yasuda, H. *J. Vac. Sci. Technol.* **1978**, *15*, 1815.

(25) Yasuda, H.; Hirotsu, T. *J. Polym. Sci.: Polym. Chem. Ed.* **1978**, *16*, 743.

(26) Jensen, R.J.; Bell, A.T.; Soong, D.S. *Plasma Chem. Plasma Process.* **1983**, *3*, 163.

(27) Yasuda, H.; Hirotsu, T. *J. Polym. Sci.: Polym. Chem. Ed.* **1977**, *15*, 2749.

(28) Nomura, H.; Kramer, P.W.; Yasuda, H. *Thin Solid Films* **1984**, *118*, 187.

(29) Badey, J.P.; Espuche, E.; Sage, D.; Chabert, B.; Jugnet, Y.; Batier, C.; Duc, T.M. *Polymer* **1996**, *37*, 1377.

(30) Kaplan, S.; Dilks, A. *J. Appl. Polym. Sci.: Appl. Polym. Sym.* **1984**, *38*, 105.

(31) Scott, T.W.; Chu, K.-C.; Venugopalan, M. *J. Polym. Sci.: Polym. Chem. Ed.* **1979**, *17*, 267.

(32) Andrade, J. D. *Surface and Interfacial Aspects of Biomedical Polymers, Surface Chemistry and Physics;* Plenum Press: New York, 1985; Vol. 1, p 180.

CHAPTER 3

MECHANICAL INTEGRITY OF LAYER-BY-LAYER ASSEMBLIES

Introduction

In the reported research on layer-by-layer (L-by-L) assemblies, the studies have concentrated on using different polyelectrolytes, the structure of these assemblies, and on the possible applications. The applications envisioned for these assemblies include conducting thin films,[1,2] sequential enzyme reactors,[3] films for nonlinear optics,[4] light-emitting and electrochromic thin films,[5-7] lithographic development[8] and asymmetric gas separation membranes.[9] The focus of these studies are on the properties that apply to each application and there have been no reports on the mechanical properties of the polyelectrolyte multilayer assemblies. This may be due to the length scale of the system which makes measurements very difficult.

It may be possible, however, to measure some properties by depositing these structures on a substrate with low tensile modulus. Elastomers have tensile moduli in the range of 1.0 MPa and serve as an ideal support for the mechanical measurements.[10] The elastomer we chose was Lycra®, a poly(ether-urea) which is available as a small diameter fiber yarn. The tensile modulus of the multilayer assembly can be measured by modeling the composite as two components in parallel where each component in the composite undergoes the same strain. A comparison will be made using the composite cylinders model first introduced by Hashin and Rosen[11] in 1964 and later refined by Christensen[12]

in 1979. This model is more complex than the "rules of mixture" model as it accounts for the differences in the Poisson's ratio, shear modulus, and bulk modulus of the two components.

In order to make these measurements, it is important that these layer-by-layer assemblies adsorb to our substrate. Several approaches are taken to allow the adsorption process: (1) Direct adsorption of polyelectrolytes onto Lycra® as this method is the simplest. This technique has been shown to initiate L-by-L formation on other systems.[13-16] (2) Chemical surface modification to incorporate charged functionalities. These techniques, namely chromic acid oxidation and sulfonation, lead to charged surfaces for polyethylene substrates.[17-19] However, there might be some difficulties using these methods as the substrate used has ether linkages that may be cleaved. (3) Plasma chemistry. We have previously shown that allylamine, plasma polymerized on poly(tetrafluoroethylene) (PTFE), supports the assembly of the polyelectrolyte multilayers and that modification should work for any other polymeric substrate.[20] However, the plasma polymer will likely enhance the tensile modulus of the Lycra® yarn since plasma polymers are crosslinked. Another technique is plasma modification using a mixture of nitrogen and hydrogen gas to incorporate amine groups onto the surface.[21] The researchers show the success of the technique through the adsorption of heparin. Amongst all these techniques, the most successful will be used to initiate charge on the Lycra® surface and multilayer assemblies will be formed on the modified surface in order to measure their tensile modulus.

Lycra®

Lycra®, a member of the Spandex® family, is an elastomer composed of block copolymers of diisocyanates and diamines or glycols. The polymerization process consists of three steps: synthesis of macroglycol, reaction with excess diisocyanate, and chain extension. Poly(tetramethylene ether) glycol, the most common macroglycol in a polyether-based Lycra®, is synthesized by cationic polymerization of tetrahydrofuran.[22] The macroglycol is treated with excess diisocyanate to form a prepolymer with isocyanate end groups. These end-groups are reacted with a diamine or a glycol to extend the chains and form the polymer. The structure of Lycra® is shown in figure 3.1. The polymer is then dry-spun to form a fiber yarn composed of several filaments (figure 3.2).[23]

Figure 3.1. Structure of Lycra® showing the butylene oxide soft segment on the left and the hard segment on the right.

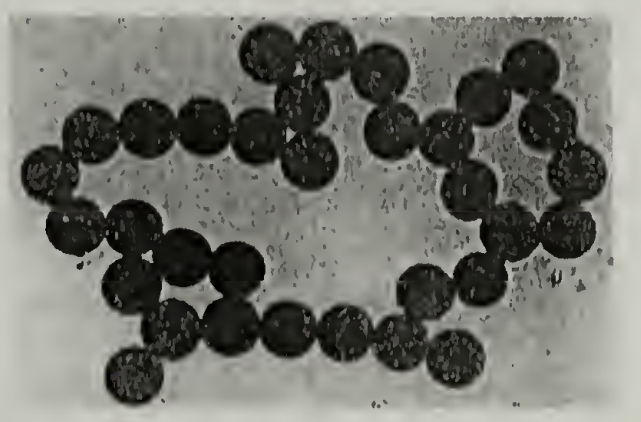

Figure 3.2. Cross section of dry-spun 423 denier Lycra® at 200X magnification.

Lycra® is an ideal substrate for the formation and testing of composites due to its properties. Like other elastomeric fibers, Lycra® has very high break elongation, high recovery from large deformation, and low modulus. The tensile modulus of polyurethanes are reported to be about 1.1 MPa.[10] The hydrolytic stability of polyether-based Lycra® is also important as the layer-by-layer assembly process involves several treatments under acidic conditions. Finally, by adjusting the processing conditions, different sized yarns can be produced so that the volume ratio of Lycra® and of the multilayer assemblies can be optimized.

Surface Modification

The surfaces of Lycra® will be modified by several methods: direct adsorption of a polyelectrolyte, chemical modification, and plasma modification. Each method is briefly described as well as it's advantages and disadvantages.

Direct Adsorption of Polyelectrolytes

Polyelectrolytes have been adsorbed onto neutral surfaces to charge the surface. Multilayer assemblies have been constructed onto glass adsorbed with PEI.[13,14] PEI has also been adsorbed onto PET, PMMA, and PS as a precursor to forming layer-by-layer assemblies.[15] Multilayer structures also form on PET that has PAH as the first adsorption solution.[16] This technique is very simple but the adhesion of the multilayers to the substrate may be weak.

Chemical Modification

Chemical modification via sulfonation or chromic acid oxidation was attempted on Lycra® to incorporate sulfonate groups or carboxylic groups, respectively. Sulfonate groups are incorporated into PP by treating it with sulfuric acid.[17] Chromic acid oxidation of LDPE leads to the formation of carboxylic acid groups onto the surface.[18,19] These techniques lead to the degradation of the sample such that the mechanical properties will decrease but the degree of degradation of Lycra® may be very severe due to the ether linkages present.

Plasma Modification

Plasma modification involves the polymerization of allylamine onto Lycra® and the functionalization of the Lycra® surface using nonpolymerizing gases. Allylamine plasma polymers have been shown to contain amine groups[24,25] that can be charged to adsorb polyelectrolytes. However, the plasma polymers may increase the mechanical properties of the Lycra® and make it more difficult to detect contributions from the multilayer assembly. Plasma modification using ammonia or nitrogen and hydrogen mixtures on PP, PVC, PTFE, PMMA, polycarbonates, and polyurethanes has been shown to promote the adsorption of heparin, which is negatively charged.[21] This modification may degrade Lycra® as some Lycra® will be ablated by the plasma gases, weakening the mechanical properties.

Mechanical Testing

The Young's Modulus E of a thin film on a substrate can be determined by using empirical composite models. These models consist of two elements which are connected either in series or in parallel as shown in figure 3.3. For a one component system, Young's Modulus is related to the stress σ and strain ε by:

$$E = \frac{\sigma}{\varepsilon}. \tag{3.1}$$

For a two component system, the volume fraction and the modulus of each component, as well as the geometry determine the overall modulus. When the elements are lined up in series (Reuss model), both elements experience the same stress. The total strain on the system is the sum of the strain on each element. The overall modulus E_T of the system is given as

$$\frac{1}{E_T} = \frac{1}{E_1}\phi_1 + \frac{1}{E_2}\phi_2 \tag{3.2}$$

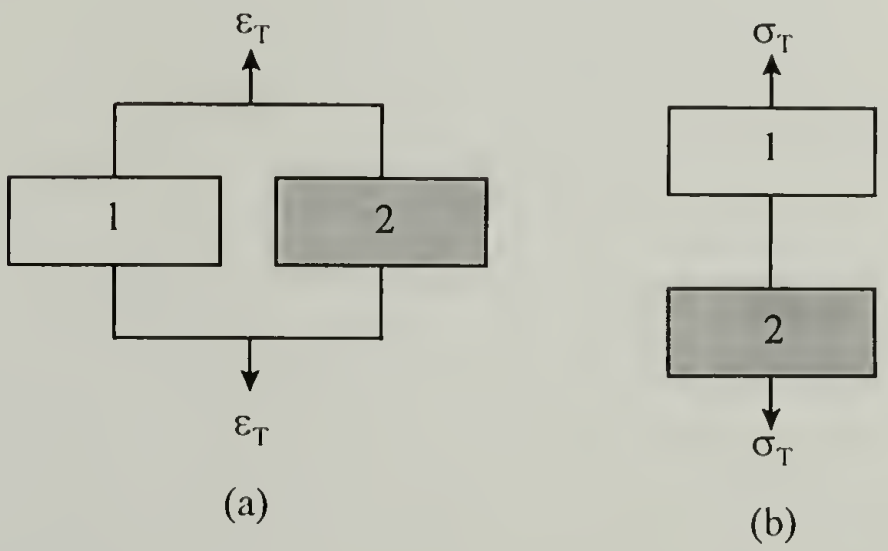

Figure 3.3. (a) The parallel model where two components experience the same strain. (b) The series model where two components experience the same stress.

where E_1 and E_2 are the modulus of each component and ϕ_1 and ϕ_2 are the volume fractions of each component. When the elements are lined up in parallel, both elements experience the same strain. The total force on the system is the sum of the force on each element. The modulus of the composite is

$$E_T = E_1\phi_1 + E_2\phi_2 . \tag{3.3}$$

The two models are compared to experimental data for polydiacetylene single crystal fibers in figure 3.4 and this shows that the parallel model agrees with the measured moduli. This is due to the structure of the composite, polymer molecules lying parallel to the fiber axis embedded in a monomer matrix, ensuring uniform strain in the deformed structure.[26]

Such a simple model may result in errors, as it does not include the effects of the differences in Poisson's ratio, shear modulus, and bulk modulus of the two materials.

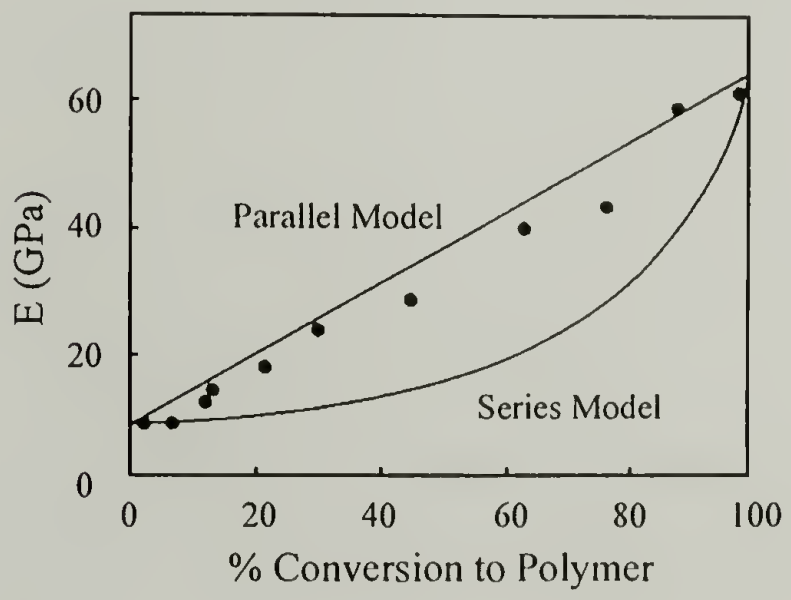

Figure 3.4. Dependence of the modulus of polydiacetylene single crystal fibers upon conversion into polymer.

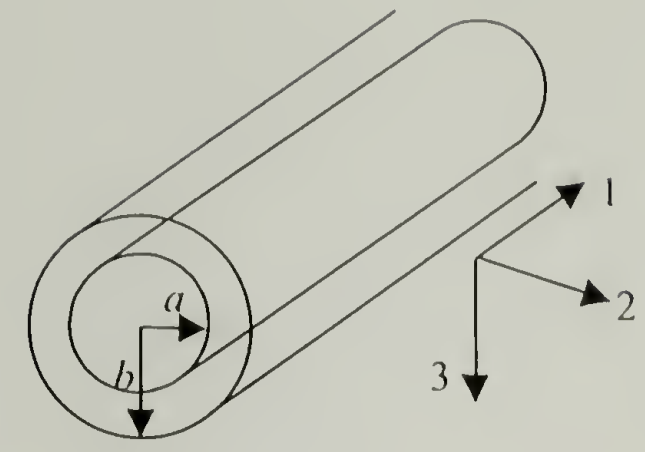

Figure 3.5. The composite cylinders model represented by one cylinder with an associated annulus of matrix material.

A more complex model which includes these terms was derived by Hashin and Rosen in 1964[11] using composite cylinders and was later refined by Christensen[12]. In this model, the fiber phase is in the form of long circular cylinders embedded in a continuous matrix phase as shown in figure 3.5. Each individual fiber of radius a is associated with an annulus of matrix material of radius b. Analysis of this model results in the following equation:

$$E_{11} = cE_f + (1-c)E_m + \frac{4c(1-c)\left(\nu_f - \nu_m\right)^2 \mu_m}{\left[(1-c)\mu_m / \left(k_f + \mu_f/3\right)\right] + \left[c\mu_m / \left(k_m + \mu_m/3\right)\right] + 1} \qquad (3.4)$$

where c is the volume fraction of the fiber, E is the tensile modulus, ν is the Poisson's ratio, μ is the shear modulus, k is the bulk modulus, and the subscripts f and m represents the fiber and the matrix, respectively. This is the exact solution as using either the theorem of minimum potential energy (giving the lower bound solution) or the theorem of minimum complementary energy (giving the upper bound solution) leads to the same equation. For a system composed of two materials having the same Poisson's ratio, it is clear that this equation simplifies to the "rules of mixtures" model. As the shear modulus

and the bulk modulus of the multilayers are unknown, these can be substituted with the results from the constitutive equations

$$\mu = \frac{E}{2(1+\nu)} \tag{3.5}$$

and

$$k = \frac{E}{3(1-2\nu)} \tag{3.6}$$

The resulting equation can be used to calculate the tensile modulus of the multilayer assembly and be used as a comparison to the rules of mixtures.

Experimental

Materials

Lycra® was obtained from DuPont as 140 denier yarns and as a 40% solution in *N,N*-dimethylacetamide (DMAC). Lycra® films were made by preparing a 6% solution in DMAC and by casting the solution onto glass slides at 80 °C. Lycra® yarns were treated with refluxing hexane for 12 hours, treated with refluxing methanol for another 12 hours, and then dried (room temperature, 0.05 mm, >24 h). Polyethylenimine (PEI) (Aldrich, $M_W \sim 25{,}000$), poly(allylamine hydrochloride) (PAH) (Aldrich, $M_n = 50{,}000\text{-}65{,}000$), and poly(sodium styrene sulfonate) (PSS) (Aldrich, $M_n = 70{,}000$) were used as received. *N,N*-dimethylacetamide (DMAC) (Fisher, certified grade), chromium (III) oxide (CrO_3)(Fisher, technical grade), sulfuric acid (Fisher, Certified ACS Plus grade),

anhydrous sodium carbonate (Fisher, Certified ACS grade), and nitric acid (Fisher, Certified ACS Plus grade) were used as received. Nitrogen/Hydrogen gas mixture (33%/67%, Merriam Graves) was used as received. Water was purified using a Millipore Milli-Q® system that involves reverse osmosis followed by ion-exchange and filtration steps.

General Methods

Plasma modification reactions were carried out in a home-built inductively coupled pyrex reactor in which flow rate, power (13.56 MHz - supplied by an Astron RS-35A power supply and a Yaesu FT-840 HF transceiver), and pressure can be controlled. X-ray photoelectron spectra (XPS) were recorded on a Perkin-Elmer - Physical Electronics 5100 spectrometer with Al K_α excitation (15 kV, 400 W) at 15° and 75° take-off angles (between the plane of the sample surface and the entrance lens of the detector optics). Atomic concentration data were determined using sensitivity factors obtained from samples of known composition: C_{1s}, 0.200; O_{1s}, 0.501; N_{1s}, 0.352; S_{2p}, 0.540. Contact angle measurements were made with a Ramé-Hart telescopic goniometer and a Gilmont syringe with a 24-gauge flat-tipped needle. Dynamic advancing (θ_A) and receding angles (θ_R) were recorded while the probe fluid (water, purified as described above) was added to and withdrawn from the drop, respectively. SEM micrographs were obtained with a JEOL-35CF scanning electron microscope at an acceleration voltage of 20 kV. Mechanical tests were conducted using an Instron 5564 mechanical tester at a crosshead speed of 22 mm/min.

Surface Modifications

Direct Adsorption of Polyelectrolytes. The direct adsorption of two different polyelectrolytes to the spandex substrate was studied to initiate L-by-L deposition. In the first attempt, film samples were allowed to sit in a 0.02 M PAH solution at pH 11 for 30 minutes Afterwards, the films were rinsed in pH 4 water for 10 minutes followed by rinsing in Milli-Q water. After rinsing, the samples were dried in a vacuum manifold overnight before analysis. The second attempt involved treatment of the film samples with a 5% PEI aqueous solution at pH 11.5 for 20 hours. After the treatment, the samples were rinsed 3 times with Milli-Q water and then dried in vacuum overnight before characterization.

Chemical Modification. Two techniques were used to modify spandex films to incorporate charge: chromic acid oxidation and sulfonation. The chromic acid oxidation solution consisted of 5 M CrO_3 in a 28 % (v/v) sulfuric acid/water solution. The solution exhibited an orange color. The solution was heated to 80 °C and the samples were floated on the solution for 2 minutes. After treatment, the films were rinsed with Milli-Q water 2 times. In the chromic acid oxidation of polyethylene films, the films are treated in nitric acid solution to remove trace chromium. This approach was attempted for the spandex films but it was found that these films immediately degrade upon exposure to the nitric acid solution. The films were subsequently treated in a 6% sodium carbonate solution for 30 minutes to remove any residual sulfuric acid and were then rinsed in Milli-Q water twice for 10 minutes. In the other method, spandex films were sulfonated

by immersing in sulfuric acid at 55 °C for 2 minutes. Afterwards, the samples were rinsed in Milli-Q water and dried in vacuum.

Plasma Modification. The first plasma modification is based on the same technique as described in the previous chapter. Spandex film samples were inserted into the reactor which was then evacuated to ~0.05 mm. Air was introduced using a needle valve and the pressure was equilibrated to 0.2 mm by adjusting the needle valve. After equilibrium pressure was reached, radiofrequency (50 W) was applied for 10 minutes. The air inlet was then closed and the reactor was evacuated to ~0.05 mm. The inlet to a vessel containing allylamine was then opened and the monomer pressure was adjusted to 0.3 mm. The flow rate was measured to be ~1.7 sccm. The allylamine plasma was operated at 50 W for 2 min. After the radiofrequency was turned off, allylamine was allowed to flow through the system for two minutes before evacuating the chamber to ~0.05 mm for 15 minutes and isolating the spandex film samples.

In a second variation, Lycra® film samples were inserted into the reactor which was then evacuated to ~0.05 mm. A nitrogen/hydrogen gas mixture was introduced using a needle valve and the pressure was equilibrated to 0.3 mm by adjusting the needle valve. After equilibrium pressure was reached, radiofrequency at 50 W was applied from 10 to 70 minutes. The flow rate was measured to be ~1.7 sccm. After the radiofrequency was turned off, the gas mixture was allowed to flow through the system for five minutes before evacuating the chamber to ~0.05 mm for 15 minutes and isolating the Lycra® film samples.

Polyelectrolyte Depositions

PAH (0.02 M) and 0.02 M PSS (concentrations based on repeat units) deposition solutions were prepared and adjusted to pH 4.0, by adding small amounts of dilute HCl and NaOH solutions and using a Fisher 825MP pH meter. For the chromic acid-oxidized samples, the pH of the first PAH adsorption solution was varied from pH 4.0 to pH 8.0. Alternating monolayers of PAH and PSS were deposited onto the surface modified Lycra® substrate by alternating submersions of the film samples in the polyelectrolyte solutions to build multilayer structures of up to 51 layers. Between the 20-minute-depositions, the films were rinsed with three aliquots of water. Spandex yarns were treated in the same manner.

Results and Discussions

Surface Modifications

Direct Adsorption of Polyelectrolytes. PAH and PEI solutions were used as first layer adsorption solutions for initiating L-by-L assembly on Lycra®. In both cases, the Lycra® films showed slight increases in the nitrogen content for both take-off angles after the polyelectrolyte adsorption. After adsorption of PAH (Lycra-PAH), the nitrogen content increases to 3.3% (vs. 1.9% for untreated samples) at 75° take-off angle. However, contact angle results show very little difference for both advancing and receding measurements. The advancing contact angle increases to 76.6° from 76.1° and

the receding angle decreases to 22.4° from 29.3°. Treatment with PEI (Lycra-PEI) showed more encouraging results as XPS and contact angle measurements both indicated surface modification. The nitrogen content at 75° take-off angle increases to 3.6% and the advancing and receding contact angle decrease to 59.9° and 11.9°, respectively.

Chemical Modification. Both of the reactions that were attempted on spandex films resulted in degradation of the films; the degradation was complete for the sulfonation reaction and no further experiments were conducted using this reaction. The chromic acid oxidation resulted in films that were slightly degraded; the film samples were slightly opaque. XPS analysis of these samples showed the presence of 1.1% sulfur at 75° take-off angle and water contact angles of 58.4° and 7° for the advancing and receding contact angles, respectively. After rinsing in sodium carbonate solution, the sulfur content decreased to 0.3% and the advancing contact angle increased to 74.9°. The degradation of the film may be advantageous as the mechanical properties of spandex are reduced.

Plasma Modification. Allylamine plasma polymerization on Lycra® generated a surface containing amine groups. The nitrogen content increased to 11.6% from 1.9% with a corresponding decrease in oxygen content from 25.6% to 15.5%. This indicates that a plasma polymerized film of allylamine forms on the Lycra® causing the attenuation of the oxygen signal from the substrate. The attenuation is not complete which may indicate that coverage may not be complete or that the plasma polymer film may be very

thin. The change in the contact angle data supports the formation of a plasma polymer film as θ_A/θ_R values decrease to 38.7°/4.7°.

Plasma treatment with a nitrogen and hydrogen gas mixture also resulted in a surface containing amine groups. The amount of nitrogen present at these surfaces is maximized between reaction times of 10 and 20 minutes. After 20 minutes, polymer etching occurs and a corresponding decrease in nitrogen content is observed. These observations are apparent from the data described in figure 3.6. Contact angle measurements of these surfaces show that the surfaces have become hydrophilic (θ_A/θ_R= 22.3°/5.5°) after 10 minutes of reaction and these values do not vary greatly for reaction times greater than 10 minutes. For adsorption of polyelectrolytes, all substrates prepared by this method were plasma-modified for 20 minutes and will be referred to as Lycra-NH_3^+.

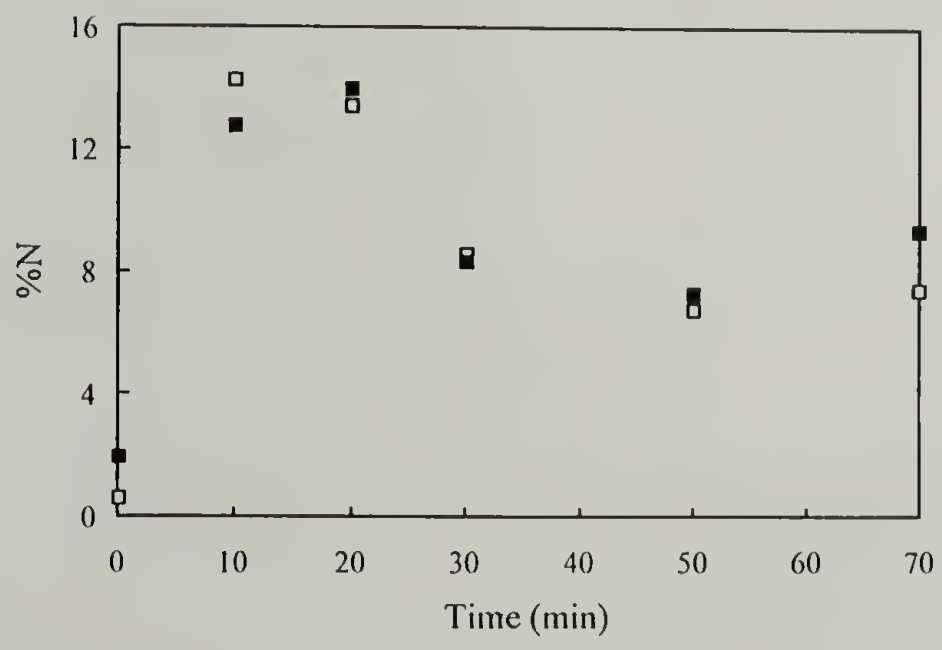

Figure 3.6. Amount of nitrogen present at the Lycra® surface after exposure to a nitrogen/hydrogen plasma at 50 W: open (□) and closed (■) symbols indicate 15° and 75° take-off angles, respectively.

Polyelectrolyte Depositions

Lycra-PAH and Lycra-PEI. For the Lycra-PAH samples, polyelectrolyte adsorption was negligible as the sulfur content of these films after 9 additional layer adsorptions was 0.4%. Nitrogen content was lower than after the initial PAH adsorption, only 1.8% nitrogen was detected. It is suspected that adsorption took place on isolated regions of the film and this technique was abandoned. Lycra-PEI samples showed greater polyelectrolyte deposition after 9 steps. The concentration of sulfur and nitrogen were 1.3% and 2.6%, respectively. The data indicates the possible formation of a L-by-L assembly as the sulfur content increases with additional deposition. However, the sulfur content after 10 layers is lower than expected when compared to multilayer depositions on other substrates. L-by-L depositions using PEI treatment form incomplete layers at the initial stages and will likely result in erroneous data for the mechanical tests thus techniques that produce complete layers are needed.

Chromic Acid Oxidation. The pH of the PAH solution was varied to maximize the amount of adsorption onto these oxidized surfaces. However, as spandex already contains nitrogen, PSS was adsorbed and the sulfur content was compared in order to compare the PAH adsorption. For the pH range tested, PAH adsorbed at pH 8 showed the highest sulfur and nitrogen content, and the greatest change in the contact angle measurements. These results are shown in table 3.1. From these results, PAH solution at pH 8 was used for all subsequent first layer adsorptions.

Table 3.1. XPS and contact angle results for PAH/PSS bilayers on oxidized spandex at different PAH solution pH.

pH	15° Take-off Angle				75° Take-off Angle				Contact Angles	
	%C	%O	%N	%S	%C	%O	%N	%S	θ_A	θ_R
No Layers	77.5	18.6	0.99	0.21	75.1	21.4	1.99	0.34	74.9	10.1
4	75.3	19.3	2.01	0.52	71.0	24.3	2.47	0.71	76.3	7.7
6	71.8	21.5	1.48	0.54	71.8	22.1	2.70	0.82	70.6	6.0
8	72.3	20.8	2.04	0.90	71.0	22.2	3.1	1.34	58.7	5.9

Multilayer films on oxidized Lycra® were formed by repetitive dipping of the treated samples into polyelectrolyte solutions. As figure 3.7 shows, the sulfur content increases as more layers are adsorbed. However after 5 layers are adsorbed, the sulfur content decreases. Further inspection of the XPS results at 75° take-off angle shows that even-number-of-layer samples have higher sulfur content (as PSS is the top layer) than the odd-number-of-layer samples which have PAH as the top layer, except for samples with 5 and 7 layers adsorbed. The 75° take-off angle is likely more lucid for these samples as the oxidized films are degraded and increases in surface roughness may skew the data obtained at shallow take-off angles. Odd-even affects indicating multilayer assembly are also apparent in most cases (the 5 layer structure is the only exception) when the nitrogen:sulfur ratio is plotted versus the number of adsorbed layers as shown in figure 3.8. The discrepancies present indicate that L-by-L assembly is inconsistent on these oxidized surfaces and the samples may not be appropriate for use in the mechanical measurements. Aberrations are also apparent in contact angle data as shown in figure 3.9.

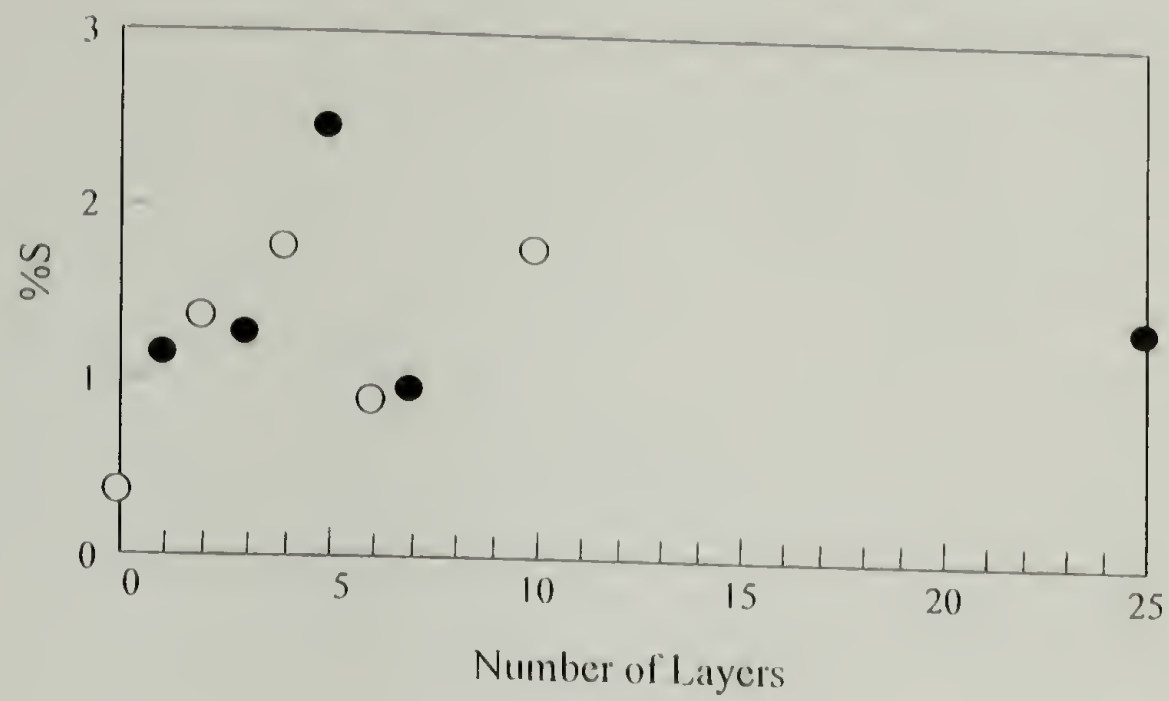

Figure 3.7. Sulfur content at 75° take-off angle as a function of the number of layers adsorbed onto oxidized Lycra®: open (○) and closed (●) symbols indicate even and odd layers, respectively.

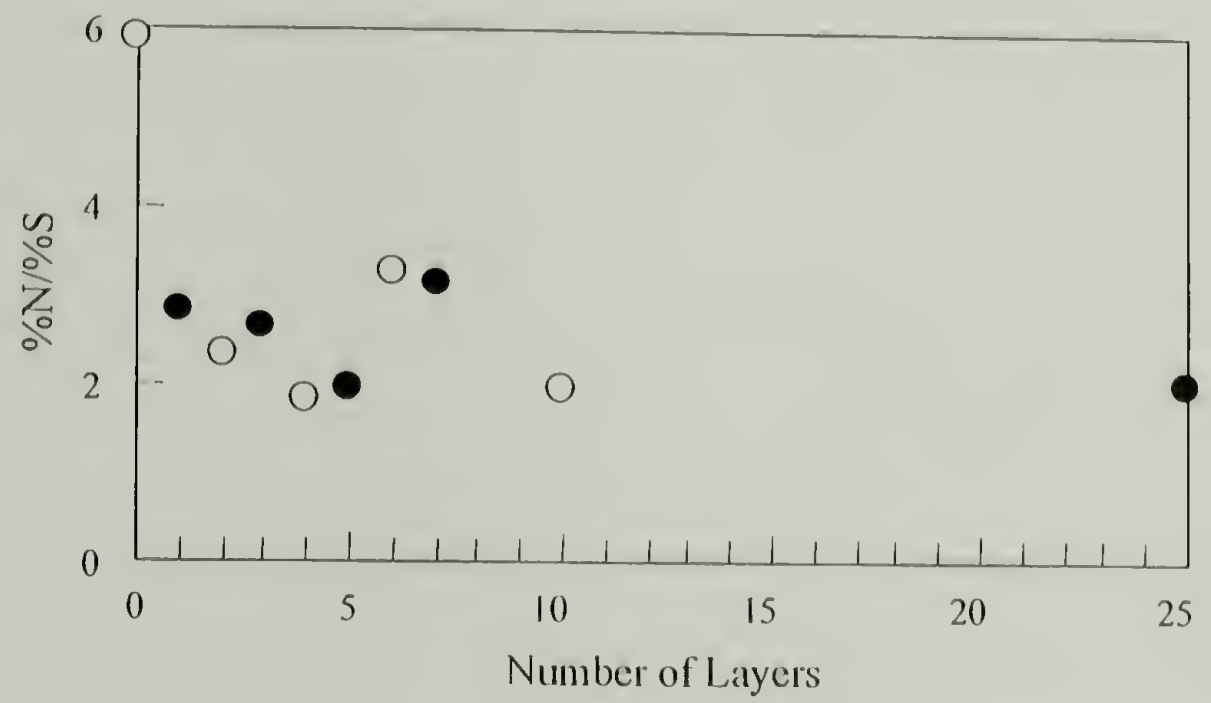

Figure 3.8. Nitrogen/sulfur ratio at 75° take-off angles as a function of the number of layers adsorbed onto oxidized Lycra®: open (○) and closed (●) symbols indicate even and odd layers, respectively.

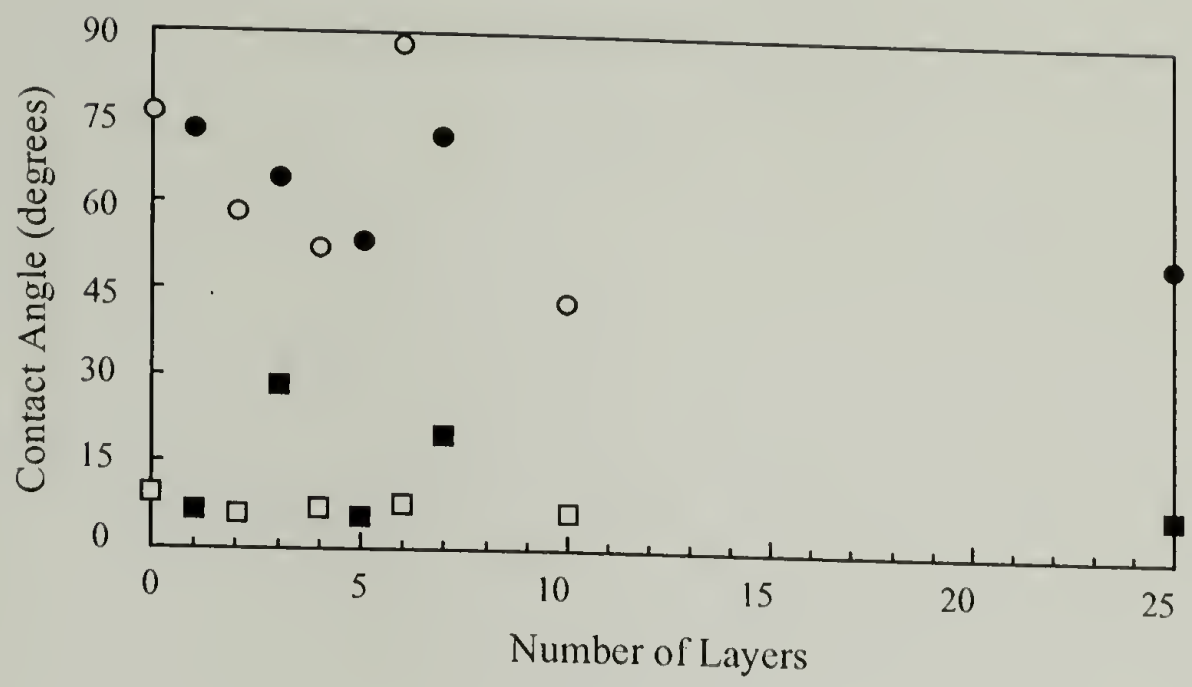

Figure 3.9. Dynamic eontact anglc data as a funetion of thc number of laycrs adsorbed onto oxidized Lyera®: open (○) and closed (●) symbols rcpresent advancing data for even and odd layers, respeetively and open (□) and closed (■) symbols indicate reecding data for even and odd layers, respeetively.

Odd-even affeets in θ_A are obscrved for most of the samples (exeept for samples with 5 and 6 layers) with higher advaneing angles for the odd numbercd laycrs. Anothcr unexpected result was the high reeeding angles measured for two of thc samples (3 and 7 layer samples) as most (if not all) L-by-L asscmblies of PSS and PAH show θ_R closc to 5°. Based on these results, it was deeided that L-by-L assemblies on oxidized Lyera® may not give eonsistent multilayered struetures and this proeedure was not uscd to pursue mechanieal property measurements.

Plasma Modifieation. As the plasma polymerization of allylamine on PTFE allowed the formation of L-by-L assemblies, it was believed that this teehnique would permit the same formation on Lyera®. Studies to assess the effeet of plasma reaetion time indieated that there may not be eomplete eoverage of thc plasma polymcr and L-by-L

adsorption studies were necessary to assess the viability of this technique. Contact angle measurements (shown in figure 3.10) indicate that the odd-even behavior that is expected for L-by-L systems is evident for samples with more than 8 layers. It is possible that in the initial layers, there might be patches present without polyelectrolytes, thus giving the anomalous behavior. As more layers are deposited, these holes are covered up. Nitrogen content also shows (figure 3.11) the odd-even behavior where even layers have higher nitrogen content than the odd layers. Examination of nitrogen content alone gives the indication of a typical multilayer assembly. Examination of the nitrogen/sulfur ratio (shown in figure 3.12), however, indicates that this system may be atypical, as higher ratios are observed at 11 and 13 layers than expected. In addition, the ratio should be 2 as for PTFE-NH_3^+, but it is close to 2.5. Further examination of the nitrogen content shows 7-8% in these layers as opposed to 6%. As the virgin material initially contains 2%

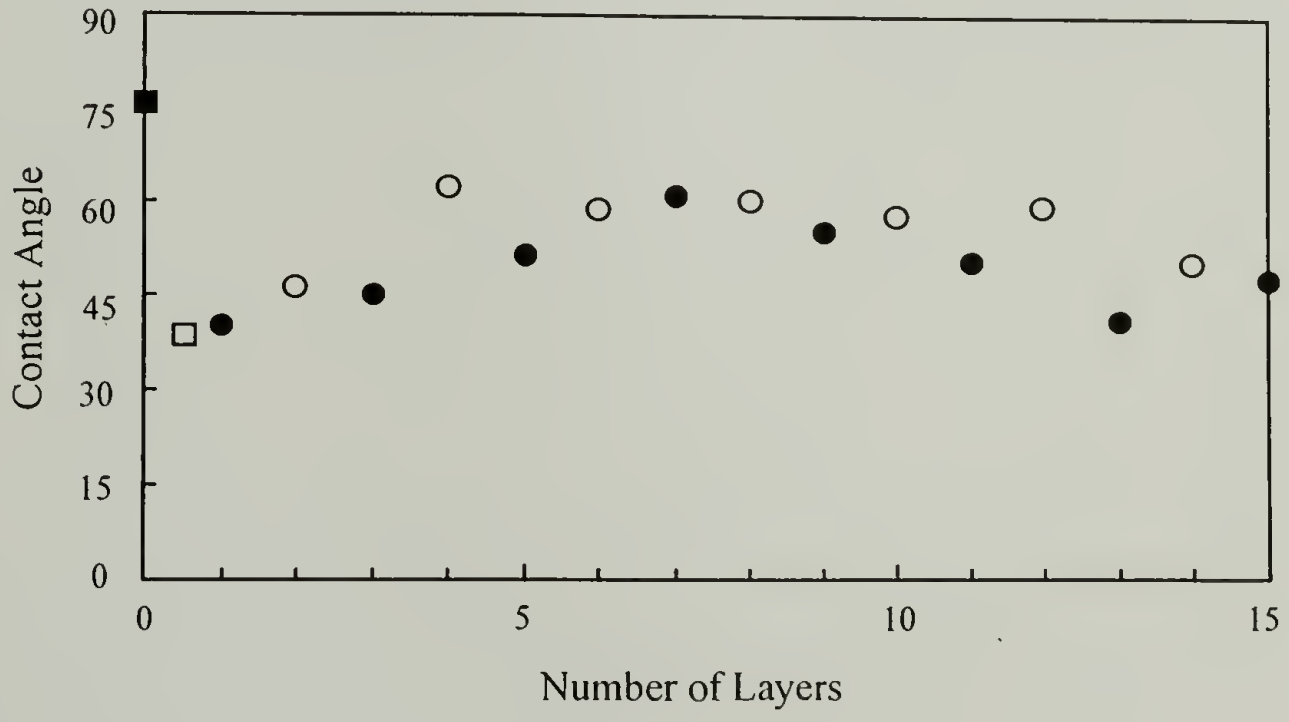

Figure 3.10. Changes in the advancing contact angle measurements as polyelectroylte layers are deposited onto plasma-polymerized allylamine on Lycra®: open (○) and closed (●) symbols represent even and odd layers, respectively, the open (□) symbol is that of the plasma polymer, and the closed (■) symbol represent the virgin material.

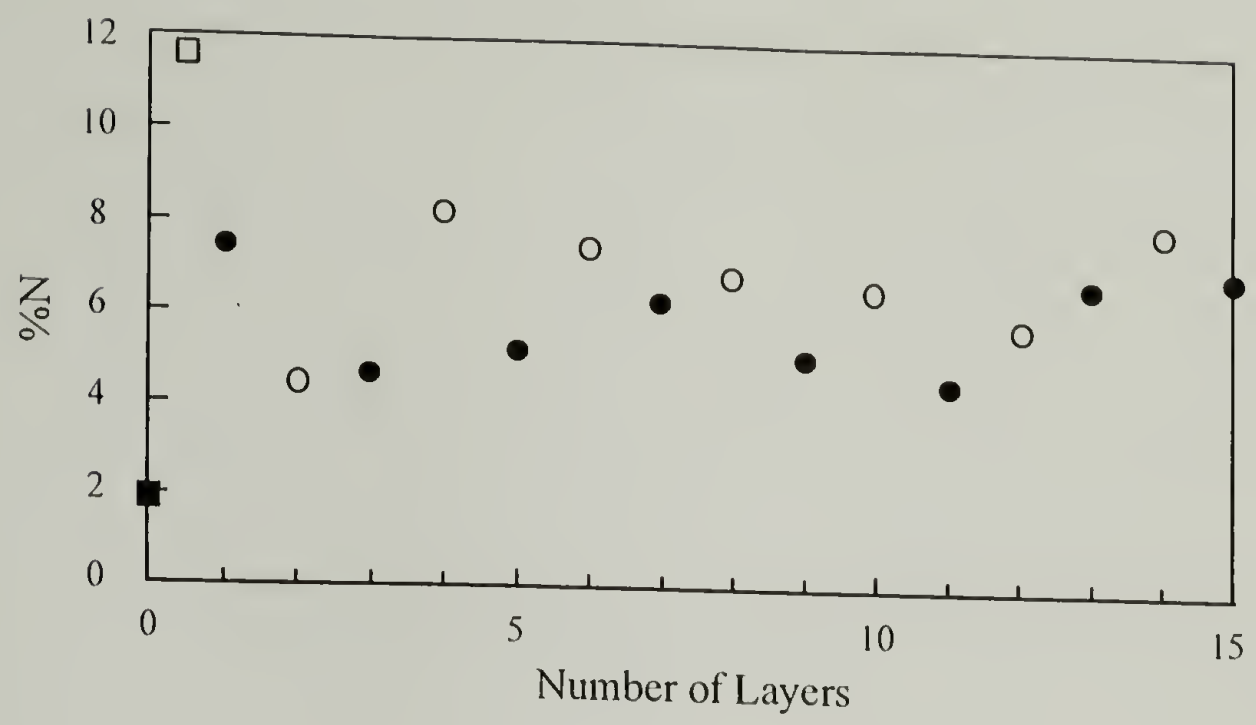

Figure 3.11. Nitrogen content measured at 75° take-off angle of the L-by-L system on plasma-polymerized allylamine on Lycra® and as layers are adsorbed: open (○) and closed (●) symbols represent even and odd layers, respectively, the open (□) symbol is that of the plasma polymer, and the closed (■) symbol represent the virgin material.

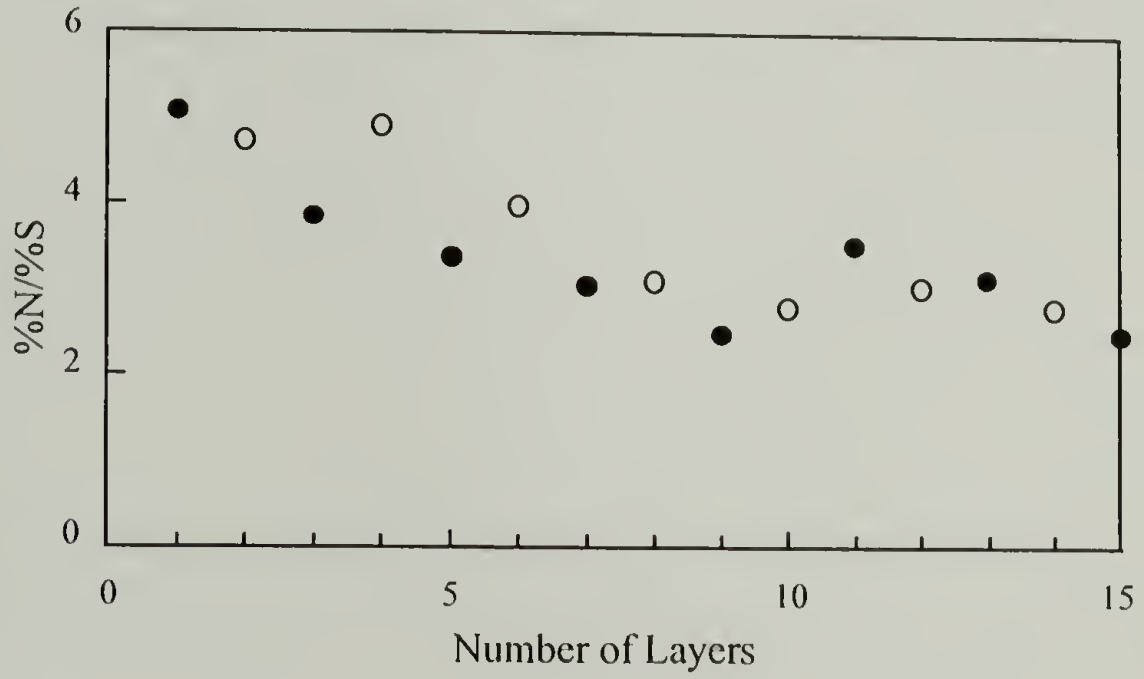

Figure 3.12. Changes in the N/S content at 75° take-off angle as polyelectroylte layers are deposited onto plasma-polymerized allylamine on Lycra®: open (○) and closed (●) symbols represent even and odd layers, respectively.

nitrogen, it is suspected that the higher nitrogen content is due to the incomplete coverage of the substrate leading to an imperfect multilayer assembly. Based on these results, a better technique is required to produce L-by-L assemblies for mechanical testing.

Plasma modification using nitrogen/hydrogen gas mixture functionalized the surface with amine groups to which PSS can adsorb. The kinetics of the first layer adsorption were determined by XPS over 45 minutes and sulfur concentration values indicate that the adsorption is complete within 20 minutes as shown in figure 3.13. Concurrent with the PSS adsorption is a desorption of some ammone groups as evidenced by the atomic % nitrogen decrease to ~2.9% from the initial ~14%. The 1st PSS layer in all multilayer assemblies was deposited using a 30 min adsorption time and subsequent layers were deposited using 20 minute adsorption times. A build-up of PSS and PAH layers by L-by-L deposition occurred on this substrate.

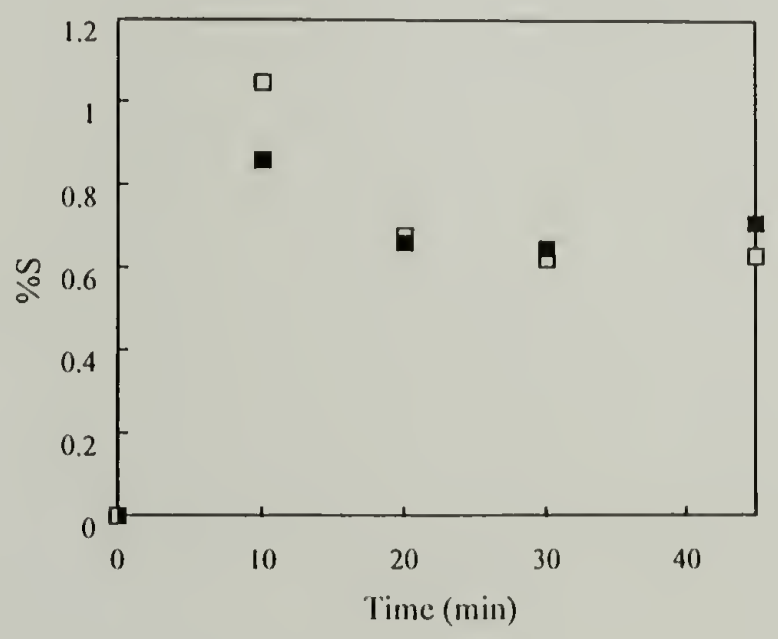

Figure 3.13. Amount of sulfur present on Lycra-NH_3^+ as the first layer (PSS) adsorption time is increased: open (□) and closed (■) symbols indicate 15° and 75° take-off angles, respectively.

Alternating deposition of PSS and PAH leads to multilayer assembly formation on Lycra-NH_3^+ as observed by the oscillating values of contact angle measurements (figure 3.14) and nitrogen:sulfur ratios (figure 3.15) as the top layer changes from PSS to PAH. As in the previous chapter, these oscillations indicate that the layers are stratified and the amplitude of the oscillation is proportional to the thickness of the layers and their degree of stratification (versus interpenetration). An odd-even effect consistent with the composition of the outermost layer is observed for all samples except for the sample with 25 layers which has a slightly higher ratio. Water contact angle data show a pronounced odd-even trend that is consistent across the series of samples with samples containing PSS as the top layer exhibiting greater wettability than those with PAH as the outermost layer. The thickness of the multilayer assembly was estimated by comparing the attenuation of the N/S ratio for this system with that of a multilayer film on PTFE modified with an allylamine plasma polymer. In the latter case, the ratio levels off after 6 layers and the thickness of each layer was measured to be 6.1 Å.[20] For this system, the ratio levels off after 10 layers which indicates that these layers are about 3 Å thick.

Mechanical Testing

Lycra® yarns were treated in the same manner as described above. The surfaces were plasma modified using a nitrogen/hydrogen gas mixture followed by polyelectrolyte deposition to form a 50 layer assembly. Samples for mechanical testing were obtained after plasma modification to study the affects of the plasma reaction on the mechanical properties of the Lycra® yarn. SEM micrographs (figure 3.16) show the surface of the

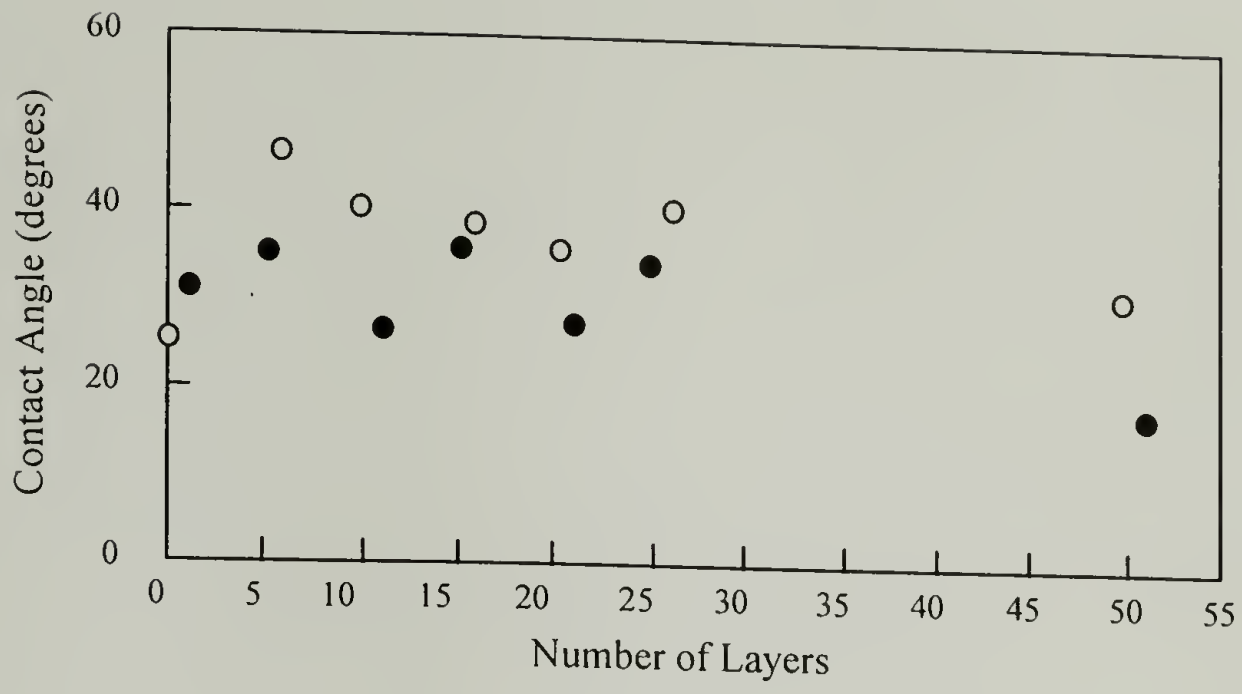

Figure 3.14. Advancing contact angle measurements of Lycra-NH_3^+ adsorbed with PSS/PAH multilayer films: closed (●) and open (○) symbols indicate an odd and even number of layers, respectively.

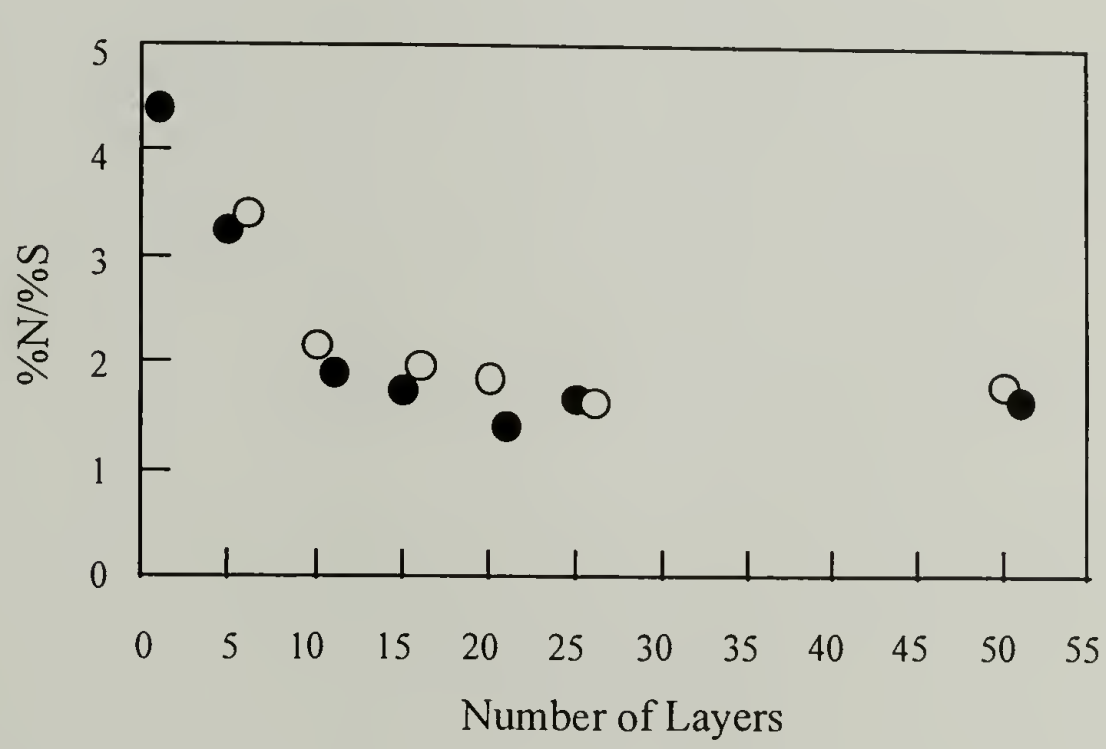

Figure 3.15. Nitrogen:sulfur atomic ratio data (XPS) versus the number of layers in the PSS/PAH multilayer film on Lycra-NH_3^+: closed (●) and open (○) symbols indicate an odd and even number of layers, respectively.

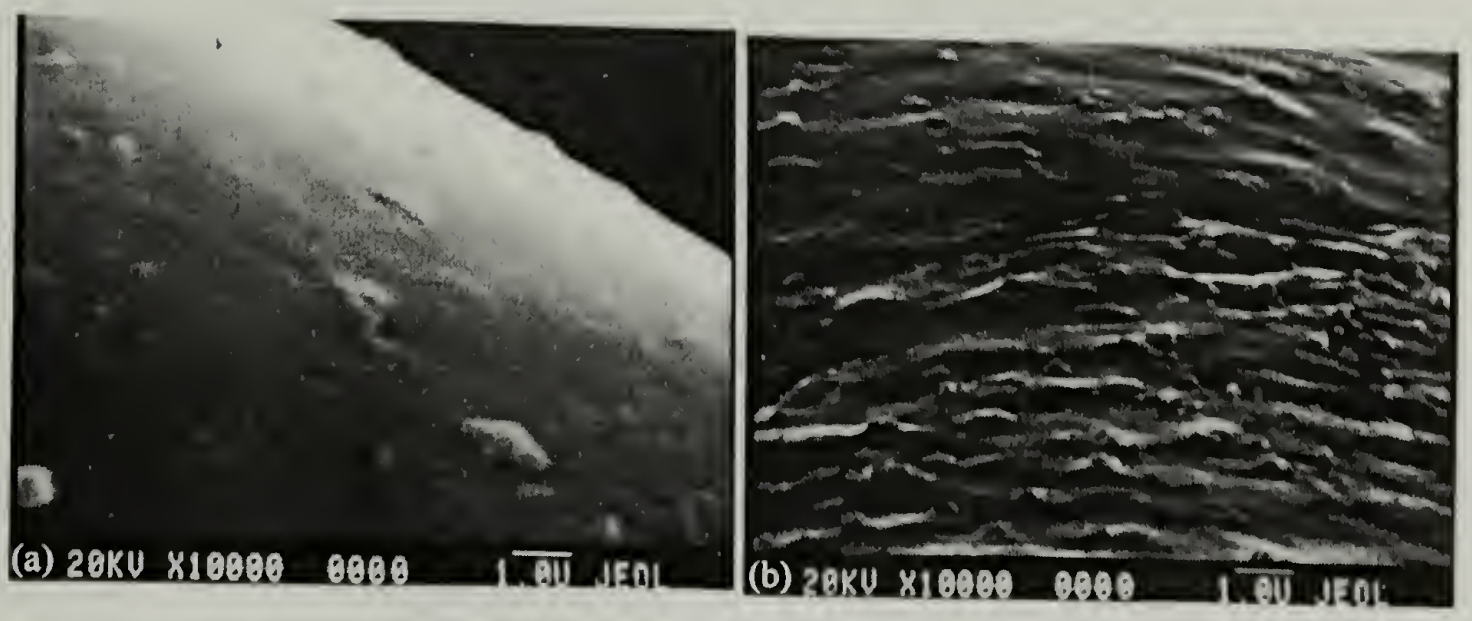

Figure 3.16. SEM micrograph of Lycra® yarn: (a) before plasma-modification and (b) after plasma-modification showing the appearance of ridges.

yarns before the plasma treatment; the surface appears smooth, but it appears rougher after treatment as the plasma modification etches amorphous regions at a greater rate than crystalline regions. The etching of the yarns was beneficial as the tensile modulus of the yarns decreases to 1.24 MPa from 2.61 MPa. After 50 layer depositions, the surface of the yarns appears smoother (figure 3.17) and the mass increase due to the layers was 19 μg for the same sample. The thickness of the assembly is estimated from the mass change to be 133 nm or 2.7nm per layer if the density of the L-by-L assembly is assumed to be 1.0 g/cm^3. This is an overestimate of the layer thickness since the single layer thickness in most L-by-L systems is less than 1 nm. As the mass contribution of the L-by-L assembly accounts for only 1.2% change in the composite, any uptake of water skews the thickness estimate. A water uptake experiment, conducted by leaving Lycra® yarn in a water solution at pH=2.9 for 25 hours (the time estimated for 50 layer

adsorption), indicates the yarn picks up 0.7% water. This leads to an overestimation in the thickness estimate of the assembly by 238%. A thickness estimate of 3 Å, obtained by comparing the N:S ratio, is used instead.

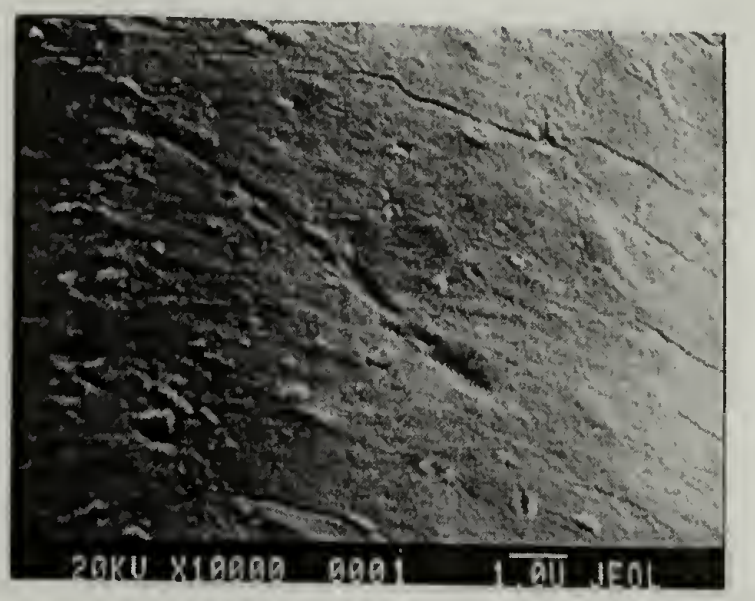

Figure 3.17. SEM micrograph of Lycra® yarn after plasma-modification followed by the adsorption of PSS/PAH polyelectrolytes forming 50 layers.

Tensile testing of the samples with 50 layers shows a stress-strain curve (figure 3.18) distinctly different than those of plasma-modified samples. The stiffness of the polyelectrolyte chains results in a higher initial slope at low strain levels. Above 2.5% strain, the multilayer assembly fails and the slope of the curve returns to that of the Lycra® support. SEM micrographs of these samples at different strains show cracks appearing in the multilayer assembly starting at about 2% strain which corresponds to the stress-strain curves. Figure 3.19 shows the progression of the crack size as the strain increases from 2% to 133%; in all cases the cracks are perpendicular to the tensile direction. The tensile modulus of the 50 layers and the Lycra® support was measured to be 7.42±0.51 MPa.

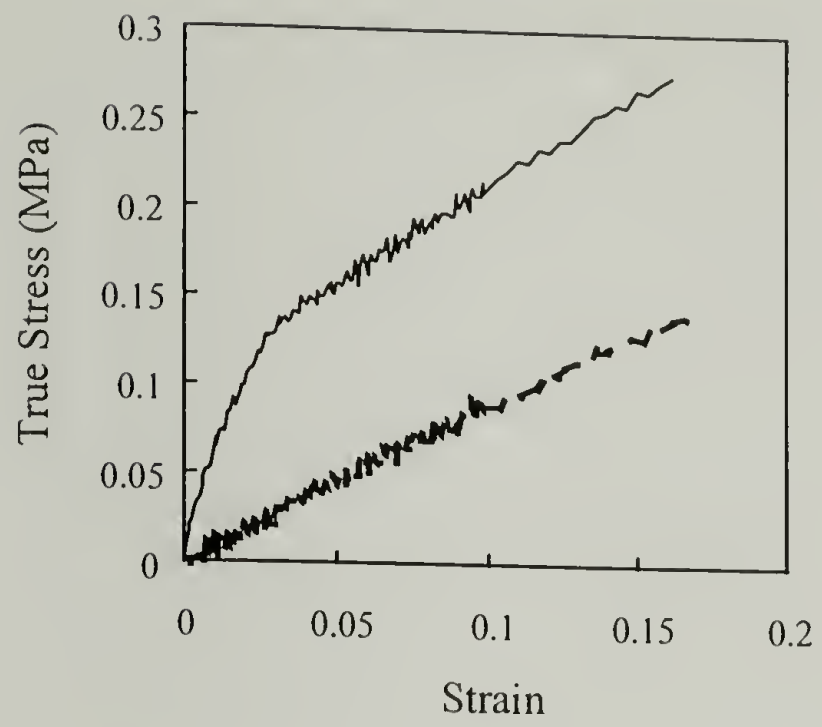

Figure 3.18. Stress-strain curve of the plasma-modified Lycra® (dashed lines) and of the plasma-modified Lycra® with 50 Layers (solid line).

By using the rule of mixtures model given in equation 3.3 (in a slightly modified form), the tensile modulus of the multilayers can be determined. As for composites in a cylindrical geometry, the volume fractions can be replaced by area relationships as follows:

$$E_T A_T = E_1 A_1 + E_2 A_2$$

where A_T is the cross-sectional area of the composite, and A_1 and A_2 are the cross-sectional areas of each component. Using the measured values of the moduli for the plasma-treated Lycra® and the composite and the measured cross-sectional area, the tensile modulus of the 50 layer structure is determined to be 8.8±0.7 GPa. This value may be an overestimation because the tensile modulus of the multilayer films is expected to be close to that of bulk polystyrene which has a reported tensile modulus of 3.0 GPa.[27]

A low value is obtained using a thickness of 8Å per layer (using the gravimetrics value accounting for the water uptake in Lycra® and assuming 30% of water in the L-by-L assembly can not be removed): of 3.3±0.3 GPa. Using this value and the critical strain of 2.5%, the strength of the coating is calculated to be 220 MPa.

It is arguable that such a simple model may contain inaccuracies and a more complex model is necessary. For this purpose, equation (3.4) is used, except that in this case, the fiber phase is that of the multilayer assembly and the matrix is that of the elastomer. The volume fraction is obtained by finding the cross-sectional areas of the multilayer assembly and of the composite structure. The Poisson's ratio for the elastomer is equivalent to a rubber (0.5) and that for the multilayer assembly is assumed to be comparable to a glassy polymer (0.3 for polystyrene). The shear modulus is 1/3 of the tensile modulus, or 0.87 MPa. The bulk modulus of most elastomers is approximately 2 GPa.[27] For the other 2 unknown variables, we can substitute the shear modulus and bulk modulus of the multilayer assembly with the tensile modulus using equations (3.5) and (3.6). Based on these assumptions, the tensile modulus of the multilayer assembly is estimated to be 8.6 GPa, which is comparable to the "rule of mixtures" model used.

As shown in figure 3.19d, at 133% strain there appears to be buckling of the Lycra® yarn as observed by the periodic ridges that appear parallel to the tensile direction. This is believed to be caused by the hard coating on the soft substrate. The hard coating has a lower Poisson Ratio than the Lycra® substrate. The Lycra® elastomer is nearly incompressible and does not want to change its volume upon deformation (the Poisson's

ratio for elastomers is ½), so in its natural state, the radius of Lycra® yarn will decrease as the yarn is extended. However, as in the present case of a hard coating, this radial decrease is hindered by the coating, which has a lower Poisson's ratio (an estimate of 1/3 is used which is equivalent to that of polystyrene). Thus the cylindrical coating on the fiber interferes radially producing radial tensile stresses at the interface and the coating is driven into hoop stress compression while the elastomer achieves radial tension. The thin hard coating on a very soft substrate can not support high compressive hoop stresses without buckling which results in the periodicity observed.

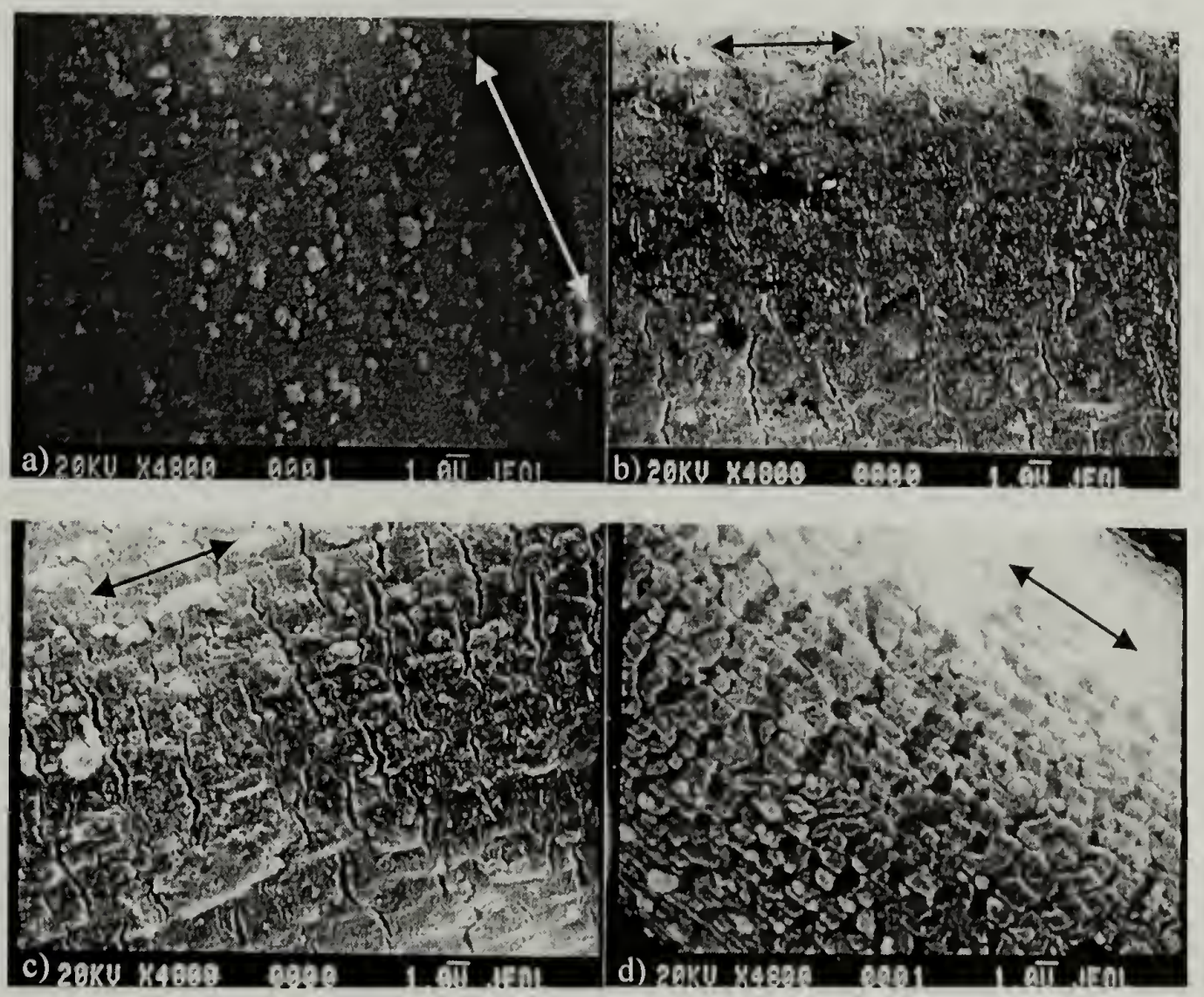

Figure 3.19. SEM micrograph of Lycra® yarn with 50 Layers under a) 2%, b) 5%, c) 17%, and d) 133% strain. Arrows in the micrographs indicate the tensile direction.

Conclusions

Several methods for the surface modification of Lycra® to initiate L-by-L assembly were attempted. Direct adsorption of polyelectrolytes does not work well with this substrate as very low amounts of nitrogen were detected after 10 adsorption steps. Chemical modifications lead to various degrees of degradation in the films, with the most extreme (sulfonation) leading to total decomposition of the film. Chromic acid oxidation leads to slight degradation of the film and the formation of L-by-L assemblies was possible although it was somewhat inconsistent. Plasma polymerization of allylamine for short durations leads to incomplete plasma polymer films; it is possible to form L-by-L assemblies on these surfaces. The most effective method for surface modification of Lycra® is the nitrogen/hydrogen plasma reaction to incorporate amine groups. Multilayer assemblies of PSS and PAH form by sequential polyelectrolyte adsorption and XPS and contact angle data indicate stratified layers. XPS analysis also indicates that the stoichiometry of the assembly process is 1.7 ammonium ions per sulfonate group. The established stoichiometry is maintained throughout multiple polyelectrolyte adsorption steps and differs from that of different substrates. Using the thickness estimate from comparing N:S data, the tensile moduli of the polyelectrolyte multilayer is estimated at 8.8±0.7 GPa. A lower estimate, assuming the thickness of each layer is 8Å, results in an estimate of 3.3±0.3 GPa which is similar to that of bulk polystyrene. The L-by-L assembly fractures after ~2.5% strain as observed in the stress-strain curve. SEM

micrographs show that these assemblies fracture at the same strain and indicate that these polyelectrolyte multilayers are brittle. The strength of the L-by-L assembly is 220 MPa using the higher modulus estimate.

Notes and References

(1) Ferreira, M.; Rubner, M.F. *Macromolecules* **1995**, *28*, 7107.

(2) Fou, A.C.; Rubner, M.F. *Macromolecules* **1995**, *28*, 7115.

(3) Onda, M.; Lvov, Y.; Ariga, K.; Kunitake, T. *J. Ferment. Bioeng.* **1996**, *82*, 502.

(4) Laschewsky, A.; Bayer, B.; Wischerhoff, E.; Arys, X.; Bertrand, P.; Delacorte, A.; Jonas, A. *Thin Solid Films* **1996**, *284*, 334.

(5) Ferreira, M.; Rubner, M.F.; Hsieh, B.R. *Mat. Res. Soc. Proc. Symp.* **1995**, *369*, 575.

(6) Onoda, M.; Yoshino, K. *Jpn. J. Appl. Phys.* **1995**, *34*, L260.

(7) Stepp, J.; Schlenoff, J.B. *J. Electrochem. Soc.* **1997**, *144*, L155.

(8) Hammond, P.T.; Whitesides, G.M. *Macromolecules* **1995**, *28*, 7569.

(9) Leväsalmi, J.-M.; McCarthy, T.J. *Macromolecules* **1997**, *30*, 1752.

(10) Smith, T.L. *Elastic Modulus, Network Structure, and Ultimate Tensile Properties of Single-Phase Polyurethane Elastomers* in *Elastomers and Rubber Elasticity*, Mark, J.E., Lal, J., Eds., American Chemical Society: Washington, D.C., 1982.

(11) Hashin, Z.; Rosen, B.W. *J. Appl. Mech.* **1964**, *31*, 223.

(12) Christensen, R.M. *Mechanics of Composite Materials*, Wiley Interscience: New York, 1979.

(13) Stockton, W.B.; Rubner, M.F. *Macromolecules* **1997**, *30*, 2717.

(14) Lvov, Y.; Ariga, K.; Kunitake, T. *Chem. Lett.* **1994**, 2323.

(15) Delcorte, A.; Bertrand, P.; Wischerhoff, E.; Laschewsky, A. *Langmuir* **1997**, *13*, 5125.

(16) Chen, W.; McCarthy, T.J. *Macromolecules* **1997**, *30*, 78.

(17) Tada, H.; Ito, S. *Langmuir* **1997**, *13*, 3982.

(18) Blais, P.; Carlsson, D.J.; Csullog, G.W.; and Wiles, D.M. *J. Coll. Interf. Sci.*, **1974**, *47*, 636.

(19) Rasmussen, J.R.; Stedronsky, E.R.; Whitesides, G.M. *J. Am. Chem. Soc.* **1977**, *99*, 4736.

(20) Hsieh, M.C.; Farris, R.J.; McCarthy, T.J. *Macromolecules* **1997**, *30*, 8453.

(21) Hollahan, J.R.; Stafford, B.B. *J. Appl. Polym. Sci.* **1969**, *13*, 807.

(22) Dreyfuss, P. *Poly(tetrahydrofuran)*, Gordon and Breach Science Publishers, New York, 1982.

(23) Ultee, A.J. *Fibers, Elastomeric*, in *Encyclopedia of Polymer Science and Engineering*; Mark, H.F., Bikales, N.M., Overberger, C.G., and Menges, G., Eds., Vol. 6, Wiley and Sons: New York, 1986, p 733.

(24) Gombotz, W.R.; Hoffman, A.S. *J. Appl. Polym. Sci.: Polym. Symp.* **1988**, *42*, 285.

(25) Hollahan, J.R.; Wydeven, T. *Science* **1973**, *179*, 500.

(26) Young, R.J.; Lovell, P.A. *Introduction to Polymers*, Chapman and Hall, New York, 1991.

(27) *Polymer Handbook*, 3rd ed.; Brandup, J., Immergut, E.H., Eds.; John Wiley & Sons: New York, 1989.

CHAPTER 4

ADHESION OF LAYER-BY-LAYER ASSEMBLIES TO CHARGED SUBSTRATES

Introduction

As a continuing effort to learn more about layer-by-layer (L-by-L) assemblies, the approach described in this chapter focuses on the adhesion strength of these assemblies on substrates with different charge densities. The adhesion of these materials is important as the reported research on applications envisioned for these assemblies all involve multilayer assemblies formed and characterized on a substrate (and not as free-standing films).[1-9] It is also not known to what degree the surfaces of these substrates are modified and thus it is important to study the effects of different charge densities on the adhesion strength of these multilayer assemblies.

The analysis of the adhesion strength of a coating is derived from Cox's research on fiber orientation and its effect on the stiffness and strength of paper and other fibrous materials.[10] Initial developments of Cox's analysis were focussed on wire-reinforced metal composites,[11] but were expanded to composites consisting of other brittle/ductile components.[12-14] As the fracture of coatings is similar to that of fibers, the analysis of adhesion strength can be extended to coatings. Throughout the reported research, it is commonly found that the adhesive shear strength of a coating is inversely proportional to

the crack spacing (distance between cracks).[15-19] The work of adhesion of the coating, which is proportional to the adhesive shear strength, can be calculated by measuring the crack spacing.

In order to study the effect of charge density on the adhesion strength of the layer-by-layer assembly, two approaches are taken to produce low and high degrees of surface charge on low density polyethylene (LDPE): (1) Chromic acid oxidation leads to the formation of carboxylic acid groups.[20,21] (2) Coating gold on LDPE followed by the adsorption of a long chain thiol, terminated with carboxylic acid groups, results in a self-assembled monolayer that is highly charged. Polyallylamine (PAH) and poly(styrene sulfonate) (PSS) are alternately adsorbed onto these surfaces to form the layer-by-layer assemblies. Once the nano-assemblies are formed, the samples are uniaxially deformed at a constant rate and examined by electron microscopy. The adhesion strength of the layer-by-layer assembly is obtained by analyzing the crack spacing of the layer-by-layer assembly fragments.

Low Density Polyethylene

Low density polyethylene is formed by the polymerization of ethylene gas in the presence of small amounts of catalyst (for example, oxygen or benzoyl peroxide) under high pressures (100-300 MPa) and high temperatures (250 °C). The resulting polymer is highly branched with 60-70% crystallinity and density of 0.91-0.94 g/cm^3. LDPE is a thermoplastic with a crystalline melting point at about 115 °C and is processable by many

methods (compression molding, extrusion, blow molding, etc.). It is solvent resistant at room temperature (but soluble in many solvents above 100 °C). The chemical resistance of LDPE (or PE in general) increases with the degree of polymerization. Similarly, the mechanical properties are also dependent on the degree of polymerization and also on the degree of branching and the molecular weight distribution. For LDPE, the tensile modulus ranges from 100 to 260 MPa.

Surface Modification

The surfaces of LDPE can be modified by several methods: chromic acid oxidation, sulfonation, or deposition of a gold layer. The first two methods support layer-by-layer assembly process as both modifications incorporate charged groups on the surface. For the gold-coated LDPE, chemisorption of a charged thiol is required before polyelectrolytes can be adsorbed.

Chromic Acid Oxidation

The surface of LDPE has been functionalized by chromic acid oxidations.[20,21] This reaction involves the immersion of LDPE in a chromic acid solution ($CrO_3/H_2O/H_2SO_4$) at 72 °C. It was found that a reaction of 5 minutes was sufficient to maximize the carboxylic acid concentration of the LDPE with the least amount of degradation (figure 4.1). The films were rinsed in water three times followed by a nitric

acid treatment at 50 °C for 15 minutes to dissolve any inorganic residues. SEM micrographs of the resulting films show the surface to be pitted (figure 4.2). The treated surface contains 60% carboxylic acid groups and 40% ketone or aldehyde moities.[21]

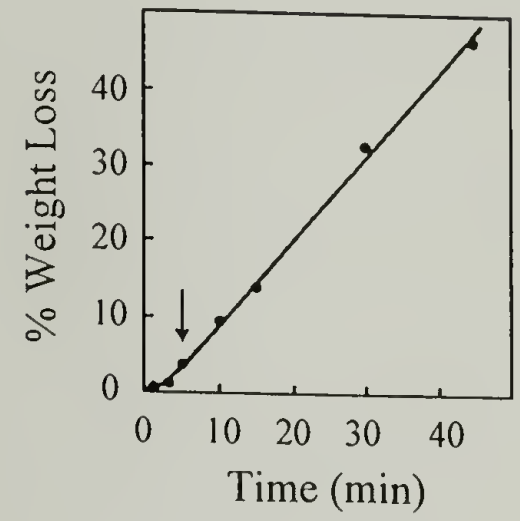

Figure 4.1. The weight loss of LDPE film on oxidation at 72 °C as a function of treatment time. The arrow indicates the time at which the density of carboxylic acid groups is at the maximum.[21]

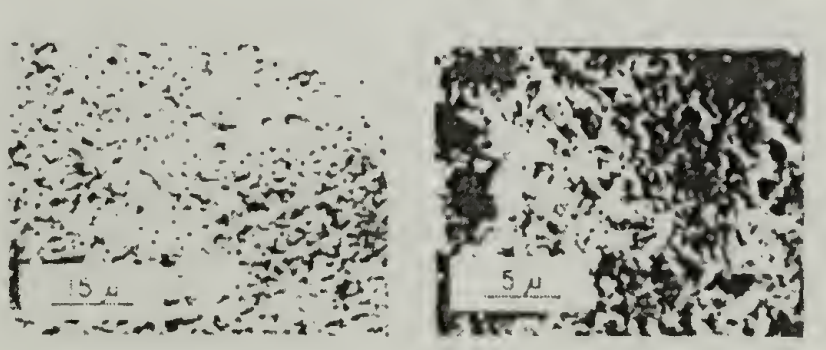

Figure 4.2. SEM micrographs of LDPE oxidized in chromic acid solution at 75 °C for 10 minutes: left, 1000X magnification; right, 3000X magnification.[21]

The mechanism of the reaction proceeds through a chromium IV ester intermediate to give an alcohol.[22] The alcohol undergoes a rapid reaction to give aldehydes and ketones as products which may oxidize further to carboxylic acids.[23, 24] The mechanism is shown in figure 4.3. The amount of carboxylic groups generated can

be quantified by attaching fluorescent groups and then measuring the intensity of the fluorescence. LDPE-COOH is labeled with 4-methyl-7-hydroxycoumarin (MHC) by converting carboxylic acids to acid chlorides and reacting with the alcohol group on MHC. The labeled LDPE was hydrolyzed to separate the MHC from the LDPE such that the fluorescence of the MHC can be measured. A second method to quantify the acid site densities is to convert the carboxylic acids to carbonyl hydrazides and label with 3-carbonylchloride-7-acetylcoumarin. The fluorescence intensity of the coumarin is measured after hydrolysis. Reaction schematics of these labeling techniques are shown in figure 4.4. Using these two different fluorimetric techniques, the absolute number of carboxylic groups generated is approximately $2*10^{15}/cm^2$.[21]

Gold Coating and Thiol Adsorption

Thin films of gold can be deposited onto substrates using thermal evaporation or sputtering. Substrates most often used are glass[25] and silicon wafers.[26,27] Thin films of gold (less than 4 nm) have been deposited onto polymeric substrates using thermal evaporation. These deposited films are discontinuous, consisting of islands with the size dependent on the surface energy of the polymer.[28]

Organothiols form self-assembled monolayers (SAM) on gold. The self-assembly process is driven by the formation of bonds between the gold surface and the thiol, the increased van der Waals interaction between the alkyl chains, and increased entropy as the solvation layer around the thiol molecules is removed. Long-chain thiols (those

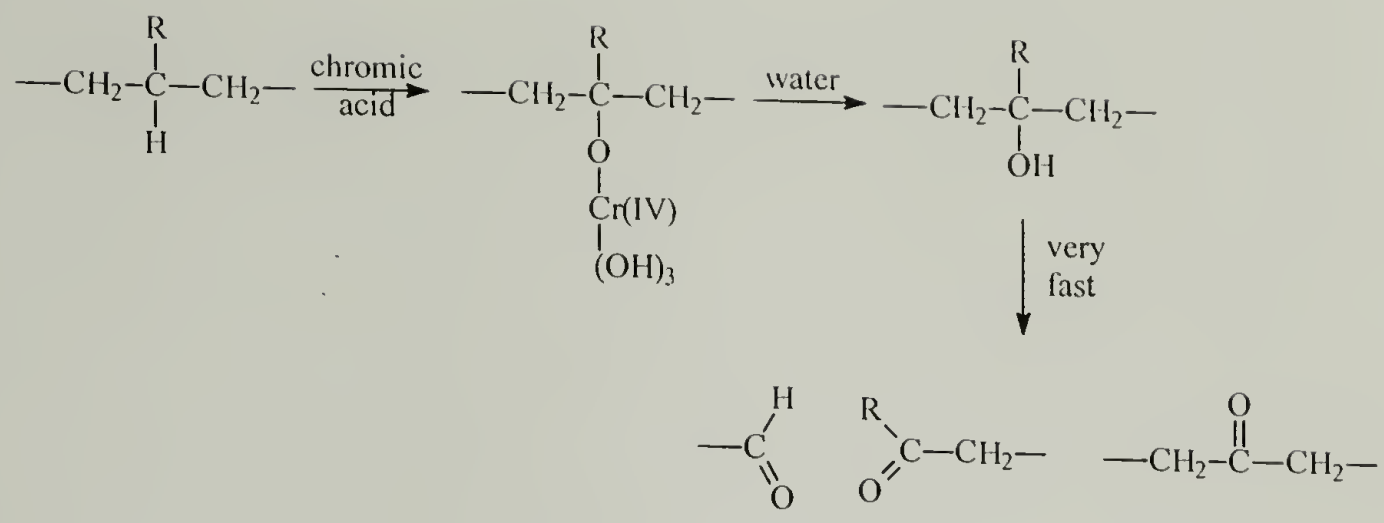

Figure 4.3. Mechanism of the chromic acid oxidation of PE.

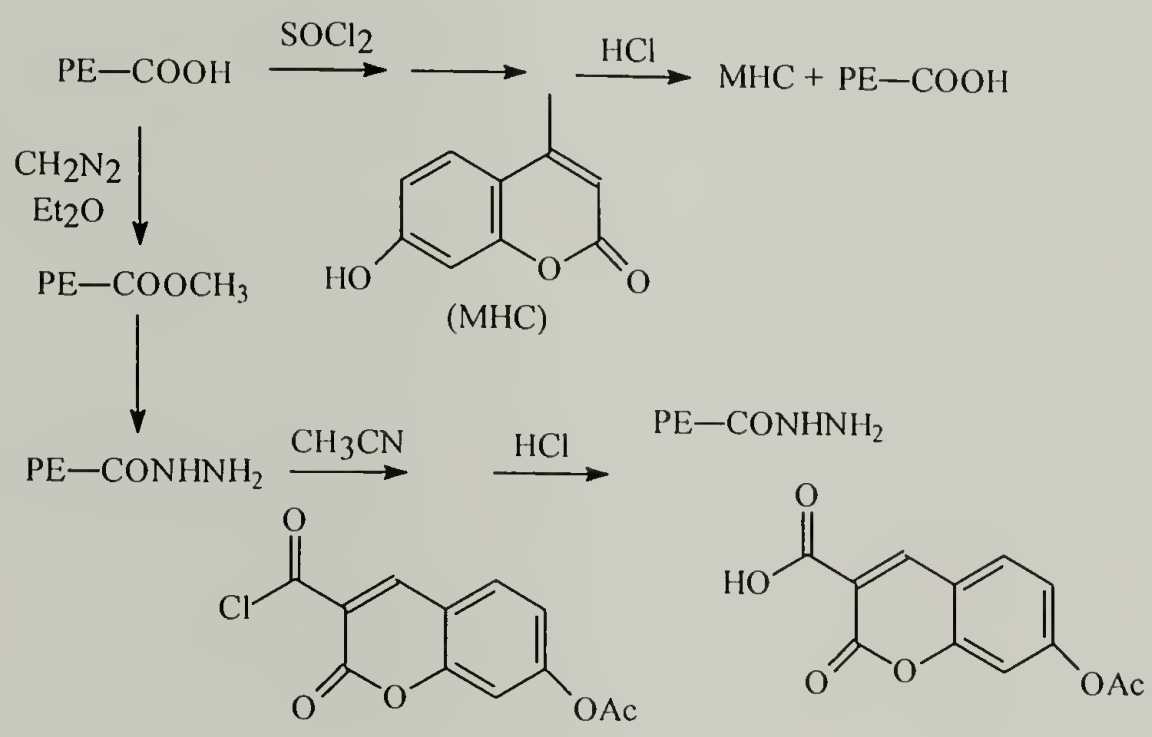

Figure 4.4. Fluorescent labeling of PE-COOH to measure the concentration of acid sites.

having more than 10 carbons) form densely packed pseudocrystalline monolayers in which the alkyl chains are all-*trans* and are tilted to the surface normal.[27,29] The amount of tilt from the surface normal has been found to be dependent on the orientation of the gold. For a Au(111), the chain tilt is ~24° (27° for a polycrystalline (111) substrate[30]) whereas for Au(100), the tilt is 14°.[31] On Au(111) surfaces, the sulfur atoms are in a hexagonal geometry with S-S spacing of 4.97Å and the area per molecule is calculated to

be 21.4Å^2.[31,32] As the chain length decreases, the amount of attractive energy of chain-chain interactions decreases, resulting in a more disordered structure with lower packing density and coverage. A real-time study of the kinetics of thiols adsorbing onto gold has been conducted using the surface plasmon technique. It was found that the adsorption mechanism involves a fast adsorption to give 80% coverage (for 12 and 16 carbon thiols) and 50% coverage (for 6 carbon thiol) followed by a slow "rearrangement" of the adsorbed thiol.[25] The adsorption of thiols containing carboxylic acid groups in the omega position onto gold has been used to form charged monolayers on which layer-by-layer assemblies can be formed.[26,33] In order get a densely packed acid surface, Chidsey suggests 16-mercaptohexadecanoic acid because the carboxylic acid group may increase the minimum chain length for self-assembly as they found that crystalline-like packing does not occur for a 11-carbon acid thiol.[34]

Fracture of Thin Films

The analysis of thin film fracture was developed from Cox's studies of the effect of fiber orientation on the stiffness and strength of paper and other fibrous materials.[10] The analysis was expanded to composites composed of rigid fibers in a ductile matrix. In 1965, Kelly and Tyson examined the tensile properties of copper composites reinforced with either tungsten or molybdenum wires.[11] In their work, they described the fracture process of continuous fibers whose breaking stress is more than the matrix's yield stress for plastic flow as follows: (1) The reinforcing fibers break when the matrix reaches the fracture stress of the fiber. (2) Once the continuous fibers are broken, the applied load is

transferred to the fibers by shear forces at the fiber/matrix interface where the fiber ends are under high shear stress. (3) The matrix continues to deform until enough stress is built up such that the fibers will fracture once more. (4) This process (shown in figure 4.5) continues until the fiber lengths are between ½ l_c and l_c where l_c is called the critical length. Although this work examined metals, this analysis was expanded to other materials. Fraser et. al: studied the surface treatment of E-glass embedded in several polymer matrices and determined the magnitude of the shear transmission across the glass fiber/polymer interface by measuring the critical fiber lengths.[12] In 1991, Nardin et. al. analyzed carbon fiber-poly(ether ether ketone) composites and showed that the physical

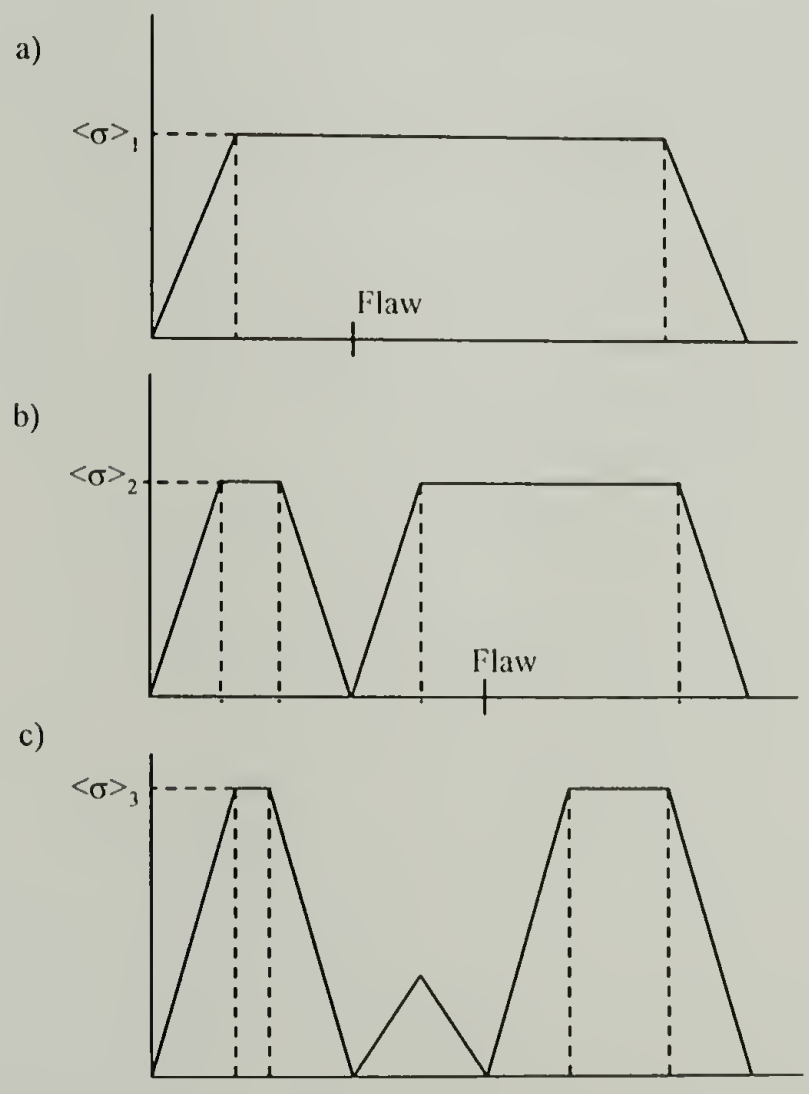

Figure 4.5. Cracking process of a fiber under tensile stress. As a critical stress level is reached, the fiber breaks at the weakest point until the fibers are between ½ l_c and l_c.[35]

interactions at the interface determined the magnitude of the interfacial shear strength.[13] In further work, they found similar results for other fibers and matrices and established a linear relationship between the interfacial shear strength and the reversible work of adhesion.[14] The slope of the line depends on the elastic moduli of the matrix and of the fiber. These analyses were conducted on fiber reinforced composites, but they have been extended to study the adhesion of coatings.

Similar to fibers in a matrix, brittle coatings on a ductile substrate crack when the composite material is under a tensile stress which exceeds the fracture strength. The crack may propagate parallel to the film near the substrate interface if the normal and shear stresses at the crack cannot be supported or relieved by local plastic deformation. The issues of coating fracture and film decohesion are discussed for chromium films on aluminum and stainless steel.[36] Film decohesion is critical for systems in which the interface fracture resistance is low (low adhesion strength) and the substrate has a high yield strength as yielding blunts film cracking at the interface and suppresses nucleation of interface cracks. There exists a critical value R which is a ratio of critical stresses for film cracking to initial decohesion represented by

$$R \approx 0.5\left(K_c^f / K_i\right)$$

where K_c^f is the mode I fracture resistance of the film and K_i is the fracture resistance along the interface. Film cracking precedes decohesion for $R<1$, otherwise both occur simultaneously. In metallic laminates, Hu and Evans show that the width of the fragments increases with decreasing yield strength and with increasing film thickness.

The thickness effects on the critical stress have also been observed by Wojciechowski et al. in their examination of Permalloy (brittle film)/Kapton laminates.[37] In their report, they found that thicker films experience earlier crack onset and have lower asymptotic crack densities than thinner films.[37] Agrawal and Raj measured the ultimate shear strength of a copper-silica interface by examining the crack spacing.[15] Initially, they approximate the shear stress as having a sinusoidal form (shown in figure 4.6):

$$\tau = \hat{\tau}\sin\frac{2\pi x}{\hat{\lambda}}, \qquad 0 \le x \le \frac{\hat{\lambda}}{2}$$

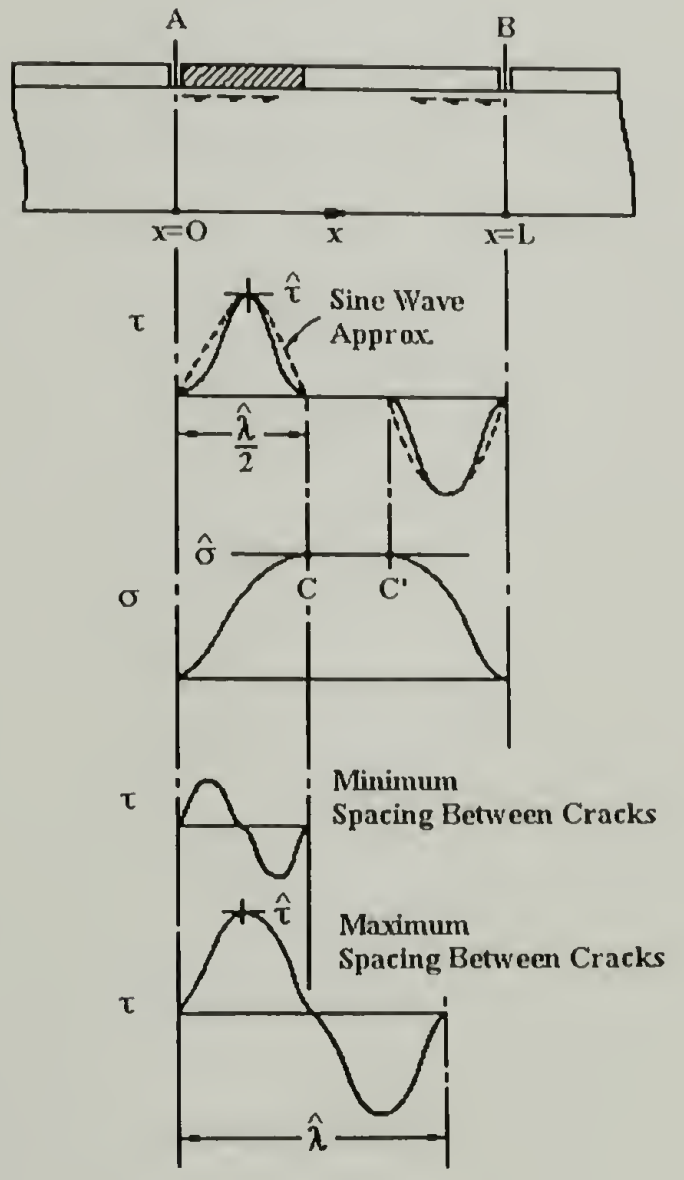

Figure 4.6. The tensile and shear stress distributions across a coating fragment as approximated by Agrawal and Raj.[15]

$$\tau=0, \qquad \frac{\hat{\lambda}}{2} < x < \left(L - \frac{\hat{\lambda}}{2}\right)$$

and

$$\tau = -\hat{\tau}\sin\frac{2\pi}{\hat{\lambda}}\left[x - \left(L - \frac{\hat{\lambda}}{2}\right)\right], \qquad \left(L - \frac{\hat{\lambda}}{2}\right) \le x \le L$$

where $\hat{\lambda}$ is the maximum crack spacing and $\hat{\tau}$ is the ultimate shear strength of the interface. To ascertain the ultimate shear strength, the tensile strength of the film $\hat{\sigma}$ is first determined by finding the fracture strain ε_f as shown in figure 4.7 and through the following relationship:

$$\hat{\sigma} = \varepsilon_f E$$

where E is the Young's modulus of the film. Once the tensile shear strength is found, the ultimate shear strength is obtained through:

$$\hat{\tau} = \frac{\pi\delta}{\hat{\lambda}}\hat{\sigma} \qquad (4.1)$$

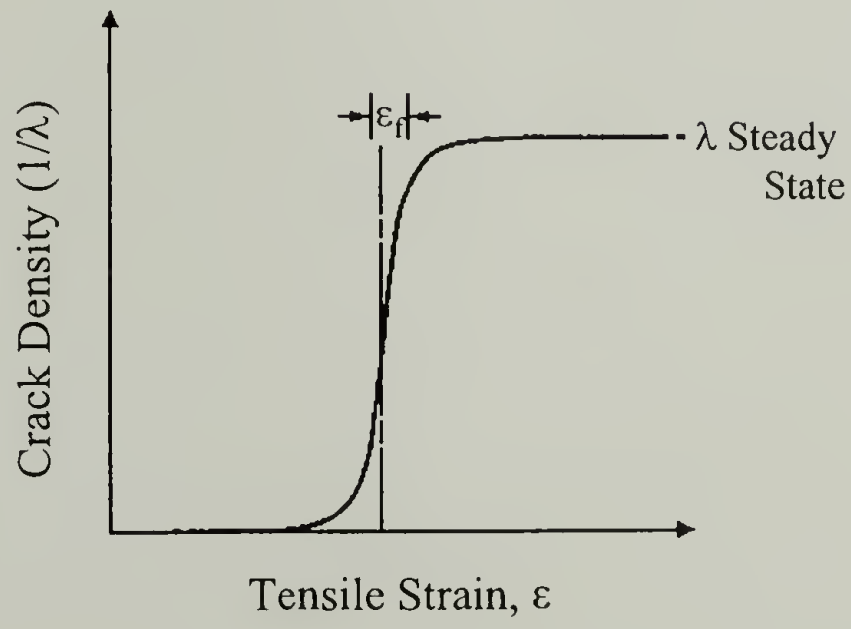

Figure 4.7. The increase in crack density as strain is applied to the laminate.[15]

where δ is the thickness of the film. Like the results from fibers, the maximum crack spacing is half that of the minimum crack spacing λ_0 ($\lambda_0 = \frac{\hat{\lambda}}{2}$). Recently, Leterrier et. al. have intensively studied glass coatings on polymer films and found similar results.[16-19] In their work, they analyzed a small element of a glass slice subjected to a tensile force as depicted in figure 4.8. The equilibrium condition for the system is

$$\delta\sigma_g + dx\tau = \delta(\sigma_g + d\sigma_g) \tag{4.2}$$

where dx is the length and σ_g is the stress in the glass layer along the loading direction x. Equation 4.2 can be rewritten as:

$$\frac{d\sigma_g}{dx} = \frac{\tau}{\delta}. \tag{4.3}$$

The integral solution to equation 4.3 is found by using the following assumptions: (1) The end effects of the coating are negligible. (2) The interfacial shear strength is constant. This assumption relies on the yield strength of the substrate being lower than the coating elongation at fracture. (3) The strength of the coating σ_{max} does not depend on the fragment size. The solution to equation 4.3 is:

$$\hat{\lambda} = 2\delta\frac{\sigma_{max}}{\tau} \tag{4.4}$$

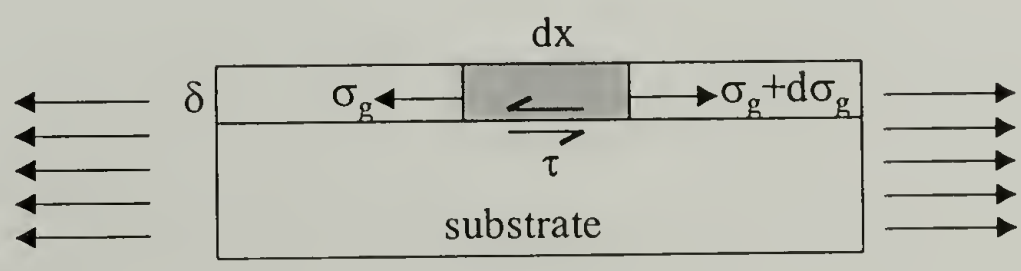

Figure 4.8. The stress state on a segment of a coating.

which is very similar to equation 4.1; the coefficient is the only difference (2 vs. π). In a previous report,[38] the mean crack spacing, $\bar{\lambda}$, was found to be related to the critical crack spacing by

$$\bar{\lambda} = 1.337\frac{\hat{\lambda}}{2} \tag{4.5}$$

Letterier used this result in combination with equation 4.4 to calculate the interfacial shear strength of glass coatings on PET films. In further analysis, they applied the relationship between the shear strength to the reversible work of adhesion *W*, previously found by Nardin for fiber composites, to their laminate composites. The work of adhesion is linearly related to the shear strength by

$$W = \frac{1}{k}\tau. \tag{4.6}$$

where *k* is a constant dependent on the moduli of the components given as

$$\frac{1}{k} = \xi^{-1}\left(E_g / E_p\right)^{1/2}.$$

ξ^{-1} is a constant independent of the system and is approximately 0.5 nm.[14] E_g and E_p refer to the Young's moduli of the glass layer and of the PET substrate, respectively. Based on these analysis, they calculated the adhesion energy of glass CVD coatings on PET films to be ~220 mJ/m^2 and attributed the high adhesion level to strong specific interactions present between silanol groups and oxygen-containing carboxyl group.[16] This compares with the estimated work of adhesion of SiO_2/PMMA of 225 mJ/m^2.[39] They continue to show (figures 4.9-4.11) that the crack onset strain (the strain at which cracks starts to appear) and the cohesive strength of the coating decrease with increasing coating thickness as the crack onset strain and the coating strength are linearly related.[19]

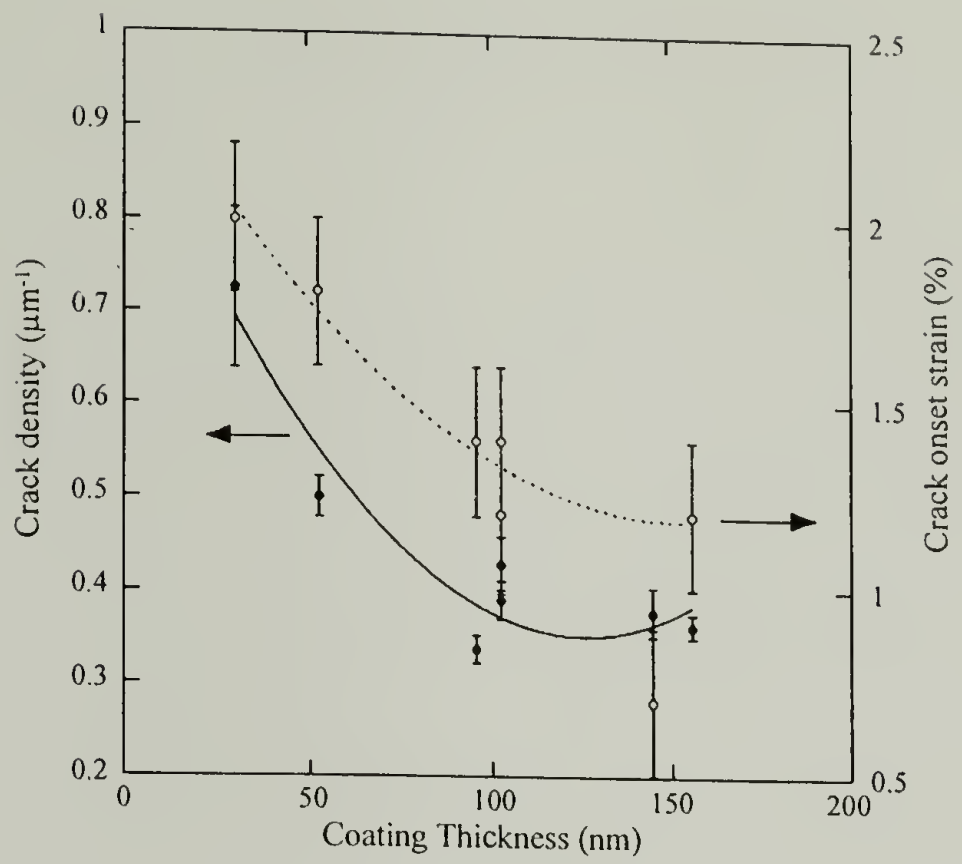

Figure 4.9. The crack density at saturation and the crack onset strain decreases as the SiO_x coating thickness increases.[19]

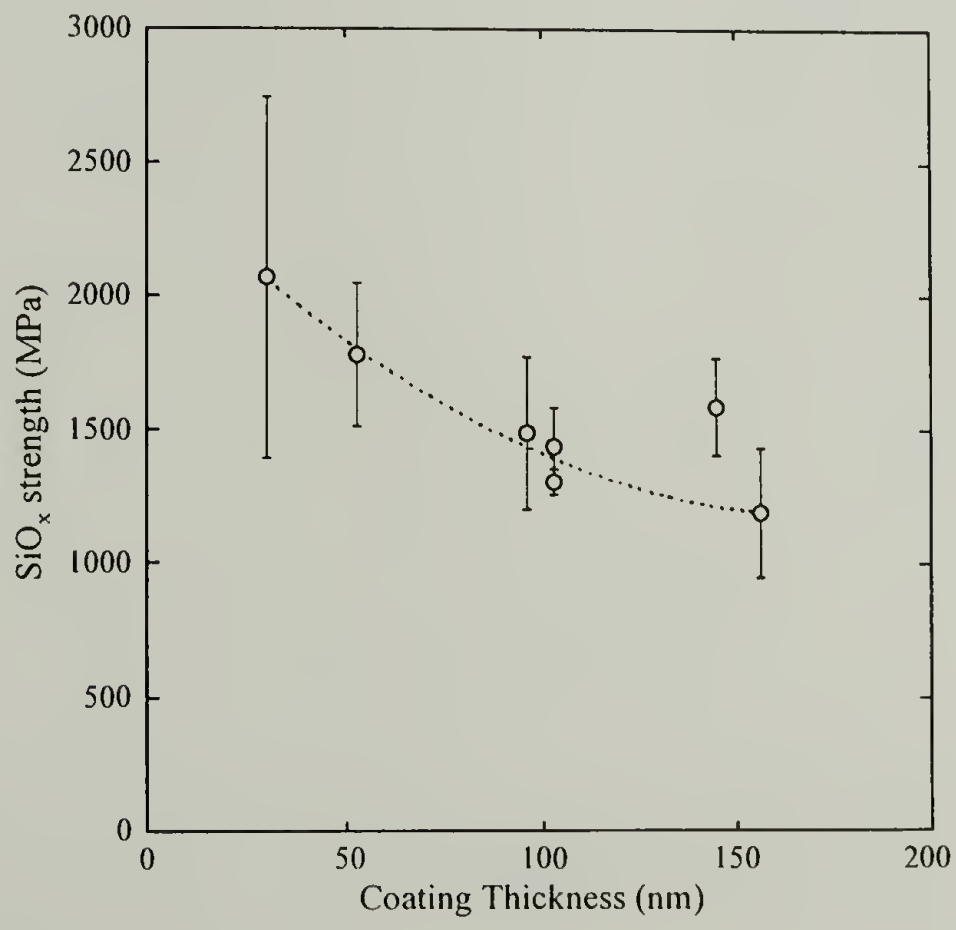

Figure 4.10. The cohesive strength of SiO_x coating decreases as the coating thickness increases.[19]

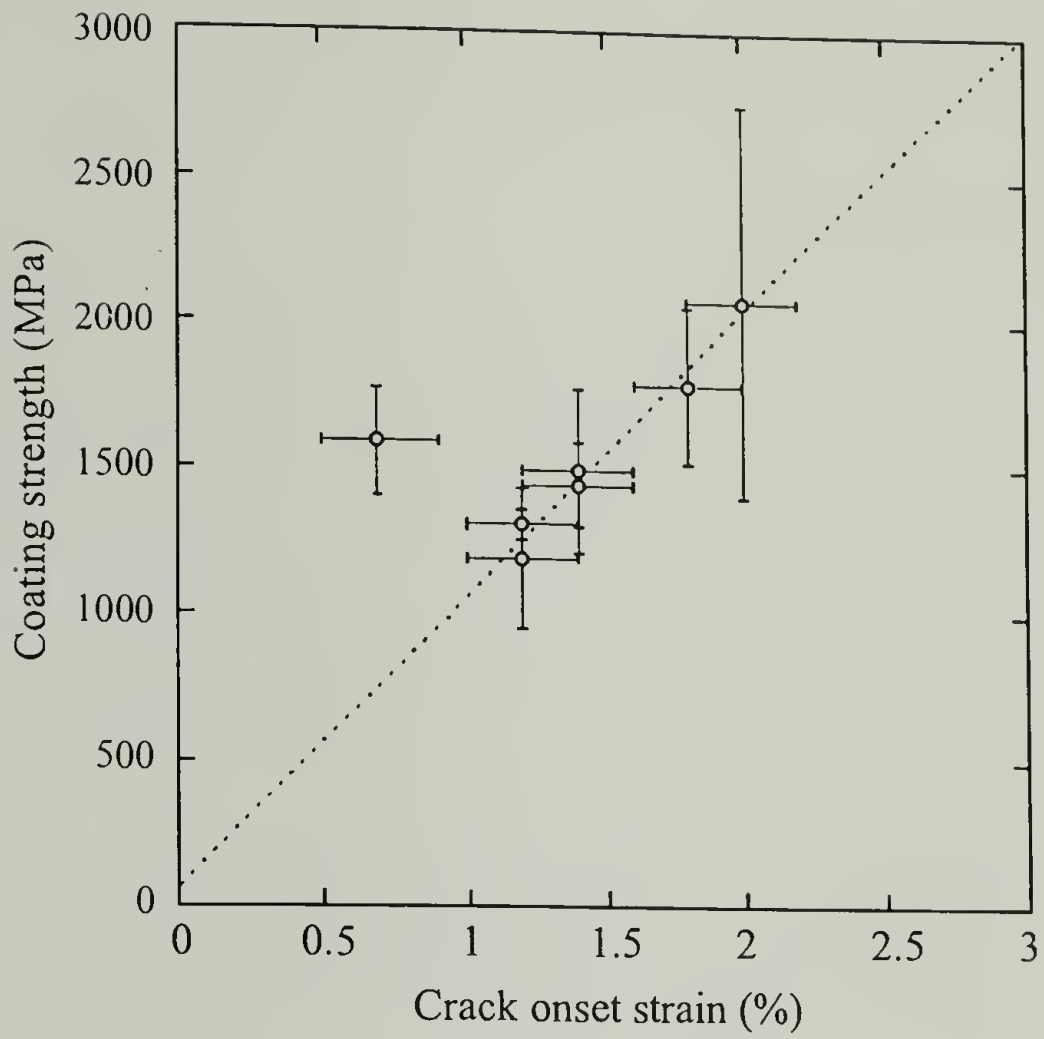

Figure 4.11. SiO_x coating strength is linearly related to the crack onset strain.[19]

Experimental

Materials

Low density polyethylene (LDPE) pellets were obtained from Dow. Poly(allylamine hydrochloride) (PAH) (Aldrich, M_n = 50,000-65,000), poly(sodium styrene sulfonate) (PSS) (Aldrich, M_n = 70,000), chromium (III) oxide (CrO_3)(Fisher, technical grade), sulfuric acid (Fisher, Certified ACS Plus grade), 16-mercaptohexadecanoic acid (Aldrich, 90%), and ethanol (Pharmco, USP grade) were used as received. Hexane (Fisher, HPLC grade) was deoxygenated by allowing nitrogen to

flow through it for 10 minutes. Water was purified using a Millipore Milli-Q® system that involves reverse osmosis followed by ion-exchange and filtration steps.

General Methods

LDPE films were made by compression molding pellets at 180°C in a Carver Laboratory Press Model Spec. 2624. Once the molding was completed, the films were immediately quenched in an ice bath to minimize crystallization. X-ray photoelectron spectra (XPS) were recorded on a Perkin-Elmer - Physical Electronics 5100 spectrometer with Al K_α excitation (15 kV, 400 W) at a take-off angle of 75° (between the plane of the sample surface and the entrance lens of the detector optics). Atomic concentration data were determined using sensitivity factors obtained from samples of known composition: C_{1s}, 0.200; O_{1s}, 0.501; N_{1s}, 0.352; S_{2p}, 0.540; Au_{4f}, 4.95. Contact angle measurements were made with a Ramé-Hart telescopic goniometer and a Gilmont syringe with a 24-gauge flat-tipped needle. Dynamic advancing (θ_A) and receding angles (θ_R) were recorded while the probe fluid (water, purified as described above) was added to and withdrawn from the drop, respectively. SEM micrographs were obtained with a JEOL-35CF scanning electron microscope at an acceleration voltage of 20 kV. AFM imaging was performed in air using a Digital Instruments Nanoscope IIIa AFM in the tapping mode™. LDPE film samples for mechanical testing, conforming to ASTM standard D 368-91 type V, are die cut using a Manual Punch Press, Model NAEF B-36. Mechanical tests were conducted using an Instron 5564 mechanical tester at a crosshead speed of 22 mm/min. Crack spacing was measured using the Zeiss Image Analysis program.

Surface Modification

Chromic Acid Oxidation. The chromic acid oxidation solution consisted of a 5 M CrO_3 in a 28 % (v/v) sulfuric acid solution. The solution was used at room temperature and the LDPE films were treated in these solutions for selected times. Afterwards, the films were removed from the chromic acid solution and were rinsed with Milli-Q water twice.

Gold Coating and Thiol Adsorption. LDPE films were gold coated using the Polaron Instruments SEM Coating Unit E5100 at 15 mAmps for 3 minutes. Afterwards, the coated films were rinsed in ethanol two times for 1 minute each and in hexane for 15 minutes. The rinsed gold-coated LDPE films were inserted into the thiol solution, prepared by saturating the deoxygenated hexane with the thiol, and allowed to react for 24 hours. Once the reaction was complete, the films were rinsed again in ethanol twice (1 minute each) and in hexane.

Polyelectrolyte Depositions

0.02 M PAH and 0.02 M PSS (concentrations based on repeat units) deposition solutions were prepared and adjusted to pH 2.9, by adding small amounts of dilute HCl and NaOH solutions and using a Fisher 825MP pH meter. For the surface modified samples, the pH of the first PAH adsorption solution was 8.0. The adsorption time for this layer was varied from 2 to 60 minutes. Alternating monolayers of PAH and PSS

were deposited onto the surface modified LDPE substrate by alternating submersions of the film samples in the polyelectrolyte solutions to build multilayer structures of up to 51 layers. Between the polyelectrolyte-depositions, the films were rinsed with three aliquots of water.

Results and Discussions

Surface Modifications

Chromic Acid Oxidation. LDPE films were submerged in chromic acid solution to generate carboxylic acid groups on the surface. The kinetics of the acid treatment were studied to find the optimal reaction time while at the same time minimizing the surface degradation. Reaction times from 1 minute to 20 minutes were examined. XPS analysis of these films shows that the atomic concentration of oxygen peaks between 2-5 minutes and decreases as the reaction time is increased further, likely due to the degradation of the LDPE (figure 4.12). Water contact angle results also show a similar trend as the advancing and receding contact angles decrease from 107°/76° to 93°/61° after 5 minutes (figure 4.13). Past 5 minutes, the water contact angle hysteresis increases which is likely caused by the increase in the roughness of the surface as a result of its degradation. Based on these results, LDPE films were treated for 5 minutes for incorporating carboxylic acid groups while at the same time minimizing the amount of surface roughening. LDPE films treated in this fashion will be abbreviated as LDPE-COOH.

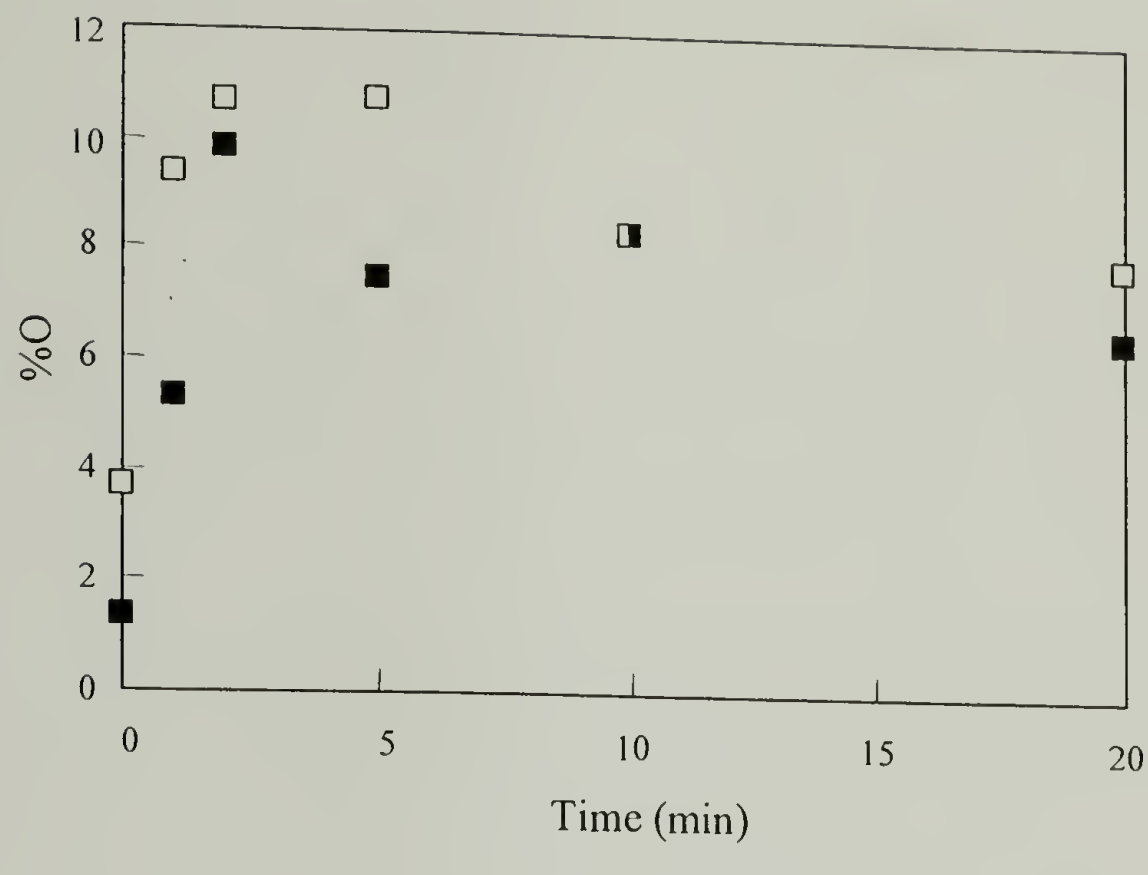

Figure 4.12. Atomic oxygen concentration of LDPE films as the chromic acid oxidation time is increased: open (□) and closed (■) symbols indicate 15° and 75° take-off angles, respectively

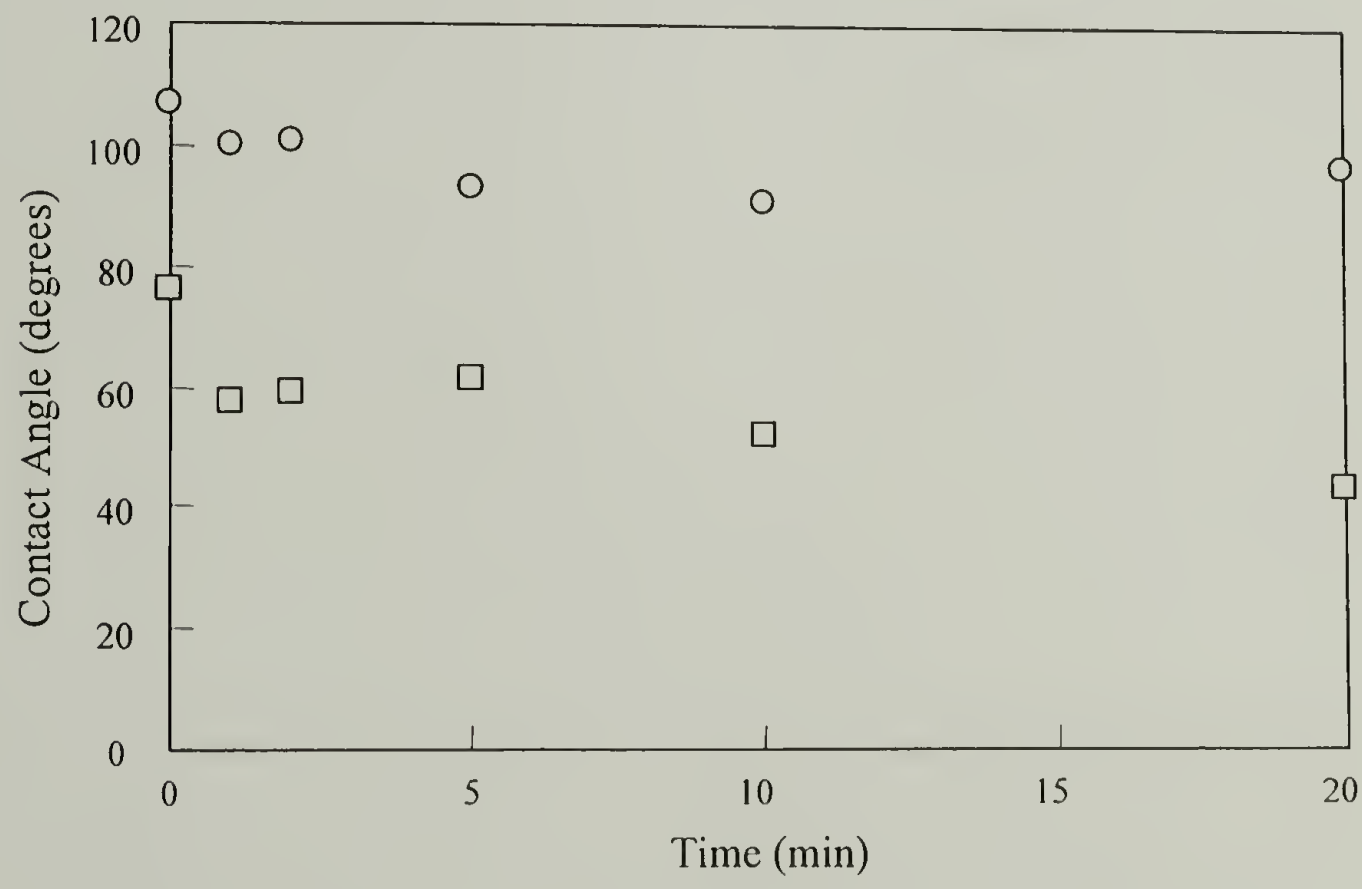

Figure 4.13. Advancing (○) and receding (□) contact angles for chromic acid oxidized LDPE as a function of treatment time.

Gold Coating and Thiol Adsorption. A thin gold coating was sputtered on LDPE in order to adsorb acid thiols. The thickness of the gold coating is estimated to be 75 nm after 3 minutes of sputtering time. XPS and contact angle analyses of gold coated LDPE films were not attempted due to the rapid contamination of gold surfaces. 16-Mercaptohexadecanoic acid was adsorbed on gold as in the reported literature for 24 hours.[40] XPS analysis of the gold-coated LDPE adsorbed with the acid thiol shows the presence of sulfur, carbon, oxygen, and gold. From the 75° take-off angle, the atomic ratios of these surfaces are comparable to the numbers that would be expected, but some carbonaceous materials are present as indicated by the higher elemental ratios (Table 4.1). Contact angle measurements also indicate the formation of the self-assembled monolayer as θ_A/θ_R decreases to 11.4°/0°, similar to a previous report on these surfaces.[41] LDPE films treated in this fashion will be abbreviated as LDPE-Au-S-x-COOH

Table 4.1. XPS results obtained at 75° take-off angle for the neat LDPE film and the gold-coated LDPE film with the acid thiol adsorbed.

Sample	%C	%O	%S	%Au	%C/%O	%C/%S	%O/%S
LDPE	98.7	1.3	0.0	0.0	75.9		
LDPE-Au-S-x-COOH	53.7	6.4	2.5	37.4	8.4	21.1	2.5

Polyelectrolyte Deposition

LDPE-COOH. The adsorption kinetics for the first layer PAH adsorption at pH 8 onto LDPE-COOH was examined for 2 to 60 minutes. Figure 4.14 shows that the atomic nitrogen concentration on the LDPE-COOH samples increases and reaches a maximum of 2.8/3.3 (15°/75° take-off angles) after 30 minutes. Dynamic contact angle measurements show little change for θ_A though θ_R decreases with adsorption time to from 62° to 35° after 30 minutes (shown in figure 4.15). From these results, adsorption times of 30 minutes were used for all polyelectrolyte adsorptions (including LDPE-Au-S-x-COOH samples).

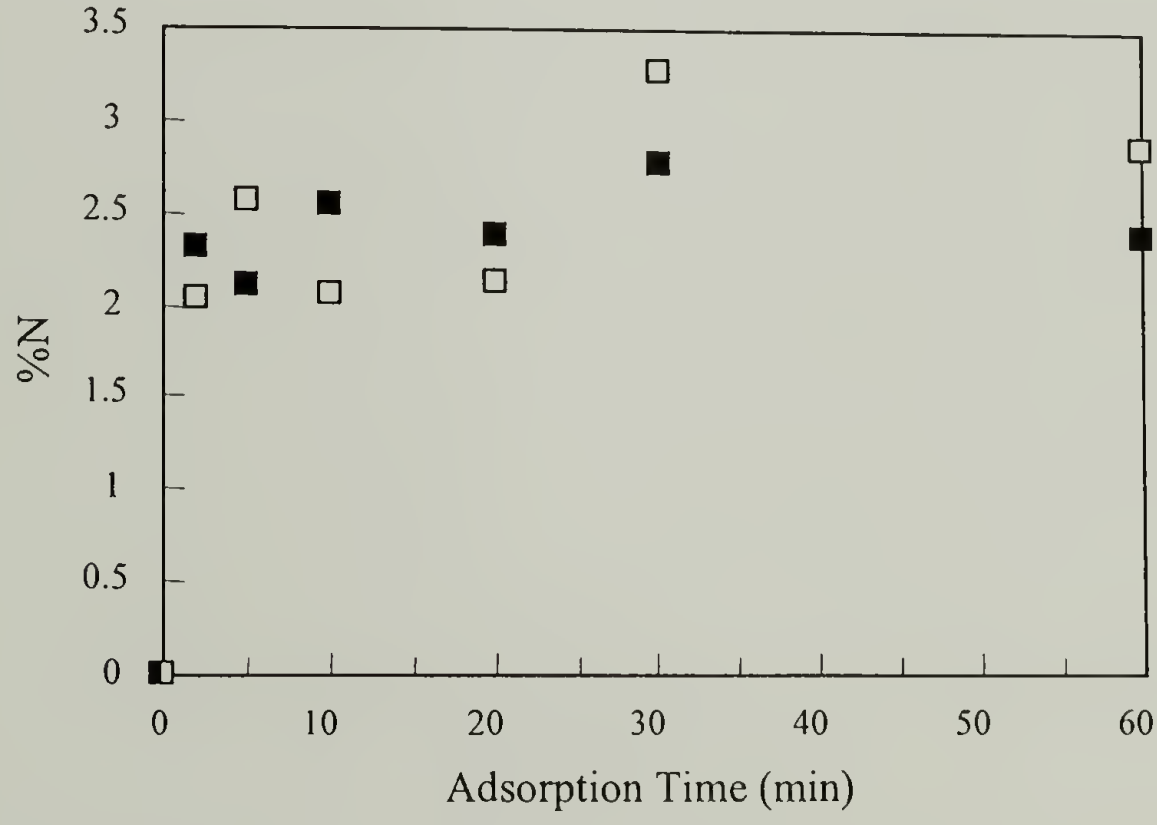

Figure 4.14. Atomic nitrogen concentration of LDPE-COOH films as PAH adsorption time is increased: open (□) and closed (■) symbols indicate 15° and 75° take-off angles, respectively

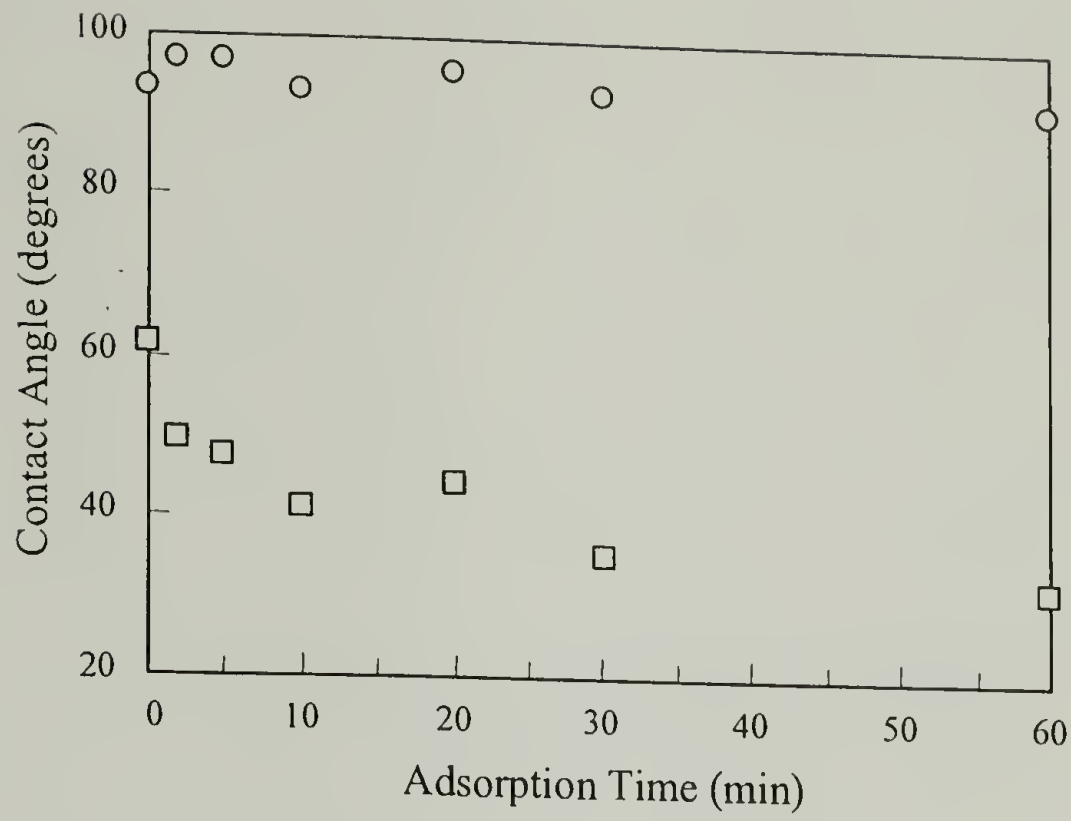

Figure 4.15. Advancing (○) and receding (□) contact angles for PAH adsorption onto LDPE-COOH as a function of treatment time.

Alternating deposition of PAH and PSS leads to multilayer assembly formation on LDPE-COOH. As in previous chapters, oscillations in the advancing contact angle measurements (figure 4.16) and in the nitrogen:sulfur ratios (figure 4.17) are observed, which indicate that the layers are stratified. Samples containing PAH as the top layer consistently exhibit higher advancing contact angles (lower wettability) than those with PSS as the outermost layer. An odd-even effect (in nitrogen:sulfur ratios) consistent with the composition of the outermost layer is observed for all samples except for the sample with 4 layers which has a slightly higher ratio. The stoichiometry of the assembly process is 2 ammonium ions per sulfonate ion indicated by the N:S ratio of ~2.

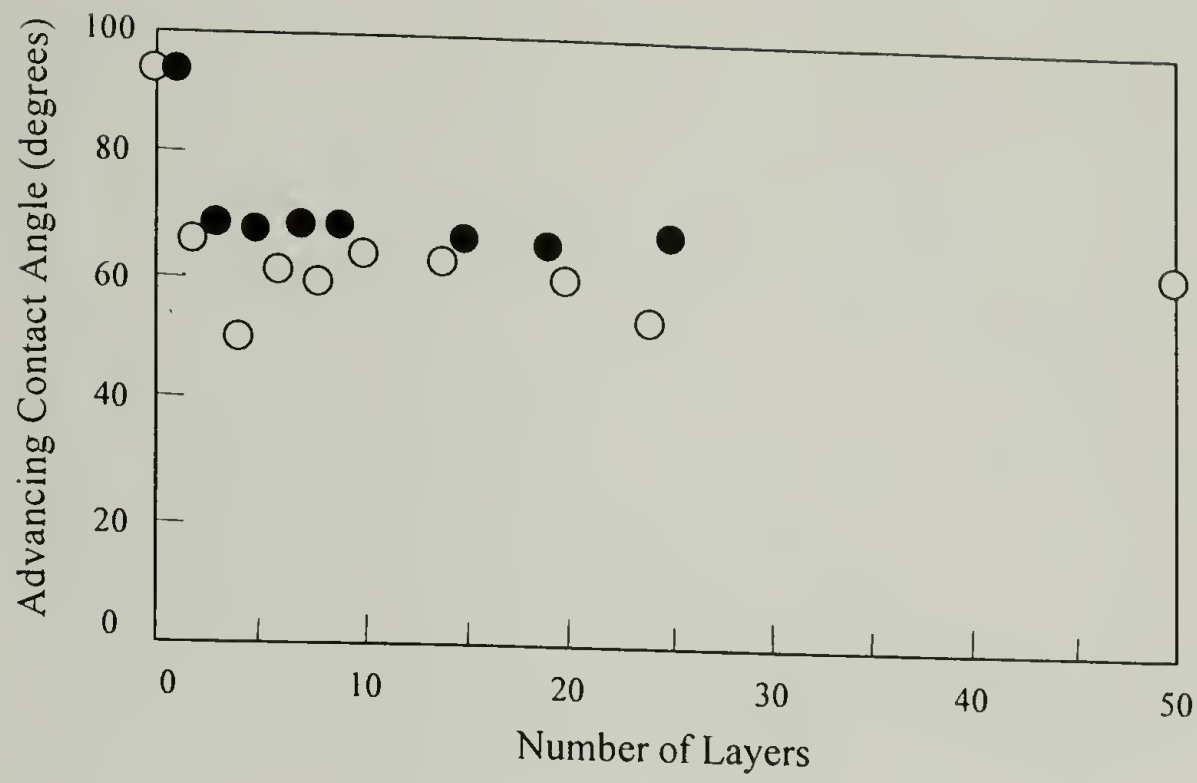

Figure 4.16. The advancing contact angle as a function of number of layers adsorbed on LDPE-COOH: closed (●) and open (○) symbols indicate an odd and even number of layers, respectively.

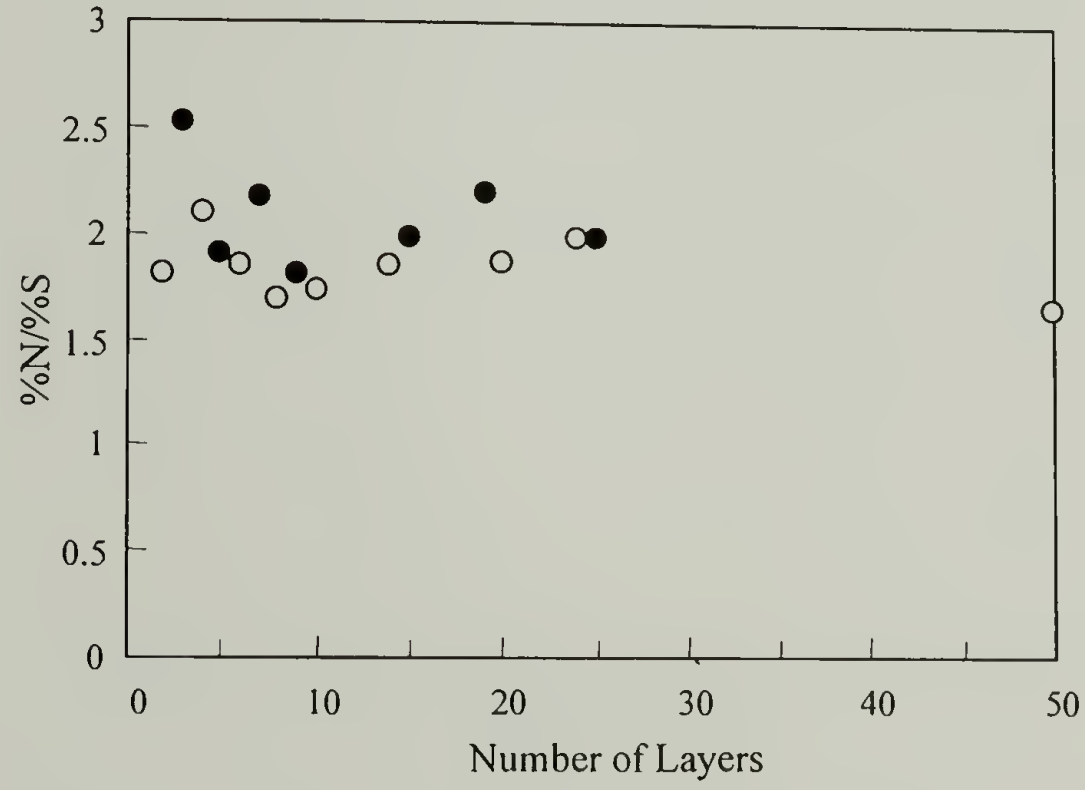

Figure 4.17. Nitrogen/sulfur ratio at 75° take-off angles as a function of the number of layers adsorbed onto LDPE-COOH: open (○) and closed (●) symbols indicate an even and odd number of layers, respectively.

LDPE-Au-S-x-COOH. As with LDPE-COOH, these samples are repeatedly immersed in alternating solutions of PAH and PSS for 30 minutes each to form multilayer assemblies. XPS analysis of LDPE-Au-S-x-COOH indicates the presence of ~37 atom % gold. Figure 4.18 shows the gold content, determined by XPS at 75° take-off angle, versus the number of layers deposited. This value decreases as the polyelectrolyte layers build up on top of the SAM and attenuate the gold signal. The 75° take-off angle data were used because we have measured a photoelectron mean free path in a series of $(PSS/PAH)_n$ samples at this angle and can use these data and this value to estimate individual layer thickness.[9,42,43] The average thickness of the individual layers is calculated using the gold XPS data (figure 4.16) plotted according to equation 2.1. Figure 4.19 shows a plot of $-\ln(N/N_O)\sin\theta$ versus n where N and N_O are the observed gold concentrations and the gold concentration after one layer was adsorbed, respectively. The slope of the line (z/λ - equation 2.1) is the average layer thickness divided by the Au_{4f} photoelectron mean free path; this analysis indicates that the average layer thickness is ~0.3λ. This is the average thickness of layers 2-5; the first PAH layer was thicker than the others and was not included in the analysis because it would have biased the average high. Leväsalmi measured a mean free path of 20Å for the Mg K_α-excited Si_{2p} electron in a $(PAH/PSS)_n$ assembly supported on a silicon wafer using XPS (75° take-off angle) and X-ray reflectivity data[9] and we can use this value to calculate[44] a mean free path of 24.4 Å for the Al K_α-excited Au_{4f} photoelectron. Assuming that the electron mean free path in LDPE-Au-S-x-COOH-supported $(PAH/PSS)_n$ is the same as that determined for Si-supported $(PAH/PSS)_n$, the average layer thickness is 7.0 Å.

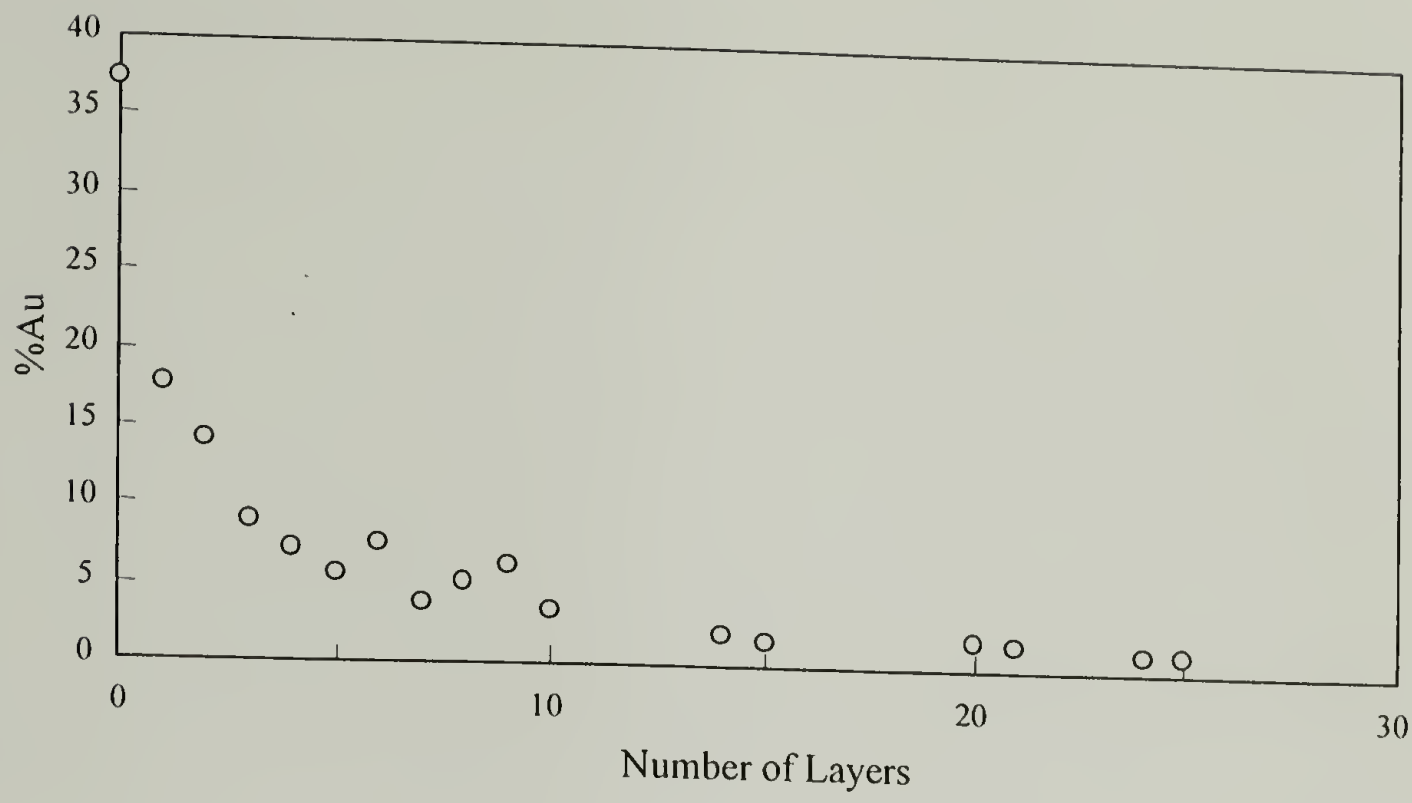

Figure 4.18. The attenuation of gold at 75° take-off angles as PAH/PSS bilayers are adsorbed onto LDPE-Au-S-x-COOH.

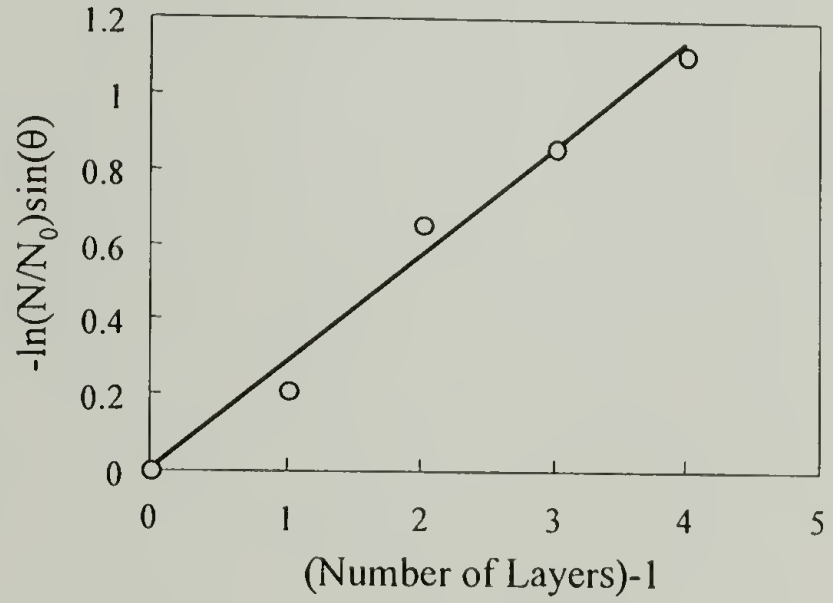

Figure 4.19. Plot of $-\ln(N/N_o)\sin\theta$ vs. number of layers in the PAH/PSS multilayer film.

As in the previous section, pronounced odd-even effects are observed in the surface composition and in the wettability. Nitrogen:sulfur ratios oscillate between relatively high values when PAH is the outermost layer and relatively low values when PSS is top-most with exceptions for samples with 10,14, and 24 layers (figure 4.20). The

first 8-9 layers are either highly stratified or very thick as the amplitude of the oscillations is great. This may be due to the high surface charge present on the SAM. After 9 layers, the amplitude of the oscillations is lower implying that there is greater interpenetration of the layers or that the layers are thinner. Some degree of scatter in the data is expected due to the fact that separate samples (each prepared by multistep procedures) are used for analysis of each multilayer assembly; samples were not reused as substrates for additional layer adsorption after analysis. Similar to layers formed on LDPE-COOH, the N:S ratio data converge to ~2 indicating that the stoichiometry of the assembly process is 2 ammonium ions per sulfonate ion. Water contact angle data (figure 4.21) show a pronounced odd-even trend that is consistent across the series of samples (2, and 8-layer samples are anomalous) with samples containing PSS as the top layer exhibiting greater wettability than those with PAH as the outermost layer.

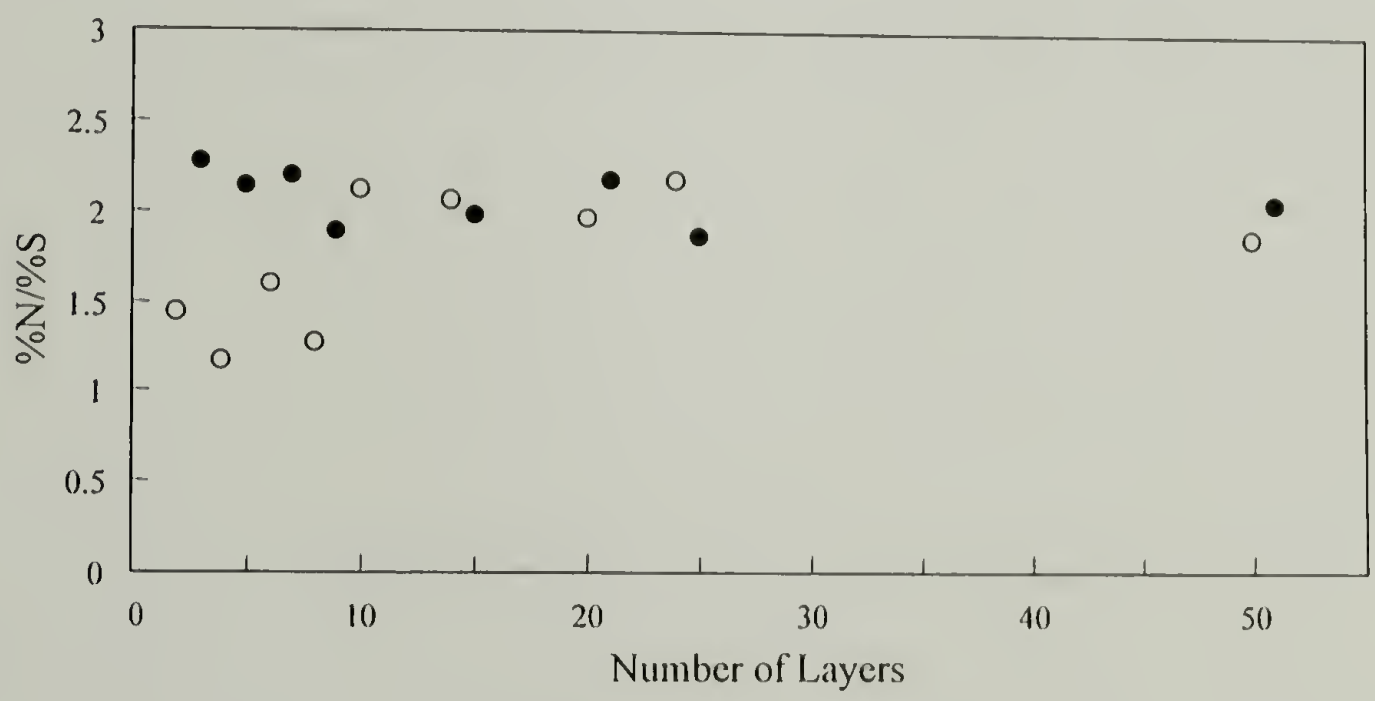

Figure 4.20. Nitrogen/sulfur ratio at 75° take-off angles as a function of the number of layers adsorbed onto LDPE-Au-S-x-COOH: open (○) and closed (●) symbols indicate even and odd layers, respectively.

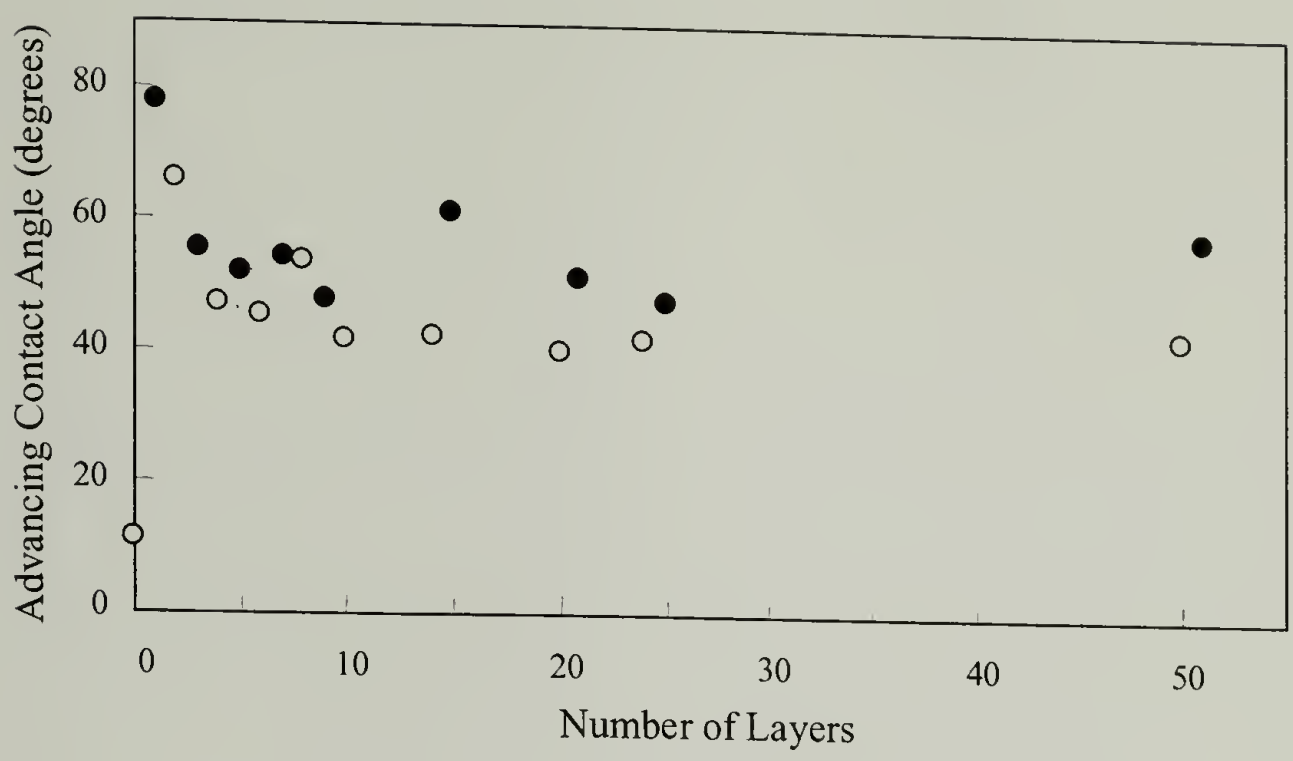

Figure 4.21. Advancing contact angle measurements on LDPE-Au-S-x-COOH as PSS/PAH polyelectrolytes are adsorbed: closed (●) and open (○) symbols indicate an odd and even number of layers, respectively.

Fracture of L-by-L Assemblies

LDPE-COOH. LDPE-COOH films and those with 50 layers adsorbed are strained at various levels and afterwards examined using AFM and SEM (SEM micrographs are shown in figure 4.22 and 4.23). LDPE-COOH films are featureless except for isolated buckling observed under 15% strain. The same features are observed for LDPE-COOH films with 50 layers at 4%, 8%, and 15% strain. This buckling may be due to some compressive forces on the films. At 50% and 100% strain, the films with the multilayer assemblies appear smooth even at high magnification (10,000 times). Cracks due to the fragmentation of the L-by-L assembly are observed for a sample strained at 150% under the same magnification. The mean crack spacing is measured at 0.50 μm. AFM analysis

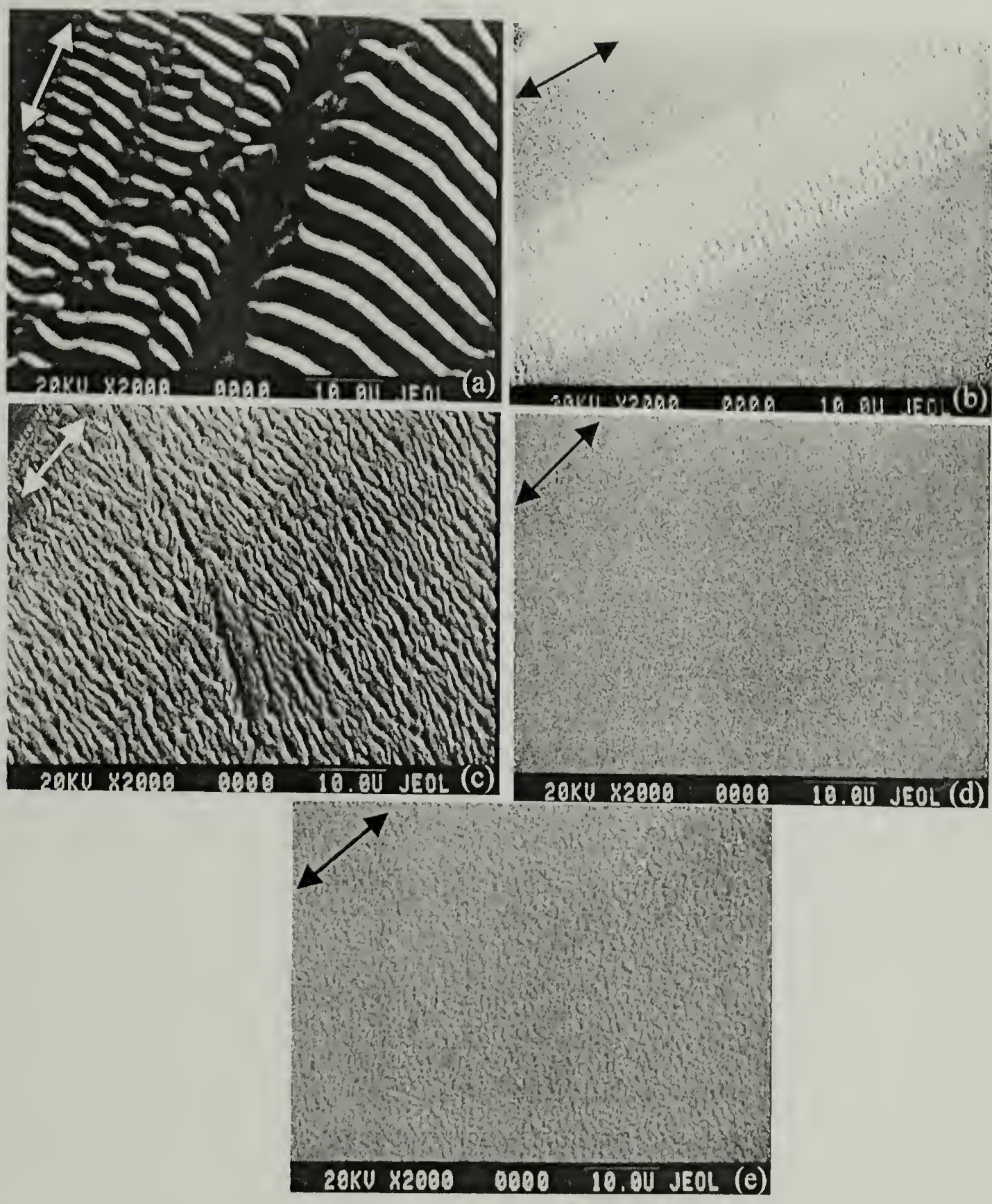

Figure 4.22. SEM micrographs (2000x) of strained LDPE-COOH films and LDPE-COOH films with 50 layers adsorbed. (a) LDPE-COOH at 15% strain showing isolated regions of buckling. (b) and (c) show isolated buckling of LDPE-COOH films with 50 layers at 4% and 15% strain, respectively. (d) LDPE-COOH film with 50 layers adsorbed at 100% strain showing no features. (e) Cracks appear in the LDPE-COOH film with 50 layers at 150% strain. The arrows indicate the direction of deformation.

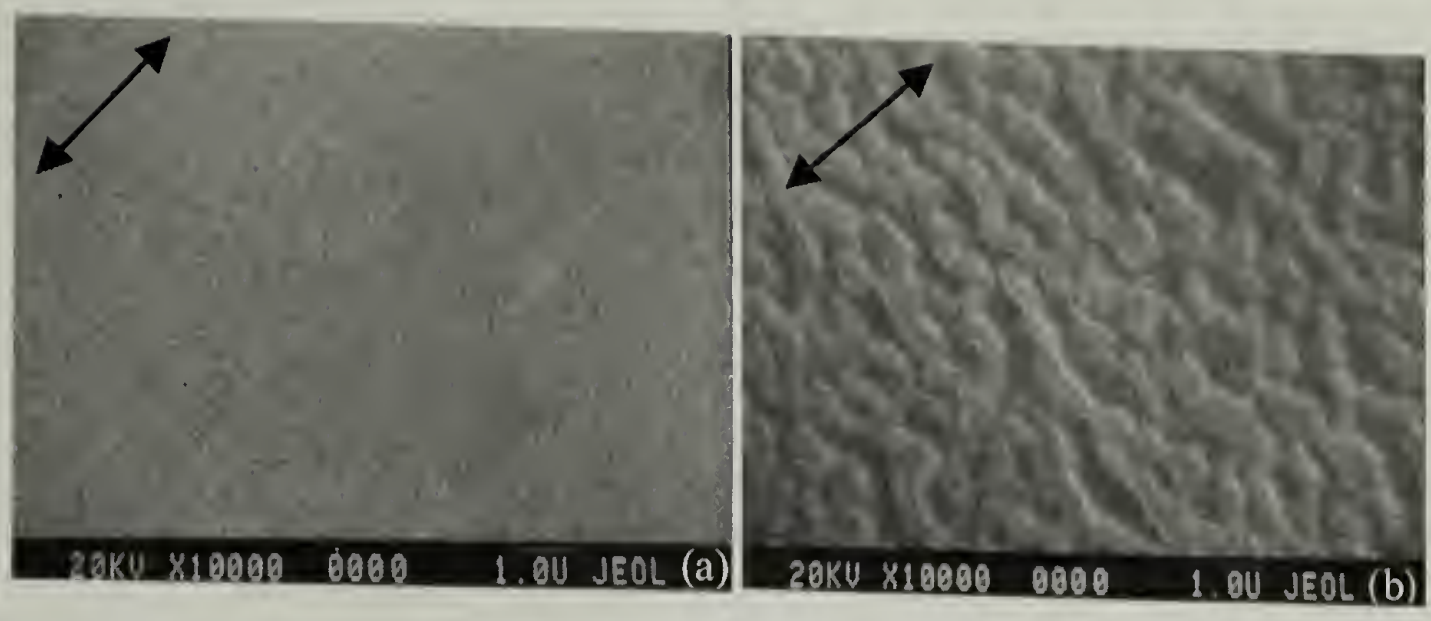

Figure 4.23. SEM micrographs (10,000x) of LDPE-COOH with 50 layers adsorbed. (a) Strained at 100%. (b) Strained at 150% showing the L-by-L assembly cracking. The arrows indicate the deformation direction.

of the height of the cracks allows the thickness of the multilayer films to be approximated at 15 nm. The work of adhesion of the L-by-L assembly to LDPE-COOH, calculated using equations (4.4) through (4.6) is at least 370±50 mJ/m^2. This is a lower estimate since the assembly would delaminate if this energy were surpassed. This number is obtained by using the measured modulus for the L-by-L assembly of 8.8 GPa, the strain to break of 2.5%, and the measured modulus for LDPE of 154 MPa.

LDPE-Au-S-x-COOH. LDPE-Au-S-x-COOH films and those with multilayer assemblies were also strained (up to 50%) and afterwards analyzed using AFM and SEM (SEM micrographs are shown in figure 4.24). Cracks due to the fragmentation of the gold layer appear in LDPE-Au-S-x-COOH film after 25% strain. This is an ominous result since cracks due to the L-by-L assembly would have to occur before reaching 25% strain in order to measure the adhesion strength. As seen in the SEM micrographs, cracks

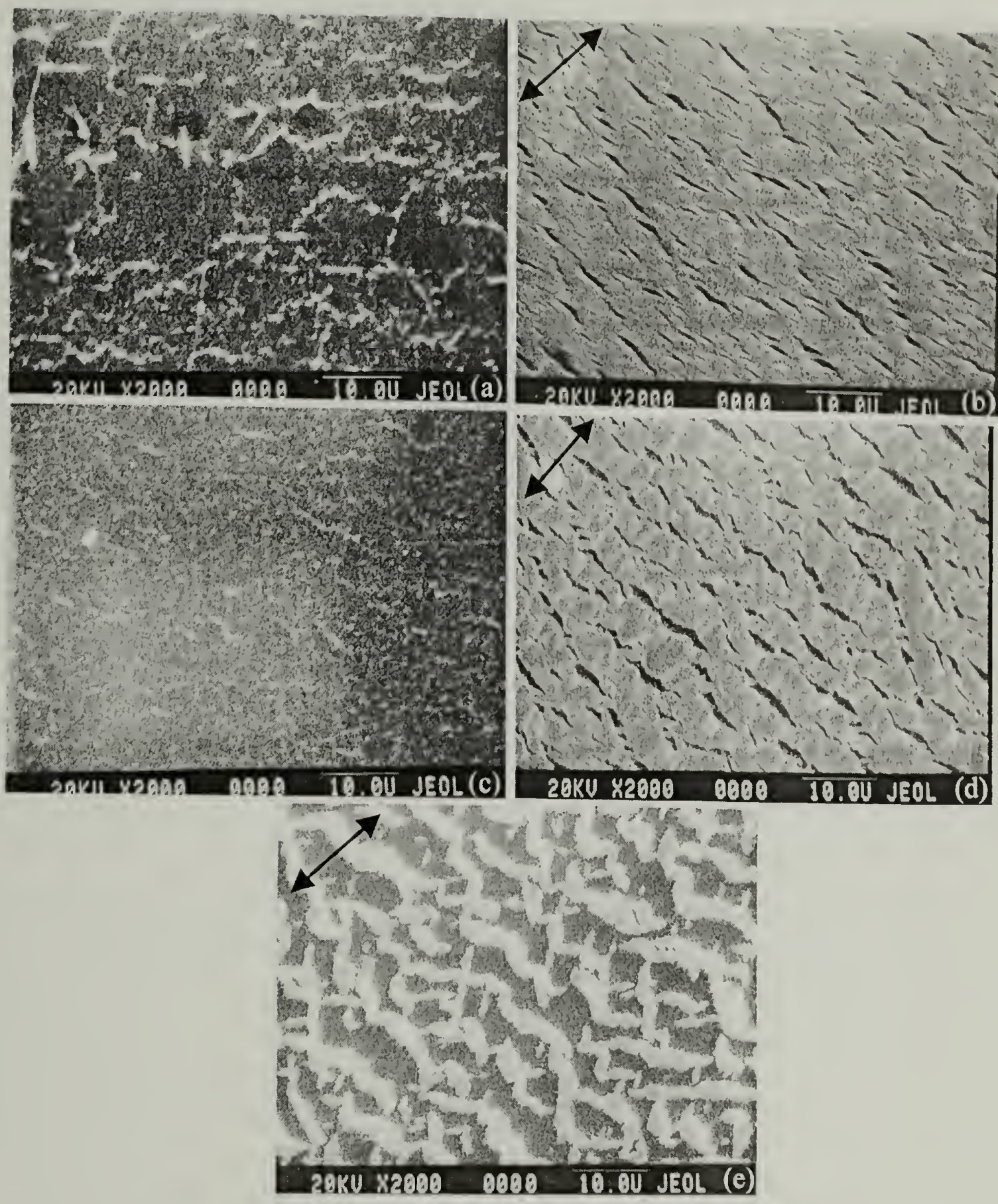

Figure 4.24. SEM micrographs (2000x) of LDPE-Au-S-x-COOH films and LDPE-Au-S-x-COOH films with 50 layers adsorbed. (a) and (b) show LDPE-Au-S-x-COOH films at 4 and 25% strain, respectively. (c), (d), and (e) show LDPE-Au-S-x-COOH films with 50 layers adsorbed at 4%, 25%, and 50% strain, respectively. Arrows indicate the direction of deformation.

were not observed until reaching 25% strain. This implies that the adhesion strength of the L-by-L assembly to the functionalized gold surface is greater than that of the gold to the LDPE substrate. The thickness of the gold/L-by-L assembly is determined to be 105 nm using AFM. The work of adhesion of gold to LDPE is calculated to be 120 mJ/m^2 using σ_{max}=160 MPa and E=80 GPa for the gold. The work of adhesion of the L-by-L assembly is greater than this number and should be higher than that obtained for the LDPE-COOH due to the higher surface charge density on this substrate.

Lycra-NH_3^+. The SEM micrograph (figure 3.19d) obtained from the deformation of the Lycra-NH_3^+ yarns adsorbed with 50 layers is analyzed as a comparison. The mean crack spacing of this L-by-L assembly is 0.94 μm. Following the same analysis as the previous two examples, the work of adhesion of the L-by-L assembly on Lycra-NH_3^+ is 200±20 mJ/m^2. This result may imply that the charge density on this substrate may be lower than that of LDPE-COOH. This is very likely as the atomic nitrogen and the atomic sulfur concentrations of LDPE-COOH-supported samples are higher than those of Lycra-NH_3^+ after a few layers are adsorbed, which implies greater concentration of ammonium ions and sulfonate ions on LDPE-COOH.

Conclusions

LPDE films were modified using two methods (chromic acid oxidation and gold coating followed by 16-mercaptohexadecanoic acid adsorption) to form substrates with different concentrations of carboxylic acid functionalities for the adsorption and formation of polyelectrolyte multilayer assemblies. XPS analysis and water contact angle measurements show that polyelectrolytes adsorb to form multilayer assemblies; the stoichiometry of the assembly process for both substrates is 2 ammonium ions per sulfonate ion. In the case of LDPE-Au-S-x-COOH and the samples with the multilayer assemblies on this substrate, the gold layer fractures before the assembly and the work of adhesion of the gold to LDPE is estimated to be 120 mJ/m^2. The LDPE-COOH films adsorbed with 50 layers initially buckle in isolated areas due to some compressive forces. Upon reaching 150% strain, the layers fracture and the adhesion energy of the assembly to LDPE-COOH is calculated to be 370±50 mJ/m^2. This number is higher than that calculated for the 50 layer assembly on Lycra-NH_3^+ (200±20 $mJ/m^{2)}$). This is likely due to higher surface charge on the LDPE-COOH samples as observed by the higher atomic nitrogen and atomic sulfur content. It should be noted that these values are conservative estimates as the layers are still adhered to the surface. These values compare favorably with those reported for other systems (W(PMMA/$SiO_{2)}$=225 mJ/m^2 and W(CVD glass/PET)=220 mJ/m^2). The adhesion of the L-by-L system is enhanced by having greater surface charge on the starting substrate.

Notes and References

(1) Ferreira, M.; Rubner, M.F. *Macromolecules* **1995**, *28*, 7107.

(2) Fou, A.C.; Rubner, M.F. *Macromolecules* **1995**, *28*, 7115.

(3) Onda, M.; Lvov, Y.; Ariga, K.; Kunitake, T. *J. Ferment. Bioeng.* **1996**, *82*, 502.

(4) Laschewsky, A.; Bayer, B.; Wischerhoff, E.; Arys, X.; Bertrand, P.; Delacorte, A.; Jonas, A. *Thin Solid Films* **1996**, *284*, 334.

(5) Ferreira, M.; Rubner, M.F.; Hsieh, B.R. *Mat. Res. Soc. Proc. Symp.* **1995**, *369*, 575.

(6) Onoda, M.; Yoshino, K. *Jpn. J. Appl. Phys.* **1995**, *34*, L260.

(7) Stepp, J.; Schlenoff, J.B. *J. Electrochem. Soc.* **1997**, *144*, L155.

(8) Hammond, P.T.; Whitesides, G.M. *Macromolecules* **1995**, *28*, 7569.

(9) Leväsalmi, J.-M.; McCarthy, T.J. *Macromolecules* **1997**, *30*, 1752.

(10) Cox, H.L. *Br. J. Appl. Phys.* **1952**, *3*, 72.

(11) Kelly, A.; Tyson, W.R. *J. Mech. Phys. Solids* **1965**, *13*, 329.

(12) Fraser, W.A.; Ancker, F.H., DiBenedetto, A.T., Elbirli, B. *Polymer Composites* **1983**, *4(4)*, 238.

(13) Nardin, M.; Asloun, E.M.; Schultz, J. *Polym. Adv. Technol.* **1991**, *2*, 115.

(14) Nardin, M.; Schultz, J. *Compos. Interfaces* **1993**, *1*, 177.

(15) Agrawal, D.C.; Raj, R. *Acta. Metall.* **1989**, *37*, 1265.

(16) Leterrier, Y.; Wyser, Y.; Månson, J.-A.E.; Hilborn, J. *J. Adhesion* **1994**, *44*, 213.

(17) Leterrier, Y.; Månson, J.-A.E. *J. Mater. Sci. Letters* **1997**, *16*, 120.

(18) Leterrier, Y.; Boogh, L.; Andersons, J.; Månson, J.-A.E. *J. Polym. Sci. Part B: Polym. Phys.* **1997**, *35*, 1449.

(19) Leterrier, Y.; Andersons, J.; Pitton, Y.; Månson, J.-A.E. *J. Polym. Sci. Part B: Polym. Phys.* **1997**, *35*, 1463.

(20) Blais, P.; Carlsson, D.J.; Csullog, G.W.; and Wiles, D.M. *J. Coll. Interf. Sci.*, **1974**, *47*, 636.

(21) Rasmussen, J.R.; Stedronsky, E.R.; Whitesides, G.M. *J. Am. Chem. Soc.* **1977**, *99*, 4736.

(22) Wiberg, K.B.; Eisenthal, R. *Tetrahedron* **1964**, *20*, 1151.

(23) Holloway, F.; Cohen, M.; Westheimer, F.H. *J. Am. Chem. Soc.* **1951**, *73*, 65.

(24) Sager, W.F. *J. Am. Chem. Soc.* **1956**, *78*, 649.

(25) DeBono, R.F.; Loucks, G.D.; Manna, D.D.; Krull, U.J. *Can. J. Chem.* **1996**, *74*, 677.

(26) Caruso, F.; Niikura, K.; Furlong, D.N.; Okahata, Y. *Langmuir* **1997**, *13*, 3422.

(27) Porter, M.D.; Bright, T.B.; Allara, D.L.; Chidsey, C.E.D. *J. Am. Chem. Soc.* **1987**, *109*, 3559.

(28) Smithson, R.L.W.; McClure, D.J.; Evans, D.F. *Thin Solid Films* **1997**, *307*, 110.

(29) Ulman, A.; Eilers, J.E.; Tillman, N. *Langmuir* **1989**, *5*, 1147.

(30) Laibinis, P.; Whitesides, G.M.; Allara, D.L.; Tao, Y.-T.; Parikh, A.N.; Nuzzo, R.G. *J. Am. Chem. Soc.* **1991**, *113*, 7152.

(31) Dubois, L.H.; Zegarski, B.R.; Nuzzo, R.G. *J. Chem. Phys.* **1993**, *98(1)*, 678.

(32) Bigelow, W.C.; Pickett, D.L.; Zisman, W.A. *J. Colloid Interface Sci.* **1946**, *1*, 513.

(33) Hammond, P.T.; Whitesides, G.M. *Macromolecules* **1995**, *28*, 7569.

(34) Chidsey, C.E.D.; Loiacono, D.N. *Langmuir* **1990**, *6*, 682.

(35) Fraser, W.A., Ancker, F.H., DiBenedetto, A.T., Elbirli, B. *Polymer Composites* **1983**, *4(4)*, 238.

(36) Hu, M.S.; Evans, A.G. *Acta. Metall.* **1989**, *37*, 917.

(37) Wojciechowski, P.H.; Mendolia, M.S. *J. Vac. Sci. Technol. A* **1989**, *7(3)*, 1282.

(38) Kimber, A.C.; Keer, J.G. *J. Mater. Sci. Letters* **1982**, *1*, 353.

(39) Fowkes, F.M.; Dwight, D.W.; Cole, D.A.; Huang, T.C. *J. Non-Cryst. Sol.* **1990**, *120*, 47.

(40) Dubois, L.H.; Zegarski, B.R.; Nuzzo, R.G. *J. Am. Chem. Soc.* **1990**, *112*, 570.

(41) Laibinis, P.E. ; Whitesides, G.M. *J. Am. Chem. Soc.* **1992**, *114*, 1990.

(42) Chen, W.; McCarthy, T.J. *Macromolecules* **1997**, *30*, 78.

(43) Phuvanartnuruks, V.; McCarthy, T.J. *Macromolecules* **1998**, *31*, 1906.

(44) Andrade, J. D. *Surface and Interfacial Aspects of Biomedical Polymers, Surface Chemistry and Physics;* Plenum Press: New York, 1985; Vol. 1, p 180.

APPENDIX A

EXTRANEOUS PLASMA CHEMISTRY INFORMATION

Plasma Reactor Setup

The electronics of the plasma reactor are described in figure A.1 with the components labeled. The transceiver, power supply, and the versatuner were purchased from Lentini Communications. The coaxial cables, the connectors, the push button switch, and the SWR tester were obtained from Radio Shack. Special connections from the coaxial cable to the components were made by the electricians and a schematic is shown in figure A.2.

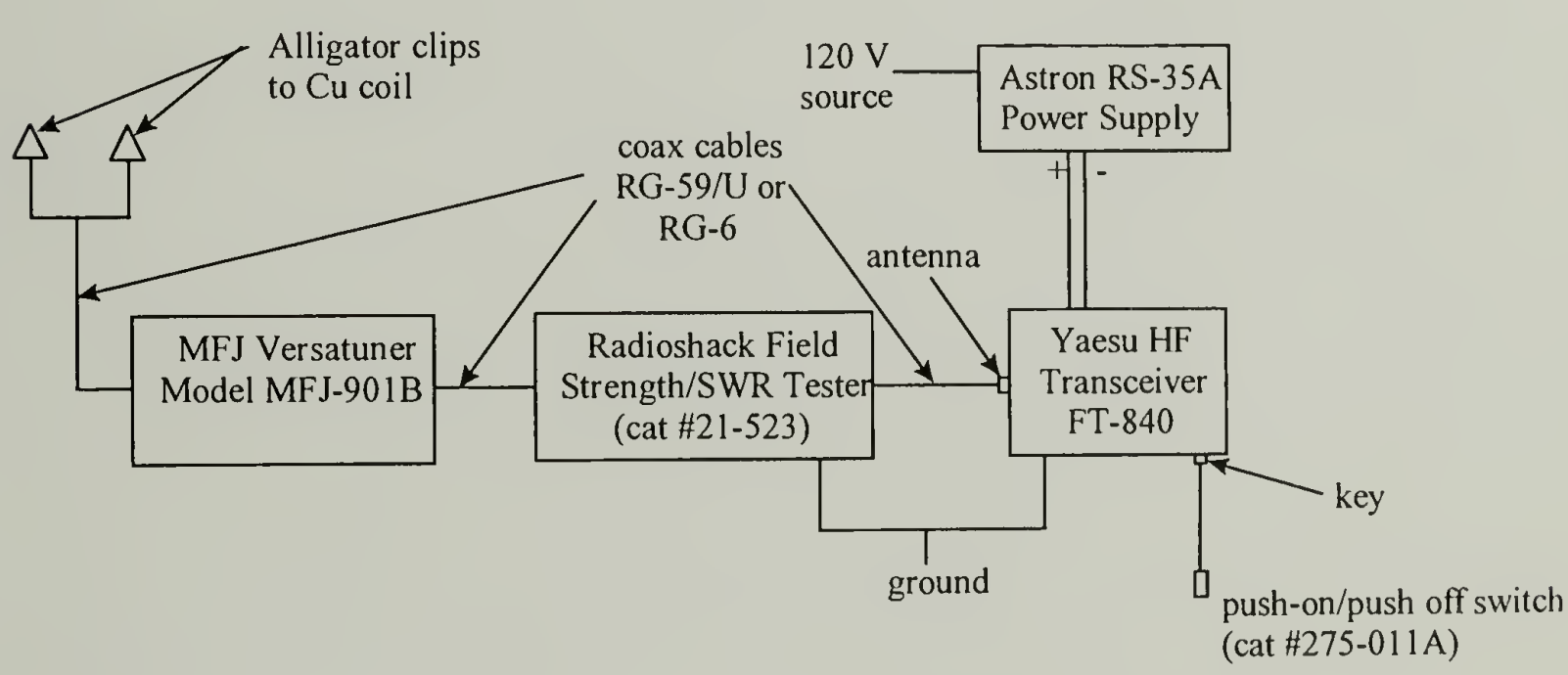

Figure A.1. Schematic of the plasma reactor setup.

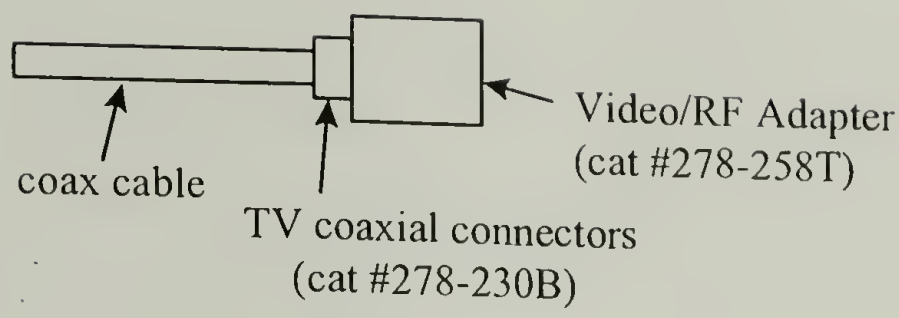

Figure A.2. Schematic of the connection at the end of the coaxial cable.

Plasma Reactor Operation

The general operating procedures for the plasma reactor are as follows: (1) Evacuate the chamber for a set time. (2) Introduce the plasma gas and let the pressure equilibrate to the desired value. (3) Measure the flow rate of the gas by closing the reactor to the vacuum pump and timing the period required to reach a certain pressure. (4) Adjust the flow rate until the desired flow rate is achieved (and at the same time keeping the pressure at the desired level). The vacuum may have to be choked off. (5) Let the gas flow through the reactor to "saturate" the reactor with the gas. (6) Turn on the reactor and "zap" the reactor with a Zerostat. At this point, the gas in the reactor should have a glow; the color of the glow depends on the elemental composition of the gas. (7) Minimize the percentage of the reflected power indicated in the SWR tester by changing the antenna (fine) and transmitter (coarse) setting on the versatuner (inductance should be at "B"). Calibrate the SWR tester after every adjustment. (8) Once the reaction is completed, turn the reactor off and let the gas flow for a few minutes to terminate any reactive groups at the surface. (9) Evacuate the sample chamber of the gas, repressurize the chamber, and remove the samples.

Bond and Ionization Energies

Table A.1. Dissociation energy for typical bonds and some common gases.

Bond/Gas	Dissociation Energy (eV)
C–C	3.61
C=C	6.35 (2.74 for π bond)
C–H	4.30
C–N	3.17
C=N	9.26
C–O	3.74
C=O	7.78
C–F	5.35
C–Cl	3.52
N–H	4.04
O–H	4.83
O–O	1.52
H_2	4.5
N_2	9.8
O_2	5.1

Table A.2. Ionization energy of noble and diatomic gases.

Gas	Ionization Energy (eV)
He	24.6
Ne	21.6
Ar	15.8
Kr	14.0
Xe	12.1
H_2	15.6
N_2	15.5
O_2	12.5

APPENDIX B

POLYELECTROLYTE SOLUTIONS AS AN ALTERNATIVE PROBE FLUID FOR CONTACT ANGLE MEASUREMENTS

Introduction

In the main section of the thesis, the probe fluid used in measuring the contact angles of surfaces was Milli-Q water. For all cases, differences in the contact angles (mostly advancing) were found indicating PSS surfaces have lower advancing contact angles than those of PAH surfaces. In most experiments, the differences between the two are significant but there are a few that are questionable. A few experiments were conducted to determine if the differences in the contact angle measurements can be enhanced by using a different probe fluid, namely a polyelectrolyte solution. It was suspected that a polyelectrolyte solution used as a probe fluid will have different values as the polyelectrolytes in the fluid will be either attracted to the surface or repelled from the surface depending on the charge present on the surface. The thought was that if PSS was the probe fluid used, surfaces with PAH as the top layer would have lower advancing contact angles (compared to water) while those with PSS as the top layer would have higher advancing contact angles.

Experimental

The materials and characterization techniques used are described as in the previous sections (see chapter 2 and chapter 4). Additionally, dynamic advancing (θ_A) and receding angles (θ_R) were recorded while the probe fluid (Milli-Q water, PSS solution, and PAH solution) was added to and withdrawn from the drop, respectively. PSS and PAH solutions were prepared in the same manner as those used for the adsorption solutions. The PSS solutions are at pH=2.9 and PAH solutions are at pH=8.

Results

^{10}PTFE-NH_3^+

Two samples were selected from these modified substrates and a number of layers were deposited on them (19 and 20 layers). The results from the contact angle measurements are shown and compared in table B.1. From these results, it can be seen that the differences in contact angle values can be enhanced when a polyelectrolyte solution is used as the probe fluid. The differences in the advancing contact angle between the 19th and 20th layer increased from 7° to 19° when the probe fluid is changed from water to PSS solution.

LDPE-COOH

Another example of the usefulness of using a polyelectrolyte solution as a probe fluid is shown for these samples. After treating LDPE samples with chromic acid for 5 minutes, advancing and receding water contact angles decrease from 107°/76° to 93°/61.4°; this implies that the surface is more hydrophilic and that acid groups may have been produced on the surface. Using PAH solution (pH=8) for the probe fluid gives similar results for the advancing contact angle (98° as compared to 107° on a virgin sample) but a dramatically lower receding contact angle (25.4° as compared to 67° on a virgin sample). The lower receding contact angle is believed to be due to the adsorbed PAH, as PAH (and other polyelectrolytes) exhibit low receding contact angle results. As the PAH solution is being added to the surface, PAH adsorbs onto the surface and changes the nature of the surface such that the receding values are akin to those of a hydrophilic surface.

Table B.1. Dynamic contact angle measurements for 19 and 20 layers on $^{10}PTFE\text{-}NH_3^+$ using PSS solution and Milli-Q water as probe fluids.

	Milli-Q Water		PSS Solution (pH=2.9)	
Sample	θ_A	θ_R	θ_A	θ_R
$^{10}PTFE\text{-}NH_3^+\text{-}(PSS/PAH)_9PSS$	57.0	5.0	74	4.3
$^{10}PTFE\text{-}NH_3^+\text{-}(PSS/PAH)_{10}$	64.1	4.7	55.5	4.3

Summary

Based on the experiments that have been conducted, it appears that polyelectrolyte solutions are good probe fluids for charged surfaces. The differences in advancing contact angle for a 19 layer sample and a 20 layer sample are 19° when the probe fluid is changed from water to PSS solution. For LDPE-COOH, the receding contact angle decreases to 25.4° for PAH solution which indicates that PAH adsorbs during the advancing process and results in receding contact angle data similar to that for other surfaces with polyelectrolytes adsorbed.

APPENDIX C

ADDITIONAL DATA FOR CHAPTER 2

Results of Adhesion Test

Peel tests were conducted on allylamine plasma-treated (10 W and 50 W) PTFE and XPS analysis was used to find the locus of failure. The results are summarized in table C.1 and shows that nitrogen from the plasma polymer was not transferred to the tape. Instead, the nitrogen content decreased, indicating that the failure occurs in the adhesive. The plasma polymer has good adhesion to PTFE at both conditions tested.

Table C.1. XPS (15° take-off angle) results for the peel test of plasma polymerized allylamine on PTFE.

Sample	Before/After Peel Test	%C	%O	%N
Tape	Before	82.8	17.2	0.0
	After $^{10}PTFE\text{-}NH_3^+$	79.2	18.7	0.0
	After $^{50}PTFE\text{-}NH_3^+$	85.5	14.5	0.0
$^{10}PTFE\text{-}NH_3^+$	Before	73.0	6.8	15.4
	After	79.8	7.5	12.7
$^{50}PTFE\text{-}NH_3^+$	Before	77.6	2.6	18.3
	After	80.4	6.3	13.3

^{10}PTFE-NH_3^+

Table C.2. Atomic composition at 15° take-off angle as layers are deposited.

Sample	%F	%C	%O	%N	%S
^{10}PTFE-NH_3^+	4.82	72.98	6.81	15.4	0.0
^{10}PTFE-NH_3^+-PSS	1.26	72.64	13.91	10.5	1.7
^{10}PTFE-NH_3^+-(PSS/PAH)	0	80.62	8.74	8.73	1.9
^{10}PTFE-NH_3^+-(PSS/PAH)PSS	3.14	70.15	17.53	7.29	1.89
^{10}PTFE-NH_3^+-$(PSS/PAH)_2$	6.97	68.45	15.33	7.44	1.8
^{10}PTFE-NH_3^+-$(PSS/PAH)_2$PSS	3.42	75.11	12.82	6.39	2.27
^{10}PTFE-NH_3^+-$(PSS/PAH)_3$	2.2	76.37	12.32	6.59	2.52
^{10}PTFE-NH_3^+-$(PSS/PAH)_3$PSS	0.61	74.71	15.76	5.99	2.93
^{10}PTFE-NH_3^+-$(PSS/PAH)_4$	2.12	73.19	15.8	6.24	2.65
^{10}PTFE-NH_3^+-$(PSS/PAH)_4$PSS	1.36	73.47	17.12	5.55	2.5
^{10}PTFE-NH_3^+-$(PSS/PAH)_5$	2.43	75.75	12.9	6.34	2.58
^{10}PTFE-NH_3^+-$(PSS/PAH)_5$PSS	1.96	72.5	16.28	6.28	2.98
^{10}PTFE-NH_3^+-$(PSS/PAH)_6$	1.55	72.92	17.93	5.18	2.42
^{10}PTFE-NH_3^+-$(PSS/PAH)_6$PSS	0.67	72.76	18.34	5.24	2.99
^{10}PTFE-NH_3^+-$(PSS/PAH)_7$	1.29	72.91	18.17	4.83	2.8
^{10}PTFE-NH_3^+-$(PSS/PAH)_7$PSS	0.84	73.17	18.02	5.07	2.9
^{10}PTFE-NH_3^+-$(PSS/PAH)_8$	2.09	72.71	18.01	4.43	2.76
^{10}PTFE-NH_3^+-$(PSS/PAH)_8$PSS	1.86	72.3	18.44	4.36	3.04
^{10}PTFE-NH_3^+-$(PSS/PAH)_9$	3.44	73.36	15.65	4.84	2.7
^{10}PTFE-NH_3^+-$(PSS/PAH)_9$PSS	0.74	72.4	18.76	5.18	2.91
^{10}PTFE-NH_3^+-$(PSS/PAH)_{10}$	0.56	73.44	17.67	5.2	3.14
^{10}PTFE-NH_3^+-$(PSS/PAH)_{10}$PSS	5.65	69.77	16.5	5.17	2.92
^{10}PTFE-NH_3^+-$(PSS/PAH)_{11}$	1.22	71.92	19.13	5.04	2.69
^{10}PTFE-NH_3^+-$(PSS/PAH)_{11}$PSS	3.42	69.84	19.47	4.62	2.65
^{10}PTFE-NH_3^+-$(PSS/PAH)_{12}$	3.9	67.92	22.33	3.86	2
^{10}PTFE-NH_3^+-$(PSS/PAH)_{12}$PSS	1.55	70.15	22.29	3.6	2.41
^{10}PTFE-NH_3^+-$(PSS/PAH)_{13}$	1.11	71.72	20.73	4.09	2.34
^{10}PTFE-NH_3^+-$(PSS/PAH)_{13}$PSS	1.9	68.42	24	3.47	2.21
^{10}PTFE-NH_3^+-$(PSS/PAH)_{14}$	0.17	70.75	22.1	4.62	2.36

Table C.3. Atomic composition at 75° take-off angle as layers are deposited.

Sample	%F	%C	%O	%N	%S
$^{10}PTFE\text{-}NH_3^+$	4.08	76.77	1.945	17.21	0.0
$^{10}PTFE\text{-}NH_3^+$-PSS	4.11	70.36	12.61	11.04	1.88
$^{10}PTFE\text{-}NH_3^+$-(PSS/PAH)	0.4	74.24	14.82	8.88	1.66
$^{10}PTFE\text{-}NH_3^+$-(PSS/PAH)PSS	1.77	72.73	15	8.37	2.13
$^{10}PTFE\text{-}NH_3^+$-$(PSS/PAH)_2$	2.8	73.46	13.83	7.92	2
$^{10}PTFE\text{-}NH_3^+$-$(PSS/PAH)_2$PSS	2.3	70.91	17.21	7.11	2.50
$^{10}PTFE\text{-}NH_3^+$-$(PSS/PAH)_3$	1.85	71	17.89	6.89	2.37
$^{10}PTFE\text{-}NH_3^+$-$(PSS/PAH)_3$PSS	1.04	71.18	18.66	6.58	2.54
$^{10}PTFE\text{-}NH_3^+$-$(PSS/PAH)_4$	2.24	69.07	19.29	6.77	2.63
$^{10}PTFE\text{-}NH_3^+$-$(PSS/PAH)_4$PSS	2.12	69.42	20.44	5.68	2.35
$^{10}PTFE\text{-}NH_3^+$-$(PSS/PAH)_5$	0.99	69.49	20.42	6.34	2.76
$^{10}PTFE\text{-}NH_3^+$-$(PSS/PAH)_5$PSS	2.09	68.88	20.3	5.9	2.84
$^{10}PTFE\text{-}NH_3^+$-$(PSS/PAH)_6$	3.05	65.71	20.42	7.75	3.08
$^{10}PTFE\text{-}NH_3^+$-$(PSS/PAH)_6$PSS	1.27	68.92	20.19	6.52	3.1
$^{10}PTFE\text{-}NH_3^+$-$(PSS/PAH)_7$	2.29	68.87	19.25	6.64	2.94
$^{10}PTFE\text{-}NH_3^+$-$(PSS/PAH)_7$PSS	2.58	67.66	20.39	6.1	3.28
$^{10}PTFE\text{-}NH_3^+$-$(PSS/PAH)_8$	2.26	68.85	18.72	6.98	3.19
$^{10}PTFE\text{-}NH_3^+$-$(PSS/PAH)_8$PSS	3.86	62.26	23.52	7	3.36
$^{10}PTFE\text{-}NH_3^+$-$(PSS/PAH)_9$	3.92	67.07	18.94	6.91	3.15
$^{10}PTFE\text{-}NH_3^+$-$(PSS/PAH)_9$PSS	0.97	68	20.57	6.97	3.5
$^{10}PTFE\text{-}NH_3^+$-$(PSS/PAH)_{10}$	0.49	69.54	18.7	7.67	3.61
$^{10}PTFE\text{-}NH_3^+$-$(PSS/PAH)_{10}$PSS	4.43	63.41	21.41	7.17	3.58
$^{10}PTFE\text{-}NH_3^+$-$(PSS/PAH)_{11}$	2.84	65.87	20.83	7.1	3.36
$^{10}PTFE\text{-}NH_3^+$-$(PSS/PAH)_{11}$PSS	2.7	63	24.62	6.28	3.4
$^{10}PTFE\text{-}NH_3^+$-$(PSS/PAH)_{12}$	1.78	64.21	25.23	5.7	2.93
$^{10}PTFE\text{-}NH_3^+$-$(PSS/PAH)_{12}$PSS	0.36	65.03	25.45	5.85	3.32
$^{10}PTFE\text{-}NH_3^+$-$(PSS/PAH)_{13}$	2.39	65.11	22.9	6.34	3.25
$^{10}PTFE\text{-}NH_3^+$-$(PSS/PAH)_{13}$PSS	1.45	65.64	24.24	5.52	3.15
$^{10}PTFE\text{-}NH_3^+$-$(PSS/PAH)_{14}$	0.37	69.92	20.75	5.97	2.99

Table C.4. Water contact angle data as layers are deposited.

Sample	θ_A	θ_R
$^{10}PTFE\text{-}NH_3^+$	63.9	6.1
$^{10}PTFE\text{-}NH_3^+$-PSS	57.9	7.7
$^{10}PTFE\text{-}NH_3^+$-(PSS/PAH)	73.4	7.1
$^{10}PTFE\text{-}NH_3^+$-(PSS/PAH)PSS	58.1	5.9
$^{10}PTFE\text{-}NH_3^+$-$(PSS/PAH)_2$	72.7	7.0
$^{10}PTFE\text{-}NH_3^+$-$(PSS/PAH)_2$PSS	59.1	5.6
$^{10}PTFE\text{-}NH_3^+$-$(PSS/PAH)_3$	66.3	6.7
$^{10}PTFE\text{-}NH_3^+$-$(PSS/PAH)_3$PSS	55.7	5.6
$^{10}PTFE\text{-}NH_3^+$-$(PSS/PAH)_4$	63.0	6.6
$^{10}PTFE\text{-}NH_3^+$-$(PSS/PAH)_4$PSS	53.6	6.7
$^{10}PTFE\text{-}NH_3^+$-$(PSS/PAH)_5$	65.1	7.2
$^{10}PTFE\text{-}NH_3^+$-$(PSS/PAH)_5$PSS	59.6	5.9
$^{10}PTFE\text{-}NH_3^+$-$(PSS/PAH)_6$	56.0	4.9
$^{10}PTFE\text{-}NH_3^+$-$(PSS/PAH)_6$PSS	49.3	6.1
$^{10}PTFE\text{-}NH_3^+$-$(PSS/PAH)_7$	60.2	7.6
$^{10}PTFE\text{-}NH_3^+$-$(PSS/PAH)_7$PSS	42.3	4.8
$^{10}PTFE\text{-}NH_3^+$-$(PSS/PAH)_8$	63.0	6.0
$^{10}PTFE\text{-}NH_3^+$-$(PSS/PAH)_8$PSS	49.0	5.1
$^{10}PTFE\text{-}NH_3^+$-$(PSS/PAH)_9$	65.6	6.9
$^{10}PTFE\text{-}NH_3^+$-$(PSS/PAH)_9$PSS	57.0	5.0
$^{10}PTFE\text{-}NH_3^+$-$(PSS/PAH)_{10}$	64.1	4.7
$^{10}PTFE\text{-}NH_3^+$-$(PSS/PAH)_{10}$PSS	53.6	4.4
$^{10}PTFE\text{-}NH_3^+$-$(PSS/PAH)_{11}$	62.7	4.6
$^{10}PTFE\text{-}NH_3^+$-$(PSS/PAH)_{11}$PSS	51.9	5.0
$^{10}PTFE\text{-}NH_3^+$-$(PSS/PAH)_{12}$	60.9	4.6
$^{10}PTFE\text{-}NH_3^+$-$(PSS/PAH)_{12}$PSS	59.3	5.1
$^{10}PTFE\text{-}NH_3^+$-$(PSS/PAH)_{13}$	70.4	4.6
$^{10}PTFE\text{-}NH_3^+$-$(PSS/PAH)_{13}$PSS	53.2	5.0
$^{10}PTFE\text{-}NH_3^+$-$(PSS/PAH)_{14}$	71.0	5.6

^{50}PTFE-NH_3^+

Table C.5. Atomic concentration at 15° take-off angle as layers are deposited.

Sample	%F	%C	%O	%N	%S
^{50}PTFE-NH_3^+	1.57	77.61	2.575	18.26	0.0
^{50}PTFE-NH_3^+-PSS	1.53	74.53	13.13	8.61	2.00
^{50}PTFE-NH_3^+-(PSS/PAH)	2.44	79.13	10.16	5.94	2.34
^{50}PTFE-NH_3^+-(PSS/PAH)PSS	2.26	81.34	8.71	5.42	2.27
^{50}PTFE-NH_3^+-$(PSS/PAH)_2$	0.54	78.72	11.57	6.47	2.71
^{50}PTFE-NH_3^+-$(PSS/PAH)_2$PSS	0	77.03	13.76	6.17	3.05
^{50}PTFE-NH_3^+-$(PSS/PAH)_3$	0.86	77	13.86	5.5	2.80
^{50}PTFE-NH_3^+-$(PSS/PAH)_3$PSS	0.39	75.43	15.88	5.33	2.97
^{50}PTFE-NH_3^+-$(PSS/PAH)_4$	0.73	73.87	16.25	6.23	2.93
^{50}PTFE-NH_3^+-$(PSS/PAH)_4$PSS	5.99	72.34	13.06	4.8	3.8
^{50}PTFE-NH_3^+-$(PSS/PAH)_5$	4.91	70.91	15.83	5.59	2.76
^{50}PTFE-NH_3^+-$(PSS/PAH)_5$PSS	0.49	74.72	16.45	5.16	3.19
^{50}PTFE-NH_3^+-$(PSS/PAH)_6$	0	13.56	13.56	4.4	2.28
^{50}PTFE-NH_3^+-$(PSS/PAH)_6$PSS	2.45	72.37	17.01	5.17	2.99
^{50}PTFE-NH_3^+-$(PSS/PAH)_7$	0	80.26	13.31	4.41	2.02
^{50}PTFE-NH_3^+-$(PSS/PAH)_7$PSS	2.12	71.79	18.72	4.42	2.95
^{50}PTFE-NH_3^+-$(PSS/PAH)_8$	0	75.27	16.39	5.55	2.79
^{50}PTFE-NH_3^+-$(PSS/PAH)_8$PSS	0	73.27	18.48	5	3.24
^{50}PTFE-NH_3^+-$(PSS/PAH)_9$	0	74.96	15.58	6.39	3.34
^{50}PTFE-NH_3^+-$(PSS/PAH)_9$PSS	0	75.74	15.94	4.71	3.61
^{50}PTFE-NH_3^+-$(PSS/PAH)_{10}$	0	78.43	13.51	4.99	3.07

Table C.6. Atomic concentration at 75° take-off angle as layers are deposited.

Sample	%F	%C	%O	%N	%S
$^{50}PTFE\text{-}NH_3^+$	0.46	72.89	2.29	24.37	0.0
$^{50}PTFE\text{-}NH_3^+$-PSS	1.31	65.61	19.39	11.18	2.50
$^{50}PTFE\text{-}NH_3^+$-(PSS/PAH)	0.6	69.21	18.14	9.49	2.56
$^{50}PTFE\text{-}NH_3^+$-(PSS/PAH)PSS	1.99	65.65	19.91	9.72	2.74
$^{50}PTFE\text{-}NH_3^+$-$(PSS/PAH)_2$	0.37	68.5	18.83	9.83	2.47
$^{50}PTFE\text{-}NH_3^+$-$(PSS/PAH)_2$PSS	0.53	65.16	22.57	8.79	2.94
$^{50}PTFE\text{-}NH_3^+$-$(PSS/PAH)_3$	1.43	68.42	19.7	8.01	2.45
$^{50}PTFE\text{-}NH_3^+$-$(PSS/PAH)_3$PSS	1.81	67.03	20.88	7.8	2.49
$^{50}PTFE\text{-}NH_3^+$-$(PSS/PAH)_4$	0.25	68.28	21.18	7.68	2.62
$^{50}PTFE\text{-}NH_3^+$-$(PSS/PAH)_4$PSS	3.97	66.13	20.8	6.43	2.68
$^{50}PTFE\text{-}NH_3^+$-$(PSS/PAH)_5$	3.8	66.03	21.17	6.47	2.52
$^{50}PTFE\text{-}NH_3^+$-$(PSS/PAH)_5$PSS	0.43	66.63	22.12	7.57	3.25
$^{50}PTFE\text{-}NH_3^+$-$(PSS/PAH)_6$	0.6	65.28	23.62	7.35	3.17
$^{50}PTFE\text{-}NH_3^+$-$(PSS/PAH)_6$PSS	1.34	64.77	23.14	7.3	3.45
$^{50}PTFE\text{-}NH_3^+$-$(PSS/PAH)_7$	0.58	67.21	22.39	6.94	2.89
$^{50}PTFE\text{-}NH_3^+$-$(PSS/PAH)_7$PSS	1.61	64.27	24.03	6.37	3.72
$^{50}PTFE\text{-}NH_3^+$-$(PSS/PAH)_8$	1.36	66.55	21.06	7.59	3.44
$^{50}PTFE\text{-}NH_3^+$-$(PSS/PAH)_8$PSS	0	68.6	21.6	6.51	3.3
$^{50}PTFE\text{-}NH_3^+$-$(PSS/PAH)_9$	0	69.66	20.57	6.7	3.07
$^{50}PTFE\text{-}NH_3^+$-$(PSS/PAH)_9$PSS	0	68.72	21.05	6.56	3.67
$^{50}PTFE\text{-}NH_3^+$-$(PSS/PAH)_{10}$	2.2	66.52	20.39	7.34	3.55

Table C.7. Water contact angle results as polyelectrolytes are adsorbed.

Sample	θ_A	θ_R
$^{50}PTFE\text{-}NH_3^+$	52.3	7.5
$^{50}PTFE\text{-}NH_3^+\text{-}PSS$	67.4	5.6
$^{50}PTFE\text{-}NH_3^+\text{-}(PSS/PAH)$	62.1	9.9
$^{50}PTFE\text{-}NH_3^+\text{-}(PSS/PAH)PSS$	60.8	7.5
$^{50}PTFE\text{-}NH_3^+\text{-}(PSS/PAH)_2$	60.9	6.5
$^{50}PTFE\text{-}NH_3^+\text{-}(PSS/PAH)_2PSS$	55.1	6.5
$^{50}PTFE\text{-}NH_3^+\text{-}(PSS/PAH)_3$	68.0	10.0
$^{50}PTFE\text{-}NH_3^+\text{-}(PSS/PAH)_3PSS$	49.6	5.9
$^{50}PTFE\text{-}NH_3^+\text{-}(PSS/PAH)_4$	55.4	7.4
$^{50}PTFE\text{-}NH_3^+\text{-}(PSS/PAH)_4PSS$	49.4	5.1
$^{50}PTFE\text{-}NH_3^+\text{-}(PSS/PAH)_5$	55.5	7.4
$^{50}PTFE\text{-}NH_3^+\text{-}(PSS/PAH)_5PSS$	46.0	5.4
$^{50}PTFE\text{-}NH_3^+\text{-}(PSS/PAH)_6$	62.4	6.4
$^{50}PTFE\text{-}NH_3^+\text{-}(PSS/PAH)_6PSS$	60.1	5.7
$^{50}PTFE\text{-}NH_3^+\text{-}(PSS/PAH)_7$	78.3	5.1
$^{50}PTFE\text{-}NH_3^+\text{-}(PSS/PAH)_7PSS$	61.1	5.0
$^{50}PTFE\text{-}NH_3^+\text{-}(PSS/PAH)_8$	88.1	5.3
$^{50}PTFE\text{-}NH_3^+\text{-}(PSS/PAH)_8PSS$	60.0	5.5
$^{50}PTFE\text{-}NH_3^+\text{-}(PSS/PAH)_9$	81.4	4.9
$^{50}PTFE\text{-}NH_3^+\text{-}(PSS/PAH)_9PSS$	61.9	5.3
$^{50}PTFE\text{-}NH_3^+\text{-}(PSS/PAH)_{10}$	84.0	5.1

APPENDIX D

ADDITIONAL DATA FOR CHAPTER 3

Lycra-PAH

Table D.1. Atomic composition at 15° take-off angle as layers are adsorbed.

Sample	%C	%O	%N	%S
Lycra®	65.88	25.87	0.59	0
Lycra-PAH	67.44	23.32	1.67	0
Lycra-PAH-PSS	62.82	26.73	1.11	0.43
Lycra-PAH-$(PSS/PAH)_2$	63.08	26.31	0.68	0.29
Lycra-PAH-$(PSS/PAH)_4$PSS	65.32	25.61	0.79	0.1

Table D.2. Atomic composition at 75° take-off angle as layers are adsorbed.

Sample	%C	%O	%N	%S
Lycra®	70.29	25.63	1.93	0
Lycra-PAH	72	22.11	3.27	0
Lycra-PAH-PSS	70.49	24.55	1.73	0.44
Lycra-PAH-$(PSS/PAH)_2$	73.8	21.09	1.53	0.47
Lycra-PAH-$(PSS/PAH)_4$PSS	72.52	23.49	1.75	0.39

Table D.3. Water contact angle measurements as layers are adsorbed.

Sample	θ_A	θ_R
Lycra®	76.1	29.3
Lycra-PAH	76.6	22.4
Lycra-PAH-PSS	58.3	7.9
Lycra-PAH-$(PSS/PAH)_2$	68.6	10.7
Lycra-PAH-$(PSS/PAH)_4$PSS	64.9	10.3

Table D.4. Atomic composition at 15° take-off angle as layers are adsorbed.

Sample	%C	%O	%N	%S
Lycra®	65.88	25.9	0.59	0
Lycra-PEI	66.08	24.8	1.8	0
Lycra-PEI-PSS	71.64	21.2	0.81	0.32
Lycra-PEI-$(PSS/PAH)_2$	62.81	22.9	0.88	0.38
Lycra-PEI-$(PSS/PAH)_4PSS$	70.68	20.4	0.82	0.61

Table D.5. Atomic composition at 75° take-off angle as layers are adsorbed.

Sample	%C	%O	%N	%S
Lycra®	70.29	25.63	1.93	0
Lycra-PEI	75.59	18.57	3.57	0
Lycra-PEI-PSS	76.33	18.02	3.05	0.95
Lycra-PEI-$(PSS/PAH)_2$	70.88	19.75	2.32	0.89
Lycra-PEI-$(PSS/PAH)_4PSS$	74.98	18.96	2.64	1.25

Table D.6. Water contact angle measurements as layers are adsorbed.

Sample	θ_A	θ_R
Lycra®	76.1	29.3
Lycra-PEI	59.9	11.9
Lycra-PEI-PSS	58	10.3
Lycra-PEI-$(PSS/PAH)_2$	61.1	8.6
Lycra-PEI-$(PSS/PAH)_4PSS$	63.4	9.4

Oxidized Lycra® (Lycra-COOH)

Table D.7. Atomic composition of Lycra-COOH at 15° take-off angle as polyelectrolytes are adsorbed.

Sample	%C	%O	%N	%S
Lycra®	65.88	25.9	0.59	0
Lycra-COOH	77.47	18.6	0.99	0.21
Lycra-COOH-PAH	71.76	21.9	1.2	0.56
Lycra-COOH-PAH/PSS	72.3	20.8	2.04	0.9
Lycra-COOH-(PAH/PSS)PAH	70.41	24.9	1.76	0.54
Lycra-COOH-$(PAH/PSS)_2$	70.11	24.2	2.44	1.07
Lycra-COOH-$(PAH/PSS)_2$PAH	66.29	27.6	2.99	1.72
Lycra-COOH-$(PAH/PSS)_3$	71.34	22.8	2.15	0.44
Lycra-COOH-$(PAH/PSS)_3$PAH	75.3	18.8	1.12	0.21
Lycra-COOH-$(PAH/PSS)_5$	70.25	25	2.01	1.07
Lycra-COOH-$(PAH/PSS)_{12}$PAH	71.2	24	1.34	0.62

Table D.8. Atomic composition of Lycra-COOH at 75° take-off angle as polyelectrolytes are adsorbed.

Sample	%C	%O	%N	%S
Lycra®	70.29	25.63	1.93	0
Lycra-COOH	75.11	21.38	1.99	0.34
Lycra-COOH-PAH	67.6	27.04	3.14	1.12
Lycra-COOH-PAH/PSS	71	22.24	3.1	1.34
Lycra-COOH-(PAH/PSS)PAH	68.53	26.11	3.3	1.26
Lycra-COOH-$(PAH/PSS)_2$	70.84	23.62	3.12	1.74
Lycra-COOH-$(PAH/PSS)_2$PAH	63.27	29.09	4.64	2.43
Lycra-COOH-$(PAH/PSS)_3$	73.64	21.19	2.84	0.88
Lycra-COOH-$(PAH/PSS)_3$PAH	73.79	20.55	2.89	0.93
Lycra-COOH-$(PAH/PSS)_5$	68.74	25.47	3.4	1.74
Lycra-COOH-$(PAH/PSS)_{12}$PAH	71.77	23.57	2.69	1.33

Table D.9. Water contact angle measurements as laycrs are adsorbed.

Sample	θ_A	θ_R
Lycra®	76.1	29.3
Lycra-COOH	74.9	10.1
Lycra-COOH-PAH	72.8	6.7
Lycra-COOH-PAH/PSS	58.7	5.9
Lycra-COOH-(PAH/PSS)PAH	64.8	28.6
Lycra-COOH-$(PAH/PSS)_2$	52.6	7.4
Lycra-COOH-$(PAH/PSS)_2$PAH	54	5.8
Lycra-COOH-$(PAH/PSS)_3$	88.4	8.4
Lycra-COOH-$(PAH/PSS)_3$PAH	72.3	19.9
Lycra-COOH-$(PAH/PSS)_5$	43.3	6.7
Lycra-COOH-$(PAH/PSS)_{12}$PAH	52	8

Plasma Polymerized Allylamine on Lycra® (Lycra-PPAAm)

Table D.10. Atomic composition at 15° take-off angle as polyelectrolytes are adsorbed.

Sample	%C	%O	%N	%S
Lycra®	65.88	25.9	0.59	0
Lycra-PPAAM	72.95	16.17	9.1	0
Lycra-PPAAM-PSS	74.35	19.01	5.46	1.18
Lycra-PPAAM-PSS/PAH	74.46	21.61	3.18	0.76
Lycra-PPAAM-(PSS/PAH)-PSS	73.12	22.56	3.24	1.08
Lycra-PPAAM-$(PSS/PAH)_2$	76.17	17.9	4.6	1.33
Lycra-PPAAM-$(PSS/PAH)_2$-PSS	71.02	25.97	2.11	0.91
Lycra-PPAAM-$(PSS/PAH)_3$	76.77	14.9	4.5	1.41
Lycra-PPAAM-$(PSS/PAH)_3$-PSS	78.71	16.25	3.57	1.46
Lycra-PPAAM-$(PSS/PAH)_4$	78.82	15.52	3.96	1.7
Lycra-PPAAM-$(PSS/PAH)_4$-PSS	77.54	18.55	2.63	1.29
Lycra-PPAAM-$(PSS/PAH)_5$	76.92	17.34	3.66	2.08
Lycra-PPAAM-$(PSS/PAH)_5$-PSS	77.06	17.85	1.94	0.72
Lycra-PPAAM-$(PSS/PAH)_6$	76.01	17.21	3.35	1.65
Lycra-PPAAM-$(PSS/PAH)_6$-PSS	74.22	19.36	4.2	2.22
Lycra-PPAAM-$(PSS/PAH)_7$	77.37	14.89	4.37	2.59
Lycra-PPAAM-$(PSS/PAH)_7$-PSS	76.45	17.51	3.68	2.35

Table D.11. Atomic composition at 75° take-off angle as polyelectrolytes are adsorbed.

Sample	%C	%O	%N	%S
Lycra®	70.29	25.63	1.93	0
Lycra-PPAAM	70.54	15.47	11.61	0
Lycra-PPAAM-PSS	73.15	17.95	7.45	1.46
Lycra-PPAAM-PSS/PAH	73.78	20.76	4.51	0.95
Lycra-PPAAM-(PSS/PAH)-PSS	73.19	20.9	4.7	1.21
Lycra-PPAAM-$(PSS/PAH)_2$	76.84	13.24	8.25	1.67
Lycra-PPAAM-$(PSS/PAH)_2$-PSS	71.54	21.74	5.19	1.53
Lycra-PPAAM-$(PSS/PAH)_3$	77.07	13.45	7.58	1.9
Lycra-PPAAM-$(PSS/PAH)_3$-PSS	78.38	13.26	6.3	2.06
Lycra-PPAAM-$(PSS/PAH)_4$	77.77	13.06	6.94	2.22
Lycra-PPAAM-$(PSS/PAH)_4$-PSS	76.25	16.58	5.13	2.04
Lycra-PPAAM-$(PSS/PAH)_5$	75.09	15.86	6.68	2.37
Lycra-PPAAM-$(PSS/PAH)_5$-PSS	74.3	18.91	4.59	1.29
Lycra-PPAAM-$(PSS/PAH)_6$	73.26	18.14	5.88	1.92
Lycra-PPAAM-$(PSS/PAH)_6$-PSS	72.89	18.23	6.75	2.13
Lycra-PPAAM-$(PSS/PAH)_7$	73.79	15.33	8.03	2.85
Lycra-PPAAM-$(PSS/PAH)_7$-PSS	73.16	17.02	7.03	2.78

Table D.12. Water contact angle measurements as layers are adsorbed.

Sample	θ_A	θ_R
Lycra®	76.1	29.3
Lycra-PPAAM	38.7	4.7
Lycra-PPAAM-PSS	40.4	7
Lycra-PPAAM-PSS/PAH	46.7	8.3
Lycra-PPAAM-(PSS/PAH)-PSS	45.3	7.2
Lycra-PPAAM-$(PSS/PAH)_2$	62.7	8
Lycra-PPAAM-$(PSS/PAH)_2$-PSS	51.8	8.4
Lycra-PPAAM-$(PSS/PAH)_3$	59	19
Lycra-PPAAM-$(PSS/PAH)_3$-PSS	61.1	10.9
Lycra-PPAAM-$(PSS/PAH)_4$	60.5	12.4
Lycra-PPAAM-$(PSS/PAH)_4$-PSS	55.5	7.7
Lycra-PPAAM-$(PSS/PAH)_5$	57.7	7.4
Lycra-PPAAM-$(PSS/PAH)_5$-PSS	50.6	6.4
Lycra-PPAAM-$(PSS/PAH)_6$	59.6	9.4
Lycra-PPAAM-$(PSS/PAH)_6$-PSS	41.2	6.7
Lycra-PPAAM-$(PSS/PAH)_7$	50.5	8.3
Lycra-PPAAM-$(PSS/PAH)_7$-PSS	48	8.8

Table D.13. Atomic composition at 15° take-off angle as polyelectrolytes are adsorbed.

Sample	%C	%O	%N	%S
Lycra®	65.88	25.9	0.59	0
Lycra-NH_3^+	74.89	11.65	13.5	0
Lycra-NH_3^+-PSS	68.07	29.64	1.68	0.62
Lycra-NH_3^+-$(PSS/PAH)_2$PSS	66.56	30.62	1.97	0.85
Lycra-NH_3^+-$(PSS/PAH)_3$	74.93	22.17	1.98	0.93
Lycra-NH_3^+-$(PSS/PAH)_5$	75.87	20.91	2.16	1.07
Lycra-NH_3^+-$(PSS/PAH)_5$PSS	75.06	21.76	2.05	1.13
Lycra-NH_3^+-$(PSS/PAH)_7$PSS	77.45	18.38	2.39	1.77
Lycra NH_3^+-$(PSS/PAH)_8$	76.32	18.93	2.87	1.88
Lycra NH_3^+-$(PSS/PAH)_{10}$	77.09	18.3	2.9	1.71
Lycra NH_3^+-$(PSS/PAH)_{10}$PSS	74.85	20.71	2.55	1.89
Lycra NH_3^+-$(PSS/PAH)_{12}$PSS	72.69	21.85	3.55	1.91
Lycra NH_3^+-$(PSS/PAH)_{13}$	75.69	19.21	3.26	1.84
Lycra NH_3^+-$(PSS/PAH)_{25}$	72.81	20.45	4.29	2.46
Lycra NH_3^+-$(PSS/PAH)_{25}$PSS	72.65	20.22	4.4	2.73

Table D.14. Atomic composition at 75° take-off angle as polyelectrolytes are adsorbed.

Sample	%C	%O	%N	%S
Lycra®	70.29	25.63	1.93	0
Lycra-NH_3^+	71.69	14.33	13.98	0
Lycra-NH_3^+-PSS	69.36	27.13	2.85	0.65
Lycra-NH_3^+-$(PSS/PAH)_2$PSS	70.96	25.47	2.73	0.84
Lycra-NH_3^+-$(PSS/PAH)_3$	71.63	24.58	2.93	0.86
Lycra-NH_3^+-$(PSS/PAH)_5$	75.49	20.24	2.92	1.35
Lycra-NH_3^+-$(PSS/PAH)_5$PSS	74.91	21.33	2.47	1.29
Lycra-NH_3^+-$(PSS/PAH)_7$PSS	74.42	20.3	3.36	1.92
Lycra NH_3^+-$(PSS/PAH)_8$	68.95	24.02	4.67	2.37
Lycra NH_3^+-$(PSS/PAH)_{10}$	76.18	17.81	3.91	2.1
Lycra NH_3^+-$(PSS/PAH)_{10}$PSS	63.55	29	4.36	3.09
Lycra NH_3^+-$(PSS/PAH)_{12}$PSS	75.6	18.14	3.91	2.35
Lycra NH_3^+-$(PSS/PAH)_{13}$	75.54	17.59	4.26	2.6
Lycra NH_3^+-$(PSS/PAH)_{25}$	70.58	21.22	5.26	2.94
Lycra NH_3^+-$(PSS/PAH)_{25}$PSS	70.03	21.34	5.37	3.25

Table D.15. Water contact angle measurements as layers are adsorbed.

Sample	θ_A	θ_R
Lycra®	76.1	29.3
Lycra-NH_3^+	25.3	5.3
Lycra-NH_3^+-PSS	31.3	6.2
Lycra-NH_3^+-$(PSS/PAH)_2PSS$	34.8	6.0
Lycra-NH_3^+-$(PSS/PAH)_3$	46.4	6.2
Lycra-NH_3^+-$(PSS/PAH)_5$	40.0	5.5
Lycra-NH_3^+-$(PSS/PAH)_5PSS$	26.8	4.4
Lycra-NH_3^+-$(PSS/PAH)_7PSS$	35.6	7.2
Lycra NH_3^+-$(PSS/PAH)_8$	38.4	5.5
Lycra NH_3^+-$(PSS/PAH)_{10}$	36.0	5.8
Lycra NH_3^+-$(PSS/PAH)_{10}PSS$	27.7	6.0
Lycra NH_3^+-$(PSS/PAH)_{12}PSS$	33.8	5.5
Lycra NH_3^+-$(PSS/PAH)_{13}$	40.0	7.2
Lycra NH_3^+-$(PSS/PAH)_{25}$	35.7	5.6
Lycra NH_3^+-$(PSS/PAH)_{25}PSS$	17.3	6.3

APPENDIX E

ADDITIONAL DATA FOR CHAPTER 4

LDPE-COOH

Table E.1. Atomic composition at 15° take-off angle as layers are adsorbed.

Sample	%C	%O	%N	%S
LDPE	96.35	3.65		
LDPE-COOH	88.86	10.75	0	0
LDPE-COOH-PAH	87.1	9.27	3.26	0
LDPE-COOH-(PAH/PSS)	82.45	13.66	2.52	1.36
LDPE-COOH-(PAH/PSS)PAH	80.95	14.74	2.9	1.41
LDPE-COOH-$(PAH/PSS)_2$	78.86	15.95	3.48	1.71
LDPE-COOH-$(PAH/PSS)_2$PAH	81.58	13.89	3.02	1.51
LDPE-COOH-$(PAH/PSS)_3$	80.52	14.65	3.06	1.77
LDPE-COOH-$(PAH/PSS)_3$PAH	80.27	14.61	3.37	1.76
LDPE-COOH-$(PAH/PSS)_4$	79.7	14.96	3.33	2.01
LDPE-COOH-$(PAH/PSS)_4$PAH	79.3	15.59	3.26	1.85
LDPE-COOH-$(PAH/PSS)_5$	76.65	18.08	3.27	1.99
LDPE-COOH-$(PAH/PSS)_7$	77.71	16.66	3.55	2.09
LDPE-COOH-$(PAH/PSS)_7$PAH	78.15	15.95	4	1.9
LDPE-COOH-$(PAH/PSS)_9$ PAH	78.88	15.37	3.87	1.88
LDPE-COOH-$(PAH/PSS)_{10}$	76.48	17.24	4.12	2.16
LDPE-COOH-$(PAH/PSS)_{12}$	77.31	16.66	3.86	2.17
LDPE-COOH-$(PAH/PSS)_{12}$PAH	78.39	15.56	3.89	2.16
LDPE-COOH-$(PAH/PSS)_{25}$	77.42	17.04	3.45	2.09

Table E.2. Atomic composition at 75° take-off angle as layers are adsorbed.

Sample	%C	%O	%N	%S
LDPE	98.7	1.3		
LDPE-COOH	92	7.47	0	
LDPE-COOH-PAH	88.6	8.16	2.77	
LDPE-COOH-(PAH/PSS)	82.76	13.32	2.52	1.4
LDPE-COOH-(PAH/PSS)PAH	83.3	12.78	2.81	1.12
LDPE-COOH-$(PAH/PSS)_2$	80.07	15.44	3.04	1.46
LDPE-COOH-$(PAH/PSS)_2$PAH	82.35	13.4	2.79	1.47
LDPE-COOH-$(PAH/PSS)_3$	81.5	13.86	3.01	1.63
LDPE-COOH-$(PAH/PSS)_3$PAH	81.67	12.92	3.7	1.7
LDPE-COOH-$(PAH/PSS)_4$	80.55	14.48	3.12	1.86
LDPE-COOH-$(PAH/PSS)_4$PAH	80.7	14.16	3.31	1.84
LDPE-COOH-$(PAH/PSS)_5$	80.51	14.67	3.05	1.77
LDPE-COOH-$(PAH/PSS)_7$	77.74	16.25	3.89	2.12
LDPE-COOH-$(PAH/PSS)_7$PAH	77.81	16.06	4.06	2.06
LDPE-COOH-$(PAH/PSS)_9$ PAH	77.9	15.88	4.27	1.95
LDPE-COOH-$(PAH/PSS)_{10}$	74.99	18.05	4.53	2.43
LDPE-COOH-$(PAH/PSS)_{12}$	73.76	18.55	5.11	2.58
LDPE-COOH-$(PAH/PSS)_{12}$PAH	73.66	18.55	5.17	2.63
LDPE-COOH-$(PAH/PSS)_{25}$	74.64	17.89	4.65	2.82

Table E.3. Water contact angle measurements as layers are adsorbed.

Sample	θ_A	θ_R
LDPE	107	76
LDPE-COOH	93	61.4
LDPE-COOH-PAH	93	35
LDPE-COOH-(PAH/PSS)	65	7.0
LDPE-COOH-(PAH/PSS)PAH	68	7.2
LDPE-COOH-$(PAH/PSS)_2$	50	7.8
LDPE-COOH-$(PAH/PSS)_2$PAH	67	6.8
LDPE-COOH-$(PAH/PSS)_3$	61	6.7
LDPE-COOH-$(PAH/PSS)_3$PAH	68	6.6
LDPE-COOH-$(PAH/PSS)_4$	59	7.7
LDPE-COOH-$(PAH/PSS)_4$PAH	68	7.8
LDPE-COOH-$(PAH/PSS)_5$	63.7	7.8
LDPE-COOH-$(PAH/PSS)_7$	62.7	9.0
LDPE-COOH-$(PAH/PSS)_7$PAH	66.7	9.8
LDPE-COOH-$(PAH/PSS)_9$ PAH	65.8	9.7
LDPE-COOH-$(PAH/PSS)_{10}$	60.2	9.7
LDPE-COOH-$(PAH/PSS)_{12}$	53.7	8.3
LDPE-COOH-$(PAH/PSS)_{12}$PAH	67.2	8.7
LDPE-COOH-$(PAH/PSS)_{25}$	63	6.4

LDPE-Au-S-x-COOH

Table E.4. Atomic composition at 15° take-off angle as layers are adsorbed.

Sample	%C	%O	%N	%S	%Au
LDPE	96.35	3.65			
LDPE-Au-S-COOH	74.3	12.09	0	1.76	11.84
LDPE-Au-S-COOH-PAH	79.2	9.75	5.82	0	4.03
LDPE-Au-S-COOH-(PAH/PSS)	75.1	15.95	3.19	3.27	2.52
LDPE-Au-S-COOH-(PAH/PSS)PAH	75	17.25	4.13	2.2	1.4
LDPE-Au-S-COOH-$(PAH/PSS)_2$	74.9	17.27	4.4	2.79	0.66
LDPE-Au-S-COOH-$(PAH/PSS)_2$PAH	73.4	17.5	5.22	2.96	0.93
LDPE-Au-S-COOH-$(PAH/PSS)_3$	75	17.83	4.56	1.88	0.7
LDPE-Au-S-COOH-$(PAH/PSS)_3$PAH	73.8	18.72	4.94	2.27	0.3
LDPE-Au-S-COOH-$(PAH/PSS)_4$	73.2	18.8	4.76	2.75	0.52
LDPE-Au-S-COOH-$(PAH/PSS)_4$PAH	72	19.17	5.66	2.64	0.54
LDPE-Au-S-COOH-$(PAH/PSS)_5$	72.6	18.95	5.21	2.85	0.37
LDPE-Au-S-COOH-$(PAH/PSS)_7$	74	17.93	5.27	2.64	0.2
LDPE-Au-S-COOH-$(PAH/PSS)_7$PAH	74.2	17.83	5.33	2.51	0.12
LDPE-Au-S-COOH-$(PAH/PSS)_{10}$	74.5	17.85	4.92	2.66	0.1
LDPE-Au-S-COOH-$(PAH/PSS)_{10}$PAH	74.5	16.92	5.53	2.99	0.08
LDPE-Au-S-COOH-$(PAH/PSS)_{12}$	74.8	17.94	4.64	2.6	0.05
LDPE-Au-S-COOH-$(PAH/PSS)_{12}$PAH	77.8	15.4	4.45	2.23	0.08
LDPE-Au-S-COOH-$(PAH/PSS)_{25}$	75.7	17.24	4.52	2.59	0
LDPE-Au-S-COOH-$(PAH/PSS)_{25}$PAH	75.1	16.55	5.97	2.42	0

Table E.5. Atomic composition at 75° take-off angle as layers are adsorbed.

Sample	%C	%O	%N	%S	%Au
LDPE	98.7	1.3			
LDPE-Au-S-COOH	53.67	6.38	0	2.54	37.4
LDPE-Au-S-COOH-PAH	68.66	6.82	5.67	1.16	17.7
LDPE-Au-S-COOH-(PAH/PSS)	66.32	13.4	3.63	2.52	14.2
LDPE-Au-S-COOH-(PAH/PSS)PAH	72.07	12.6	4.42	1.96	8.97
LDPE-Au-S-COOH-$(PAH/PSS)_2$	68.91	16.2	4.13	3.56	7.25
LDPE-Au-S-COOH-$(PAH/PSS)_2$PAH	72.11	15.3	4.75	2.24	5.6
LDPE-Au-S-COOH-$(PAH/PSS)_3$	69.88	15.6	4.31	2.73	7.5
LDPE-Au-S-COOH-$(PAH/PSS)_3$PAH	71.22	16.6	5.72	2.62	3.88
LDPE-Au-S-COOH-$(PAH/PSS)_4$	72.34	15.9	3.73	2.95	5.1
LDPE-Au-S-COOH-$(PAH/PSS)_4$PAH	71.18	15.1	4.88	2.6	6.27
LDPE-Au-S-COOH-$(PAH/PSS)_5$	70.36	17.8	5.77	2.74	3.32
LDPE-Au-S-COOH-$(PAH/PSS)_7$	69.56	19.2	6.28	3.05	1.95
LDPE-Au-S-COOH-$(PAH/PSS)_7$PAH	71.2	18.1	5.98	3.02	1.66
LDPE-Au-S-COOH-$(PAH/PSS)_{10}$	67.85	19.4	7.3	3.73	1.72
LDPE-Au-S-COOH-$(PAH/PSS)_{10}$PAH	71.58	17.8	6.18	2.86	1.6
LDPE-Au-S-COOH-$(PAH/PSS)_{12}$	71.77	18.2	6.18	2.86	1.03
LDPE-Au-S-COOH-$(PAH/PSS)_{12}$PAH	75.82	15.6	4.89	2.63	1.01
LDPE-Au-S-COOH-$(PAH/PSS)_{25}$	70.94	19.7	6	3.22	0.11
LDPE-Au-S-COOH-$(PAH/PSS)_{25}$PAH	71.12	19	6.54	3.2	0.12

Table E.6. Water contact angle measurements as layers are adsorbed.

Sample	θ_A	θ_R
LDPE	107	76
LDPE-Au-S-COOH	11.4	0
LDPE-Au-S-COOH-PAH	77.6	0
LDPE-Au-S-COOH-(PAH/PSS)	65.8	0
LDPE-Au-S-COOH-(PAH/PSS)PAH	55.3	0
LDPE-Au-S-COOH-$(PAH/PSS)_2$	46.8	0
LDPE-Au-S-COOH-$(PAH/PSS)_2$PAH	51.5	0
LDPE-Au-S-COOH-$(PAH/PSS)_3$	45.3	0
LDPE-Au-S-COOH-$(PAH/PSS)_3$PAH	54.2	0
LDPE-Au-S-COOH-$(PAH/PSS)_4$	53.7	0
LDPE-Au-S-COOH-$(PAH/PSS)_4$PAH	47.4	0
LDPE-Au-S-COOH-$(PAH/PSS)_5$	41.8	0
LDPE-Au-S-COOH-$(PAH/PSS)_7$	42.3	0
LDPE-Au-S-COOH-$(PAH/PSS)_7$PAH	61	0
LDPE-Au-S-COOH-$(PAH/PSS)_{10}$	40.2	0
LDPE-Au-S-COOH-$(PAH/PSS)_{10}$PAH	51.2	0
LDPE-Au-S-COOH-$(PAH/PSS)_{12}$	42	0
LDPE-Au-S-COOH-$(PAH/PSS)_{12}$PAH	47.4	0
LDPE-Au-S-COOH-$(PAH/PSS)_{25}$	42.8	0
LDPE-Au-S-COOH-$(PAH/PSS)_{25}$PAH	58.3	0

APPENDIX F

ULTRAHYDROPHOBIC COATINGS OF PLASMA-POLYMERIZED FLUOROMONOMERS

Introduction

The wettability of solid surfaces with a liquid (usually water) has been of interest since the beginning of this century as an attempt to improve the water-repellency of surfaces. The wetting of a liquid on a surface is measured in terms of a contact angle θ that describes the angle between the tangent of the liquid droplet at the air/liquid/solid interface and the solid surface. The theoretical treatment on the effects of surface roughness on wettability and on contact angle hysteresis was discussed in chapter 1. In brief, increasing the roughness ratio of a hydrophobic surface results in an increase in both the advancing contact angle and the contact angle hysteresis before a critical roughness is reached, at which point the hysteresis decreases (curve (D) in figure 1.9). Experimentally, the effects of roughness on wettability were first reported by Lee in 1936.[1] He observed that increasing the roughness factor of a high-aromatic tar on plate glass from 1 to 1.44 leads to an increase in the contact angle from 138.2° to 152.8°. The effects of roughness on contact angle hysteresis were observed by Dettre and Johnson and by Bartell and Shepard.[2,3]

Recently, materials possessing high contact angles have been synthesized by plasma polymerization of fluorocarbons; the contact angles of the resulting surfaces are

dependent on the type of surface morphology generated. The highest water contact angle for a CF_3-rich (smooth) surface was reported as 120° on a coating of a polymethacrylic ester having perfluorinated side-chains.[4] Washo reports a contact angle between 165-170° for a plasma polymerized tetrafluoroethylene using a RF inductively coupled flow reactor.[5] The plasma polymer is in powder form and the micrographs show a high surface roughness with crater-like features. For D.C. plasma polymerized vinylidene fluoride[6], the contact angles were found to be 162° at the anode versus 119° at the cathode with corresponding roughness of 270 nm and 90 nm, respectively. The highest contact angle reported for plasma polymerized -CF_3 substituted perfluorohexenes was 127° with a corresponding mean roughness of 0.38 nm.[7] In these reports, the contact angle hysteresis was not reported and the extent of the hydrophobicity of these surfaces is not known. In this section, we present a study of the effect of the fluorocarbon structure on the plasma polymer formed and on the wettability of the plasma polymer.

Experimental

General Procedures

PET films (DuPont Mylar, 5 mil) were rinsed with distilled water and methanol, extracted in refluxing hexane for 2 h, and then dried (room temperature, 0.05 mm, >24 h). Perfluorohexane (PFH) (99%, Aldrich), 3,3,4,4,5,5,6,6,6-nonafluoro-1-hexene (NFH) (99%, Aldrich), perfluoro-2-methyl-2-pentene (PFMP) (98%, Aldrich), 2,2,3,3,4,4,4-

heptafluorobutyl acrylate (HFBA) (97%, Aldrich), 1,1,1,3,3,3-hexafluoroisopropyl acrylate (HFIA) (99%, Aldrich), 2,2,3,3,3-pentafluoropropyl acrylate (PFPA) (98%, Aldrich), and ethyl heptafluorobutyrate (EHFB) (97%, Aldrich) were used as received. Water was purified using a Millipore Milli-Q® system that involves reverse osmosis followed by ion-exchange and filtration steps. Plasma polymerizations were carried out in a home-built inductively coupled pyrex reactor in which flow rate, power (13.56 MHz - supplied by an Astron RS-35A power supply and a Yaesu FT-840 HF transceiver), and pressure can be controlled. X-ray photoelectron spectra (XPS) were recorded on a Perkin-Elmer - Physical Electronics 5100 spectrometer with Al K_α excitation (15 kV, 400 W) at a take-off angle of 75° (between the plane of the sample surface and the entrance lens of the detector optics). Atomic concentration data were determined using sensitivity factors obtained from samples of known composition: C_{1s}, 0.200; O_{1s}, 0.501; N_{1s}, 0.352; F_{1s}, 1.00. Contact angle measurements were made with a Ramé-Hart telescopic goniometer and a Gilmont syringe with a 24-gauge flat-tipped needle. Dynamic advancing (θ_A) and receding angles (θ_R) were recorded while the probe fluid (water, purified as described above) was added to and withdrawn from the drop, respectively. AFM imaging was performed in air using Digital Instruments Nanoscope IIIa AFM in tapping mode™. SEM micrographs were obtained with a JEOL-35CF scanning electron microscope at an acceleration voltage of 20 kV. Some samples were easily damaged by the electron beam; platinum-carbon replicas were made of those surfaces and FESEM micrographs were obtained with a JEOL-6320FXV scanning electron microscope at an acceleration voltage of 5 kV.

Plasma Chemistry

PET film samples were taped onto a glass slide with one sample upstream and another downstream. The glass slide was inserted into the reactor which was then evaeuated to ~0.05 mm. Monomer gas was introduced using a needle valve and the pressure was equilibrated to the desired pressure by adjusting the needle valve. After equilibrium pressure was reaehed and the reactor was exposed to the monomer for at least 10 minutes, radiofrequency at 20 W was applied for 15 minutes. The flow rate was measured to be ~1.7 secm. The monomer pressures used were 0.3 mm, 0.4 mm, and 0.5 mm. After the radiofrequency was turned off, monomer gas was allowed to flow through the system for 10 minutes before evacuating the ehamber to ~0.05 mm for 10 minutes and isolating the PET film samples.

Results and Discussions

Plasma Chemistry

The plasma polymerization of the fluoromonomers was eonducted in the home-built plasma reactor deseribed in chapter 2. Film samples of PET were cut to dimensions appropriate for our analytical teehniques (generally 1.5 x 4 cm), taped to the ends of the glass plate, and were exposed to a monomer gas plasma (20 W) for 15 min. One sample, loeated eloser to the vaeuum, will be ealled the downstream sample, and another sample,

located closer to the monomer source, will be called the upstream sample. The initial water contact angle measurements for PET are θ_A=85.5° and θ_R=47.1°.

Saturated Fluoromonomer (PFH)

Plasma polymerization of PFH does not produce powders under the conditions examined. The amount of plasma polymer deposited decreased as the pressure was increased from 0.3 mm to 0.5 mm, as observed from the decrease in fluorine content (55.7% to 25.0%) and the concomitant increase in oxygen content due to the PET substrate (1.4% to 22.0%). The advancing contact angle varied from 115° to 118° and the hysteresis increased from 43° to 50° as the pressure is increased. The roughness ratio as measured by the AFM did not change and the increase in hysteresis may by due to more -CF_3 groups present. The lack of powder formation was not surprising since under the conditions tested; it is difficult for the monomer to polymerize in the gas phase, due to lack of unsaturation. It was previously suggested that polymerization in the gas phase is a necessary condition for powder formation.[8-10]

Unsaturated Fluoromonomers

Two fluoromonomers in this class were examined, NFH and PFMP. NFH is a long chain with the double bond in the 1 position and is expected to polymerize in the gas phase and form a powder. PFMP is more hindered at its unsaturation and may have more difficulty polymerizing in the gas phase. The structures of these two monomers are

shown in figure F.1. The XPS and contact angle results are summarized in table F.1. For all samples except NFH at 0.3 mm downstream, the measured F/C ratios are below the theoretical F/C ratio.

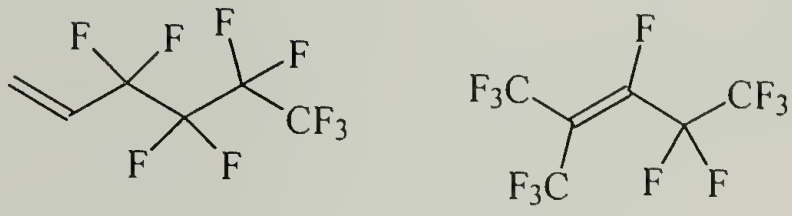

NFH PFMP

Figure F.1. Monomer structure of NFH and PFMP.

Table F.1. XPS and contact angle data for plasma polymers of NFH and PFMP. The theoretical F/C ratio for NFH is 1.5 and for PFMP is 2.0.

Monomer	Pressure (mm)	Position	F/C	θ_A	θ_R
NFH	0.3	downstream	1.78	112°	83°
		upstream	1.44	129°	80°
	0.4	downstream	1.15	136°	65°
		upstream	1.19	116°	67°
	0.5	downstream	1.29	169°/122°	168°/69°
		upstream	1.16	110°	71°
PFMP	0.3	downstream	1.48	113°	76°
		upstream	1.42	110°	77°
	0.4	downstream	1.42	116°	74°
		upstream	1.34	114°	83°
	0.5	downstream	0.74	113°	73°
		upstream	1.43	114°	77°

For NFH monomer, powder deposition occurred at 0.5 mm on the downstream sample resulting in a highly nonwettable surface (θ_A=169° and θ_R=168°). However, the powder formed under these conditions does not adhere well as observed by the change in contact angle measurements (θ_A=122° and θ_R=69°) when the size of the water droplet is increased past a certain size. The upstream sample under the same conditions did not exhibit the same hydrophobic properties (θ_A=110° and θ_R=71°). This difference in wettability is due to the difference in the surface morphology and not to the chemical composition as both samples have very similar F/C ratios. Figure F.2 shows the surface topography as measured by AFM. The roughness ratio for the downstream sample (with the powder) is 1.64 versus 1.05 for the upstream sample (no powder).

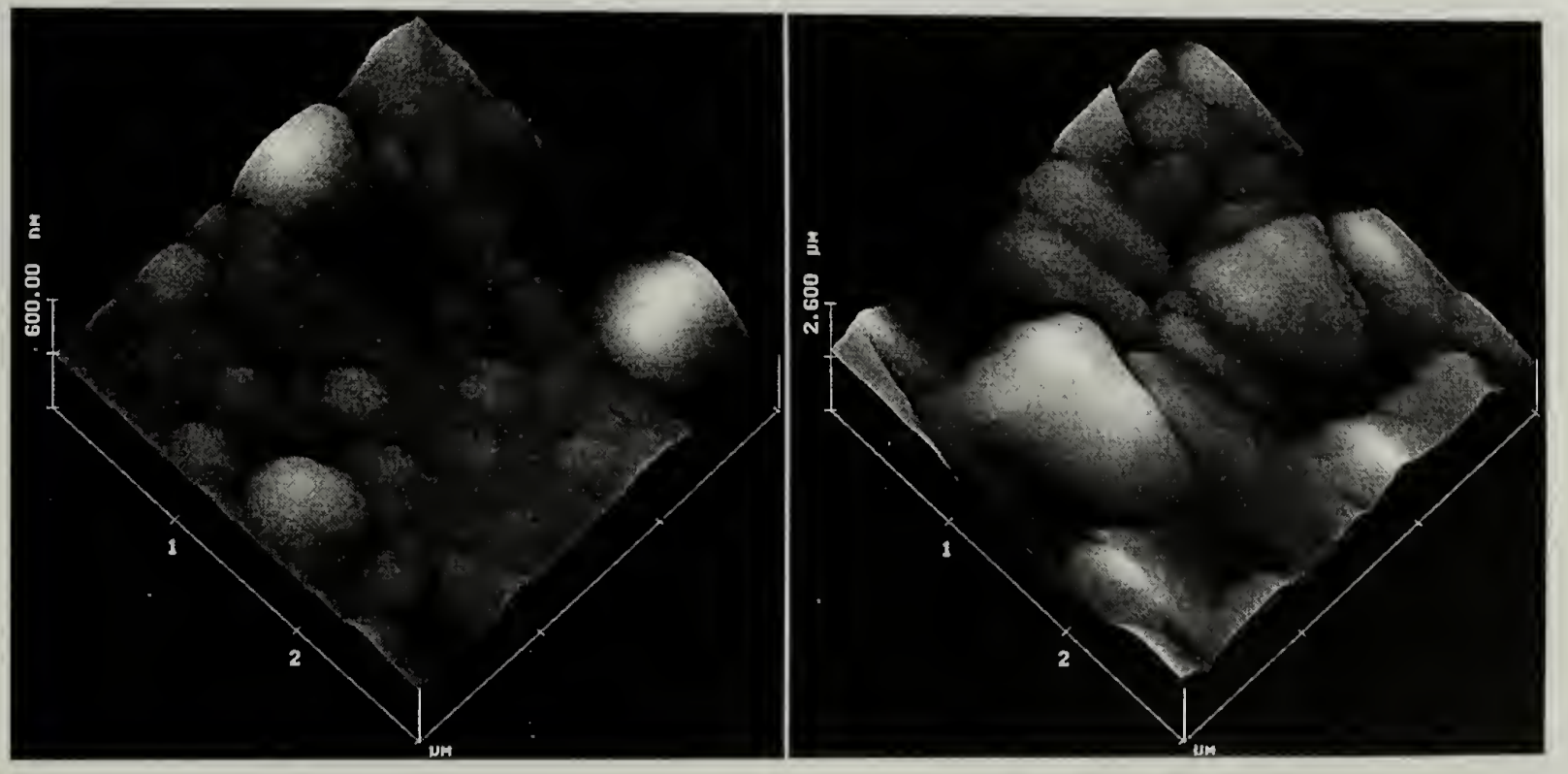

Upstream (110°/71°) Downstream (169°/168°)

Figure F.2. AFM trace of NFH plasma polymer prepared at 0.5 mm for the upstream (r=1.05) and downstream sample (r=1.64).

Plasma polymerization of PFMP monomer did not form powder for the conditions examined. The F/C ratio varied around 1.4 with the exception of the downstream sample at 0.5 mm (F/C=0.74) due to the appearance of the PET substrate which also contributed to a measured 18% oxygen content. All samples tested have similar wetting properties. Powder did not form for this monomer due to the structural constraint at the double bond. A high polymerization rate in the gas phase is needed in order for powder to form, otherwise the formation of films is more favored.[8] The $-CF_3$ substituent in the 2 position structurally hinders the polymerization process in the gas phase and slows the reaction rate leading to film formation rather than powder formation.

Fluorinated Acrylates and EHFB

Four monomers were chosen to determine the effects of the length and branching of the fluorinated alkyl acrylates and the effect of the degree of saturation of monomers containing carbonyl groups. HFBA and PFPA are compared as the chain-length differs by one carbon unit. PFPA and HFIA are compared as the former monomer has a straight chain versus a branched structure for the latter. Finally, EHFB lacks the double bond but has a carbonyl moiety and serves as an ideal candidate for comparing the effect of the degree of saturation versus that of the acrylates. The structures of these monomers are shown in figure F.3. The XPS and contact angle results are summarized in table F.2. Powder formation was observed for all the monomers tested.

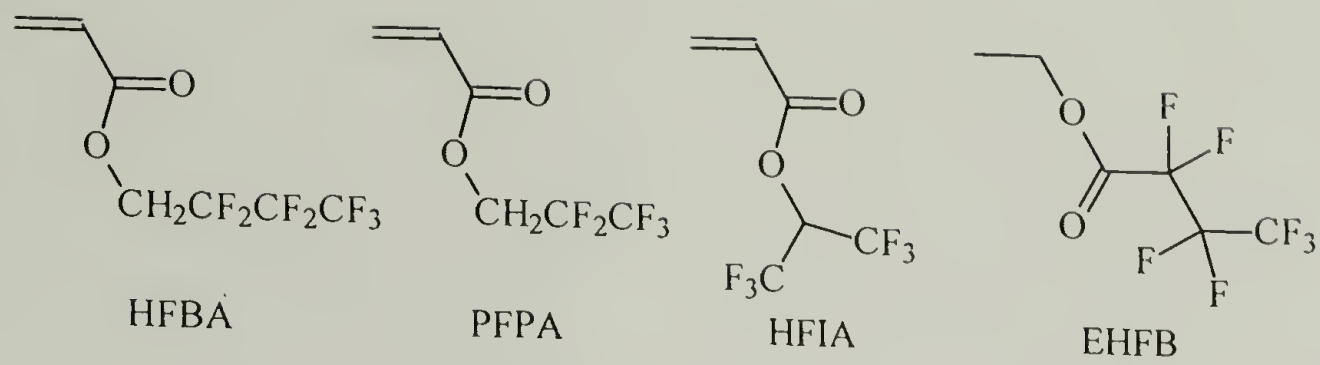

Figure F.3. Chemical structures of the acrylates and butyrate tested.

Table F.2. XPS and contact angle data for HFBA, PFPA, HFIA, and EHFB. The theoretical F/C, F/O, and C/O ratios are noted in the first row for each monomer.

Monomer	Pressure (mm)	Position	F/C	F/O	C/O	θ_A	θ_R
HFBA			1.0	3.5	3.5		
	0.3	downstream	1.12	6.2	5.5	105°	63°
	0.4	downstream	0.91	4.4	4.8	102°	58°
		upstream	0.84	3.2	3.8	174°	173°
PFPA			0.83	2.5	3.0		
	0.3	downstream	0.79	3.2	4.0	118°/96°	43°/15°
		upstream	0.69	2.5	3.6	106°	35°
	0.4	downstream	0.89	4.1	4.6	90°	54°
		upstream	0.70	2.5	3.6	118°	33°
	0.5	downstream	0.86	3.4	3.9	93°	54°
		upstream	0.71	2.4	3.4	169°/147°	7.8°
HFIA			1.0	3.0	3.0		
	0.3	downstream	1.67	13	7.6	108°	72°
		upstream	1.25	5.2	4.1	116°	51°
	0.4	downstream	1.00	6.0	6.0	164°	153°
		upstream	1.17	4.1	3.5	119°	46°
EHFB			1.17	3.5	3.0		
	0.3	downstream	0.93	7.8	8.3	126°	41°
		upstream	0.69	2.5	3.6	112°	52°
	0.4	downstream	0.93	7.0	7.5	164°	149°
		upstream	0.78	3.8	4.9	110°	47°

Powder deposition for HFBA was achieved at 0.4 mm upstream. For the two HFBA samples that did not form powder, the F/O and C/O ratios for the resulting film are higher than for the starting monomer which signifies that some carbonyl groups were lost during the plasma polymerization, probably in the form of carbon dioxide. This contrasts with the powder formed by HFBA which shows F/O and C/O ratios close to that of the starting monomer. The highly hydrophobic nature for the end-resulting surface is attributed to the high roughness resulting from the powder deposition as the F/C ratio for the polymer powder is slightly lower than those of the polymer film. Figure F.4 shows AFM surface profiles for the upstream and downstream sample treated at 0.4 mm pressure which verifies the increased roughness for the more nonwettable surface.

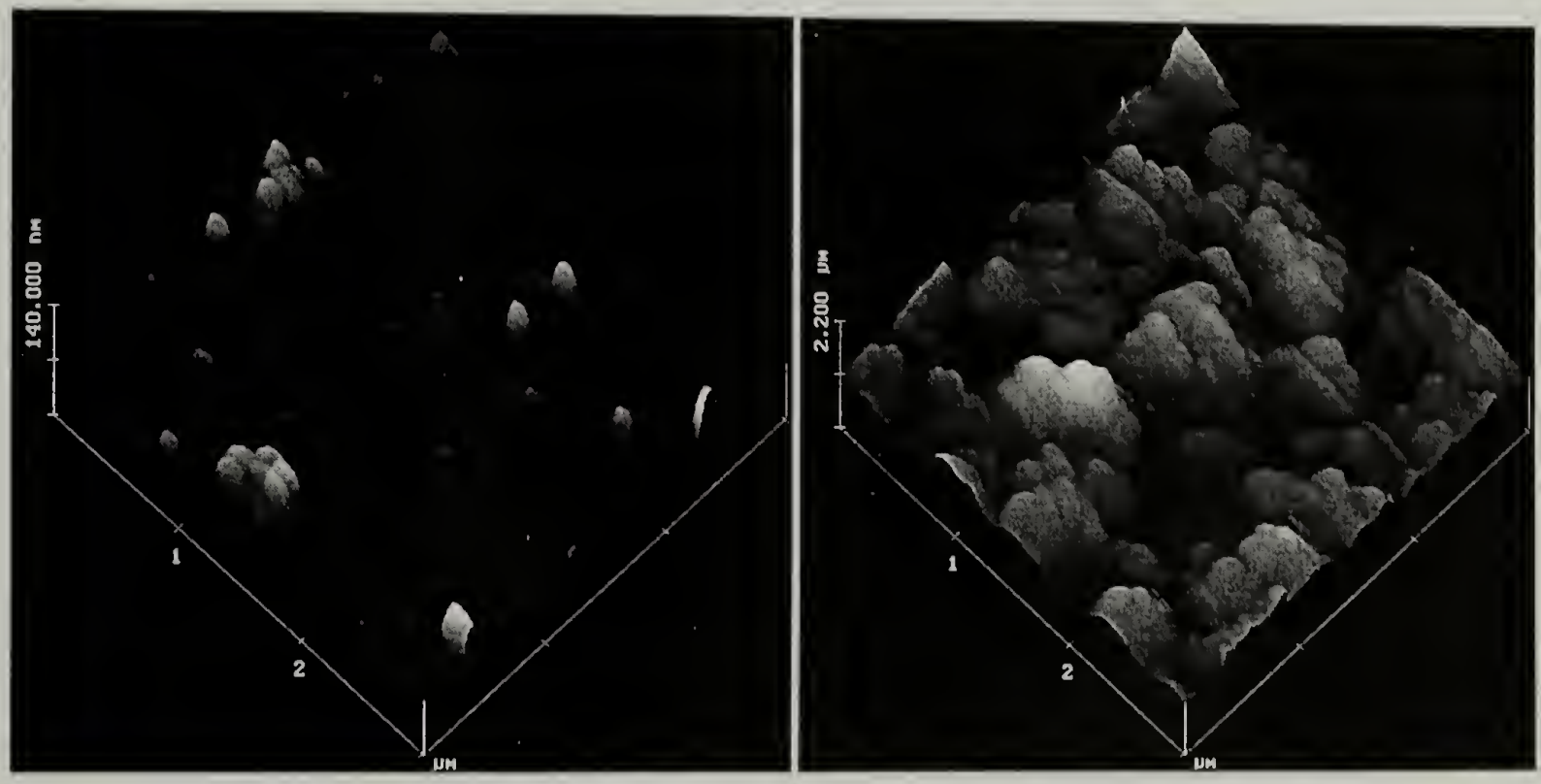

Downstream (102°/58°) Upstream (174°/173°)

Figure F.4. AFM trace of HFBA plasma polymer prepared at 0.4 mm for the upstream (r=2.56) and downstream sample (r=1.00).

For PFPA, powder deposition did not take place until 0.5 mm pressure. Similar to HFBA downstream samples, PFPA downstream samples show higher F/O and C/O ratio than that for the starting monomer indicating that some carbonyl groups were lost. The ratios for the upstream samples including the powder polymer are comparable to the starting monomer. The powder polymer shows a high advancing contact angle (θ_A=169°), but the water droplet wets the surface as the droplet is withdrawn (θ_R=7.8°). One possible explanation of this result is that there is sufficient mobility of the carbonyl group in the acrylate polymer that it reorients itself to the surface after the surface is exposed to the water drop thus producing a wetting surface.[11,12] Another possible explanation is that for this polymer, the roughness factor is below the critical noncomposite-composite transition where increasing the roughness greatly magnifies the hysteresis. Whatever the reason may be, it is noted that the high advancing contact angle of this surface is due to surface roughness as AFM shows the differences for the upstream and downstream samples (Figure F.5).

Powder formation of HFIA occurred at 0.4 mm pressure on the downstream sample. In all samples, F/C, F/O, and C/O ratios are higher for the resulting plasma polymer than for the starting monomer which indicates the loss of CO_2. The powder sample shows a F/C ratio of 1 matching the expected ratio while the other two ratios are doubled, which contrasts with the HFBA and PFPA powders that have nearly equal ratios to their respective monomers. This suggests that the polymerization mechanism of HFIA in the gas phase differs from HFBA and PFPA, perhaps through the climination of the carbonyl group instead of through the double bond.[13,14] This may explain the decrease in

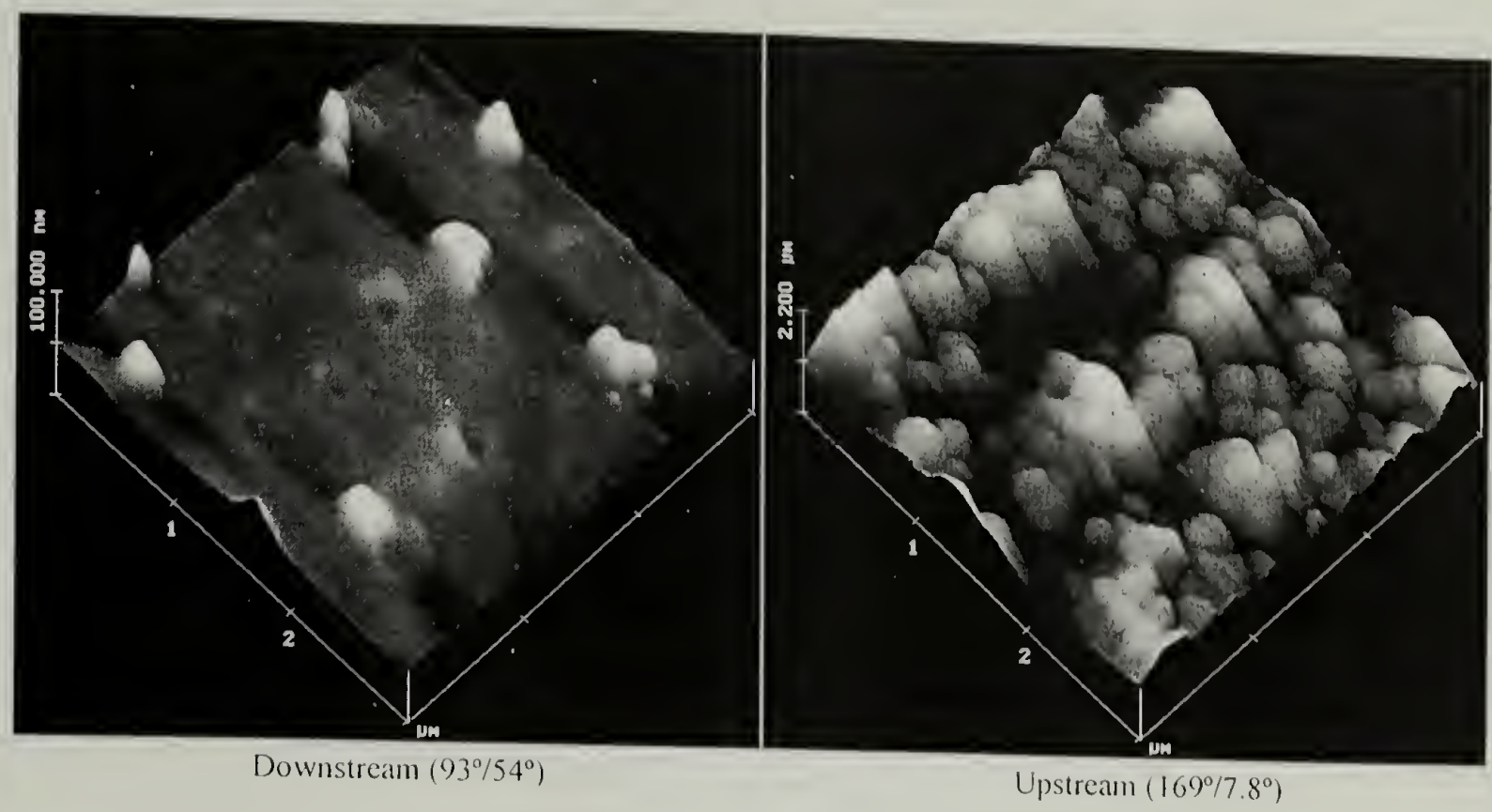

Downstream (93°/54°)

Upstream (169°/7.8°)

Figure F.5. AFM trace of PFPA plasma polymer prepared at 0.5 mm for the upstream (r=2.26) and downstream sample (r=1.00).

adhesion of the powder to the substrate. Because of this, direct measurement of the surface roughness using AFM was not possible. In a direct comparison with PFPA, the branched acrylate formed powders at a lower pressure and the water droplet does not adhere to the sample upon exposure (θ_R=153°). The remaining carbonyl groups in these samples may not be as mobile as in the case of the linear fluoroalkyl acrylate due to the branched group. Platinum-carbon replicas of the surface were made in order to examine the surface roughness of these materials using the AFM. Like the previous samples that show highly nonwettable surfaces, surface roughness again is the important factor as the downstream sample has a roughness ratio of 2.82 (θ_Λ=164°) while the upstream sample has a ratio of 1.14 (θ_Λ=119°), as is shown in figure F.6.

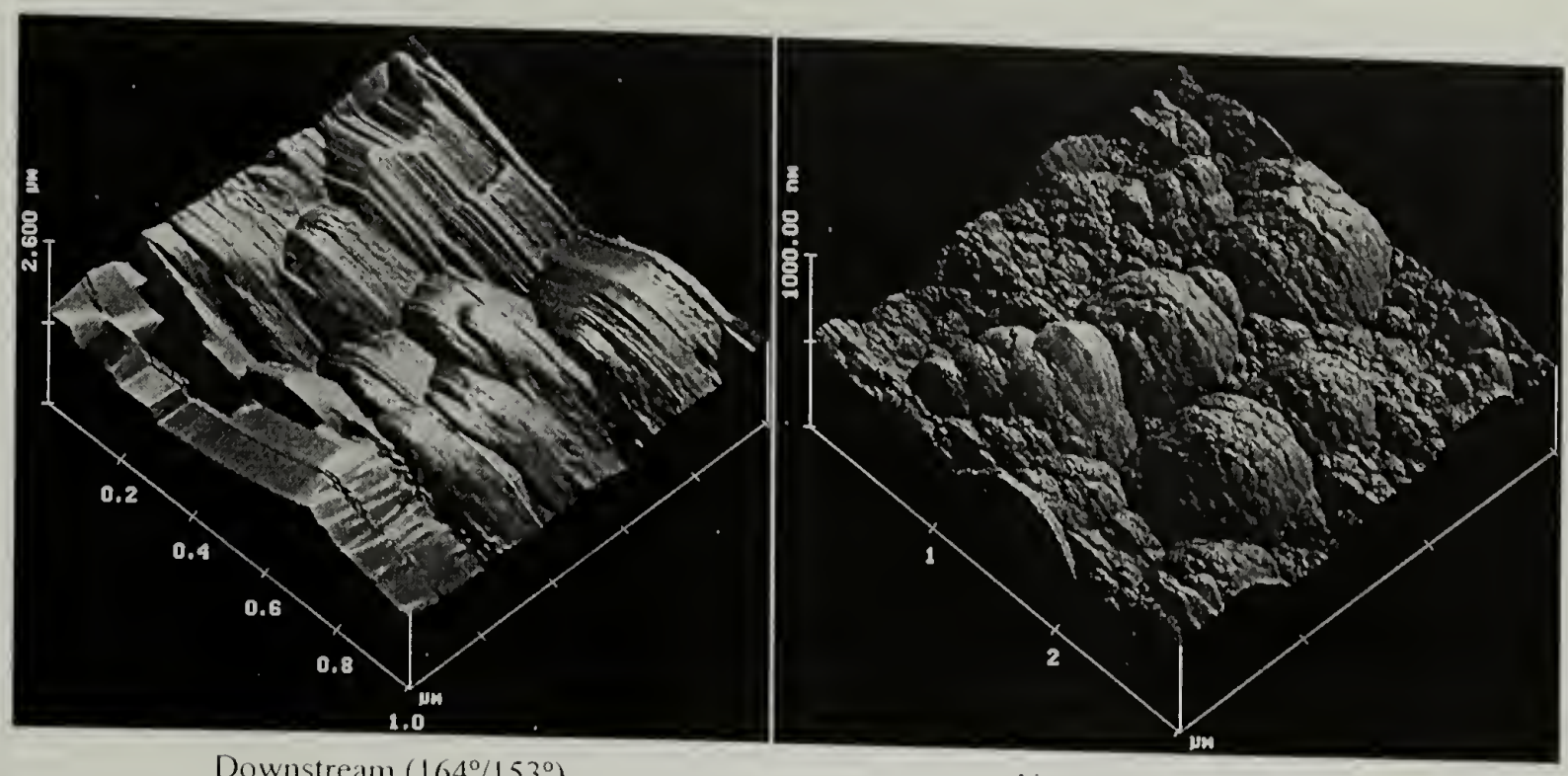

Downstream (164°/153°)

Upstream (119°/146°)

Figure F.6. AFM trace of HFIA plasma polymer prepared at 0.4 mm for the upstream (r=1.14) and downstream sample (r=2.82).

EHFB monomer plasma polymerized in the gas phase and formed a powder at 0.4 mm; these results are similar to those of HFBA and HFIA. The monomer most likely polymerized through the elimination of some carbonyl groups as higher F/O and C/O ratios than that for the starting monomer (doubled) are observed. Similar to the HFIA plasma polymer which also may polymerize through the carbonyl group, these powders show weak adhesion as direct roughness measurements using AFM were not possible; surface replicas had to be prepared. Water droplets on these surfaces roll off the surface as was the case of HFBA and HFIA samples. The surface roughness of these samples again plays a major role in their wetting properties. Their surfaces are compared in figure F.7.

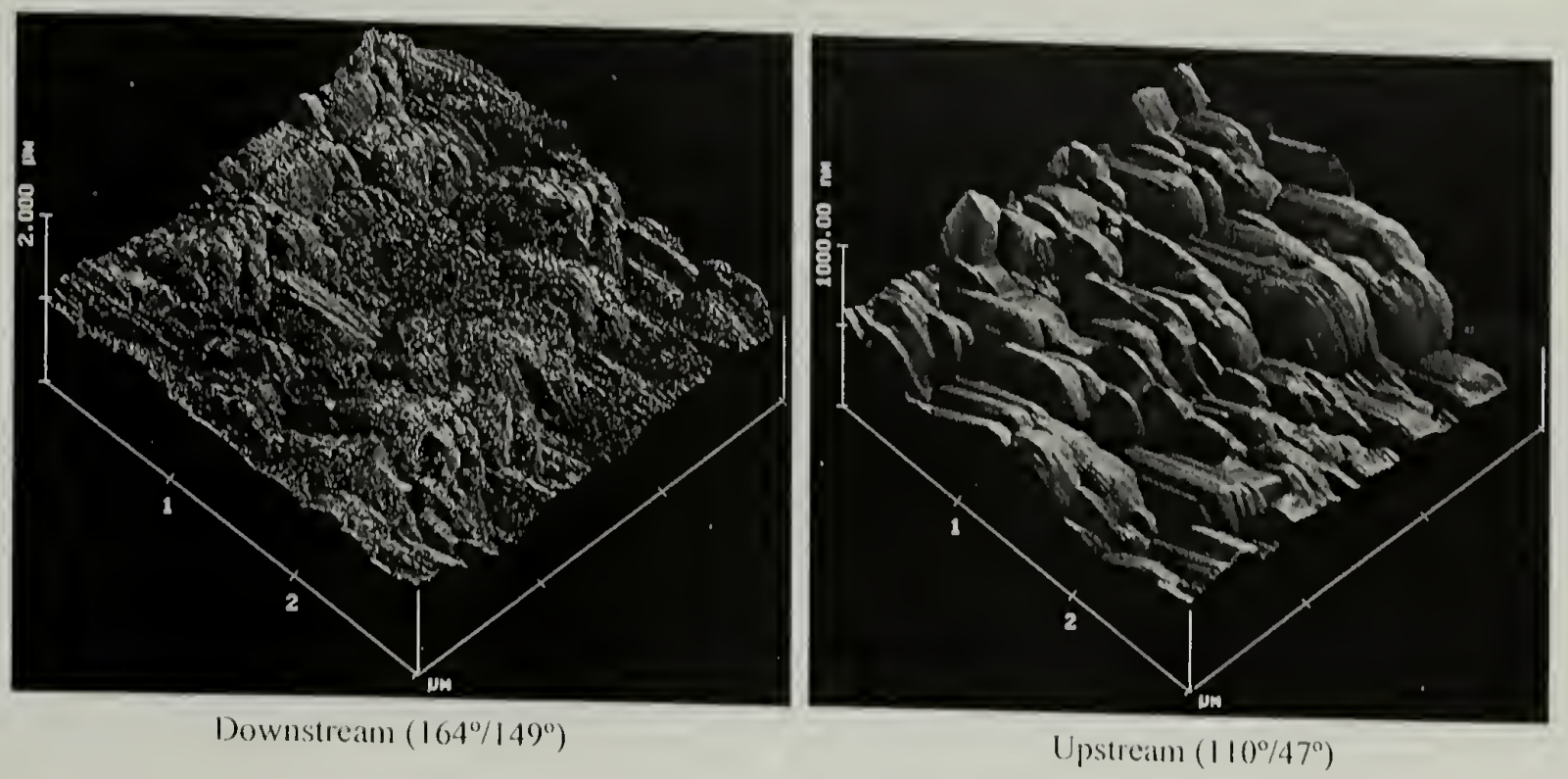

Downstream (164°/149°)

Upstream (110°/47°)

Figure F.7. AFM trace of EFHB plasma polymer prepared at 0.4 mm for the upstream (r=1.18) and downstream sample (r=3.29).

Summary

Various fluorocarbon gases have been plasma polymerized on PET, forming hydrophobic surfaces. The most hydrophobic surfaces were generated with monomers that contain either carbonyl groups or double bonds and form powders. It is observed that monomers that have difficulty polymerizing in the gas phase, whether saturated, as in the case of PFH, or if the site of the double bond is structurally hindered, as in PFMP, do not form the necessary rough surface which is a prerequisite to highly nonwettable surfaces. For the other monomers examined, a minimum monomer concentration, as controlled by the monomer pressure, was necessary to form powder structures. When the powder successfully deposits on the support surface, a hydrophobic surface was formed. The chemical composition is not a major contributor as the F/C ratio of these powders is at

most 1.3 whereas it is slightly higher than 2.0 for Teflon with a corresponding advancing contact angle of about 110°. For the monomers that have high F/O and C/O ratios (HFIA and EHFB), some polymerization occurs through the elimination of the carbonyl group and forms a low adherent powder coating. A minimum length for the fluorinated alkyl chain in the acrylate is necessary for high receding contact angle. The length must be at least 3 carbons or the chain must be branched.

Notes and References

(1) Lee, A.R. *J. Soc. Chem. Ind.* **1936**, *55*, 23T.

(2) Dettre, R.H.; Johnson, R.E., Jr. *Adv. Chem. Ser.* **1964**, *43*, 136.

(3) Bartell, F.E.; Shepard, J.W. *J. Phys. Chem.* **1953**, *57*, 211.

(4) Shafrin, E.G.; Zisman, W.A. *Adv. Chem. Ser.* **1964**, *43*, 145.

(5) Washo, B.D. *Org. Coat. Apply. Polym. Sci.* **1982**, *47*, 69.

(6) Sato, D.; Jikei, M.; Kakimoto, M. *Polym. Prepr.(Am. Chem. Soc. Div. Polym. Chem.)* **1998**, *39(2)*, 926.

(7) Wang, J.-H.; Chen, J.J.; Timmons, R.B. *Chem. Mater.* **1996**, *8*, 2212.

(8) Kobayashi, H.; Bell, A.T.; Shen, M. *J. Appl. Polym. Sci.* **1973**, *17*, 885.

(9) Kobayashi, H.; Bell, A.T.; Shen, M. *Macromolecules* **1974**, *7*, 277.

(10) Yasuda, H. *Plasma Polymerization*; Academic Press: New York, 1985.

(11) Lavielle, L., and Schultz, J. *J. Coll. Interface Sci.* **1985**, *106*, 438.

(12) Lavielle, L.; Lischetti, G.; Sanfield, A.; and Schultz, J. *J. Coll. Interface Sci.* **1990**, *138*, 134.

(13) Ohno, M.; Ohno, K.; Sohma, J. *J. Polym. Sci. Part A: Polym. Chem.* **1987**, *25*, 1273.

(14) Denes, F.; Sarmadi, A.M.; Hop, C.E.C.A.; Young, R.A. *Polym. Prepr.(Am. Chem. Soc. Div. Polym. Chem.)* **1993**, *34(1)*, 685.

BIBLIOGRAPHY

Agrawal, D.C.; Raj, R. *Acta. Metall.* **1989**, *37*, 1265.

Andrade, J. D. *Surface and Interfacial Aspects of Biomedical Polymers, Surface Chemistry and Physics;* Plenum Press: New York, 1985; Vol. 1, p 180.

Ashley, J.C. *IEEE Trans. Nucl. Sci.* **1980**, *NS-27*, 1454.

Ashley, J.C.; Williams, M.W. *Rad. Res.* **1980**, *81*, 364.

Ashley, J.C. *J. Electron Spectroscopy* **1982**, *29*, 177.

Badey, J.P.; Espuche, E.; Sage, D.; Chabert, B.; Jugnet, Y.; Batier, C.; Duc, T.M. *Polymer* **1996**, *37*, 1377.

Bartell, F.E.; Shepard, J.W. *J. Phys. Chem.* **1953**, *57*, 211.

Bigelow, W.C.; Pickett, D.L.; Zisman, W.A. *J. Colloid Interface Sci.* **1946**, *1*, 513.

Blaakmeer, J.; Böhmer, M.R.; Cohen Stuart, M.A.; Fleer, G.J. *Macromolecules* **1990**, 23, 2301.

Blais, P.; Carlsson, D.J.; Csullog, G.W.; and Wiles, D.M. *J. Coll. Interf. Sci.*, **1974**, *47*, 636.

Böhmer, M.R.; Evers, O.A.; Scheutjens, J.M.H.M. *Macromolecules* **1990**, 23, 2288.

Caruso, F.; Niikura, K.; Furlong, D.N.; Okahata, Y. *Langmuir*, **1997**, *13*, 3427.

Caruso, F.; Niikura, K.; Furlong, D.N.; Okahata, Y. *Langmuir* **1997**, *13*, 3422.

Cassie, A.B.D; Baxter, S. *Trans. Faraday Soc.* **1944**, *40*, 546.

Cassie, A.B.D. *Discuss. Faraday Soc.* **1948**, *3*, 11.

Chen, W.; McCarthy, T.J. *Macromolecules* **1997**, *30*, 78.

Cheung, J.H.; Stockton, W.B.; Rubner, M.F. *Macromolecules* **1997**, *30*, 2712.

Chidsey, C.E.D.; Loiacono, D.N. *Langmuir* **1990**, *6*, 682.

Clark, D.T.; Thomas, H.R. *J. Polym. Sci., Polym. Chem. Ed.* **1977**, *15*, 2843.

Coburn, J.W.; Kay, E. *IBM J. Res. Develop.* **1979**, *23*, 33.

Cosgrove, T.; Obey, T.M.; Vincent, B. *J. Colloid Interface Sci.* **1986**, *111 (2)*, 409.

Cox, H.L. *Br. J. Appl. Phys.* **1952**, *3*, 72.

d'Agostino, R. *J. Vac. Sci. Technol. A* **1985**, *3(6)*, 2627.

DeBono, R.F.; Loucks, G.D.; Manna, D.D.; Krull, U.J. *Can. J. Chem.* **1996**, *74*, 677.

Decher, G.; Hong, J.-D.; Schmitt, J. *Thin Solid Films* **1992**, *210/211*, 831.

Decher, G.; Schmitt, J. *Progr. Colloid. Polym. Sci.* **1992**, *89*, 160.

Decher, G.; Lvov, Y.; Schmitt, J. *Thin Solid Films* **1994**, *244*, 772.

Decher, G. *Multilayer Films (Polyelectrolytes)*, in *The Polymeric Materials Encyclopedia: Synthesis, Properties and Applications*; Salamone, J.C., Ed., Vol. 6, CRC Press: Boca Raton, 1996, p 4540.

Delcorte, A.; Bertrand, P.; Wischerhoff, E.; Laschewsky, A. *Langmuir* **1997**, *13*, 5125.

Delcorte, A.; Bertrand, P.; Arys, X.; Jonas, A.; Wischerhoff, E.; Mayer, B.; Laschewsky, A. *Surface Science* **1996**, *366*, 149.

Denes, F.; Sarmadi, A.M.; Hop, C.E.C.A.; Young, R.A. *Polym. Prepr.(Am. Chem. Soc. Div. Polym. Chem.)* **1993**, *34(1)*, 685.

Dettre, R.H.; Johnson, R.E., Jr. *Adv. Chem. Ser.* **1964**, *43*, 136.

Dias, A.J.; McCarthy, T.J. *Macromolecules* **1987**, *20*, 2068.

Dubois, L.H.; Zegarski, B.R.; Nuzzo, R.G. *J. Am. Chem. Soc.* **1990**, *112*, 570.

Dubois, L.H.; Zegarski, B.R.; Nuzzo, R.G. *J. Chem. Phys.* **1993**, *98(1)*, 678.

Evers, O.A.; Fleer, G.J.; Scheutjens, J.M.H.M.; Lyklema, J. *J. Colloid Interface Sci.* **1986**, *111 (2)*, 446.

Ferreira, M.; Cheung, J.H.; Rubner, M.F. *Thin Solid Films*, **1994**, *244*, 806.

Ferreira, M.; Rubner, M.F. *Macromolecules* **1995**, *28*, 7107.

Fou, A.C.; Rubner, M.F. *Macromolecules* **1995**, *28*, 7115.

Fou, A.C.; Onitsuka, O.; Ferreira, M.; Rubner, M.F.; Hsieh, B.R. *J. Appl. Phys.* **1996**, *79*, 7501.

Fowkes, F.M.; Dwight, D.W.; Cole, D.A.; Huang, T.C. *J. Non-Cryst. Sol.* **1990**, *120*, 47.

Fraser, W.A.; Ancker, F.H., DiBenedetto, A.T., Elbirli, B. *Polymer Composites* **1983**, *4(4)*, 238.

Gombotz, W.R.; Hoffman, A.S. *J. Appl. Polym. Sci.: Polym. Symp.* **1988**, *42*, 285.

Hall, S.M.; Andrade, J.D.; Ma, S.M.; King, R.N. *J. Electron Spectroscopy* **1979**, *17*, 181.

Hammond, P.T.; Whitesides, G.M. *Macromolecules* **1995**, *28*, 7569.

Hollahan, J.R.; Wydeven, T. *Science* **1973**, *179*, 500..

Holloway, F.; Cohen, M.; Westheimer, F.H. *J. Am. Chem. Soc.* **1951**, *73*, 65.

Hu, M.S.; Evans, A.G. *Acta. Metall.* **1989**, *37*, 917.

Jensen, R.J.; Bell, A.T.; Soong, D.S. *Plasma Chem. Plasma Process.* **1983**, *3*, 163.

Johnson, R.E., Jr.; Dettre, R.H. *Adv. Chem. Ser.* **1964**, *43*, 112.

Johnson, R.E., Jr.; Dettre, R.H. *J. Phys. Chem.* **1964**, *68*, 1744.

Kaplan, S.; Dilks, A. *J. Appl. Polym. Sci.: Appl. Polym. Sym.* **1984**, *38*, 105.

Kelly, A.; Tyson, W.R. *J. Mech. Phys. Solids* **1965**, *13*, 329.

Kimber, A.C.; Keer, J.G. *J. Mater. Sci. Letters* **1982**, *1*, 353.

Kleinfeld, E.R.; Ferguson, G.S. *Science* **1994**, *265*, 370.

Kleinfeld, E.R.; Ferguson, G.S. *Chem. Mater.* **1995**, *7*, 2327.

Kobayashi, H.; Bell, A.T.; Shen, M. *J. Appl. Polym. Sci.* **1973**, *17*, 885.

Kobayashi, H.; Bell, A.T.; Shen, M. *Macromolecules* **1974**, *7*, 277.

Krishnamurthy, V.; Kamel, I.L.; Wei, Y. *J. Polym. Sci.: Part A: Polym. Chem.* **1989**, *27*, 1211.

Laibinis, P.; Whitesides, G.M.; Allara, D.L.; Tao, Y.-T.; Parikh, A.N.; Nuzzo, R.G. *J. Am. Chem. Soc.* **1991**, *113*, 7152.

Laibinis, P.E. ; Whitesides, G.M. *J. Am. Chem. Soc.* **1992**, *114*, 1990.

Laschewsky, A.; Bayer, B.; Wischerhoff, E.; Arys, X.; Bertrand, P.; Delacorte, A.; Jonas, A. *Thin Solid Films* **1996**, *284*, 334.

Laurent, D.; Schlenoff, J.B. *Langmuir* **1997**, *13*, 1552.

Lavielle, L., and Schultz, J. *J. Coll. Interface Sci.* **1985**, *106*, 438.

Lavielle, L.; Lischetti, G.; Sanfield, A.; and Schultz, J. *J. Coll. Interface Sci.* **1990**, *138*, 134.

Lee, A.R. *J. Soc. Chem. Ind.* **1936**, *55*, 23T.

Leterrier, Y.; Wyser, Y.; Månson, J.-A.E.; Hilborn, J. *J. Adhesion* **1994**, *44*, 213.

Leterrier, Y.; Månson, J.-A.E. *J. Mater. Sci. Letters* **1997**, *16*, 120.

Leterrier, Y.; Boogh, L.; Andersons, J.; Månson, J.-A.E. *J. Polym. Sci. Part B: Polym. Phys.* **1997**, *35*, 1449.

Leterrier, Y.; Andersons, J.; Pitton, Y.; Månson, J.-A.E. *J. Polym. Sci. Part B: Polym. Phys.* **1997**, *35*, 1463.

Leväsalmi, J.-M.; McCarthy, T.J. *Macromolecules* **1997**, *30*, 1752.

Liston, E.M.; Martinu, L.; Wertheimer, M.R. *Plasma Surface Modification of Polymers for Improved Adhesion: A Critical Review*, in *Plasma Surface Modification of Polymers*, Strobel, M.; Lyons, C.; Mittal, K.L., Eds., Utrecht: The Netherlands, 1994.

Lvov, Y.; Decher, G.; Möhwald, H. *Langmuir* **1993**, *9*, 481.

Lvov, Y.; Decher, G.; Sukhorukov, G. *Macromolecules* **1993**, *26*, 5397.

Lvov, Y.; Haas, H. Decher, G.; Möhwald, H.; Kalachev, A. *J. Phys. Chem.* **1993**, *97*, 12835.

Lvov, Y.; Ariga, K.; Kunitake, T. *Chem. Lett.* **1994**, 2323.

Lvov, Y.; Haas, H.; Decher, G.; Möhwald, H. *Langmuir* **1994**, *10*, 4232.

Lvov, Y.; Ariga, K.; Ichinose, I.; Kunitake, T. *Langmuir* **1996**, *12*, 3038.

Lvov, Y.; Ariga, K.; Onda, M.; Ichinose, I.; Kunitake, T. *Langmuir* **1997**, *13*, 6195.

Marra, J.; van der Schee, H.A.; Fleer, G.J.; Lyklema, J. In *Adsorption from Solution*; Ottewill, R.H., Rochester, C.H., Eds.; Academic Press: New York, 1983, p 245.

Morita, S.; Bell, A.T.; Shen, M. *J. Polym. Sci.: Polym. Chem. Ed.* **1979**, *17*, 2775.

Morosoff, N.; Newton, W.; Yasuda, H. *J. Vac. Sci. Technol.* **1978**, *15*, 1815.

Morosoff, N. *Surface Modification by Plasma Polymerization*, in *Innovations in Materials Processing*, Bruggeman, G., Weiss, V., Eds., Plenum: New York, 1985.

Morosoff, N. *An Introduction to Plasma Polymerization*, in *Plasma Deposition, Treatment, and Etching of Polymers*, d'Agostino, R., Ed., Academic Press: San Diego, 1990.

Morra, M.; Occhiello, E.; Garbassi, F. *Langmuir* **1989**, *5*, 872.

Nardin, M.; Asloun, E.M.; Schultz, J. *Polym. Adv. Technol.* **1991**, *2*, 115.

Nardin, M.; Schultz, J. *Compos. Interfaces* **1993**, *1*, 177.

Nomura, H.; Kramer, P.W.; Yasuda, H. *Thin Solid Films* **1984**, *118*, 187.

Ohno, M.; Ohno, K.; Sohma, J. *J. Polym. Sci. Part A: Polym. Chem.* **1987**, *25*, 1273.

Onda, M.; Lvov, Y.; Ariga, K.; Kunitake, T. *J. Ferment. Bioeng.* **1996**, *82*, 502.

Onoda, M.; Yoshino, K. *Jpn. J. Appl. Phys.* **1995**, *34*, L260.

Papenhuijzen, J.; Fleer, G.J; Bijsterbosch, B.H. *J. Colloid Interface Sci.* **1985**, *104*, 530.

Papenhuijzen, J.; van der Schee, H.A.; Fleer, G.J. *J. Colloid Interface Sci.* **1985**, *104*, 540.

Phuvanartnuruks, V.; McCarthy, T.J. *Macromolecules* **1998**, *31*, 1906.

Plunkett, R.J. U.S. Pat. 2,230,654, **1941**.

Porter, M.D.; Bright, T.B.; Allara, D.L.; Chidsey, C.E.D. *J. Am. Chem. Soc.* **1987**, *109*, 3559.

Powell, C.J. *Surface Science* **1974**, *44*, 29.

Rasmussen, J.R.; Stedronsky, E.R.; Whitesides, G.M. *J. Am. Chem. Soc.* **1977**, *99*, 4736.

Sager, W.F. *J. Am. Chem. Soc.* **1956**, *78*, 649.

Sato, D.; Jikei, M.; Kakimoto, M. *Polym. Prepr.(Am. Chem. Soc. Div. Polym. Chem.)* **1998**, *39(2)*, 926.

Schmitt, J.; Grunewald, G,; Decher, G.; Pershan, P.S.; Kjaer, K.; Losche, M. *Macromolecules* **1993**, *26*, 7058.

Scott, T.W.; Chu, K.-C.; Venugopalan, M. *J. Polym. Sci.: Polym. Chem. Ed.* **1979**, *17*, 267.

Shafrin, E.G.; Zisman, W.A. *Adv. Chem. Ser.* **1964**, *43*, 145.

Smithson, R.L.W.; McClure, D.J.; Evans, D.F. *Thin Solid Films* **1997**, *307*, 110.

Steinhardt, R.G.; Hudis, J.; Perlman, M.L. *Phys. Rev.* **1972**, *B5*, 1016.

Stepp, J.; Schlenoff, J.B. *J. Electrochem. Soc.* **1997**, *144*, L155.

Sterrett, T.L.; Sachdeva, R.; Jerabek, P. *J. Mater. Sci. Mater. Med.* **1992**, *3*, 402.

Stockton, W.B.; Rubner, M.F. *Macromolecules* **1997**, *30*, 2717.

Sukhorukov, G.B.; Schmitt, J.; and Decher, G. *Ber. Bunsenges. Phys. Chem.* **1996**, *100*, 948.

Sun, Y.; Hao, E.; Zhang, X.; Yang, B.; Shen, J.; Chi, L.; Fuchs, H. *Langmuir* **1997**, *13*, 5168.

Tran, C.N.B.; Walt, D.R. *J. Colloid Interface Sci.* **1989**, *132*, 373.

Tsukruk, V.V.; Rinderspacher, F.; Bliznyuk, V. *Langmuir* **1997**, *13*, 2171.

Ulman, A. *An Introduction to Ultrathin Organic Films from Langmuir-Blodgett to Self-Assembly*; Academic Press: New York, 1991.

Ulman, A., Ed. *Thin Films, vol. 20, Organic Thin Films and Surfaces: Directions for the Nineties*; Academic Press: New York, 1995.

Ulman, A.; Eilers, J.E.; Tillman, N. *Langmuir* **1989**, *5*, 1147.

Van der Schee, H.A.; Lyklema, J. *J. Phys. Chem.* **1984**, 88, 6661.

Vargo, T.G.; Gardella, Jr., J.A.; Meyer, A.E.; Baier, R.E. *J. Polym. Sci.: Part A: Polym. Chem.* **1991**, *29*, 555.

Vögtle, F. *Supramolecular Chemistry*; Wiley: Chichester, 1993.

Wang, J.-H.; Chen, J.J.; Timmons, R.B. *Chem. Mater.* **1996**, *8*, 2212.

Washo, B.D. *Org. Coat. Apply. Polym. Sci.* **1982**, *47*, 69.

Watanabe, S.; Regan, S.L. *J. Am. Chem. Soc.* **1994**, *116*, 8855.

Wenzel, R.N. *Ind. Eng. Chem.* **1936**, *28*, 988.

Wiberg, K.B.; Eisenthal, R. *Tetrahedron* **1964**, *20*, 1151.

Wojciechowski, P.H.; Mendolia, M.S. *J. Vac. Sci. Technol. A* **1989**, *7(3)*, 1282.

Yamagishi, F.G.; Granger, D.D.; Schmitz, A.E.; Miller, L.J. *Thin Solid Films* **1981**, *84*, 427.

Yasuda, H.; Hirotsu, T. *J. Polym. Sci.: Polym. Chem. Ed.* **1977**, *15*, 2749.

Yasuda, H.; Hirotsu, T. *J. Polym. Sci.: Polym. Chem. Ed.* **1978**, *16*, 743.

Yasuda, H. *Plasma Polymerization*; Academic Press: New York, 1985.

Yeh, Y.-S.; Iriyama, Y.; Matsuzawa, Y.; Hanson, S.R.; Yasuda, H. *J. Biomed. Mater. Res.* **1988**, *22*, 795.

Young, T. *Phil. Trans.* **1805**, *95*, 65.